Response to Anonymous Referee #1

We would like to thank the reviewer for their comprehensive and thoughtful review, and helpful comments which are addressed individually in the response below. The reviewer's comments are included in blue & italics.

GENERAL COMMENTS

As clearly stated in the title, this manuscript presents results from the 2016 "CINDI-2" intercomparison campaign relating to retrievals of key trace species (NO2, O4, O3 and HCHO) using either MAX-DOAS or zenith sky UV/Visible spectrometers. These types of measurements have grown to considerable importance in the field of atmospheric composition in recent years, and are expected to continue to increase rapidly in number and range of applications, making a very careful campaign such as CINDI-2 of great interest to a broad community. Importantly, the major types of instruments now in widespread use (such as Pandora, SAOZ, the former EnviMeS MAX-DOAS and the Hoffman mini-DOAS) all participated in the campaign which ensures the relevance of the CINDI-2 results to the actual measurements being made around the world.

The manuscript is comprehensive and clearly written, and many of the author team are among the world experts in this field, and overall, I believe is very suitable for publication in AMT.

I do have a number of general comments and questions. I believe it will help the reader better understand the philosophy and approach of CINDI-2 if each of these could be briefly addressed in either the introduction or the discussion section of the manuscript.

1. It is evident that while great attention was paid to ensure the consistency of certain aspects of the measurements and retrievals, other aspects – which would also affect the results - were left to the individual groups. I am sure the decisions of the organisers in this regard were made with thought but it is not always clear to the reader what the motivation was for the different inclusions and exclusions and how these related to the stated aims.

This comment touches on a very important topic and most of the choices were motivated by findings of the first CINDI campaign and MADCAT. There definitely are reasons why some aspects of the intercomparison exercise were prescribed (such as the measurement schedule and the retrieval settings) while others were not (the analysis code and some of the calibration procedures). The organisers of the CINDI-2 intercomparison were aiming at providing a procedure that (1) forced every participating instrument to look simultaneously in the same direction (and to do this as precisely as practically achievable) and hence sample the same airmass and (2) to prescribe the use of analysis settings that were as consistent as realistically possible to enforce a more coordinated analysis.

One step further would have been to also prescribe the analysis software but allowing the individual groups to stick with their own preferred analysis software (which most participants would continue to use after CINDI-2 anyway) led to a more realistic intercomparison, and hence to a more realistic assessment of the participating instrument/group by using the combination of individual instrument plus individually used analysis software but prescribing all other settings and procedures.

Main reasons for not enforcing strict guidelines for the calibration steps were that (1) some of the key calibration steps (wavelength registration and slit function determination) can be obtained in the field using solar lines and dedicated software, (2) calibration facilities were not available to analyse other key instrumental responses, such as stray-light level, detector linearity response or polarization response, and (3) some neglected calibration steps are of minor importance for DOAS-type retrievals (e.g. radiometric response). However, the possibility to address better the missing aspects, and in

particular calibration related issues, will be considered when preparing future campaigns. A short paragraph has been added at the end of Section 2.2 (Campaign design) to motivate better why a lot of effort was spent on certain aspects.

2. To what extent, can the results of the intercomparison obtained in idealised and tightly co-ordinated conditions be applied the operational, geographically-distributed real-world measurement sites? Recommendations for the networks seem minimal (elevation scans are mentioned).

This is also a very important comment and helpful feed-back for us. The NDACC UV/Vis Working Group provides recommendations for measurements and data analysis which are mandatory for the inclusion of an instrument (and station) into the NDACC network. These recommendations (referred to as NDACC UV/Vis Appendix) have been substantially updated to also include guidelines for MAX-DOAS measurements and data analysis, and they will be published on the NDACC web page by the end of December 2019. A short statement has been added to address this, which is quoted under item 5 further below.
We have also added a separate section entitled 'Recommendations for network operation and future campaigns' before the conclusions. A part of the conclusions has been moved into this section and some addition text addressing this comment has also been added.

3. Limited of course by my own experience, it seems quite unusual for an intercomparison to be carried out without a designated reference instrument or standard, and instead to use the median of the participants as a reference. (Although in the case of formaldehyde a subgroup of better performing instruments is identified and so this is closer to an orthodox reference group). As far as I can see, this means there can be no traceability of any of the measurements? I would also add that in places I found the text has the potential to be misleading by referring to "the reference" in the abstract and conclusions, which readers might read in isolation to the rest of the paper.

We have clarified the use of reference data sets in the text. Reasons for why we used the median of the participating instruments rather than one single instrument (or a small group of instruments) is to keep the comparison fairer and not to 'favour' a couple of instruments. If an instrument with an absolute calibration would have been available then using that instrument would certainly have made sense, but there is no absolute reference for such measurements. The approach adopted here is similar to what was used in previous UV-Vis intercomparisons, i.e. identifying a group of mutually consistent instruments and use the median from their measurements as a best estimate ('most probable') of the 'true' value. For NO_2, it appeared that a large number of instruments were found to be in mutual agreement within limits derived from previous campaigns, for HCHO only a small sub-group presented a satisfactory level of agreement.

4. In many places the manuscript notes the efforts made to eliminate spatial and temporal mismatches between the participating instruments, but this does not seem linked to the scales of temporal and spatial variability expected for these species, and indeed, in section 3.7 it seems NO2 varies on a finer scale.

Efforts were made to substantially improve the spatial and temporal coincidence between measurements, in comparison to what was done in previous campaigns. However, practical limitations (related to the large variety of participating instruments) also had to be considered. It was found – a posteriori – that the scale of variability of NO_2 was in fact small enough to still dominate the variance of the measurements (despite the fact that these measurements were synchronized to better than one minute in time and all telescope pointing in the same azimuthal direction within a few degrees of accuracy, and in the same elevation to better than 1 degree). And this has also been stated in Section 3.7. E.g. the following sentence has been added: 'This means that in this intercomparison, atmospheric

variability limits the reproducibility and representativeness of individual MAX-DOAS measurements for species such as NO_2.'

5. From time to time the stated aims seem to interfere with each other. To really understand the differences between instruments requires a somewhat different approach compared to undertaking a strict performance evaluation, particularly if the aim is to simulate realistic conditions in the field. This point is closely related to (1) about the overall design of the exercise and what is or isn't being evaluated.

To address and clarify this point, we have added a statement in Section 1, paragraph 4, that the aim of the intercomparison is '… to assess the participating instruments in their ability to retrieve the same geophysical quantities (i.e. slant columns of NO_2, O_4, HCHO and O_3) when measured and processed in a controlled way (i.e. using a prescribed measurement protocol and retrieval settings)'.

We have also added/changed the following statement in the conclusion so that is now reads: ' This assessment process, undertaken as part of the CINDI-2 intercomparison campaign, provides the UV-visible absorption spectroscopy research community with guidelines and a procedure on how to assess the performance of MAX-DOAS and DOAS instruments, in particular for the inclusion into NDACC (see NDACC webpage for access to the UV/Vis Appendix describing these recommendations). It is expected that a similar level of consistency, as seen during CINDI-2, can be obtained in the field if recommended settings are implemented and used by each participant of the network. More control in this aspect of homogeneity can be obtained through centralized processing, which is the aim of the currently developed ESA FRM4DOAS project (see http://frm4doas.aeronomie.be/).'

SPECIFIC COMMENTS

Page 2
Lines 9-12 The "major aims" don't quite agree with what appears later (Section 2.3, page 5 lines 31-32).

We agree with the reviewer (thanks very much for picking this up) and have changed the text in the abstract and in Section 2.3 to be consistent.

Lines 12-14 I don't see how you can do "trend analysis" without traceability to a standard?

For trend analysis, the measurement precision and its stability in time (i.e. making sure that measurements are not affected by drifts or discontinuities of any type) should be most important. This means that suitability for trend analysis cannot be determined from a campaign in isolation, since an instrument showing a perfect behavior during two weeks can always be affected by longer term drifts or biases once in operation. However, successful participation to successive campaigns is one way to verify stability. This is e.g. the approach used in the Dobson/Brewer network communities. Another possible approach is to regularly operate traveling standard instruments at the different sites of a network.

Line 20 The word "unprecedented" seems over hyped

We have changed this to 'unique'.

Line 25 "bias and offset of the individual data sets against the reference". I think this is likely to mislead the reader of the abstract because it implies the existence of a reference instrument.

We agree and have changed the text to '…. the selected refence (which is the median of either all data or a subset), …'

Lines 23-26 This seems like the "reproducibility" in usual metrological terms.

As far as I understand, this is correct. However, we used here the same mathematical terms previously used in UV/Vis instrument intercomparisons to be consistent with the analysis performed e.g. during the first CINDI or earlier intercomparisons.

Line 28 ". . . a quantitative assessment of the measurement performance" – it seems to me more like the "consistency" ?

We have changed the text to: 'It introduces a quantitative assessment of the consistency between all the participating instruments for the MAX-DOAS and zenith-sky DOAS techniques.' If an instrument was not performing well, this could be clearly identified.

Page 3
Line 38 "The interest of ESA for . . ." change to either "The interest of ESA in " or "The desire of ESA for" or similar.

Done.

Lines 40-41 "planned at the horizon 2022-2023" – I don't know what this phrase means sorry.

This phrase has been deleted.

Page 4
Line 7 Touching again on the philosophy of CINDI-2, it seems to me just the consistency, there are other aspects of "high quality" needed for "long-term measurements, trend analysis and satellite data validation".

See response to the corresponding comment above.

Line 8 ". . . it is essential . . . to contribute to a harmonisation" – it can't be "essential" to"contribute"! These seem to be aims (1) and (3) from the abstract re-worded.

We agree that this wasn't worded well and the text has been changed to accommodate the comment. The part of the sentence "… and to contribute to a harmonisation of the measurement settings and retrieval methods." has been deleted.

Line 9-10 Did you in fact contribute to a harmonisation of the measurement settings and retrieval methods outside of the intercomparison itself, ie for the networks to use in practice?

Yes, we did and this has been incorporated in the updated NDACC UV/Vis Appendix (Protocol for NDACC UV/Vis instrument operation and data analysis) which will be published on the NDACC web page later this month (Dec 2019). This has been added under Conclusions (paragraph 5).

Page 5
Lines 5-10 This is very interesting in terms of the philosophy of CINDI-2. It is stated some groups performed more advanced pre-processing, but in general, as far as I can tell, the results from these groups was not weighted any differently from groups that didn't do these steps. Is that logical?

Yes, it actually is. Since many of the instruments can differ in the detail of their particular setup, it would have been difficult to fairly assess the instruments performance on grounds of pre-processing without really looking thoroughly at each of the instruments and its pre-calibration features. However, it would certainly be valuable if future campaigns would look into the pre-processing and calibration of the instruments in a more coordinated way (e.g. through organization of a calibration campaign ahead of the field campaign) and this has now also been added in a new section dealing specifically with recommendations based on the CINDI-2 results and experiences.

Lines 9-10 Rather than standardise these steps, wouldn't it be more valuable to assess their contribution to better results?

That is a good point and we have addressed this by adding additional text under the new Section 5 (Recommendations for network operation and future campaigns), last paragraph (bullet #2).

Lines 9-10 Could this be something to recommend to field instruments?

Yes, it certainly can and the NDACC UV/Vis Appendix also contains information on further documentation containing guidelines for calibrations which will shortly also be available on the NDACC UV/Vis working group web site as well and is currently available here: http://frm4doas.aeronomie.be/ProjectDir/Deliverables/FRM4DOAS_D4_MAXDOAS_Best_Practices_Document_20180110_v1_0.pdf

Line 14 "containers". For the first time this word appears, I suggest "shipping containers", and also the first time it appears in the captions (Figure 1). After the first time, just "container" would be ok. A "container" out of context could be of any size.

We have changed this to: '… mobile units (similar to shipping containers) were temporarily installed for the campaign period.' The containers are not strictly speaking shipping containers but 'mobile units' which look similar to shipping containers.

Line 14 "temporary containers were rented" – I would prefer "shipping containers were rented and temporarily installed".

We have changed the text accordingly (see above).

Line 24 Strictly, 287 degrees isn't WNW, which is 292.5 degrees from north.

True, that is strictly speaking correct and we have added 'approximately'. We were working of a table that stated that WNW is associated with angles between 281.25° – 303.75°.

Line 24 Rather than "N=0", it would be clearer to say "north"

Agreed and this has been changed accordingly.

Line 29 Change "Like in" to "As in "

Done.

Lines 30-32 The objectives don't quite match the three listed earlier (such as in the abstract). Now there are only two.

This was already previously raised (first comment of the 'specific comments section') and has been changed in the text so it is consistent in Section 2.3 and the abstract.

Lines 31-32 The second objective was previously to "discuss the performance" now it is to "define a robust methodology for performance assessment". Is it to define a methodology or to apply it?

The objective is to define a methodology which is then also applied to the CINDI-2 data products. The text has been changed accordingly.

Lines 36-39 It is interesting that the retrieval settings and parameters were specified but not the software. I am struggling to understand the logic of this. I think this decision is worth more explanation. It would be possible to compare a purely raw instrumental quantity, wouldn't it?

We understand were the reviewer is coming from but since all analysis software packages basically solve the same mathematical equations (which are part of the DOAS technique), the differences lie in the details of the implementation (in particular wavelength registration issues) rather than in the

actual analysis software. Hence the approach to harmonize and prescribe the settings as much as possible but allow for individual software packages to be used.

Page 6

Lines 1-7 This is another curious feature of the design of the campaign. To me there seems a conflict between the daily meetings which help understand better what is going on, and the strictness of the campaign designed to assess performance. In the field this luxury would certainly not be available.

It is certainly correct that in the field, it is often not possible to get this kind of feed-back and the semi-blind intercomparison procedure is in this regard a compromise between (1) a strict 'blind' intercomparison which would not allow for any exchange of information between the participants and (2) the opportunity especially (but not only!) for more inexperienced participants to gain a lot of experience and knowledge, and if possible, to have an independent referee intervene if there is an obvious problem with instrumentation that can be fixed (e.g. a problem with the hardware, such as the elevation pointing). The information provided at the daily meetings also encouraged the participants to be more engaged in the intercomparison overall without giving away how well their individual measurements were doing.

Line 14 "operation" should be "operational"

Done.

Line 27 The sentence "The convention for the azimuth angle . . . " appears in the wrong place

We agree and this has been fixed; the explanation is now been provided earlier on under Section 2.2.

Line 28 "synchronicity" should be "synchronisation" (unless we are talking about Jung or pop music from the early 1980s)

Fair enough and done.

Line 32 I would have thought "an NDACC" rather than "a NDACC" (but this is because I am expecting the reader to read "NDACC" as "en dack".)

Agreed & done.

Page 7

Line 12 "unprecedented" seems over-hyped to me – don't you really just mean that it was "improved" or "greatly improved" since CINDI-1?

We appreciate the comment and have reworded the sentence accordingly.

Line 13 "synchroncity" -> "synchronisation"

Done.

Line 14 ". . . the impact of atmospheric noise on the data comparisons could be reduced to a minimum" - How do you know though that the level of co-ordination is enough though? Do you know what time scales and spatial scales you expect the species to vary over? Later on, you imply that actually the co-ordination was not sufficient for N20.

Good point and we have toned the statement down accordingly.

Line 29 Could you have mandated separate times for UV and visible?

Possibly, but we were not aware of that issue when the measurement schedule was designed, and this would also have meant that it would have affected everybody's schedule not just the Pandora instruments.

Line 34 I don't think "MPIC" has previously been defined.

The full name has been added in brackets.

Page 7 line 30 – Page 8 line 4
Presumably however none of this, except (3), would be available in a field setting? This to me seems a conflict between the different aims of CINDI-2.

Both, (2) and (3) should be straight forward to implement in a field application. All this is discussed in much more detail in Donner et al., 2019 which has been submitted and is currently under review (the reference has been updated accordingly). It is certainly true that option (1) requires the availability of a strong lamp but for a campaign such as CINDI-2, this was definitely a very valuable additional test and helped each of the groups to find out more about the accuracy of the elevation pointing of their instrument.

Page 8
Line 12 "we used" – until now the manuscript has been written using the traditional third person passive voice.

Agreed & this has been changed to the passive form.

Lines 25-38 There doesn't seem to be any mention of the type of location Cabauw is in terms of rural versus urban and the expected pollution levels.

Good point. We have added a short description of the Cabauw measurement site under Section 2:

"In short, the CESAR site at Cabauw is overall a rural site, with only a few pollution sources nearby, but the wider vicinity of Cabauw is densely populated, with the cities of Utrecht, Amsterdam, The Hague and Rotterdam less than 60 km away and a dense highway grid within 25 km, so that the site experiences recurring pollution events, e.g. such as from the daily morning and afternoon rush hours."

Page 9
Lines 18-19 Some of the instruments show a drift over the course of the campaign. Should we therefore expect instruments in the field also to show potentially significant drifts over time?

Possibly, and CINDI-2 really helped us to appreciate how important it is for the measurement quality to verify the accuracy and stability of the elevation scans. This also means that in the field, it is important to regularly monitor the accuracy of the elevation scans to avoid any drift, bias or discontinuity in data series, hence we made a recommendation to this end (2nd paragraph on conclusions).

Lines 35-38 The decision to allow resubmissions is also interesting – I assume the justification is that these types of mistakes would be able to be identified and corrected independently by the instrument operator in a network setting?

Yes, that is correct. For a resubmission, the groups had to state clearly what mistakes they made and how they were remedied. Admittedly, in a real word situation (e.g. due to time constraints) we might not always look carefully enough at our data sets but if we would, we should be able to identify and correct the issues which were identified.

Page 10
Lines 6-14 This seems to create a problem though, because in the field, this would not generally be possible?

We don't quite understand why this is a problem. We don't mean to imply that everything we applied during the intercomparison has to be 100% reproducible in a field situation and we think it is ok that

we create somewhat more idealized conditions which show us how well we can agree if we pay attention and get everything is right as possible.

Page 11
Line 25 -"drastically reduced" – that would depend on the temporal and spatial variability though?

Good point. We have toned the text down somewhat and changed ‘drastically’ into ‘considerably’ and changed ‘should accurately reflect’ to ‘should more accurately reflect’

Line 26 "and/or atmospheric variability" – I don’t understand what you mean here. The sentence seems to contradict itself to me. The sampling and mis-match errors are only small or large relative to the spatial and temporal scale of atmospheric variability. If the comparison noise is caused by atmospheric variability then isn’t that a mismatch?

We agree with the reviewer and have deleted ‘and/or atmospheric variability’.

Line 33 "similar as performed" -> "similar to as performed" or "similar to those performed"

Done.

Page 12
Lines 22-30 The implication is that the fit residuals should represent a lower bound to the measurement uncertainty, but perhaps another sentence of justification is needed for this.

A statement to this effect has been added.

Line 30 – If the real NO2 is varying on short scales that in itself is not an error of the measurement, but it would affect the agreement with a given satellite pixel.

We agree and we expect that the scale of variability of NO_2 is much smaller than the scale of any NO_2 satellite measurement. The main issue is therefore to assess the representativeness of correlative measurements for comparison to satellite data.

Line 39 "keeps" should be "stays"

Done. We have changed it to ‘remains’.

Page 13
Lines 1-2 ". . . for this molecule most of the residual variance between good instruments can be explained by measurement noise" needs re-wording. I think I know what you mean but the words by themselves don’t make much sense.

We have reworded the sentence to ‘… for this molecule most of the residual variance from regressions involving good instruments can be explained by instrument shot noise.’

Line 9 Replace "a couple" by "two".

Done.

Line 19 Replace "largest" with "the largest"

Done.

Lines 18-21 This must be very relevant for field instruments?

Yes, we agree. This is already covered under Section 3.4 so we didn’t want to repeat it here again.

Line 30 ". . . specific limits have been set. . ." You should add something like ". . . specific limits have been set to use for performance evaluation". The way it is now, it takes the reader some time to work out what these limits are all about.

Done.

Lines 28-37
Intuitively, I don't find this approach very reasonable. It seems you choose limits somewhat arbitrarily (or at least let's say making use of subjective judgement), and then go through a binary pass or fail evaluation. Especially in figure 19, some of the dots which pass seem to be right on the limit, and some of the failed points fall only just outside it. I appreciate for network use such as NDACC there might need to be a definite threshold, but otherwise the use of pass/fail seems to degrade the information you have gained through the experiment. Perhaps you could discuss this point briefly.

We agree that this is not straight forward and a bit of a delicate issue as well. Even though we tried to introduce some elements of objectivity, the choice of a limit is fundamentally arbitrary (but not totally subjective since it is based on statistical arguments). Since the limits were chosen to exceed the median of the measurements (this has now also been added to Figure 18 and in the text), instruments that exceed them can be seen as "out of the norm". This does not necessarily mean that such measurements are problematic and this is why we are checking several parameters. Failing in one parameter, especially if very close to the limit is not a problem per se but failing in two or more usually is.

Page 14
Line 1 "statistic" should be "statistics" if I've understood the sentence correctly.

Done.

Lines 11-17 Just repeating an earlier comment, the use of green versus orange when the two instruments could be a distance of epsilon other side of an arbitrary line seems odd to me. The use of pink for being four times outside the limit makes more sense.

See discussion above.

Lines 37-38 I thought the DOAS settings were all prescribed?

This sentence has been deleted, AIOFM have made a mistake and chose the wrong ozone cross-section. They have re-analysed their data with the correct ozone cross-section and we have updated the figures correspondingly. This did affect Figures 13, 18, 20 and 22, and Fig-S22, Fig-S23 and Fig-S24 from the Supplement, and some text in Appendix B.

Page 15
Line 8 "wavelengths" should be "wavelength"

Done.

Line 9 A better wording might be "and only failed to satisfy one criterion in the O4 .."

Done.

Lines 8-10 I suggest breaking this sentence into two parts for easier comprehension.

Done.

Lines 23-24 I suggest replacing "at the same time they are meeting" with "at the same time meet"

Done.

Line 24 Replace "On the opposite" with a phrase such as "On the other hand" or "Conversely".

Done.

Line 25 "satisfies" should be "satisfy"

Done.

Page 16
Line 1 ". . . a reduction in of the atmospheric changes on the intercomparison exercise." A reduction compared to what? (CINDI-1 I assume).

We agree that this needs to be fixed and have added to the sentence so it reads: '… atmospheric changes on the intercomparison exercise in comparison to CINDI.'

Line 4 "very well coordinated" sounds like boasting to me!

Fair enough and we have dropped this phrase.

Line 14 ". . . with a selected reference" seems misleading to me, because it implies a specified reference instrument, which was not part of the intercomparison.

We agree and have changed the text accordingly: '… with a reference data set was performed (see Section 3.5 for details on how the reference data sets were derived) …'

Lines 23-25 "The median bias against the reference is generally low . . .". Again I think this might mislead the reader who hasn't read the whole paper, who would assume there was a particular reference instrument.

To clarify this, we have replaced '… the reference…' with '… the reference data sets …'

Line 30 Replace "&" (ampersand symbol) with the word "and".

Done.

Line 33 Personally, I don't think you can say "guideline" in the singular like this, but others might disagree.

Agreed and changed.

Line 34 Replace "like the one" with "such as the one".

The sentence has been changed and the phrase has been dropped.

Page 17
Line 4 "instruments" should have an apostrophe - "instruments' " or re-word to "the elevation point calibration of instruments".

Done.

Lines 7-8 "a thoroughly planned and carefully managed campaign" sounds like boasting to me.

Fair enough and this has been toned down in the text and this sentence has been moved to the new Section 5 (Recommendations …).

Lines 18-26 This sounds really good and would be very valuable to the community.

The feedback is much appreciated and this will clearly be considered in the design of the next UV/Vis intercomparison. This has now also been moved into Section 5.

Page 32 (Figure 3)
The individual plots are very small but adequate for qualitative use of the figure.

That was the intention. If ok with the reviewer, we would prefer to leave the plot as is.

Page 40 (Figure 11)
Delete the unwanted carriage return in the caption.

Done.

Page 46 (Figure 17)
"The dashed lines indicate the limits . . . " For the caption, you need to provide more information, in particular that these limits have been chosen (rather than derived), for the sake of distinguishing outliers.

Done.

Page 49 (Figure 20)
In my printed version of the manuscript I find the pink and orange a little bit hard to distinguish. (The green and orange have excellent contrast.)

Good point, we have fixed this by replacing pink with black.

Page 51 (Figure 22)
The numbers in the green boxes are quite hard to read, and also to some extent those in the red and orange boxes.

We agree and have fixed this figure so that the numbers are much clearer to see.

Response to Anonymous Referee #2

We would like to thank the reviewer for their thorough review and helpful comments which are addressed individually in the response below. The reviewer's comments are included in blue and italics.

This manuscript is a well written and extensive intercomparison between UV-Visible spectrometers during a field study with a highly refined strategy. The work demonstrates very good agreement between slant column densities of the gases mentioned in the title during the campaign. These efforts are necessary for understanding agreement between instruments and for use in subsequent profile retrievals and satellite validation. The work is clearly relevant to Atmospheric Measurement Techniques and I recommend that it be published with minor revisions. Below are general and then specific comments.

General comment:
The manuscript goes through extensive procedures that were designed to synchronize measurements to be of the same volume of air at the same time. This synchronization has been improved as compared to the prior campaign, and results are improved. This result indicates that there are significant variations in the actual slant column densities at the same elevation angles if viewed at even slightly different times. The result is not surprising for short-lived pollution gases that probably have a variety of nearby sources, but it indicates that subsequent inversions to vertical concentration profiles and vertical column densities may have challenges due to variations in the vertical concentration profile that occur during the measurement profile. This point is discussed on page 12, lines 21-31, but is not given as much importance as is necessary for this finding.

To emphasis this finding further, we have added a brief summary of what has been discussed in Section 3.7 (former page 12, lines 21-31) to the conclusions as part of the 1. bullet point.

On the other hand, it seems that this point may be the origin of the "conclusion" on lines 13-14 of page 17 that the design "was not fully adequate for profile inversion experiments". This conclusion should be removed or reworded because the present work does not show inversion experiments and thus cannot conclude on them. If the point was meant to be that variability in space and time is observed, then that is a conclusion. Please make clear both the important point of variability in time and space and discuss relevance for inversions, but do not conclude about inversions that are not shown here.

We have changed the sentence as suggested and added more discussion to this first bullet point (partly also covered by the response to the comment above).

Specific comments:
Page 3, line 34. It should be discussed here that when the instruments that measure profiles sequentially at un-synchronized field studies (as they will typically be used after CINDI-2) that the variability during the profile will affect profile inversions. Potentially the Boesch et al. (2018) AMT paper could be cited.

This is an important point and one of the CINDI-2 companion papers on profile retrievals, 'Intercomparison of MAX-DOAS vertical profile retrieval algorithms: studies on field data from the CINDI-2 campaign' by Tirpitz et al. (see also entry in the reference list) which has just been submitted to AMT, would be the more appropriate publication for this discussion. A brief discussion has also been added in Section 5, 1. bullet point under 'Despite these achievements, a few critical points were identified that deserve more attention in future deployments.'

Page 4, line 24. The Apituley et al. manuscript to be submitted to AMT is really important to the present publication. Is this manuscript submitted? If it is not submitted by the time of this manuscript being decided upon, details should be added here.

Since Apituley et al. is not yet submitted, we have added some information re the measurement site (CESAR) and the CINDI-2 campaign in general:

'In short, the CESAR site at Cabauw is overall a rural site, with only a few pollution sources nearby, but the wider vicinity of Cabauw is densely populated, with the cities of Utrecht, Amsterdam, The Hague and Rotterdam less than 60 km away and a dense highway grid within 25 km, so that the site experiences recurring pollution events, e.g. such as from the daily morning and afternoon rush hours.

The MAX-DOAS instruments were also complemented with a suite of in-situ, profiling and mobile observations which are described in detail by Apituley et al. (to be submitted to AMT, 2019). In particular, a long-path DOAS measuring near surface mixing ratios of NO_2 and HCHO but also a range of other species such as HONO and SO_2 (see e.g. Merten et al, 2011, for a description of the technique) was operated at the CESAR site for the period of the campaign. Several mobile MAX-DOAS measurements were also made around Cabauw, and between Rotterdam and Utrecht (e.g. Merlaud, 2013). in addition to the static ones. NO_2 profiles were measured with NO_2 sondes (Sluis et al, 2010) and lidar (e.g. Volten et al., 2009), as well as through in-situ observations using the Cabauw meteorological tower. Extensive aerosol information was also gathered using Raman aerosol lidar and in situ samplers.'

Page 5, lines 9-10. The suggestion for future studies should be in the discussion rather than here. Potentially giving an indication to "see section N.M" would be appropriate.

We agree and since this suggestion is also discussed as part of the previous Conclusions section, now part of the newly added Section 5 (Recommendations for network operation and future campaigns), at the end (2nd bullet point), we have deleted this sentence.

Page 6, line 31. Please give the approximate solar zenith angles of these UTC cutoffs so that they can be more easily translated to other work.

This information has been added.

Page 7, line 14. The text says "atmospheric noise", but this effect is not noise but variability given later analysis. Reword.

This has been reworded as suggested.

Page 10, lines 23-29. It may be appropriate to note that retrievals using a zenith reference spectrum within the same elevation sequence (rather than a fixed noon reference) often reduces difficulty in fitting, and thus more instruments could get useful HCHO data if other analysis methods were used.

We agree with the reviewer that using a sequential reference spectrum can potentially reduce instrumental effects, or the impact of misfits to strong absorbers like O_3. However, this has not really been true for CINDI-2 and the agreement seems worse, most likely because noise is added due to the fact that not all instruments are able to capture the sequential reference exactly in the same way.

Page 12, line 24. The word "noise" is used, but this effect is not noise, but rather "variability" due to viewing different airmasses (in time or space).

We have changed the wording from 'noise' to 'difference between the individual data sets'.

Page 12, line 39. Replace "keeps larger" with "remains larger".

Done.

Page 13, line 16. Change "dependency" to "dependence".

Done.

Figure 7 needs a color/symbol key

This has been added as requested.

Table A1. The reference to Vandaele et al. (1998) is not in the references. The paper that I believe is cited seems to indicate the spectrum is at 294K rather than 298K. Please clarify this citation and temperature. This citation and temperature occur in other appendices. Please assure that all sources are fully cited in these appendix tables.

We agree with the reviewer and have added the reference and corrected the citations.

Intercomparison of NO_2, O_4, O_3 and HCHO slant column measurements by MAX-DOAS and zenith-sky UV-Visible spectrometers during the CINDI-2 campaign

Karin Kreher[1], Michel Van Roozendael[2], Francois Hendrick[2], Arnoud Apituley[3], Ermioni Dimitropoulou[2], Udo Frieß[4], Andreas Richter[5], Thomas Wagner[6], Johannes Lampel[4,7], Nader Abuhassan[8,31], Li Ang[9,7], Monica Anguas[10,8], Alkis Bais[11,9], Nuria Benavent[10,8], Tim Bösch[5], Kristof Bognar[12,0], Alexander Borovski[13,1], Ilya Bruchkouski[14,2], Alexander Cede[18,15,3,31], Ka Lok Chan[16,4,26], Sebastian Donner[6], Theano Drosoglou[11,9], Caroline Fayt[2], Henning Finkenzeller[17,5], David Garcia-Nieto[10,8], Clio Gielen[2], Laura Gómez-Martín[18,22], Nan Hao[19,35], Bas Henzing[20], Jay R. Herman[8,31], Christian Hermans[2], Syedul Hoque[21,17], Hitoshi Irie[21,17], Junli Jin[22,18], Paul Johnston[23,19], Junaid Khayyam Butt[24,0], Fahim Khokhar[24,0], Theodore K. Koenig[17,5], Jonas Kuhn[4,6], Vinod Kumar[26,25,1], Johannes Lampel[4,33], Cheng Liu[21,6], Jianzhong Ma[22,18], Alexis Merlaud[2], Abhishek K. Mishra[25,1], Moritz Müller[15,3,27,32], Monica Navarro-Comas[18,22], Mareike Ostendorf[5], Andrea Pazmino[28,3], Enno Peters[5,29,30], Gaia Pinardi[2], Manuel Pinharanda[28,3], Ankie Piters[3], Ulrich Platt[4], Oleg Postylyakov[13,1], Cristina Prados-Roman[18,22], Olga Puentedura[18,22], Richard Querel[23,19], Alfonso Saiz-Lopez[10,8], Anja Schönhardt[5], Stefan F. Schreier[30,24], Andrée Seyler[5], Vinayak Sinha[25,1], Elena Spinei[8,25,31], Kimberly Strong[12,0], Frederik Tack[2], Xin Tian[9,7], Martin Tiefengraber[15,3,27,32], Jan-Lukas Tirpitz[4], Jeroen van Gent[2], Rainer Volkamer[17,5], Mihalis Vrekoussis[5,32,28,33,29], Shanshan Wang[10,8,34,27], Zhuoru Wang[35,26], Mark Wenig[16,4], Folkard Wittrock[5], Pinhua H. Xie[9,7], Jin Xu[9,7], Margarita Yela[18,22], Chengxin Zhang[21,6], Xiaoyi Zhao[12,0,3,64]

[1] BK Scientific, Mainz, Germany
[2] Royal Belgian Institute for Space Aeronomy, Brussels, Belgium
[3] Royal Netherlands Meteorological Institute, De Bilt, The Netherlands
[4] Institute of Environmental Physics, University of Heidelberg, Heidelberg, Germany
[5] Institute of Environmental Physics, University of Bremen, Bremen, Germany
[6] Max Planck Institute for Chemistry, Mainz, Germany
[7] Airyx GmbH, Justus-von-Liebig-Straße 14, 69214 Eppelheim, Germany
[8] NASA Goddard Space Flight Center, USA
[9] Anhui Institute of Optics and Fine Mechanics, Chinese Academy of Sciences, Hefei, China
[10] Department of Atmospheric Chemistry and Climate, Institute of Physical Chemistry Rocasolano, Madrid, Spain
[11] Laboratory of Atmospheric Physics, Aristotle University of Thessaloniki, Thessaloniki, Greece
[12] Department of Physics, University of Toronto, Toronto, Canada
[13] A. M. Obukhov Institute of Atmospheric Physics, Russian Academy of Sciences, Moscow, Russia
[14] Belarusian State University, Minsk, Belarus
[15] LuftBlick Earth Observation Technologies, Mutters, Austria
[16] Meteorologisches Institut, Ludwig-Maximilians-Universität München, Munich, Germany
[17] Department of Chemistry & Cooperative Institute for Research on Environmental Sciences (CIRES), University of Colorado, Boulder, USA
[18] National Institute for Aerospace Technology (INTA), Madrid, Spain
[19] European Organisation for the Exploitation of Meteorological Satellites (EUMETSAT), Darmstadt, Germany
[20] Netherlands Organisation for Applied Scientific Research (TNO), the Netherlands
[21] Center for Environmental Remote Sensing, Chiba University, Chiba, Japan
School of Earth and Space Sciences, University of Science and Technology of China, Hefei, Anhui, China
[17,22] Center for Environmental Remote Sensing, Chiba University, Chiba, Japan
[18] Meteorological Observation Center, China Meteorological Administration, Beijing, China &
Chinese Academy of Meteorological Science, China Meteorological Administration, Beijing, China
[23,19] National Institute of Water and Atmospheric Research, Lauder, New Zealand
[24,0] National University of Sciences and Technology, Islamabad, Pakistan
[25,1] Department of Earth and Environmental Sciences, Indian Institute of Science Education and Research Mohali, Punjab, India
[26,2] School of Earth and Space Sciences, University of Science and Technology of China, Hefei, Anhui, China
National Institute for Aerospace Technology (INTA), Madrid, Spain

Formatted: Not Highlight
Formatted: Not Highlight
Formatted: Not Highlight
Formatted: Left, Add space between paragraphs of the same style, Don't suppress line numbers
Formatted: Font: 10 pt, English (United Kingdom)
Formatted: Left, Don't adjust space between Latin and Asian text, Don't adjust space between Asian text and numbers

[2][3] Department of Atmospheric and Cryospheric Sciences, University of Innsbruck, Innsbruck, Austria
[28] Laboratoire Atmosphère, Milieux, Observations Spatiales, Université de Versailles Saint-Quentin-en-Yvelines, Centre National de la Recherche Scientifique, Guyancourt, France
[29][4] now at Institute for the Protection of Maritime Infrastructures, German Aerospace Center (DLR), Bremerhaven, Germany
[30] Institute of Meteorology, University of Natural Resources and Life Sciences, Vienna, Austria
[31][5] Virginia Polytechnic Institute and State University, Blacksburg, VA, USA
[32][6] Center of Marine Environmental Sciences (MARUM), University of Bremen, Bremen, Germany
[33][9] Energy, Environment and Water Research Center (EEWRC), The Cyprus Institute, Nicosia, Cyprus

~~Remote Sensing Technology Institute, German Aerospace Center (DLR), Oberpfaffenhofen, Germany~~
[34][7] Shanghai Key Laboratory of Atmospheric Particle Pollution and Prevention, Department of Environmental Science & Engineering, Fudan University, Shanghai, China
[35][8] Remote Sensing Technology Institute, German Aerospace Center (DLR), Oberpfaffenhofen, Germany
~~Center of Marine Environmental Sciences (MARUM), University of Bremen, Bremen, Germany~~
[29] ~~Energy, Environment and Water Research Center (EEWRC), The Cyprus Institute, Nicosia, Cyprus~~
[30] ~~now at Institute for the Protection of Maritime Infrastructures, German Aerospace Center (DLR), Bremerhaven, Germany~~
[31] ~~NASA Goddard Space Flight Center, USA~~
[32] ~~Department of Atmospheric and Cryospheric Sciences, University of Innsbruck, Innsbruck, Austria~~
[33] ~~Airyx GmbH, Justus-von-Liebig-Straße 14, 69214 Eppelheim, Germany~~
[3][4] now at Measurement and Analysis Research Section, Environment and Climate Change Canada, Toronto, M3H 5T4, Canada
[35] ~~European Organisation for the Exploitation of Meteorological Satellites (EUMETSAT), Darmstadt, Germany~~

Correspondence to: Karin Kreher (karin.kreher@bkscientific.eu)

Abstract. In September 2016, 36 spectrometers from 24 institutes measured a number of key atmospheric pollutants for a period of 17 days during the Second Cabauw Intercomparison campaign for Nitrogen Dioxide measuring Instruments (CINDI-2) that took place at Cabauw, The Netherlands (51.97° N, 4.93° E). We report on the outcome of the formal semi-blind intercomparison exercise, which was held under the umbrella of the Network for the Detection of Atmospheric Composition Change (NDACC) and the European Space Agency (ESA). The three major goals of CINDI-2 were (1) to characterise and better understand the differences between a large number of Multi-AXis Differential Optical Absorption Spectroscopy (MAX-DOAS) and zenith-sky DOAS instruments and analysis methods, ~~to discuss the performance of the various types of instruments~~ (2) to define a robust methodology for performance assessment of all participating instruments and (3) to contribute to a harmonisation of the measurement settings and retrieval methods. This, in turn, creates the capability to produce consistent high-quality ground-based data sets, which are an essential requirement to generate reliable long-term measurement time series suitable for trend analysis and satellite data validation.

The data products investigated during the semi-blind intercomparison are slant columns of nitrogen dioxide (NO_2), the oxygen collision complex~~dimer~~ (O_4) and ozone (O_3) measured in the UV and visible wavelength region, formaldehyde (HCHO) in the UV spectral region and NO_2 in an additional (smaller) wavelength range in the visible. The campaign design and implementation processes are discussed in detail including the measurement protocol, calibration procedures and slant column retrieval settings.

Formatted: Add space between paragraphs of the same style, Adjust space between Latin and Asian text, Adjust space between Asian text and numbers, Tab stops: 1.62 cm, Left + 3.23 cm, Left + 4.85 cm, Left + 6.46 cm, Left + 8.08 cm, Left + 9.69 cm, Left + 11.31 cm, Left + 12.92 cm, Left + 14.54 cm, Left + 16.16 cm, Left + 17.77 cm, Left + 19.39 cm, Left + 21 cm, Left + 22.62 cm, Left + 24.23 cm, Left + 25.85 cm, Left

Formatted: Don't add space between paragraphs of the same style, Don't adjust space between Latin and Asian text, Don't adjust space between Asian text and numbers, Tab stops: Not at 1.62 cm + 3.23 cm + 4.85 cm + 6.46 cm + 8.08 cm + 9.69 cm + 11.31 cm + 12.92 cm + 14.54 cm + 16.16 cm + 17.77 cm + 19.39 cm + 21 cm + 22.62 cm + 24.23 cm + 25.85 cm

Formatted: Normal

Formatted: Not Highlight

Formatted: Not Highlight

Strong emphasis was put on the careful alignment and synchronisation of the measurement systems, resulting in a unique ~~a unprecedented~~ set of measurements made under highly comparable air mass conditions.

The CINDI-2 data sets were investigated using a regression analysis of the slant columns measured by each instrument and for each of the target data products. The slope and intercept of the regression analysis respectively quantify the mean systematic bias and offset of the individual data sets against the selected reference (which is obtained from the median of either all data sets or a subset), and the RMS error provides an estimate of the measurement noise or dispersion. These three criteria are examined and for each of the parameters and each of the data products, performance thresholds are set and applied to all the measurements. The approach presented here has been developed based on heritage from previous intercomparison exercises. It introduces a quantitative assessment of the ~~measurement performance of~~ consistency between all the participating instruments for the MAX-DOAS and zenith-sky DOAS techniques.

1 Introduction

Passive UV-visible spectroscopy using scattered sunlight as a light source provides one of the most effective methods for routine remote sensing of atmospheric trace gases from the ground. While zenith-sky observations have been used for several decades to monitor stratospheric gases such as NO_2, O_3, BrO and OClO (e.g. Noxon, 1975; Platt et al., 1979; Solomon et al., 1987; Pommereau and Goutail, 1988; Richter et al., 1999; Liley et al., 2000; Hendrick et al., 2011, Yela et al., 2017), measurements scanning the sky vertically at several elevation angles between horizon and zenith have been established more recently. In addition to total columns, the so-called MAX-DOAS (Multi-Axis Differential Optical Absorption Spectroscopy; Hönninger et al., 2004) technique also allows the derivation of vertically resolved information on a number of tropospheric species such as NO_2, HCHO, BrO, glyoxal, IO, HONO, SO_2, etc. (see e.g. Hönninger and Platt, 2002; Wittrock et al., 2004; Heckel et al., 2005; Lee et al., 2008, 2009; Sinreich et al., 2010; Frieß et al., 2011; Hendrick et al., 2014, Prados-Roman et al., 2018) as well as aerosols (see e.g. Wagner et al., 2004; Frieß et al., 2006; Clémer et al., 2010, Ortega et al., 2016). The number of MAX-DOAS instruments used worldwide has grown considerably in recent years notably in support of satellite validation (e.g. Wang et al., 2017a; Herman et al., 2018) and for urban pollution studies (e.g. Gratsea et al., 2016; Wang et al., 2017b) and this increase in deployment of MAX-DOAS instrumentation for tropospheric observations, together with the diversity of the designs and operation protocols, has created the need for regular formal intercomparisons which should include as many different instruments as possible.

In 2005 and 2006, two field campaigns were held at Cabauw, The Netherlands, involving MAX-DOAS instruments as part of DANDELIONS (Dutch Aerosol and Nitrogen Dioxide Experiments for vaLIdation of OMI and SCIAMACHY). This project was dedicated to the validation of satellite NO_2 measurements by the Ozone Monitoring Instrument (OMI) and SCIAMACHY (Scanning Imaging Absorption SpectroMeter for Atmospheric CartographY) and aerosol measurements by OMI and the Advanced Along-Track Scanning Radiometer (AATSR) (Brinksma et al., 2008). This was followed by the first Cabauw Intercomparison campaign for Nitrogen Dioxide measuring Instruments (CINDI) which was organised in 2009 under the auspices of the European Space Agency (ESA), the Network for the Detection of Atmospheric Composition Change (NDACC) and the European Union (EU) FP6 Global Earth Observation and MONitoring (GEOMON) project. This effort resulted in the first successful large-scale intercomparison of both MAX-DOAS and zenith-sky ground-based remote sensors of NO_2 and O_4 slant columns (Roscoe et al., 2010). Datasets of NO_2, aerosols and other air pollution components observed during CINDI were documented in a number of peer-reviewed articles (Piters et al., 2012; Roscoe et al., 2010; Pinardi et al., 2013; Zieger et al., 2011; Irie et al., 2011 and Frieß et al., 2016), providing an assessment of the performance of ground-based remote sensing instruments for the observation of NO_2, HCHO and aerosol. Recommendations were issued regarding the operation and calibration of the instruments, the retrieval settings, and the

observation strategies for use in ground-based networks for air quality monitoring and satellite data validation. Several important findings were highlighted in view of preparing future campaigns, in particular (1) the need for accurate calibration and monitoring of the elevation angle of MAX-DOAS scanners and (2) for intercomparison purposes, the importance of synchronising measurements in time and space very accurately. The lack of such a synchronisation was indeed considered as being responsible for a large part of the scatter observed during CINDI (Roscoe et al., 2010), which limited the interpretation of the results.

Seven years after CINDI, a second campaign (CINDI-2) was undertaken at the same site (Cabauw Experimental Site for Atmospheric Research - CESAR) from 25 August until 7 October 2016. Its goal was to intercompare the new and extended generation of ground-based remote-sensing and in-situ air quality instruments. The interest of ESA ~~for~~ in such intercalibration activities is motivated by the ongoing development of several UV-visible space missions targeting air quality monitoring such as the Copernicus Sentinel 5 Precursor (S-5P) satellite launched in October 2017 and the future Copernicus Sentinel 4 and 5 satellites.~~planned at the horizon 2022-2023.~~ The validation and ongoing support of measurements from such space missions is essential and requires dedicated ground-truth measurement systems. Because tropospheric measurements from space-borne nadir UV-visible sensors show little or no vertical discrimination and inherently provide measurements of the total tropospheric amount, surface in-situ measurements are generally unsuitable for such a validation effort. Instead, validation requires a technique that can deliver column-integrated and vertically resolved information on the key tropospheric species measured by satellite instruments such as NO_2, HCHO and SO_2 with a horizontal representativeness compatible with the resolution of space measurements (e.g. 3.5x7 km^2 for S-5P).

Hence, the specific goals of CINDI-2 were to support the creation of high-quality ground-based data sets as needed for long-term measurements, trend analysis and satellite data validation. To achieve this, it is essential to characterise ~~and better understand~~ the differences between a large number of MAX-DOAS and zenith-sky DOAS instruments and analysis methods~~, and to contribute to a harmonisation of the measurement settings and retrieval methods.~~ and to assess the participating instruments in their ability to retrieve the same geophysical quantities (i.e. slant columns of NO_2, O_4, HCHO and O_3) when measured and processed in a controlled way (i.e. using a prescribed measurement protocol and retrieval settings). The design of the CINDI-2 campaign and the development of the measurement protocol, adhered to specifically during the official intercomparison phase, was based on the experience gained during the first CINDI campaign in 2009 as well as more recent projects and campaigns such as the MAD-CAT campaign in Mainz, Germany, in 2013 (e.g. Peters et al., 2017).

This paper is organized as follows. In Section 2, the campaign design is discussed including an overview of the participating groups and their instruments, and a discussion of the measurement protocol details. In Section 3, the results of the semi-blind slant column intercomparison are presented, and in Section 4, a systematic approach is proposed to quantitatively assess the performance of the participating instruments for the different target trace gas data products. Section 5 provides recommendations for observation networks and future intercomparison campaigns and Section 6 summarizes the campaign outcomes ~~and provides recommendations for future intercomparison campaigns~~.

2 Intercomparison campaign design and measurement protocol

The CESAR site was accessible for the installation of the instruments from 25 August 2016 onwards, with the formal semi-blind intercomparison being held for 17 days from 12 – 28 September 2016. Here, we concentrate on this official intercomparison phase of the CINDI-2 campaign, and measurements and results are discussed for this time period only. A general description of the overall campaign including a more detailed discussion of the CESAR site and all ancillary measurements can be found in Apituley et al.

Formatted: Not Highlight
Formatted: Not Highlight
Formatted: Subscript, Not Highlight
Formatted: Not Highlight
Formatted: Subscript, Not Highlight
Formatted: Not Highlight
Formatted: Subscript, Not Highlight
Formatted: Not Highlight
Formatted: Not Highlight
Formatted: Not Highlight
Formatted: Not Highlight
Formatted: Not Highlight
Formatted: Not Highlight

(to be submitted to AMT, 202019). In short, the CESAR site at Cabauw is overall a rural site, with only a few pollution sources nearby, but the wider vicinity of Cabauw is densely populated, with the cities of Utrecht, Amsterdam, The Hague and Rotterdam less than 60 km away and a dense highway grid within 25 km, so that the site experiences recurring pollution events, e.g. such as from the daily morning and afternoon rush hours.

2.1 **The MAX-DOAS instruments were also complemented with a suite of in-situ, profiling and mobile observations which are described in detail by Apituley et al. (to be submitted to AMT, 2020). In particular, a long-path DOAS measuring near surface mixing ratios of NO_2 and HCHO but also a range of other species such as HONO and SO_2 (see e.g. Merten et al, 2011, for a description of the technique) was operated at the CESAR site for the period of the campaign. Several mobile MAX-DOAS measurements were also made around Cabauw, and between Rotterdam and Utrecht (e.g. Merlaud, 2013) in addition to the static observations. NO_2 profiles were measured with NO_2 sondes (Sluis et al, 2010) and lidar (e.g. Volten et al., 2009), as well as through in-situ observations using the Cabauw meteorological tower. Extensive aerosol information was also gathered using Raman aerosol lidar and in situ samplers.**

2.22.1 Instruments

Table 1Table 1 lists the groups and instruments that were included in the CINDI-2 semi-blind intercomparison, and an overview of the relevant instrumental details is given in Table 2Table 2. Among the 36 participating instruments, 17 were two-dimensional (2D) MAX-DOAS systems allowing for scans in both elevation and azimuth, 16 were one-dimensional (1D) MAX-DOAS systems performing elevation scans in one fixed azimuthal direction, one was an imaging DOAS instrument (Imaging MaPper for Atmospheric observaTions - IMPACT, Peters et al., submitted 2019) for which only measurements in the common viewing direction were submitted, and the last two instruments were zenith-sky DOAS systems of the SAOZ (Système d'Analyse par Observation Zénithale) (Pommereau and Goutail, 1988) and most recent Mini SAOZ version. The complete technical specifications for each instrument can be found in Section 3 of the Supplement.

Instruments have been sorted into different categories. Custom-built systems refer to instruments developed by scientific organisations for their own research activities. Other categories denote commercial systems of various types. Pandora instruments (Herman et al., 2009) are being developed at NASA/LuftBlick, commercialised by the SciGlob company and deployed as part of the Pandonia Global Network (PGN) (http://pandonia.net/). EnviMes[1] MAX-DOAS instruments (Lampel et al., 2015) have been recently commercialised based on expertise developed at the University of Heidelberg. Mini-DOAS instruments (e.g. Hönninger et al., 2004; Bobrowski, 2005) are produced in Germany by Hoffmann GmbH (http://www.hmm.de/).

No particular guidelines were given concerning the spectral calibration of instruments, which means that participating groups were free to apply calibration steps of various levels of complexity. In addition to standard calibration procedures involving dark current and electronic offset corrections, wavelength registration and slit function determination, some groups performed more advanced pre-processing steps such as radiometric calibration, stray-light and interpixel variability correction or an explicit correction for detector response non-linearity, the latter being a known feature of Avantes spectrometers. For future campaigns, it might be useful to standardise calibration procedures in order to better control the impact of possible instrumental effects on intercomparison results.

[1] Now: SkySpec from Airyx GmbH (www.airyx.de)

Formatted: Font: 10 pt
Formatted: Font: 10 pt
Formatted: Font: 10 pt
Formatted: Font: 10 pt
Formatted: Subscript
Formatted: Subscript
Formatted: Font: (Default) Times New Roman, English (United Kingdom)
Formatted: Font: (Default) Times New Roman, English (United Kingdom)
Formatted: Font: (Default) Times New Roman, English (United Kingdom)
Formatted: Font: (Default) Times New Roman, English (United Kingdom)
Formatted: Font: (Default) Times New Roman, 10 pt, English (United Kingdom), Subscript
Formatted: Font: (Default) Times New Roman, English (United Kingdom)
Formatted: Font: (Default) Times New Roman, English (United Kingdom)
Formatted: Font: (Default) Times New Roman, 10 pt, English (United Kingdom), Subscript
Formatted: Font: (Default) Times New Roman, 10 pt, English (United Kingdom)
Formatted: Font: (Default) Times New Roman, English (United Kingdom)
Formatted: Font: (Default) Times New Roman, English (United Kingdom)
Formatted: Font: (Default) Times New Roman, English (United Kingdom)
Formatted: Font: (Default) Times New Roman, English (United Kingdom)
Formatted: Font: (Default) Times New Roman, English (United Kingdom)
Formatted: Font: (Default) Times New Roman, English (United Kingdom)
Formatted: Font: 12 pt
Formatted: Font: 10 pt
Formatted: Font: 10 pt

2.32.2 Campaign design

To allow for optimal synchronisation of the measurements, all the spectrometers participating in the semi-blind intercomparison exercise were installed in close proximity to each other on the remote-sensing site (RSS) of the CESAR station (see Figure 1Figure 1 and Apituley et al., to be submitted to AMT, 202019). To achieve this, temporary mobile units (similar to shipping containers) were rented. temporarily installed for the campaign period.

The rationale behind this setup was to arrange the instruments in such a way to minimise ambiguity in air masses observed simultaneouslythat the same air masses could be sampled by all spectrometers at the same time. This is essential for tropospheric NO_2 but also for aerosol and HCHO, since all these species can feature rapidly changing concentrations in both space and time. Considering the large number of systems that needed to be accommodated, two rows of containers were deployed with the bottom row being similar to the one deployed during the previous CINDI campaign. This bottom row of containers was predominantly used to host the 1D MAX-DOAS instruments and the two zenith-sky systems. A second row of containers was deployed on top of the first one, with the stacked double-containers providing additional height. All 2D MAX-DOAS systems were installed on the roof of the top-level containers allowing for more flexibility on the azimuth scan settings and avoiding any risk of interference with the 1D systems. All the 1D MAX-DOAS instruments used the same azimuth viewing direction of 287° (i.e. approximately WNW, with North (N) being 0°N=0 and East (E) 90° etc.) which was already used during the first CINDI campaign since it provided an unobstructed view to the horizon. This direction was also one of the azimuth directions used by the 2D MAX-DOAS systems (see also discussion of the measurement protocol in Section 2.4).

In Sections 2.4 – 2.6, further procedures aiding the comparability of the MAX-DOAS measurements such as the overall measurement protocol, elevation angle calibrations and slant column retrieval settings are discussed in more detail. Prescribing these procedures as strictly as possible was highlighted during previous campaigns as important (see in particular Roscoe et al., 2010) and the campaign design of CINDI-2 focused on implementing such recommendations.

2.42.3 Semi-blind intercomparison

AsI like in previous intercomparison campaigns of the same type (see e.g. Vandaele et al., 2005; and Roscoe et al., 1999, 2010), a semi-blind intercomparison protocol was adopted. The CINDI-2 intercomparison exercise had two three key objectives: (1) To characterise the differences between a large number of measurement systems and approaches, and (2) to to discuss the performance of the various types of instrument and define a robust methodology for performance assessment of all participating instruments and (3) to provide guidelines to further harmonise the measurement settings and analysis methods. The adopted semi-blind intercomparison protocol was based on the following approach:

a) The data acquisition schedule applied by the participants was strictly prescribed to coordinate the timing and geometry of each individual measurement as exactly as possible, so that the same air mass could be measured by all instruments with good synchronisation.

b) For each data product, a set of retrieval settings and parameters was prescribed (see Appendix A). These were mandatory for participation in the semi-blind exercise. The data analysis software, however, was not prescribed and the different software types used by each institute are listed in Table 3Table 3.

c) All slant column data sets measured during the previous day were submitted to an independent campaign referee (K. Kreher) and her assistant (E. Dimitropoulou) every morning by 10:00 local time. At daily meetings in the afternoon (usually at 16:00), the results of the slant column comparison for measurements from the previous day were displayed anonymously,

Formatted: Font: 10 pt

Formatted: Not Highlight

Formatted: Not Highlight

Formatted: Not Highlight

Formatted: Not Highlight

Formatted: Font: 10 pt

i.e. without any assignment to the different instruments. Basic analysis plots exploring the differences in the data sets measured during the previous days were shown and discussed.

d) The referee notified instrument representatives if there was an obvious problem with their submitted data set so that this issue could be addressed and, if possible, corrected for the remainder of the campaign.

e) After the formal campaign had finished, all participants had about three weeks to undertake the analysis according to the prescribed measurement and analysis protocol (see Section 2.4), and the final slant column data sets had to be submitted by 18 October 2016. After this date, any resubmissions were only accepted if the group could clearly state the reasons why the data set needed to be updated, e.g. if an error was found in the analysis and needed to be remedied. Further details on this process are given in Section 3.3 and Appendix B.

The semi-blind intercomparison exercise focused on a limited number of key data products of direct relevance for satellite validation and NDACC operational continuity. These data products are listed in Table 4~~Table 4~~. Depending on the specific characteristics of their instrumentation, participants were free to submit~~contribute~~ all or only a subset of the data products.

Formatted: Font: 10 pt

~~2.5~~2.4 Measurement protocol

As discussed above, it was recognised in previous intercomparison campaigns (see in particular Roscoe et al., 2010) that the achievable level of agreement between MAX-DOAS sensors is often limited by imperfect co-location and a lack of synchronisation. This problem is especially critical for tropospheric NO_2 comparisons, because of the large variability of this pollutant on very small scales. However, it is also relevant for other gases such as HCHO, O_4, SO_2, glyoxal, etc. For this reason, it was decided to co-locate all the MAX-DOAS instruments on the same observation platform (see Section 2.2) and additionally to impose a strict protocol on the timing of the spectral acquisition.

The baseline for all MAX-DOAS instruments was to point towards a fixed azimuth direction (287°~~, i.e. west-north-westerly~~) throughout the day. This direction was chosen because of the very close to obstruction-free line of sight towards the horizon. In addition, the 2D MAX-DOAS instruments performed azimuthal scans simultaneously according to a strict measurement schedule. ~~The convention for the azimuth angle is 0° for North, 90° for East, etc.~~ The scheme described below was designed to ensure the maximum of synchronisation~~city~~ between the same type of instruments (e.g. azimuthal scans by 2D MAX-DOAS) but also between the different types of instruments (1D and 2D MAX-DOAS, and zenith-sky DOAS). A distinction was made between twilight (morning and evening) and daytime conditions, for which separate data acquisition protocols were prescribed. According to the geometry of the solar position during the campaign, the daytime period (excluding twilight) was defined to be from 6:00 to 16:45 UTC~~.~~ with 6:00 UTC corresponding to an SZA of approximately 83° - 87° and 16:45 UTC to an SZA of approximately 76° - 82°, depending on the exact date during the campaign.

To allow for an NDACC-type intercomparison of stratospheric measurements (e.g. Vandaele et al., 2005), zenith-sky twilight observations were also performed. The acquisition scheme for the dawn observations prescribed 39 measurements with a duration of 3 min each (integration time: 170s; overhead time: 10s), starting at 04:00:00 UTC and ending at 05:57:00 UTC. This sequence was followed by a 180s (3 min) interval allowing for a transition to the MAX-DOAS mode of which the first scans started at 06:00:00 UTC. For measurements at dusk, 40 acquisitions were recorded with a duration of 180s each starting at 16:45:00 UTC and ending at 18:45:00 UTC.

During daytime, the acquisition scheme for MAX-DOAS and zenith-sky systems included four sequences of 15 minutes per hourly slot starting at 06:00:00 UTC. Individual acquisitions (at one given angle) were set to one-minute-long in all cases. For 1D systems, the pointing azimuth direction was set to 287° with elevation angles of 1, 2, 3, 4, 5, 6, 8, 15, 30 and 90°. For 2D systems, the azimuth

angles 45, 95, 135, 195, 245 and 355° were successively sampled in addition to the reference angle of 287°. In each azimuthal direction, four elevation angles (1, 3, 5, 15°) were scanned except for the reference azimuth of 287° where the same elevations as prescribed for the 1D MAX-DOAS systems were used. One zenith reference spectrum was recorded every 15 minutes, and for 2D systems or instruments equipped with a sun tracker, almucantar scans and/or direct-sun measurements were performed between the 10th and 15th minute of the sequence. For zenith-sky instruments, one-minute-long acquisitions were performed during the whole day from 06:00.00 UTC to 16:44:00 UTC.

Figure 2~~Figure 2~~ (upper plot) provides an overview of the number of days each instrument was on duty during the intercomparison period. It also illustrates (lower plot) the accuracy with which the different groups were able to match the imposed measurement protocol. As can be seen, the instruments were in operation most of the time during the 17 days of the semi-blind period and most of them were able to follow the schedule to better than one minute. In comparison to past campaigns, the~~is~~ ~~unprecedented~~ level of synchronisation~~city~~ was clearly improved which significantly reduced the need for smoothing or interpolating data in time ~~(see Section 3.7)~~. As a result, the impact of the atmospheric variability~~noise~~ on the data comparisons could be reduced ~~to a minimum.~~considerably, but not completely eliminated (see Section 3.7).

As discussed above, the measurement procedure was strict but in spite of this comprehensive protocol, there was still some freedom left on how to implement details of the acquisitions. E.g. for managing the acquisition time, most groups decided to move the telescope and gather the spectra within the prescribed one minute time period, while INTA (inta-17) gathered spectra for one minute and then moved the telescope. As a result, a time shift was accumulated when compared to other groups (see Figure 2). Chiba-9 also shows a noticeable time shift due to constraints in the acquisition software that prevented the strict implementation of the protocol. In the case of niwa-30, the large time shift in the UV was due to instrument imposed alternating between measurements in the visible and UV wavelength regions (hence only one spectral range could be synchronised with the protocol).

Likewise, it must be noted that Pandora instruments also take separate measurements for the visible and the UV range, where a blocking filter is inserted in the optical path for the UV measurements in order to reduce spectral stray light. Therefore, a compromise had to be found in the time synchronization bracketing the requested measurement time. This is the reason for the systematic offsets for Pandoras in the bottom panel of Figure 2. Another consequence of this was that the total measurement time of Pandora instruments was about half the time of the other participating instruments, which affects the noise levels for Pandoras described throughout this paper to some extent.

~~2.6~~2.5 Calibration of the MAX-DOAS elevation scans

Because of the importance of the elevation pointing accuracy for MAX-DOAS measurements at low elevation and as recommended after the first CINDI intercomparison (Roscoe et al., 2010), different calibration tests involving all the participating instruments were undertaken during both the warm-up and semi-blind intercomparison phases. Three different approaches were used:

1) On several evenings, MPIC (Max Planck Institute for Chemistry) installed an Opel car 1999 xenon lamp with a 17 cm diameter lens at a distance of 1280 m from the measurement site (angular lamp extension ~0.008°) in the main viewing azimuth direction (287°) of the MAX-DOAS instruments. It served as a common light source at long distance, and MAX-DOAS instruments recorded downward and upward scan spectra pointing towards the lamp.
2) A white stripe on a black target at known elevation close to the instruments was scanned.
3) Intensities were measured regularly during horizon scans (see Section 3.2 for details).

Formatted: Font: 10 pt

Formatted: Font: Not Bold

Additional calibration measurements using a near-distance lamp placed a few meters away from instruments were also performed by IUP-Heidelberg and several other groups. Overall, these calibration procedures allowed the pointing accuracy of the different instruments and their stability during the campaign to be fully characterized (see Donner et al., ~~to be submitted to AMT,~~ in review, 2019). As such they played an important role for the interpretation of the semi-blind intercomparison results (see Section 3.7).

~~2.7~~2.6 Slant column retrieval settings

To minimise the sources of difference between measurements, a set of common retrieval settings and parameters was prescribed ahead of the campaign. The use of these settings was mandatory for participation in the semi-blind exercise. The detailed spectral retrieval settings imposed for each data product referenced in Table 1~~Table 1~~ are given in Appendix A. These settings were based on the NDACC protocol for UV-Vis measurements (http://www.ndaccdemo.org/data/protocols) as well as results from the first CINDI campaign (e.g. Pinardi et al., 2013), the MAD-CAT campaign (http://joseba.mpch-mainz.mpg.de/mad_analysis.htm) and the QA4ECV project (http://www.qa4ecv.eu/). Although not necessarily optimal, they represent a common baseline applicable to all data sets in a consistent way. Concerning the choice of the Fraunhofer reference spectrum, ~~we used~~ daily reference spectra obtained from the mean of all zenith-sky spectra acquired between 11:30:00 and 11:41:00 UTC were used. Slant columns retrieved against this reference spectrum are hereinafter referred to as differential slant column densities (dSCDs).

Formatted: Font: 10 pt

Note that additional retrievals were also performed using sequential reference spectra (zenith-sky observations taken close to the time of the respective horizon measurements). These data were, however, not included in the formal semi-blind intercomparison since they essentially lead to similar comparison results as the analyses using daily reference spectra. They were also not available from all groups. Moreover, the use of daily reference spectra presents the advantage of being directly applicable to twilight measurements and provides a better test of the instrumental stability over several hours of operation. As already noted in Section 2.1, the determination of the instrumental slit function and its eventual wavelength dependence was under the responsibility of the participating groups.

3 Semi-blind intercomparison results

3.1 Overview of slant column measurements and meteorological conditions

The meteorological conditions during CINDI-2 were exceptionally favourable for the location and season. The uppermost panel of Figure 3 shows the hourly sunshine duration and surface temperature records for the whole semi-blind intercomparison period (for more details, see Apituley et al., to be submitted to AMT, 20~~19~~). The first four days of the semi-blind phase were characterized by a clear sky with some haze in the morning and very high air temperatures for the season (>30°C), allowing for efficient formaldehyde production. The next seven days were cloudier with lower temperatures. The last six days of the semi-blind exercise were also characterized by mostly clear sky or occasionally broken cloud conditions.

All other panels of Figure 3 display the time variation of each of the dSCD data products included in the intercomparison, as measured by the IUP Bremen instrument, which had excellent data coverage throughout the campaign duration. Green lines represent zenith-sky measurements, red lines off-axis data at 30° elevation, and blue lines off-axis measurements up to 15° elevation. Results show a large variability of the NO_2, O_4 and HCHO tropospheric columns while ozone data display the expected regular diurnal pattern mainly due to the variation of the stratospheric light path during the ascent and descent of the sun. Due to the unusually favourable weather conditions, higher than expected values were observed for tropospheric HCHO while tropospheric NO_2 was at its lowest during the first Sunday (18 September) of the intercomparison campaign. The variability of the tropospheric trace gas content and the exceptionally large number of clear-sky sunny conditions were ideal for comparison purposes.

3.2 Horizon scans

Horizon scans, which consist of measuring the change in intensity when scanning the sky radiance across the horizon line, were systematically performed every day at noon during the semi-blind intercomparison period. Although difficult to calibrate absolutely because the horizon is generally not free of obstacles (e.g. trees, buildings or terrain height fluctuations), they provide a simple and valuable technique for monitoring the elevation pointing stability of MAX-DOAS instruments. Figure 4~~Figure 4~~ shows an example of the variation of the intensity at 440 nm, as reported by the IUP-Bremen instrument (blue circles). Considering that the intensity measured as a function of the elevation angle yields the integral over the telescope's point spread function, measurements were fitted using an error function (Gaussian integral) according to equation 1:

$$S = A\left[erf\left(\frac{x-x_0}{B}\right)+1\right] + C(x-x_0) + D \qquad \text{Eq. (1)}$$

where x is the elevation angle, and A, B, C and D are fitting parameters. The centre (x_0), also fitted, provides a measure of the horizon elevation.

The analytic derivative of equation 1 is a Gaussian curve of which the full width at half maximum (FWHM) is given by:

$$FWHM = 2\sqrt{\ln(2)}\,B \qquad \text{Eq. (2)}$$

We used this quantity to estimate the effective field of view (FOV) of the instrument (see Figure 4~~Figure 4~~, red line).

Applying this fitting methodology, horizon scans delivered daily by each group were systematically analysed. Figure 5 presents an overview of the time evolution of the horizon elevation derived from each instrument (and their median values represented by red lines), all of them being measured in the visible wavelength range except for knmi-21. The same analysis was also performed at UV wavelengths. A summary of the resulting median and 1σ standard deviation FOV derived from each instrument is presented in Figure 6~~Figure 6~~.

The time series of horizon scans provide a useful assessment of the stability and precision of the elevation pointing devices used by the different instruments. In some cases, horizon scans allowed the identification of calibration biases, which could then be addressed by the instrument teams and corrected straight away. This is in particular the case for the dlrustc-13 and -14 instruments. Considering the effective field of view (FOV), a large variability between the instruments was identified. This generally reflects differences in the optical design of the different systems. However, horizon scans can also be influenced by atmospheric conditions and by perturbations of the light intensity at the horizon (e.g. due to fog, high aerosol loads or refraction at temperature inversions). Nevertheless, it is striking to note in Figure 6~~Figure 6~~ that horizon elevations tend to be systematically higher at visible wavelengths than at UV ones. Likewise, FOVs measured in the UV tend to be wider than in the visible. This variation is larger than expected from typical chromatic aberration effects in telescope lenses. The reason for this behaviour is not fully understood but it is likely related to the wavelength dependence of the surface albedo, which may affect the horizon scan fitting process (for more details, see Donner et al. in review,~~,~~ 2019).

3.3 History of slant column data set revisions

As described in Section 2.3, semi-blind dSCD data sets had to be submitted by 18 October 2016, i.e. three weeks after the end of the formal intercomparison period. However, resubmissions were accepted after this date when a clear justification was provided for the change. The main motivation for accepting late revisions was to remedy well-identified mistakes. Details of the submitted revisions, including justifications for the changes and corresponding dates, are given in Appendix B.

Formatted: Font: 10 pt

Formatted: Font: 10 pt

Formatted: Font: 10 pt

Formatted: Font: 10 pt

3.4 Pre-processing of the slant column data

Before further processing, the dSCD measurements from all groups were checked to remove unphysical values and obvious outliers. For this purpose, the following filters were applied: 1) dSCD data exceeding 10 times the daily median values from the instrument were excluded, 2) data points with fitting RMS exceeding 4 times the daily median RMS were removed.

In addition, the results from the horizon scan analysis (see Section 3.2) were used to readjust the elevation angle of instruments presenting absolute elevation offsets larger than 1.5°. This correction was performed assuming a reference horizon elevation of 0.1°, as determined independently using lamp measurements performed at night combined with an analysis of terrain height variations (Donner et al., ~~to be submitted to AMT,~~ in review, 2019). The impact of this angular correction is illustrated in Figure 7~~Figure 7~~ for NO_2 dSCD measurements, which are here represented in terms of their relative difference with respect to median values from a selection of the participating instruments (for more details see Section 3.5, and Figure 8~~Figure 8~~). As can be seen, the large biases observed during the first few days of the campaign for some instruments were due to systematic mispointing effects well compensated by the correction. The impact of the correction is largest for NO_2, but it is also significant for other tropospheric species, in particular ~~for~~ O_4. This again stresses the importance of accurately calibrating the elevation scanner of MAX-DOAS instruments.

Formatted: Font: 10 pt

Formatted: Font: 10 pt

3.5 Determination of reference comparison data sets

As in previous campaigns, the intercomparison of dSCD measurements was based on pre-selected reference data sets. In CINDI-2, these were based on the calculation of median dSCDs obtained from a selection of measurements presenting an acceptable agreement. Here, the selection of the reference groups, different for each data product, was performed after an initial regression analysis using the median of all data as reference. Only groups satisfying the performance criterion for the regression slopes were retained (see Section 4 and Table 4 for more details). The data sets included in the median references are displayed in Figure 8~~Figure 8~~ for both MAX-DOAS and zenith-sky twilight data products. In the particular case of HCHO, the selection was performed through visual inspection of the dSCD comparisons. Only data sets displaying consistent behaviour at 30° elevation (the angle generally used to retrieve first guess total tropospheric columns using the geometrical approximation; see Hönninger and Platt, 2002) were retained for building the reference. This can be appreciated in Figure 9~~Figure 9~~ where time series of the HCHO dSCDs measured by each group are compared to the reference values. As can be seen, many data sets display noisy and/or unphysical negative values and only the four selected groups (bira-4, iupb-18, mpic-28 and niwa-29) present mutually consistent values. Note that a similar approach was used for the selection of the HCHO dSCD reference in Pinardi et al. (2013).

Formatted: Font: 10 pt

Formatted: Font: 10 pt

3.6 Initial assessment of the overall agreement between measurement data sets

Tables 5 and 6 show the mean relative differences (in percent) from the reference dSCDs and their 1st sigma standard deviation for all participating instruments and, respectively, for all MAX-DOAS products and for all zenith-sky DOAS products. Extreme outliers (values exceeding percentile 97) are excluded from the analysis, as well as MAX-DOAS ozone measurements since these show very small off-axis enhancements (see Figure 8~~Figure 8~~). Both tables provide an overall initial assessment of the intercomparison results indicating that for most data products (except HCHO), instruments generally agree within a few percent for the most relevant range of elevation angles of 1°-10° for MAX-DOAS data and for an SZA of 80°-93° for zenith-sky twilight data. One can also see that the overall agreement between instruments is better in the visible than in the UV spectral range.

Formatted: Font: 10 pt

For HCHO (last two columns of Table 5), the differences between the instruments are comparatively larger and, in some cases, extreme. However, restricting the analysis to the first four days of the measurement campaign (when the air temperature was warmer and the HCHO dSCDs higher) reduces discrepancies significantly and, although a higher spread remains compared to any of the other products, one can conclude that under such favourable conditions a large number of the participating instruments provide consistent HCHO dSCD measurements. For amoiap-2, however, the instrument was operated in different modes during different time periods with some modes being more advantages for the HCHO data analysis than others. The group found that when only HCHO data acquired during the optimal time period is used, the mean relative difference is substantially lower, approximately -16%. More details on the instrument and the different modes are provided in Borovski et al. 2017a and Borovski et al. 2017b.

The last row of Tables 5 and 6 shows the median values from the table entrees for each column. The median of the differences is by construction close to zero (but not exactly zero since the median reference values are derived from a selected subset of the participating instruments), while the median of the standard deviations provides an estimate of the most probable size of the deviations against the reference. For example, the median value for zenith-sky DOAS NO2uv shows the highest deviation from the reference when compared to the other zenith-sky DOAS products. For the MAX-DOAS data products, as expected, HCHO shows by far the highest deviation.

3.7 Regression analysis

The approach adopted for the ~~formal~~ CINDI-2 intercomparison follows from previous exercises, in particular the CINDI campaign (Roscoe et al., 2010) and previous NDACC intercomparisons (Vandaele et al., 2005; Roscoe et al., 1999). It is based on the systematic analysis of regression plots between individual measurements and corresponding median reference values (see Section 3.5). Assuming negligible uncertainties on the reference dSCDs, we use a simple linear least-squares regression method weighted by reported dSCD uncertainties. Owing to the strict measurement protocol imposed for the campaign, most measurement points could be compared one-to-one without the need for further interpolation or averaging. When interpolation was necessary, a simple linear procedure was used to bring measurements in line with the campaign protocol (see Section 2.4). This implies that, in comparison to previous similar exercises, sampling and mismatch errors (air mass co-location errors) could be ~~drastically~~ reduced considerably, so that comparison noise and biases should more accurately reflect the intrinsic instrumental performances ~~and/or atmospheric variability~~. This question is further investigated below.

Linear correlation plots between the dSCDs for each instrument and the median value of all the measurements were systematically generated for the complete semi-blind intercomparison time period for each data product, and for each elevation angle and azimuth viewing direction. This allowed identification of, e.g., whether a specific issue arose from particular observation geometries for one or several instruments. Concerning zenith-sky twilight analyses, zenith measurements were selected in a limited range of solar zenith angles (from 75° to 93°) representative of typical twilight measurements, similar to as performed within NDACC for stratospheric ozone and NO_2 monitoring (see e.g. Hendrick et al., 2011) where an SZA range from 86°-91° is used. Figure 10~~Figure 10~~ and 11 show examples of the regression analysis for the case of MAX-DOAS NO_2 and O_4 measured in the visible spectral range. A more complete overview of the regression results obtained for all species can be found in the Supplement where the regression analysis is shown for all elevation angles and viewing directions. As can be seen, a tight correlation is observed for most of the participating instruments. The values for the slope (S), intercept (I), and the RMS calculated as part of the regression analysis are shown in each of the instrument panels. The slope and intercept parameters, respectively, quantify the mean systematic bias and offset of individual data sets against the median reference, while the RMS error provides an estimate of the measurement noise or dispersion.

Formatted: Font: 10 pt

A similar analysis is presented in Figure 12~~Figure 12~~ for HCHO. Note the much larger relative noise obtained for this weak absorber, and the larger dispersion of the results. For this molecule, low-noise research grade instruments perform significantly better than other systems. A similar conclusion was reached in Pinardi et al. (2013) (see in particular Figure 18). Note however, that instruments equipped with compact Avantes spectrometers (e.g. the Pandora and EnviMes instruments) also provide good results despite a larger noise level.

It is interesting to further investigate the dSCD noise levels and their dependencies. Two approaches are generally used to characterize the random uncertainties of dSCD measurements. The first one consists of inspecting the dSCD uncertainties produced by the DOAS least-squares fitting procedure. Assuming normally distributed residuals, these uncertainties provide a good estimate of the random uncertainty due to instrument noise. Figure 13~~Figure 13~~ (panel a) displays DOAS fit dSCD errors normalised to their median for the 12 data products investigated in this exercise for all instruments and all elevation angles. For each box, the bottom and top edges of the box indicate the 25th and 75th percentiles, respectively, while the whiskers extend to the most extreme data points. Median dSCD error values are given for reference on the upper x-axis. Next to the fitting errors, in the right panel of Figure 13~~Figure 13~~, are represented the RMS residuals from regression analyses, normalised in the same way as the dSCD errors. Owing to the good synchronisation achieved during CINDI-2, these RMS values provide a good estimate of the comparison noise against median dSCD references. Assuming ideal comparison conditions (i.e. perfect co-location in time and space under stable atmospheric conditions), one would expect these two independent estimates of random uncertainties to converge towards a common value. This happens to be approximately the case for HCHO and for most of the twilight (stratospheric) data products, except for the O3vis product. In contrast, however, regression noise values derived for NO_2 and O_4 dSCDs appear to be much larger than their corresponding fitting uncertainties, and in the case of the NO2vis product, the difference is most pronounced.

The results shown in Figure 13 indicate that despite the measurement synchronisation (to better than 1 minute) and the fact that all instruments were oriented and pointing towards the same air masses, the variability of the NO_2 and possibly aerosol or cloud features can be large enough to introduce a difference between the individual data sets~~noise~~ in the comparison exceeding the measurement uncertainty by an order of magnitude. This means that in this intercomparison, atmospheric variability limits the reproducibility and representativeness of individual MAX-DOAS measurements for species such as NO_2. Accordingly, it can be argued that for low-noise instruments the random uncertainty on tropospheric NO_2 dSCD measurements is by far dominated by atmospheric variability effects and the details of how this variability is smoothed out by the measurement system (in particular the FOV of the MAX-DOAS telescope and the integration time are key parameters). This also suggests that using DOAS fit errors as a measure of the dSCD error covariance (as often applied in MAX-DOAS profile inversion schemes, see e.g. Clémer et al., 2010; Vlemmix et al., 2015; Frieß et al., 2018) is not appropriate especially for tropospheric NO_2 retrievals. Instead, a more representative estimate of the random error should be derived from the measured variability of the observed dSCD, with the DOAS fit uncertainties being a lower boundary for the measurement uncertainties at best.~~.~~ This issue has been further investigated in a recent publication by Bösch et al. (2018).

This interpretation is strongly corroborated by Figure 14~~Figure 14~~, where the angular dependence of regression noise results is displayed (in green) for the NO2vis, O4vis and HCHO products. As can be seen, the comparison noise on NO_2 dSCDs is largest at the lowest elevation angles and regularly decreases at larger elevations. This behaviour, which is less marked but also observed for O_4, is consistent with atmospheric variability effects since one expects that inhomogeneities of the tropospheric NO_2 field will affect more strongly observations at lowest elevation angles (which have strongest sensitivity to near-surface NO_2). In contrast, the HCHO comparison noise is virtually independent from the elevation angle and close in size to the fitting noise. Note that even at the highest elevation of 30°, the comparison noise on NO_2 and O_4 dSCDs remain~~keep~~s larger than the fitting noise, suggesting that atmospheric variability remains a dominant effect at all the angles used for profile inversion. Figure 15 displays results from the same analyses

Formatted: Font: 10 pt
Formatted: Font: 10 pt
Formatted: Font: 10 pt
Formatted: Font: 10 pt, Not Bold
Formatted: Font: 10 pt, Not Bold
Formatted: Font: 10 pt, Not Bold, Not Italic
Formatted: Font: 10 pt, Not Bold
Formatted: Font: 10 pt, Not Bold, Not Italic
Formatted: Font: 10 pt, Not Bold
Formatted: Font: 10 pt, Not Bold, Subscript
Formatted: Font: 10 pt, Not Bold
Formatted: Font: 10 pt
Formatted: Font: 10 pt

but restricted to reference data sets. Similar conclusions are reached for NO_2 and O_4. In the case of HCHO, the noise level drops considerably, which reflects the high sensitivity of instruments selected for building the HCHO reference. Interestingly, one can also see that regression RMS and fitting residuals now match almost perfectly (and at all elevation angles) meaning that for this molecule most of the residual variance from regressions involving good instruments can be explained by instrument shot noise. ~~between good instruments can be explained by measurement noise.~~ Figure 16 displays results obtained when selecting Pandora instruments only. In comparison to other systems, Pandoras are characterised by a larger field of view (see Figure 6) which probably explains the smaller regression RMS observed for NO_2 and O_4 (likely due to a more efficient smoothing of the atmospheric variability).

Figure 17~~Figure 17~~ provides a different view of the data set already presented in Figure 10~~Figure 10~~, displaying the slope, intercept and RMS for the NO_2 (visible) regression analysis graphically for all measurement days and viewing directions, and for several elevation angles (1°, 3°, 5°, 8°, 15°, and 30°). Similar plots have been generated for all the trace gas data products and are provided in Sections 1 and 2 of the Supplement. Note that for twoa ~~couple of~~ instruments (chiba-9, amoiap-2), only one elevation angle from the above set is available due to technical reasons intrinsic to these instruments. The limits indicated with dashed lines are introduced and discussed further in Section 4. Figure 17~~Figure 17~~ can be compared with similar figures in Roscoe et al. (2010) (Figure 6) and Pinardi et al. (2013) (Figure 7) allowing results from both CINDI campaigns to be linked. It is interesting to note that although the range of variability on the slope and intercept parameters was similar in both campaigns, the proportion of instruments matching the 5% limit on the slope was significantly improved in CINDI-2 indicating a general improvement of the overall consistency of the measurements.

As to be expected from well-calibrated instruments, the three regression parameters displayed in Figure 17~~Figure 17~~ generally do not show any marked angular dependence~~y~~. However, some data sets display larger deviations and sometimes also significant angular dependencies. For these cases, the lowest elevation angles often show the largest deviations (e.g. intercept and RMS for nasa-31 and dlrustc-13, slope for uto-36) but not always (e.g. RMS for cu-boulder-11 and slope for iupb-37). Although this certainly does not explain all discrepancies, it is interesting to note that, in many cases, the largest deviations are observed for instruments that did not supply (or could only partially supply) horizon scan information and therefore could not benefit from the angular correction applied in pre-processing (see Section 3.4).

4 Investigation of instrument performance

With MAX-DOAS-type instruments having gained popularity in recent years and their usage becoming more widespread, the need for a reliable and clearly documented assessment process is becoming more pressing. A semi-blind intercomparison campaign such as CINDI-2 provides the ideal conditions to obtain a data set for such a process and the opportunity to involve as many MAX-DOAS instruments as possible.

Three criteria based on the regression analysis discussed in Section 3.7 (slope, intercept and RMS) have been selected to assess the performance of each of the participating instruments with regard to the eight MAX-DOAS and four zenith-sky products. For each of these parameters, specific limits have been set for the performance evaluation as listed in Table 4. These were semi-empirically derived from a visual inspection of the distribution of the slope, intercept and RMS values for each of the eight CINDI-2 MAX-DOAS and four zenith-sky data products. The histograms and limits (indicated with red lines) for the eight MAX-DOAS data products are displayed in Figure 18 for the slope, intercept and RMS from the regression analysis. Note that the NO_2 and O_3 criteria were adapted from previous NDACC campaigns (see I~~i~~ntroduction for further details). For other products, limits were set arbitrarily

Formatted: Font: 10 pt

Formatted: Font: 10 pt

Formatted: Font: 10 pt

Formatted: Font: 10 pt

to capture the most probable values while excluding clear outliers. The limits were, however, chosen to exceed the median of the measurements (indicated with blue lines). The blue lines represent the percentiles 16 and 84 (84 only for RMS) and it can be seen that the certification criteria have been chosen to exceed these limits. One exception is HCHO, since for this product the difference between well performing and less well performing instruments was much larger than for the other products.

It must be acknowledged that the performance limits defined in this work (as in previous NDACC intercomparisons) are representative of the current state-of-the-art of the instrumentation, and to some extent also reflect the measurement conditions in Cabauw. Another campaign being performed e.g. in a cleaner or more stable site could lead to different values for the limits.

Figure 19~~Figure 19~~ shows a summary of the same regression statistics previously discussed in Section 3.7 and displayed in Figure 10~~Figure 10~~ and 15 but with all individual elevation angles added up resulting in one single value for each parameter, instrument and data product. This means that only 3 values are displayed for each instrument. The green shaded areas denote the limits defined in Figure 18 with all parameters falling within the limits being displayed as blue dots while values in red are not meeting the respective criterion. Note that not all of the 36 instruments measure NO2vis. For the slope of the NO2vis regression analysis shown in the top panel, two instruments (uto-36 and amoiap-2) fall outside the limit. One other instrument (iupb-37, the imaging instrument) is not meeting the criterion set for the intercept (see middle panel) and one (nasa-31) for the RMS (bottom panel). One of such summary plots has been produced for each of the eight MAX-DOAS and four zenith-sky data products which can be individually viewed in Sections 1 and 2 of the Supplement.

Formatted: Font: 10 pt

Formatted: Font: 10 pt

To further summarize the outcome of the regression analysis and provide an overview of all 8 MAX-DOAS data products,

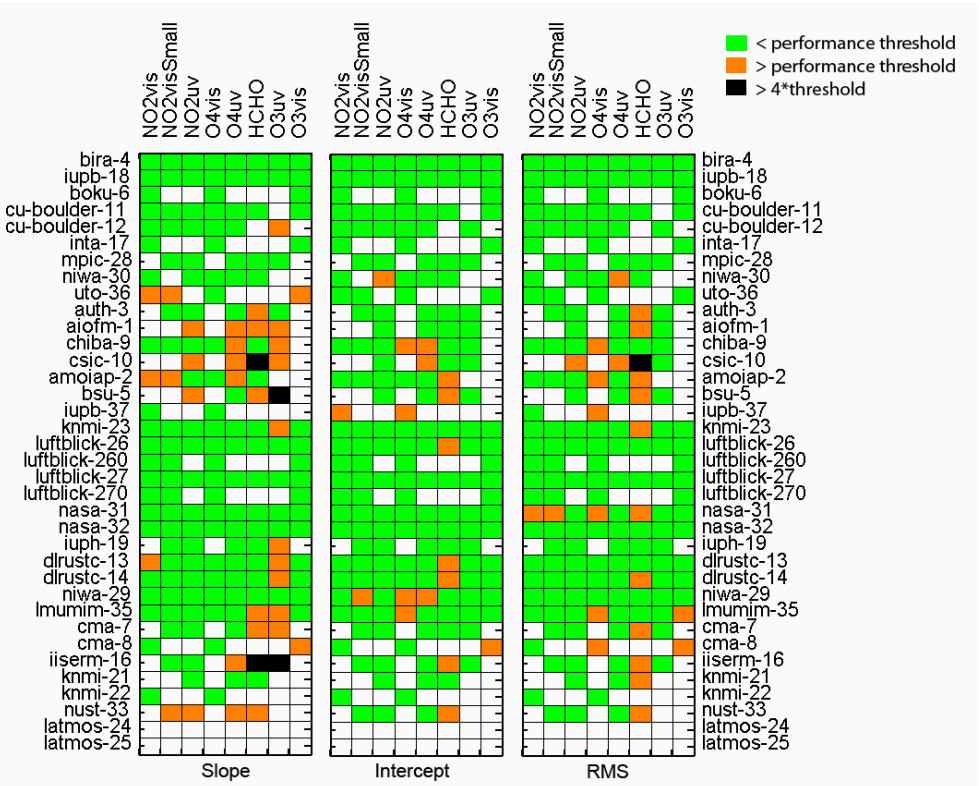

Figure 20~~Figure 20~~ displays the three selected parameters for all participating instruments. The performance is colour coded with regard to parameters falling inside the performance limit (green) or not meeting the criterion (orange). In exceptional cases where the slope or RMS is exceeding the threshold by more than a factor of 4, the performance is colour-coded in black~~pink~~. Just under one-third of all the instruments do meet all the criteria. Figure 21 shows the same summary for the four zenith-sky data products. In this case, more instruments meet all criteria and none of the products have any parameters which exceed any performance threshold by a factor of 4 or more.

Figure 22~~Figure 22~~ further synthesizes all results into one overview plot. This assessment matrix shows the outcome for all 36 instruments, eight data products for MAX-DOAS and four data products for zenith-sky mode. Any box coloured with green denotes that all three assessment criteria for that instrument and data product have been fulfilled. Boxes marked with yellow and orange denote that one or two criteria, respectively, have not been met, while red means that all three criteria have not been met and black~~pink~~ indicates that this data set has at least one extreme outlier. Additionally, both the reported dSCD regression RMS and the DOAS fit RMS are used to sort the data products accordingly, with the smallest median RMS being assigned the lowest number in each case.

Formatted: Normal

Formatted: Font: 10 pt, Do not check spelling or grammar

Formatted: Font: 10 pt, Check spelling and grammar

Formatted: Font: 9 pt

Formatted: Font: 10 pt

The order in which the instruments are displayed in Figure 22~~Figure 22~~ is identical to Figures 20 and 21 with the instruments being grouped into five different categories: Custom-built, Pandora, EnviMes, miniDOAS and SAOZ. Custom-built instruments are assembled in-house and often designed with specific research purposes in mind. This category displays the greatest diversity in performance, and it includes the highest performing instruments as well as the instrumentation with the biggest difficulties meeting the set criteria of the performance assessment. In some cases, this can be related to the level of experience of the research group involved in building the instrument and/or in operating the instrument and performing the data analysis.

The first seven custom-built instruments listed in Figure 22~~Figure 22~~ meet all criteria for all measured MAX-DOAS data sets with the following three instruments also being close to fulfilling almost all criteria for most of the data. The last six instruments listed under the custom-built category, however, struggle to either meet two criteria or to meet all criteria for one of the measured data products. Additionally, HCHO or O3uv data sets measured by three of the instruments (~~aiofm-1,~~ csic-10, ~~and~~ bsu-5 and iiserm-16) contain extreme outliers. ~~In the case of aiofm-1, the extreme outliers in the O3uv data set can be at least partly attributed to an issue with the DOAS settings, most probably related to the ozone cross-sections used during the data processing.~~

The seven Pandora and five EnviMes instruments show overall a more consistent picture. Four of the Pandoras are meeting all categories and two of the other Pandoras satisfy all but one of the criteria for one or two of the data products. Nasa-31, however, experienced problems during operation and had some dirt inside the head sensor which was moving around and blocking part of the instrument FOV as well as having a loose tracker shaft. This caused significantly reduced signal-to-noise and an increased pointing uncertainty (see the large error bar for this instrument in Figure 6) that had negative consequences for all data products analyzed in the campaign. These problems were detected during the campaign and an attempt was made to fix them. In spite of these issues, most criteria were still met. It should be noted though that the behaviour displayed by nasa-31 did not fully represent the observational capabilities of a Pandora, as clearly evidenced by results from other instruments of the same type. The EnviMes instruments performed overall well when measuring NO_2 but struggled more to fulfil all criteria for the HCHO and O3uv data sets apart from niwa-29 which satisfied all criteria for HCHO and O3uv while not satisfying one of the criteria for both of the O_4 data sets and one of the NO_2 data sets. Most of the six miniDOAS instruments measured NO_2 satisfactorily in all three wavelength~~s~~ ranges and only failed to~~not~~ satisfy one criterion in the O_4 data sets. However, they~~but~~ experienced discernible difficulties when measuring HCHO and O_3 which includes all criteria failed and extreme outliers.

The zenith-sky twilight data set (rightmost four columns in Figure 22) show a consistent performance for all custom-built, Pandora, EnviMes and SAOZ type instruments and all four data products (apart from nasa-31, see discussion above) with in most cases (90%) all criteria satisfied and in just eight cases one criterion not satisfied. The performance of the miniDOAS instruments is for the zenith-sky data more variable with one instrument (cma-8) not satisfying any of the criteria for O3vis and another (nust-33) failing two out of three criteria for the NO2uv product. The two SAOZ instruments measure zenith-sky data only and either satisfy all criteria or just do not meet one of them.

The ranking provided in each of the individual boxes in Figure 22~~Figure 22~~ is based on the dSCD regression RMS (first value) and the RMS calculated as part of the data fitting routine (second value), the instruments with the smallest RMS (i.e. the smallest measurement noise) being assigned the lowest number. Overall, the combined ranking reflects the performance assessment of the individual instruments, but there are a couple of noteworthy deviations. For example, the data products measured by auth-3 have very large numbers corresponding to a high RMS (high measurement noise in comparison to other systems) but at the same time ~~they are~~ meet~~ing~~ almost all performance criteria. On the other hand~~opposite~~, the data products measured by aiofm-1 have an excellent fit RMS rating corresponding to a very low measurement noise, while none of the data products satisfy~~ies~~ all criteria and

Formatted: Font: 10 pt

Formatted: Font: 10 pt

Formatted: Font: 10 pt

O3uv has at least one extreme outlier. This apparent inconsistency reflects the nature of the performance assessment methodology, which puts larger emphasis on the assessment of systematic biases on measured dSCDs than on the noise. We have also seen that the comparison noise in regression analyses is for some of the products (NO_2, O_4) dominated by atmospheric/observation geometry effects rather than by actual instrumental noise.

The performance matrix shown in Figure 22~~Figure 22~~ can be used to assess the participating groups and their instruments regarding their capability to measure NO_2, O_3 and HCHO concentrations and aerosols (using O_4 measurements) at sufficiently high quality to allow reliable geophysical studies or satellite validation efforts. Based on their RMS rating and the fact that they meet all the other criteria as well, the top most four instruments listed in Figure 22~~Figure 22~~ and the Luftblick 26 and 27 systems can be considered as the best performing instruments during CINDI-2. In addition to offering an instantaneous picture of the level of performance of the current international MAX-DOAS research community, these results also provide the background information needed for the formal assessment and certification of instruments contributing to the NDACC network.

Formatted: Font: 10 pt

Formatted: Font: 10 pt

5 Recommendations for network operation and future campaigns

The CINDI-2 intercomparison exercise included more target trace gas species, and more instruments and participants from many different institutes than previously attempted in any other UV-visible spectroscopy intercomparison exercise. This provided a logistical challenge, which was addressed by setting up a carefully managed campaign. Beyond the detailed consistency assessment documented in this work, several lessons were learned that are expected to be of benefit to measurements conducted at network sites.

1. The accuracy and stability of the MAX-DOAS elevation scans was found to be critical, especially for measurements at low elevation angles. Therefore, we recommend to regularly calibrate elevation scan devices using one of the methods described in Donner et al. (in review, 2019). Moreover, for instruments not equipped with an internal pointing verification system (e.g. digital inclinometer or self-calibrating sun-tracker) horizon scans should be regularly performed, ideally on a daily basis, in order to verify the long-term stability of the pointing elevation.
2. The degree of geometric and temporal synchronisation prescribed for the instruments has revealed that spatial and temporal variability in the atmosphere is significantly greater than the total effect of instrument-derived uncertainties. As a result, atmospheric variability limits the reproducibility and representativeness of individual MAX-DOAS measurements for species such as NO_2. For this molecule, we estimate that the variability has a spatial scale that is at least as fine as many tens to a few hundreds of meters. This order of magnitude is consistent with the horizontal distances sampled by the average FOV (1 degree) and the horizontal separation of the instrument telescopes. It implies that random error estimates on NO_2 dSCDs should account for atmospheric variability effects in addition to spectral fitting uncertainties. To a lesser extent, the same reasoning applies to O_4 dCSD measurements.
3. For high-quality HCHO measurements, radiance measurements should reach a signal-to-noise ratio of 1000 or better in the spectral range from 335 nm to 360 nm, corresponding to HCHO dSCD uncertainties of $5x10^{15}$ molec/cm^2 or better. At this level of random uncertainty (and in contrast to the NO_2 case), HCHO spectral fitting errors still dominate over atmospheric variability effects.

One also anticipates that future similar intercalibration campaigns will strongly benefit from the lessons learned during and after CINDI-2. As already pointed out, the campaign was successful in improving (1) the spatial and temporal synchronicity of the measurements, and (2) the characterisation of the pointing elevation accuracy from all instruments and their impact on the DOAS analysis results. Despite these achievements, a few critical points were identified that deserve more attention in future deployments.

1. The data acquisition protocol, which proved to be very useful for instrument synchronisation, was not fully adequate for monitoring the spatial variability in highly variable trace gases such as NO_2. As discussed in Section 3.7, results from CINDI-2 indicate that in spite of the improvement in measuring the same airmass, the variability in some of the trace gases can still be large enough to introduce noise which is clearly exceeding the measurement uncertainty, suggesting that using DOAS fit errors as a measure of the dSCD error covariance is not appropriate. A more representative estimate of the random error should be derived instead from the measured variability of the observed dSCDs (see e.g. Bösch et al., 2018). For future campaigns, we hence recommend to adopt a strategy combining full elevation scans suitable for profile inversion at one or two reference azimuths, and azimuth scans at one elevation for evaluation of the spatial variability in trace gas concentration.
2. Although the campaign had a strong focus on elevation scan calibration, other aspects of the instrument calibration were handled with far less attention. Results from the data analysis, however, indicated that some of the observed discrepancies were related to a lack of proper instrumental characterisation before the campaign (e.g. detector non-linearity or spectral stray-light), and it is likely that some of the remaining deviations are related to unresolved calibration issues. For future campaigns, a better strategy should be developed to improve the characterization of participating instruments in preparation for field deployment. This could, e.g. be organised in the form of a preparatory calibration campaign hosted by a suitably equipped lab. The focus of this exercise should be put on instrumental characteristics of major importance for DOAS-type instruments, i.e. in particular instrumental line shape, spectral stray-light, polarization response, detector response (dark-current and linearity), field of view of telescope, elevation scanner accuracy and reproducibility, and instrument throughput and sensitivity.

Formatted: List Paragraph, Numbered + Level: 1 + Numbering Style: 1, 2, 3, … + Start at: 1 + Alignment: Left + Aligned at: 0.63 cm + Indent at: 1.27 cm

Formatted: Font: 10 pt

~~5~~6 Conclusions

The CINDI-2 intercomparison campaign had a strong focus on synchronisation and collocation of the measurements as well as on the determination of the pointing accuracy, which altogether resulted in a reduction of the impact of atmospheric changes on the intercomparison exercise in comparison to CINDI. While each participating institute used their own instrumentation and analysis software (Tables 2 and 3), specific measurement procedures and retrieval settings were prescribed and strictly adhered to.

This comprehensive ~~and very well coordinated~~ measurement protocol was highly successful in synchronising the timing of the measurements between all the instruments (Figure 2). The different approaches applied to determine the pointing accuracy of the instruments and their stability during the campaign provided important information for monitoring the instrument performance (see Figure 6). Moreover, this information was used to correct the data analysis in cases where the measurements were compromised by pointing inaccuracies leading to further improvements in consistency (see e.g. Figure 7). The horizon scans, in particular, were useful for identifying calibration biases, which could be addressed and corrected for the remainder of the campaign. Based on the experiences made during CINDI-2, it is highly recommended to include horizon scans into the daily measurement routine at monitoring sites and for any future MAX-DOAS intercomparison exercise. The different methods for the elevation calibration used during the CINDI-2 campaign are discussed in more detail in Donner et al. (~~to be submitted to AMT,~~ in review, 2019).

In line with previous intercomparisons, a regression analysis of the dSCDs measured by each instrument with a ~~selected~~ reference data set ~~(see Sections 3.5 for details)~~ was performed (see Section 3.5 for details on how the reference data sets were derived) and a whole range of correlation plots between the dSCDs and the reference were generated in a systematic manner (Figures 10-12 and Sections 1 and 2 of the Supplement). The slope and intercept of the regression analysis respectively quantify the mean systematic bias and offset of the individual data sets against the reference, and the regression RMS error provides an estimate of the overall

comparison noise (see e.g. Figure 17). These three performance criteria were further investigated, and for each of the parameters and data products, specific limits were set and applied to all the measurements (Table 4 & Figure 18). Figures 19-22 visualize the summary of the regression analysis and provide an overview of the performance of each of the instruments regarding the eight MAX-DOAS and four zenith-sky data products.

The general level of agreement achieved for the different data products is summarized in Table 7. The median bias against the reference data sets is generally low (<5% for most products) and comparison noise levels are of the order of 3-4 10^{15} molec./cm^2 for NO_2, 1.5 10^{42} molec.^{2}/cm^5 for O_4 and 1.0 10^{16} molec./cm^2 for HCHO. The table also lists the typical dSCD retrieval uncertainties that can be expected from high quality and standard instruments, respectively. These uncertainties are compatible with satellite validation requirements (for further details, e.g. see https://sentinels.copernicus.eu/web/sentinel/technical-guides/sentinel-5p/validation). The results summarized in Table 7 agree well with the mean relative differences and standard deviation from the reference listed for all participating instruments in Tables 5 and 6, which also show that most instruments agree within a few percent for all MAX-DOAS and~~&~~ twilight DOAS products (apart from HCHO and O_3).

This assessment process, undertaken as part of the CINDI-2 intercomparison campaign, provides the UV-visible absorption spectroscopy research community with ~~a~~ guidelines and a procedure on how to assess the performance of MAX-DOAS and DOAS instruments, in particular for the inclusion into NDACC (see NDACC webpage for access to the UV/Vis Appendix describing these recommendations). It is expected that a similar level of consistency, as seen during CINDI-2, can be obtained in the field if recommended settings are implemented and used by each participant of the network. ~~and~~ More control in this aspect of homogeneity can be obtained through centralized processing, which is the aim of the currently developed ESA FRM4DOAS project ~~in a future centralised MAX-DOAS processing system such as~~like the one being developed in the ESA FRM4DOAS project (see http://frm4doas.aeronomie.be/).

The semi-blind CINDI-2 intercomparison exercise, presented here, concludes with the comparison and assessment of the retrieved dSCDs of a limited number of mature data products (NO_2, O_4, O_3 and HCHO). However, additional species (e.g. HONO, glyoxal, BrO, H_2O) were also measured during the campaign, some of them being the subject of ongoing studies to be published separately. In particular, the tropospheric ozone column retrieval has been investigated in depth (Wang et al., 2018) and a publication on HONO retrievals is under way (Wang et al., ~~to be~~ submitted to AMT, 2019) as a follow-up of the first HONO intercomparison during the MAD-CAT campaign (Wang et al., 2017c). In addition to dSCD measurements, the subsequent steps in MAX-DOAS retrievals, i.e. their conversion into vertical column and profile information is also further investigated in a CINDI-2 profiling working group and as part of the ESA FRM$_4$DOAS project (Frieß et al., 2018; Tirpitz et al., ~~to be~~ submitted to AMT, 2019). Furthermore, other aspects of the campaign measurements are being further exploited, such as mobile car-DOAS observations, reference in-situ measurements and instruments' elevation pointing calibration (Donner et al.~~, to be submitted to AMT,~~ in review, 2019).

~~The CINDI-2 intercomparison exercise included more target trace gas species, and more instruments and participants from many different institutes than previously attempted in any other UV-visible spectroscopy intercomparison exercise. This provided a logistical challenge, which was successfully addressed by employing a thoroughly planned and carefully managed campaign. It is anticipated that future similar intercalibration campaigns will strongly benefit from the lessons learned during and after CINDI-2. As already pointed out, the campaign was very successful in improving (1) the spatial and temporal synchronicity of the measurements, and (2) the characterisation of the pointing elevation accuracy from all instruments and their impact on the DOAS analysis results. Despite these achievements, a few critical points were identified that deserve more attention in future deployments.~~

Formatted: Comment Text, Line spacing: 1.5 lines

Formatted: Font: 10 pt, English (United Kingdom)

Formatted: Font: 10 pt, English (United Kingdom)

Formatted: Font: 10 pt, English (United Kingdom)

Formatted: Font: 10 pt, English (United Kingdom)

Formatted: Font: 10 pt, English (United Kingdom)

Formatted: Font: 10 pt, English (United Kingdom)

Formatted: Not Superscript/ Subscript

Formatted: Font: 10 pt

~~1. The data acquisition protocol, which proved to be very useful for instrument synchronisation, was not fully adequate for profile inversion experiments. For future campaigns, we recommend to adopt a strategy combining full elevation scans suitable for profile inversion at one or two reference azimuths, and azimuth scans at one elevation for evaluation of the spatial variability in trace gas concentration.~~

~~2. Although the campaign had a strong focus on elevation scan calibration, other aspects of the instrument calibration were handled with far less attention. Results from the data analysis, however, indicated that some of the observed discrepancies were related to a lack of proper instrumental characterisation before the campaign (e.g. detector non-linearity or spectral stray-light), and it is likely that some of the remaining deviations are related to unresolved calibration issues. For future campaigns, a better strategy should be developed to improve the characterization of participating instruments in preparation for field deployment. This could, e.g. be organised in the form of a preparatory calibration campaign hosted by a suitably equipped lab. The focus of this exercise should be put on instrumental characteristics of major importance for DOAS-type instruments, i.e. in particular instrumental line shape, spectral stray-light, polarization response, detector response (dark-current and linearity), field of view of telescope, elevation scanner accuracy and reproducibility, and instrument throughput and sensitivity.~~

Author contributions. FH, MVR, AA, UF, AR, TW, JL and AP designed, planned and organised the CINDI-2 intercomparison campaign. KK was the referee for the intercomparison during the campaign and for the follow-up data analysis. ED contributed as the assistant referee. All co-authors contributed to the campaign either as participants and instrument operators and/or by performing the data analysis, data quality control and data submission. MVR performed the intercomparison data analysis. KK and MVR interpreted the results and wrote the manuscript with feed-back and contributions from all other co-authors.

Competing interests. The authors declare that they have no conflict of interest.

Acknowledgements. We gratefully acknowledge the KNMI staff at Cabauw for their excellent technical and infrastructure support during the campaign. CINDI-2 received funding from the Netherlands Space Office (NSO). Funding for this study was provided by ESA through the CINDI-2 (ESA Contract No.4000118533/16/I-Sbo) and FRM4DOAS (ESA Contract No. 4000118181/16/I-EF) projects and partly within the EU 7th Framework Programme QA4ECV project (Grant Agreement no. 607405). The BOKU MAX-DOAS instrument was funded and the participation of S. F. Schreier was supported by the Austrian Science Fund (FWF): I 2296-N29. The participation of the University of Toronto team was supported by the Canadian Space Agency (through the AVATARS project) and the Natural Sciences and Engineering Research Council (through the PAHA project). The instrument was funded by the Canada Foundation for Innovation and is usually operated at the Polar Environment Atmospheric Research Laboratory (PEARL) by the Canadian Network for the Detection of Atmospheric Change (CANDAC). Funding for CISC was provided by the UVAS ("Ultraviolet and Visible Atmospheric Sounder") project SEOSAT/INGENIO, ESP2015-71299-R, MINECO-FEDER, UE. The activities of the IUP Heidelberg were supported by the DFG project RAPSODI (grant No. PL 193/17-1). SAOZ and Mini-SAOZ instruments are supported by the Centre National de la Recherche Scientifique (CNRS) and the Centre National d'Etudes Spatiales (CNES). INTA acknowledges support from the National funding projects HELADO (CTM2013-41311-P) and AVATAR (CGL2014-55230-R). AMOIAP acknowledges support from the Russian Science Foundation (grant 16-17-10275) and Russian Foundation for Basic Research (grants 16-05-01062 and 18-35-00682). K.L. Chan received trans-national access funding from ACTRIS-2 (H2020 Grant Agreement N° 654109). R. Volkamer acknowledges funding from NASA's Atmospheric Composition Program (NASA-16-NUP2016-0001), and US National Science Foundation (award AGS-1620530). H. Finkenzeller is recipient of a NASA graduate fellowship. M. Vrekoussis acknowledges support from the University of Bremen and the DFG Research Center/Cluster of Excellence "The Ocean in the Earth System-MARUM". Financial support through the University of Bremen

Formatted: Font: 10 pt

Formatted: Font: (Default) Times New Roman, 10 pt, Italic, English (United Kingdom)

Formatted: Font: (Default) Times New Roman, 10 pt, English (United Kingdom)

Formatted: Justified, Line spacing: 1.5 lines

Formatted: Font: (Default) Times New Roman, 10 pt, Italic, English (United Kingdom)

Formatted: Font: (Default) Times New Roman, 10 pt, English (United Kingdom)

Formatted: Font: 10 pt

Formatted: Normal

Institutional Strategy in the framework of the DFG Excellence Initiative is gratefully acknowledged for A. Schönhardt. Pandora instrument deployment was supported by Luftblick through ESA Pandonia Project and NASA Pandora Project at Goddard Space Flight Center under NASA Headquarters' Tropospheric Composition Program.

Formatted: Font: (Default) Times New Roman, Font color: Auto, Pattern: Clear

67 References

Apituley, A., et al.: Second Cabauw Intercomparison of Nitrogen Dioxide Measuring Instruments (CINDI-2) – Campaign Overview, to be submitted to AMT, 20~~19~~20.

Bobrowski, N.: Volcanic Gas Studies by Multi Axis Differential Optical Absorption Spectroscopy, Ph.D. thesis, University of Heidelberg, Germany, 2005.

Bösch, T., Rozanov, V., Richter, A., Peters, E., Rozanov, A., Wittrock, F., Merlaud, A., Lampel, J., Schmitt, S., de Haij, M., Berkhout, S., Henzing, B., Apituley, A., den Hoed, M., Vonk, J., Tiefengraber, M., Müller, M., and Burrows, J. P.: BOREAS – a new MAX-DOAS profile retrieval algorithm for aerosols and trace gases, Atmos. Meas. Tech., 11, 6833-6859, https://doi.org/10.5194/amt-11-6833-2018, 2018.

Borovski, A., Elokhov, A., Postylyakov, O., and Bruchkouski, I., Study of different operational modes of the IAP 2-port-DOAS instrument for investigation of atmospheric trace gases during CINDI-2 campaign, Proc. SPIE 10424, 104240Y, 2017a, doi: 10.1117/12.2278234.

Borovski, A., Postylyakov, O., Elokhov, A., and Bruchkovski, I., Study of different operational modes of the IAP 2-port-DOAS instrument for atmospheric trace gases investigation during CINDI-2 campaign basing on residual noise analysis, Proc. SPIE 10466, 104662Z, 2017b, doi: 10.1117/12.2285798.

Brinksma, E. J., Pinardi, G., Volten, H., Braak, R., Richter, A., Schönhardt, A., Van Roozendael, M., Fayt, C., Hermans, C., Dirksen, R. J., Vlemmix, T., Berkhout, A. J. C., Swart, D. P. J., Oetjen, H., Wittrock, F., Wagner, T., Ibrahim, O. W., de Leeuw, G., Moerman, M., Curier, R. L., Celarier, E. A., Cede, A., Knap, W. H., Veefkind, J. P., Eskes, H. J., Allaart, M., Rothe, R., Piters, A. J. M., and Levelt, P. F.: The 2005 and 2006 DANDELIONS NO_2 and aerosol intercomparison campaigns, J. Geophys. Res., 113, D16S46, doi:10.1029/2007JD008808, 2008.

Clémer, K., Van Roozendael, M., Fayt, C., Hendrick, F., Hermans, C., Pinardi, G., Spurr, R., Wang, P., and De Mazière, M .: Multiple wavelength retrieval of tropospheric aerosol optical properties from MAXDOAS measurements in Beijing, Atmos. Meas. Tech., 3, 863-878, 2010.

~~Donner, S., Kuhn, J., Van Roozendael, M., Bais, A., Beirle, S., Bösch, T., Bognar, K., Bruchkouski, I., Chan, K.L., Drosoglou, T., Fayt, C., Friess, U., Hendrick, F., Hermans, C., Jin, J., Li, A., Ma, J., Peters, E., Pinardi, G., Richter, A., Schreier, S.F., Seyler, A., Strong, K., Tirpitz, J. L., Wang, Y., Xie, P., Xu, J., Zhao, X. and Wagner, T., Evaluating different methods for elevation calibration of MAX-DOAS instruments during the CINDI-2 campaign, to be submitted to AMT, 2019.~~Donner, S., Kuhn, J., Van Roozendael, M., Bais, A., Beirle, S., Bösch, T., Bognar, K., Bruchkousky, I., Chan, K. L., Drosoglou, T., Fayt, C., Frieß, U., Hendrick, F., Hermans, C., Jin, J., Li, A., Ma, J., Peters, E., Pinardi, G., Richter, A., Schreier, S. F., Seyler, A., Strong, K., Tirpitz, J.-L., Wang, Y., Xie, P., Xu, J., Zhao, X., and Wagner, T.: Evaluating different methods for elevation calibration of MAX-DOAS instruments during the CINDI-2 campaign, Atmos. Meas. Tech. Discuss., https://doi.org/10.5194/amt-2019-115, in review, 2019.

Fleischmann, O. C., Hartmann, M., Burrows, J. P., and Orphal, J.: New ultraviolet absorption cross-sections of BrO at atmospheric temperatures measured by time-windowing Fourier transform spectroscopy, Journal of Photochemistry and Photobiology A: Chemistry, 168, 117–132, 2004.

Formatted: Font: Times New Roman, 10 pt, Font color: Auto, Pattern: Clear

Formatted: Font: 10 pt, Do not check spelling or grammar

Formatted: Font: 10 pt, Do not check spelling or grammar

Frieß, U., Monks, P., Remedios, J., Rozanov, A., Sinreich, R., Wagner, T., and Platt, U.: MAXDOAS O_4 measurements: a new technique to derive information on atmospheric aerosols: 2. Modeling studies, J. Geophys. Res., 111, D14203, doi:10.1029/2005JD006618, 2006.

Frieß, U., Sihler, H., Sander, R., Pöhler, D., Yilmaz, S., and Platt, U.: The vertical distribution of BrO and aerosols in the Arctic: Measurements by active and passive differential optical absorption spectroscopy. Journal of Geophysical Research, 116, D00R04. https://doi.org/10.1029/2011JD015938, 2011.

Frieß, U., Klein Baltink, H., Beirle, S., Clémer, K., Hendrick, F., Henzing, B., Irie, H., de Leeuw, G., Li, A., Moerman, M. M., van Roozendael, M., Shaiganfar, R., Wagner, T., Wang, Y., Xie, P., Yilmaz, S., and Zieger, P.: Intercomparison of aerosol extinction profiles retrieved from MAX-DOAS measurements, Atmos. Meas. Tech., 9, 3205-3222, https://doi.org/10.5194/amt-9-3205-2016, 2016.

Frieß, U., Beirle, S., Alvarado Bonilla, L., Bösch, T., Friedrich, M. M., Hendrick, F., Piters, A., Richter, A., van Roozendael, M., Rozanov, V. V., Spinei, E., Tirpitz, J.-L., Vlemmix, T., Wagner, T., and Wang, Y.: Intercomparison of MAX-DOAS Vertical Profile Retrieval Algorithms: Studies using Synthetic Data, Atmos. Meas. Tech. Discuss., https://doi.org/10.5194/amt-2018-423, in review, 2018.

Gratsea, M., Vrekoussis, M., Richter, A., Wittrock, F., Schönhardt, A., Burrows, J., Kazadzis, S., N. Mihalopoulos, N., Gerasopoulos, E., Slant column MAX-DOAS measurements of nitrogen dioxide, formaldehyde, glyoxal and oxygen dimer in the urban environment of Athens. Atmospheric Environment, 135, 118–131. https://doi.org/10.1016/j.atmosenv.2016.03.048, 2016.

Heckel, A., Richter, A., Tarsu, T., Wittrock, F., Hak, C., Pundt, I., Junkermann, W., and Burrows, J. P.: MAX-DOAS measurements of formaldehyde in the Po-Valley, Atmos. Chem. Phys., 5, 909-918, https://doi.org/10.5194/acp-5-909-2005, 2005.

Hendrick, F., Pommereau, J.-P., Goutail, F., Evans, R.D., Ionov, D., Pazmino, A., Kyrö, E., Held, G., Eriksen, P., Dorokhov, V., Gil, M., and Van Roozendael, M.: NDACC/SAOZ UV-visible total ozone measurements: improved retrieval and comparison with correlative ground-based and satellite Observations, Atmos. Chem. Phys., 11, 5975–5995, doi:10.5194/acp-11-5975-2011, 2011.

Hendrick, F., Müller, J.-F., Clémer, K., Wang, P., De Mazière, M., Fayt, C., Gielen, C., Hermans, C., Ma, J. Z., Pinardi, G., Stavrakou, T., Vlemmix, T., and Van Roozendael, M.: Four years of ground-based MAX-DOAS observations of HONO and NO_2 in the Beijing area, Atmos. Chem. Phys., 14, 765–781, doi:10.5194/acp-14-765-2014, 2014.

Herman, J., A. Cede, E. Spinei, G. Mount, M. Tzortziou, and N. Abuhassan: NO_2 column amounts from ground-based Pandora and MFDOAS spectrometers using the direct-sun DOAS technique: Intercomparisons and application to OMI validation, J. Geophys. Res., 114, D13307, doi:10.1029/2009JD011848, 2009.

Herman, J., Spinei, E., Fried, A., Kim, J., Kim, J., Kim, W., Cede, A., Abuhassan, N., Segal-Rozenhaimer, M.: NO_2 and HCHO measurements in Korea from 2012 to 2016 from Pandora spectrometer instruments compared with OMI retrievals and with aircraft measurements during the KORUS-AQ campaign. Atmospheric Measurement Techniques, 11(8), 4583–4603, https://doi.org/10.5194/amt-11-4583-2018, 2018.

Hönninger G. and Platt, U.: Observations of BrO and its vertical distribution during surface ozone depletion at Alert, Atmos. Environ., 36, 2481–2489, 2002.

Hönninger, G., von Friedeburg, C., and Platt, U.: Multi axis differential optical absorption spectroscopy (MAX-DOAS), Atmos. Chem. Phys., 4, 231–254, doi:10.5194/acp-4-231-2004, 2004.

Irie, H., Takashima, H., Kanaya, Y., Boersma, K. F., Gast, L., Wittrock, F., Brunner, D., Zhou, Y., and Van Roozendael, M.: Eight-component retrievals from ground-based MAX-DOAS observations, Atmos. Meas. Tech., 4, 1027–1044, doi:10.5194/amt-4-1027-2011, 2011.

Lampel, J., Friess, U. and Platt, U.: The impact of vibrational Raman scattering of air on DOAS measurements of atmospheric trace gases, Atmos. Meas. Tech., 8, 3767–3787, doi :10.5194/amt-8-3767-2015, 2015.

Lee, C., Richter, A., Lee, H., Kim, Y. J., Burrows, J. P., Lee, Y. G., and Choi, B. C.: Impact of transport of sulfur dioxide from the Asian continent on the air quality over Korea during May 2005. Atmospheric Environment, 42(7), 1461–1475. https://doi.org/10.1016/j.atmosenv.2007.11.006, 2008.

Lee, H., Irie, H., Kim, Y. J., Noh, Y., Lee, C., Kim, Y., and Chun, K. J.: Retrieval of Aerosol Extinction in the Lower Troposphere Based on UV MAX-DOAS Measurements. Aerosol Science and Technology, 43(5), 502–509. https://doi.org/10.1080/02786820902769691, 2009.

Liley, J., Johnston, P., McKenzie, R., Thomas, A., and Boyd, I.: Stratospheric NO_2 variations from a long time series at Lauder, New Zealand, J. Geophys. Res., 105, 11 633–11 640, 2000.

Meller, R. and Moortgat, G. K.: Temperature dependence of the absorption cross sections of formaldehyde between 223 and 323 K in the wavelength range 225–375 nm, Journal of Geophysical Research: Atmospheres, 105, 7089–7101 2156–2202, 2000.

Merlaud, A.: Development and use of compact instruments for tropospheric investigations based on optical spectroscopy from mobile platforms, Presses univ. de Louvain, 2013.

Merten, A., Tschritter, J., and Platt, U.: Design of differential optical absorption spectroscopy long-path telescopes based on fiber optics, Appl. Opt, 10, 738–754, http://ao.osa.org/abstract.cfm?URI=ao-50-5-738, 2011.

Noxon, J. F.: Nitrogen dioxide in the stratosphere and troposphere measured by ground-based absorption spectroscopy, Science,189, 547–549, 1975.

Ortega, I., Coburn, S., Berg, L.K., Lantz, K., Michalsky, J., Ferrare, R., Hair, J., Hostetler, C. and Volkamer, R.: The CU 2D-MAX-DOAS instrument - part 2: Raman Scattering Probability Measurements and Retrieval of Aerosol Optical Properties, Atmos. Meas. Techn., 9, 3893-3910, doi:10.5194/amt-2015-385, 2016.

Peters, E., Pinardi, G., Seyler, A., Richter, A., Wittrock, F., Bösch, T., Van Roozendael, M., Hendrick, F., Drosoglou, T., Bais, A. F., Kanaya, Y., Zhao, X., Strong, K., Lampel, J., Volkamer, R., Koenig, T., Ortega, I., Puentedura, O., Navarro-Comas, M., Gómez, L., Yela González, M., Piters, A., Remmers, J., Wang, Y., Wagner, T., Wang, S., Saiz-Lopez, A., García-Nieto, D., Cuevas, C. A., Benavent, N., Querel, R., Johnston, P., Postylyakov, O., Borovski, A., Elokhov, A., Bruchkouski, I., Liu, H., Liu, C., Hong, Q., Rivera, C., Grutter, M., Stremme, W., Khokhar, M. F., Khayyam, J., and Burrows, J. P.: Investigating differences in DOAS retrieval codes using MAD-CAT campaign data, Atmos. Meas. Tech., 10, 955-978, https://doi.org/10.5194/amt-10-955-2017, 2017.

Peters, E., Ostendorf, M., Bösch, T., Seyler, A., Schönhardt, A., Schreier, S.F., Henzing, J.S., Wittrock, F., Richter, A., Vrekoussis, M. and Burrows, J.P.: Full-azimuthal imaging-DOAS observations of NO_2 and O_4 during CINDI-2, Atmos. Meas. Tech., 12, 4171–4190, https://doi.org/10.5194/amt-12-4171-2019, 2019~~, submitted to AMT, 2019.~~

Pinardi, G., Van Roozendael, M., Abuhassan, N., Adams, C., Cede, A., Clémer, K., Fayt, C., Frieß, U., Gil, M., Herman, J., Hermans, C., Hendrick, F., Irie, H., Merlaud, A., Navarro Comas, M., Peters, E., Piters, A. J. M., Puentedura, O., Richter, A., Schönhardt, A., Shaiganfar, R., Spinei, E., Strong, K., Takashima, H., Vrekoussis, M., Wagner, T., Wittrock, F., and Yilmaz, S.: MAX-DOAS formaldehyde slant column measurements during CINDI: intercomparison and analysis improvement, Atmos. Meas. Tech., 6, 167-185, https://doi.org/10.5194/amt-6-167-2013, 2013.

Formatted: Font: 10 pt, Do not check spelling or grammar

Formatted: Font: (Default) Times New Roman, 10 pt, English (United Kingdom), Do not check spelling or grammar

Formatted: Font: (Default) Times New Roman, 10 pt, English (United Kingdom), Do not check spelling or grammar

Formatted: Font: (Default) Times New Roman, 10 pt, English (United Kingdom), Do not check spelling or grammar

Formatted: Font: (Default) Times New Roman, 10 pt, English (United Kingdom), Do not check spelling or grammar

Formatted: Font: (Default) Times New Roman, 10 pt, English (United Kingdom), Do not check spelling or grammar

Formatted: edtbold, Font: 12 pt

Formatted: edtbold, Font: Times New Roman, 10 pt, Font color: Auto, Pattern: Clear

Formatted: edtbold, Font: 12 pt

Piters, A. J. M., Boersma, K. F., Kroon, M., Hains, J. C., Van Roozendael, M., Wittrock, F., Abuhassan, N., Adams, C., Akrami, M., Allaart, M. A. F., Apituley, A., Beirle, S., Bergwerff, J. B., Berkhout, A. J. C., Brunner, D., Cede, A., Chong, J., Clémer, K., Fayt, C., Frieß, U., Gast, L. F. L., Gil-Ojeda, M., Goutail, F., Graves, R., Griesfeller, A., Großmann, K., Hemerijckx, G., Hendrick, F., Henzing, B., Herman, J., Hermans, C., Hoexum, M., van der Hoff, G. R., Irie, H., Johnston, P. V., Kanaya, Y., Kim, Y. J., Klein Baltink, H., Kreher, K., de Leeuw, G., Leigh, R., Merlaud, A., Moerman, M. M., Monks, P. S., Mount, G. H., Navarro-Comas, M., Oetjen, H., Pazmino, A., Perez-Camacho, M., Peters, E., du Piesanie, A., Pinardi, G., Puentedura, O., Richter, A., Roscoe, H. K., Schönhardt, A., Schwarzenbach, B., Shaiganfar, R., Sluis, W., Spinei, E., Stolk, A. P., Strong, K., Swart, D. P. J., Takashima, H., Vlemmix, T., Vrekoussis, M., Wagner, T., Whyte, C., Wilson, K. M., Yela, M., Yilmaz, S., Zieger, P., and Zhou, Y.: The Cabauw Intercomparison campaign for Nitrogen Dioxide measuring Instruments (CINDI): design, execution, and early results, Atmos. Meas. Tech., 5, 457–485, doi:10.5194/amt-5-457-2012, 2012.

Platt, U., Perner, D., and Patz, H. W.: Simultaneous Measurement of Atmospheric CH2O, O3, and NO2 by Differential Optical Absorption, J. Geophys. Res., 84, 6329–6335, 1979.

Pommereau, J.-P. and Goutail, F.: O_3 and NO_2 ground-based measurements by visible spectrometry during Arctic winter and spring 1988, Geophys. Res. Lett., 15, 891–894, 1988.

Prados-Roman, C., Gómez-Martín, L., Puentedura, O., Navarro-Comas, M., Iglesias, J., de Migo, J. R., Pérez, M., Ochoa, H., Barlasina, M. E., Carbajal, G. and Yela., M.: Reactive bromine in the low troposphere of Antarctica: estimations at two research sites, Atmos. Chem. Phys., 18, 8549-8570, https://doi.org/10.5194/acp-18-8549-2018, 2018.

Puķīte, J., Kühl, S., Deutschmann, T., Platt, U., and Wagner, T.: Extending differential optical absorption spectroscopy for limb measurements in the UV, Atmos. Meas. Tech., 3, 631–653, https://doi.org/10.5194/amt-3-631-2010, 2010.

Richter, A., Eisinger, M., Ladstätter-Weißenmayer, A.,Wittrock, F., and Burrows, J. P.: DOAS zenith-sky observations: 2.Seasonal variations of BrO over Bremen (53°N) 1994–1995, J. Atmos.Chem., 32, 83–99, 1999.

Roscoe, H. K., Johnston, P. V, Van Roozendael, M., Richter, A., Sarkissian, A., Roscoe, J., Preston, K. E., Lambert, J.-C., Hermans, C., Decuyper, W., Dzienus, S., Winterrath, T., Burrows, J. B., Goutail, F., Pommereau, J.-P., D'Almeida, E., Hottier, J., Coureul, C., Didier, R., Pundt, I., Bartlett, L. M., McElroy, C. T., Kerr, J. E., Elokhov, A., Giovanelli, G., Ravegnani, F., Premuda, M., Kostadinov, I., Erle, F., Wagner, T., Pfeilsticker, K., Kenntner, M., Marquard, L. C., Gil, M., Puentedura, O., Yela, M., Arlander, D. W., Kastad Hoiskar, B. A., Tellefsen, C. W., Karlsen Tornkvist, K., Heese, B., Jones, R. L., Aliwell, S. R., Freshwater, R. A., Slant Column Measurements of O_3 and NO_2 During the NDSC Intercomparison of Zenith-Sky UV-Visible Spectrometers in June 1996. J. Atmos. Chem., 32, 281–314, 1999.

Roscoe, H. K., Van Roozendael, M., Fayt, C., du Piesanie, A., Abuhassan, N., Adams, C., Akrami, M., Cede, A., Chong, J., Clémer, K., Friess, U., Gil Ojeda, M., Goutail, F., Graves, R., Griesfeller, A., Grossmann, K., 5 Hemerijckx, G., Hendrick, F., Herman, J., Hermans, C., Irie, H., Johnston, P. V., Kanaya, Y., Kreher, K., Leigh, R., Merlaud, A., Mount, G. H., Navarro, M., Oetjen, H., Pazmino, A., Perez-Camacho, M., Peters, E., Pinardi, G., Puentedura, O., Richter, A., Schönhardt, A., Shaiganfar, R., Spinei, E., Strong, K., Takashima, H., Vlemmix, T., Vrekoussis, M., Wagner, T., Wittrock, F., Yela, M., Yilmaz, S., Boersma, F., Hains, J., Kroon, M., Piters, A., and Kim, Y. J.: Intercomparison of slant column measurements of NO_2 and O_4 by MAX-DOAS and zenith-sky UV and visible spectrometers, Atmos. Meas. Tech., 3, 1629–1646, doi:10.5194/amt-3-1629-2010, 2010.

Rothman, L. S., Gordon, I. E., Barber, R. J., Dothe, H., Gamache, R. R., Goldman, A., Perevalov, V. I., Tashkun, S. A., and Tennyson, J.: HITEMP, the high-temperature molecular spectroscopic database, J. Quant. Spectrosc. Ra., 111, 2139–2150, https://doi.org/10.1016/j.jqsrt.2010.05.001, 2010.

Serdyuchenko, A., Gorshelev, V., Weber, M., Chehade, W., and Burrows, J.: High spectral resolution ozone absorption cross-sections, Atmospheric Measurement Techniques, 7, 1867–8548, 2014.

Formatted: Font: Times New Roman, 10 pt, Font color: Auto, Do not check spelling or grammar, Pattern: Clear

Formatted: Font: 10 pt, Do not check spelling or grammar

Formatted: Font: 10 pt, Do not check spelling or grammar

Sinreich, R., Coburn, S., Dix, B., and Volkamer, R.: Ship-based detection of glyoxal over the remote tropical Pacific Ocean, Atmos. Chem. Phys., 10, 11359-11371, https://doi.org/10.5194/acp-10-11359-2010, 2010.

Sluis, W. W., Allaart, M. A. F., Piters, A. J. M., and Gast, L. F. L.: The development of a nitrogen dioxide sonde, Atmos. Meas. Tech., 3, 1753–1762, https://doi.org/10.5194/amt-3-1753-2010, 2010.

Solomon, S., A. L. Schmeltekopf, and R. W. Sanders, On the interpretation of zenith sky absorption-measurements, J. Geophys. Res., 92, 8311–8319, 1987.

Thalman, R. and Volkamer, R.: Temperature dependent absorption cross-sections of O 2–O 2 collision pairs between 340 and 630 nm and at atmospherically relevant pressure, Physical chemistry chemical physics, 15, 15 371–15 381, 2013.

Tirpitz, J.-L, Frieß, U., Hendrick, F., Alberti, C., Allaart, M., Apituley, A., Bais, A. Beirle, S., Berkhout, S., Bognar, K., Bösch, T., Bruchkouski, I., Cede, A., Chan, K.L., den Hoed, M., Donner, S., Drosoglou, T., Fayt, C., Friedrich, M.M., Frumau, A., Gast, L., Gielen, C., Gomez-Martín, L., Hao, N., Hensen, A., Henzing, B., Hermans, C., Jin, J., Kreher, K., Kuhn, J., Lampel, J., Li, A., Liu, C., Liu, H., Ma, J., Merlaud, A., Peters, E., Pinardi, G., Piters, A., Platt, U., Puentedura, O., Richter, A., Schmitt, S., Spinei, E., Stein Zweers, D., Strong, K., Swart, D., Tack, F., Tiefengraber, M., van der Hoff, R., van Roozendael, M., Vlemmix, T., Vonk, J., Wagner, T., Wang, Y., Wang, Z., Wenig, M., Wiegner, M., Wittrock, F., Xie, P., Xing, C., Xu, J., Yela, M., Zhang, C., and Zhao, X.: et al., Intercomparison of MAX-DOAS vVertical pProfile rRetrieval aAlgorithms: studies on field data from the CINDI-2 campaignField measurements during the CINDI-2 campaign, to be submitted to AMT, (2019).

Vandaele, A. C., Hermans, C., Simon, P. C., Carleer, M., Colin, R., Fally, S., Merienne, M.-F., Jenouvrier, A., and Coquart, B.: Measurements of the NO2 absorption cross-section from 42 000 cm-1 to 10 000 cm-1 (238–1000 nm) at 220 K and 294 K, Journal of Quantitative Spectroscopy and Radiative Transfer, 59, 171–184, 1998.

Vandaele, A. C., et al.: An intercomparison campaign of ground-based UV-visible measurements of NO_2, BrO, and OClO slant columns: Methods of analysis and results for NO_2, Journal of Geophysical Research, 110(D8), D08305, https://doi.org/10.1029/2004JD005423, 2005.

Vlemmix, T., Hendrick, F., Pinardi, G., De Smedt, I., Fayt, C., Hermans, C., Piters, A., Wang, P., Levelt, P., and Van Roozendael, M.: MAX-DOAS observations of aerosols, formaldehyde and nitrogen dioxide in the Beijing area: comparison of two profile retrieval approaches, Atmos. Meas. Tech., 8, 941–963, doi:10.5194/amt-8-941-2015, 2015.

Volten, H., E. J. Brinksma, A. J. C. Berkhout, J. Hains, J. B. Bergwerff, G. R. Van der Hoff, A. Apituley, R. J. Dirksen, S. Calabretta-Jongen, and D. P. J. Swart, NO2 lidar profile measurements for satellite interpretation and validation, J. Geophys. Res., 114, D24301, doi:10.1029/2009JD012441, 2009.

Wagner, T., Dix, B., von Friedeburg, C., Frieß, U., Sanghavi, S., Sinreich, R., and Platt, U.: MAX-DOAS O_4 measurements: a new technique to derive information on atmospheric aerosols – principles and information content, J. Geophys. Res., 109, D22205, doi:10.1029/2004JD004904, 2004.

Wang, Y., Beirle, S., Lampel, J., Koukouli, M., De Smedt, I., Theys, N., Li, A., Wu, D., Xie, P., Liu, C., Van Roozendael, M., Stavrakou, T., Müller, J.-F., and Wagner, T.: Validation of OMI, GOME-2A and GOME-2B tropospheric NO_2, SO_2 and HCHO products using MAX-DOAS observations from 2011 to 2014 in Wuxi, China: investigation of the effects of priori profiles and aerosols on the satellite products, Atmos. Chem. Phys., 17, 5007-5033, https://doi.org/10.5194/acp-17-5007-2017, 2017a.

Wang, Y., Lampel, J., Xie, P., Beirle, S., Li, A., Wu, D., and Wagner, T.: Ground-based MAX-DOAS observations of tropospheric aerosols, NO_2, SO_2 and HCHO in Wuxi, China, from 2011 to 2014, Atmos. Chem. Phys., 17, 2189-2215, https://doi.org/10.5194/acp-17-2189-2017, 2017b.

Formatted: Font: Times New Roman, 10 pt, Font color: Auto, Do not check spelling or grammar, Pattern: Clear

Formatted: Hyperlink, Font: Times New Roman, 10 pt, Font color: Auto, Do not check spelling or grammar, Pattern: Clear

Formatted: Font: Times New Roman, 10 pt, Font color: Auto, Do not check spelling or grammar, Pattern: Clear

Field Code Changed

Formatted: Font: 10 pt, Do not check spelling or grammar

Formatted ...

Formatted: Font: 10 pt, Do not check spelling or grammar

Formatted: Font: 10 pt, Do not check spelling or grammar

Wang, Y., Beirle, S., Hendrick, F., Hilboll, A., Jin, J., Kyuberis, A. A., Lampel, J., Li, A., Luo, Y., Lodi, L., Ma, J., Navarro, M., Ortega, I., Peters, E., Polyansky, O. L., Remmers, J., Richter, A., Puentedura, O., Van Roozendael, M., Seyler, A., Tennyson, J., Volkamer, R., Xie, P., Zobov, N. F., and Wagner, T.: MAX-DOAS measurements of HONO slant column densities during the MAD-CAT campaign: inter-comparison, sensitivity studies on spectral analysis settings, and error budget, Atmos. Meas. Tech., 10, 3719-3742, https://doi.org/10.5194/amt-10-3719-2017, 2017c.

Wang, Y., J. Puķīte, T. Wagner, S. Donner, S. Beirle, A. Hilboll, M. Vrekoussis, A. Richter, A. Apituley, A. Piters, M. Allaart, H. Eskes, A. Frumau, M. Van Roozendael, J. Lampel, U. Platt, S. Schmitt, D. Swart, and J. Vonk, Vertical profiles of tropospheric ozone from MAX-DOAS measurements during the CINDI-2 campaign: Part 1— Development of a new retrieval algorithm. Journal of Geophysical Research: Atmospheres, 123. https://doi. org/10.1029/2018JD028647, 2018.

Wang, Y., Apituley, A., ~~Kumar, V., Borovski, A.,~~ Bais, A., Beirle, S., Benavent, N., Borovski, A., Bruchkouski, I., Chan, K.L., Donner, S., Drosoglou, T., Finkenzeller, H., Friedrich, M.M., ~~Finkenzeller, H.,~~ Frieß~~s~~, U., Garcia-Nieto, D., Gómez-Martín, L., ~~Hilboll, A.,~~ Hendrick, F., Hilboll, A., ~~Bruchkouski, I.,~~ Jin, J., Johnston, P., ~~Kreher, K.,~~ Koenig, T.K., Kreher, K., Kumar, V., Kyuberis, A., Lampel, J., Liu, C., Liu, H.~~, Lodi, L.~~, ~~Lampel, J., Saiz López, A.,~~ Ma, J.~~, Puentedura Rodríguez, O.~~, Polyansky, O.L., Postylyakov, O., ~~Polyansky, O.L.,~~ Querel, R., Saiz-López, A., ~~Van Roozendael, M., Volkamer, R.M.,~~ Schmitt, S., Tian, X., Tirpitz, J.L., ~~Tian, X.,~~ Van Roozendael, M., Volkamer, R., Wang, Z.~~, Xing, C.~~, Xie, P., Xing, C., Xu, J., Yela, M., Zhang, C., and Wagner, T.: Inter-comparison of MAX-DOAS measurements of tropospheric HONO slant column densities and vertical profiles during the CINDI-2 Campaign, ~~to be~~ submitted to Atmos. Meas. Tech., 2019.

Wittrock, F., Oetjen, H., Richter, A., Fietkau, S., Medeke, T., Rozanov, A., and Burrows, J. P.: MAX-DOAS measurements of atmospheric trace gases in Ny-Alesund – Radiative transfer ˚ studies and their application, Atmos. Chem. Phys., 4, 955–966, doi:10.5194/acp-4-955-2004, 2004.

Yela, M., Gil-Ojeda, M., Navarro-Comas, M., Gonzalez-Bartolomé, D., Puentedura, O., Funke, B., Iglesias, J., Rodríguez, S., García, O., Ochoa, H., and Deferrari, G.: Hemispheric asymmetry in stratospheric NO_2 trends, Atmos. Chem. Phys., 17, 13373-13389, https://doi.org/10.5194/acp-17-13373-2017, 2017.

Zieger, P., Weingartner, E., Henzing, J., Moerman, M., de Leeuw, G., Mikkilä, J., Ehn, M., Petäjä, T., Clémer, K., van Roozendael, M., Yilmaz, S., Frieß, U., Irie, H., Wagner, T., Shaiganfar, R., Beirle, S., Apituley, A., Wilson, K., and Baltensperger, U.: Comparison of ambient aerosol extinction coefficients obtained from in-situ, MAX-DOAS and LIDAR measurements at Cabauw, Atmos. Chem. Phys., 11, 2603–2624, doi:10.5194/acp-11-2603-2011, 2011.

Formatted: Indent: Left: 0 cm, First line: 0 cm

Formatted: Do not check spelling or grammar

Table 1: List of participating groups and corresponding instrument IDs in alphabetical order according to their acronym.

Institute	Country	Acronym	Instrument ID
Anhui Institute of Optics and Fine Mechanics	China	AIOFM	aiofm-1
A. M. Obukhov Institute of Atmospheric Physics, Russian Academy of Sciences, Moscow	Russia	AMOIAP	amoiap-2
Aristotle University of Thessaloniki	Greece	AUTH	auth-3
Royal Belgian Institute for Space Aeronomy	Belgium	BIRA-IASB	bira-4
University of Natural Resources and Life Sciences, Vienna	Austria	BOKU	boku-6
Belarusian State University	Belarus	BSU	bsu-5
Chiba University	Japan	CHIBA	chiba-9
China Meteorological Administration	China	CMA	cma-7, cma-8
Spanish National Research Council	Spain	CSIC	csic-10
University of Colorado	USA	CU-Boulder	cu-boulder-11, cu-boulder-12
Deutsches Zentrum für Luft- und Raumfahrt/ University of Science and Technology of China	Germany/ China	DLR-USTC	dlrustc-13, dlrustc-14
Indian Institute of Science Education and Research Mohali	India	IISERM	iiserm-16
National Institute for Aerospace Technology	Spain	INTA	inta-17
University of Bremen	Germany	IUP-Bremen	iupb-18, iupb-37
University of Heidelberg	Germany	IUP-Heidelberg	iuph-19
Royal Netherlands Meteorological Institute	The Netherlands	KNMI	knmi-21, knmi-22, knmi-23
Laboratoire Atmosphère, Milieux, Observations Spatiales	France	LATMOS	latmos-24, latmos-25
Ludwig-Maximilians-Universität München	Germany	LMU-MIM	lmumim-35
LuftBlick Earth Observation Technologies	Austria	Luftblick	luftblick-26, luftblick-27, luftblick-260, luftblick-270
Max Planck Institute for Chemistry, Mainz	Germany	MPIC	mpic-28
NASA Goddard Space Flight Center	USA	NASA	nasa-31, nasa-32
National Institute of Water and Atmospheric Research	New Zealand	NIWA	niwa-29, niwa-30
National University of Sciences and Technology	Pakistan	NUST	nust-33
University of Toronto	Canada	UTO	uto-36

Table 2: Overview of the main characteristics of the instruments taking part in the semi-blind intercomparison campaign. The table lists the type, specific ID and model name for each participating instrument (columns 1-3). In columns 4-5, it also specifies whether instruments could take azimuthal scans (ASc) and/or be operated in direct-sun mode (DS). The spectral range, spectral resolution and field of view (FOV) are summarized in columns 6-8. Note that the FOV given in column 8 is the value provided as part of the instrument specification which may differ from the effective FOV shown in Figure 6. Light coupling (column 9) denotes whether spectrometers were fed by means of optical fibers (F) or using a telescope or lens directly coupled to the entrance slit (D). Detector type and temperature are listed in columns 10-11.

Instrument type	Instrument ID	Instrument name	ASc	DS	Spectral range	Spectral res. (nm)	FOV (°)	Light coupl.	Detector type	Detector T (°C)
Custom-built MAX-DOAS	bira-4	2D MAX-DOAS	y	y	300-390/ 400-560	0.37/ 0.58	1.0/ 0.5	F	CCD	-50/ -50
	iupb-18	2D MAX-DOAS	y	n	305-390/ 406-579	0.5/ 0.85	1.0	F	CCD	-35/ -30
	boku-6	2D MAX-DOAS	y	n	419-553	0.8	0.8	F	CCD	-60
	cu-boulder-11	2D MAX-DOAS	y	y	325-470/ 430-680	0.7/ 1.2	0.7	F	CCD	-30
	cu-boulder-12	1D MAX-DOAS	n	n	300-465/ 380-490	0.8/ 0.5	0.7	F	CCD	-30/ 0
	inta-17	RASAS-III	y	n	420-540	0.55	1.0	F	CCD	-30
	mpic-28	Tube MAX-DOAS	n	n	305-464	0.6	0.7	F	CCD	20
	niwa-30	ACTON275 MAX-DOAS	n	n	290-363/ 400-460	0.54	0.5	F	CCD	-20
	uto-36	2D MAX-DOAS	y	y	340-560	0.75	0.62	F	CCD	-70
	auth-3	Phaethon	y	y	300-450 nm	0.4	1.0	F	CCD	5
	aiofm-1	2D MAX-DOAS	y	n	290-380 nm	0.4	0.2	F	CCD	-30
	chiba-9	CHIBA-U MAX-DOAS	n	n	310-515 nm	0.4	<1	F	CCD	room T
	csic-10	1D MAX-DOAS	n	n	300-500 nm	0.5	0.7	F	CCD	-70
	amoiap-2	2-port DOAS	n	n	315-385/ 395-465/ 420-490 nm	0.4	0.3	F	CCD	-40
	bsu-5	MARSB	n	n	300-500 nm	0.4	0.2-1.0	D	CCD	-40
	iupb-37	Imaging-DOAS	y	n	420-500 nm	0.8	1.2	F	CCD	-30
Pandora	knmi-23	Pandora-1S	y	y	290-530	0.6	1.5	F	CCD	20
	luftblick-26	Pandora-2S	y	y	280-540	0.6	1.5	F	CCD	20
	luftblick-260	Pandora-2S	y	y	380-900	1.1	1.5	F	CCD	20
	luftblick-27	Pandora-2S	y	y	280-540	0.6	1.5	F	CCD	20
	luftblick-270	Pandora-2S	y	y	380-900	1.1	1.5	F	CCD	20
	nasa-31	Pandora-1S	y	y	280-540	0.6	1.6	F	CCD	20
	nasa-32	Pandora-1S	y	y	280-540	0.6	1.6	F	CCD	20
EnviMes	iuph-19	2D EnviMes	y	y	300-460/ 440-580	0.6/ 0.5	<0.5	F	CCD	20

	dlrustc-13	1D EnviMes	n	n	300-460/ 450-600	0.6/ 0.6	0.4	F	CCD	20
	dlrustc-14	1D EnviMes	n	n	300-460/ 450-600	0.6/ 0.6	0.4	F	CCD	20
	niwa-29	1D EnviMes	n	n	305-460/ 410-550	0.6	<0.5	F	CCD	20
	lmumim-35	2D EnviMes	y	n	300-460/ 450-600	0.6/ 0.9	0.4	F	CCD	20
Mini-DOAS Hoffmann GmbH	cma-7	Mini-DOAS-UV	n	n	300-450	0.7	0.8	F	LinArr	room T
	cma-8	Mini-DOAS-Vis	n	n	400-710	1.6	0.8	F	LinArr	room T
	iiserm-16	Mini-DOAS-UV	n	n	316-466	0.7	0.7	F	CCD	-10.4
	knmi-21	Mini-DOAS-UV	n	n	290-443	0.6	0.45	F	LinArr	-5
	knmi-22	Mini-DOAS-Vis	n	n	400-600	0.5	0.4	F	LinArr	-5
	nust-33	Mini-DOAS-UV	n	n	320-465	0.7	1.2	F	CCD	room T
SAOZ	latmos-24	SAOZ	n	n	270-640 nm	1.3	20	D	LinArr	ambient T + dT
	latmos-25	Mini-SAOZ	n	n	270-820 nm	0.7	8	F	CCD	room T

Table 3: Overview of analysis software used by each of the participating institutes.

Data analysis software	Institute acronym
QDOAS	AUTH, BIRA-IASB, CSIC, CU-Boulder, LMU-MIM
QDOAS & WinDOAS	AIOFM, NUST
QDOAS & in-house developed software	UTO
DOASIS	DLR-USTC, IUP-Heidelberg
DOASIS & WinDOAS	IISERM,
DOASIS & in-house developed software (STRATO)	NIWA
WinDOAS	CMA, MPIC
WinDOAS & in-house developed software	BSU
Blick Software Suite	LuftBlick, NASA
Blick Software Suite & in-house developed software	KNMI
NLIN	BOKU, IUP-Bremen
LANA	INTA
SAOZ SAM v5.9 & Mini SAOZ in-house developed software	LATMOS
JM2 (Japanese MAX-DOAS profile retrieval algorithm, version 2)	CHIBA
Andor Solis & in-house developed software	AMOIAP

Table 4: Data products included in the semi-blind intercomparison exercise and wavelength intervals selected for the analysis. Performance limits on bias (deviation from unity slope), offset and RMS of dSCD linear regressions are also listed for each of the eight data products.

Data product	Spectral interval (nm)	Bias (%)	Offset (molec/cm^2)	RMS (molec/cm^2)
NO2vis	425 – 490	5	1.5 10^{15}	8.0 10^{15}
NO2visSmall	411 – 445	5	1.5 10^{15}	8.0 10^{15}
NO2uv	338 – 370	6	2.0 10^{15}	1.0 10^{16}
O4vis*	425 – 490	5	0.7 10^{42}	3.0 10^{42}
O4uv*	338 – 370	6	0.8 10^{42}	3.0 10^{42}
HCHO	336.5 – 359	10	5.0 10^{15}	1.0 10^{16}
O3vis	450 – 520	4	0.2 10^{18}	1.0 10^{18}
O3uv	320 – 340	4	1.0 10^{18}	4.0 10^{18}

* Note: the units for O_4 are molec^2/cm^5

Table 5: Mean relative difference from the reference and standard deviation (in percent) for all participating instruments and MAX-DOAS data products (apart from ozone). The last column provides the values for HCHO when only considering measurements made during the first 4 days of the campaign period (12-15 Sep. 2016).

Instrument ID	NO2vis	NO2visSmall	NO2uv	O4vis	O4uv	HCHO	HCHO (12-15/09)
bira-4	-0.0 (2.0)	0.7 (2.0)	1.7 (2.1)	0.6 (2.0)	1.0 (1.7)	5.2 (6.9)	1.0 (2.9)
iupb-18	-2.2 (2.7)	-1.2 (2.4)	0.1 (2.2)	-0.7 (2.2)	-1.2 (2.5)	-2.9 (6.4)	0.0 (3.6)
boku-6	0.7 (2.6)	--	--	0.3 (2.0)	--	--	--
cu-boulder-11	0.9 (4.9)	-1.8 (4.3)	-3.7 (5.1)	-0.7 (3.2)	-0.4 (3.3)	-19.9 (32.0)	-7.1 (11.7)
cu-boulder-12	-3.9 (1.5)	-0.6 (1.6)	-0.6 (2.9)	-0.7 (1.6)	-0.2 (4.7)	--	--
inta-17	0.7 (2.6)	--	--	-0.2 (2.6)	--	--	--
mpic-28	--	1.4 (2.1)	3.4 (3.3)	--	0.9 (2.2)	-0.2 (14.5)	-4.0 (5.4)
niwa-30	-2.6 (2.3)	--	-0.2 (10.0)	-0.1 (2.5)	1.1 (6.5)	-24.5 (36.1)	-11.5 (7.7)
uto-36	-6.4 (3.2)	-5.0 (3.1)	--	-3.6 (3.1)	--	--	--
auth-3	--	-2.4 (3.4)	-3.4 (8.2)	--	0.5 (8.5)	7.9 (62.1)	16.3 (26.3)
aiofm-1	--	--	-15.8 (5.3)	--	-7.3 (5.1)	18.2 (54.7)	-0.2 (16.3)
chiba-9	-2.3 (3.4)	-1.3 (3.6)	1.0 (4.0)	6.5 (6.8)	10.6 (4.1)	0.1 (24.0)	-2.6 (13.3)
csic-10	--	--	-17.7 (12.5)	--	0.5 (8.4)	-131.5 (164.8)	--
amoiap-2	-7.3 (3.3)	-7.9 (3.2)	-6.3 (9.9)	-0.8 (8.5)	-10.7 (8.0)	-70.5 (80.0)	-31.7 (12.1)
bsu-5	--	--	-6.5 (6.5)	--	-5.0 (5.1)	33.3 (90.5)	13.2 (22.9)
iupb-37	3.3 (6.8)	--	--	-4.2 (7.0)	--	--	--
knmi-23	1.9 (2.3)	2.8 (2.3)	3.3 (6.8)	1.3 (1.5)	4.2 (4.2)	-12.3 (47.1)	-12.2 (17.9)
luftblick-26	-0.4 (1.4)	-0.4 (1.3)	0.6 (2.6)	-0.0 (1.3)	0.6 (3.0)	-17.6 (32.5)	-11.9 (16.7)
luftblick-260	3.4 (2.1)	2.8 (2.3)	--	-0.3 (1.5)	--	--	--
luftblick-27	-1.3 (1.8)	-1.0 (1.6)	-0.5 (2.8)	0.8 (1.4)	-1.0 (2.7)	-12.6 (28.0)	-9.0 (13.4)
luftblick-270	-0.5 (1.7)	0.7 (2.0)	--	-0.6 (1.3)	--	--	--
nasa-31	1.1 (6.2)	1.0 (5.9)	1.2 (5.7)	-0.1 (4.2)	-1.0 (5.1)	-21.5 (38.0)	-11.4 (15.7)
nasa-32	0.5 (1.7)	0.2 (1.7)	-0.2 (3.0)	1.0 (1.5)	-0.5 (3.1)	-10.6 (30.6)	-7.4 (9.6)
iuph-19	--	-2.1 (3.0)	-1.0 (3.2)	--	-1.2 (3.0)	-32.1 (28.8)	-14.2 (7.9)
dlrustc-13	-3.9 (3.7)	-3.1 (3.5)	-4.2 (3.8)	-3.1 (2.4)	0.8 (2.3)	-42.6 (42.0)	-14.1 (8.1)
dlrustc-14	-1.3 (3.0)	-0.4 (2.7)	-0.1 (2.7)	-1.5 (2.3)	1.7 (2.0)	-57.5 (60.0)	-17.7 (9.9)
niwa-29	-6.5 (12.0)	-5.1 (13.3)	-4.0 (14.8)	-0.2 (4.0)	3.8 (6.2)	-10.5 (15.8)	--
lmumim-35	2.1 (4.4)	1.2 (4.1)	-0.4 (3.7)	7.1 (7.8)	-3.9 (3.0)	-9.0 (22.5)	-8.5 (8.3)
cma-7	--	-1.5 (5.4)	-2.1 (5.4)	--	1.7 (5.4)	-26.2 (35.5)	-20.7 (13.8)
cma-8	-4.0 (4.1)	--	--	0.7 (7.8)	--	--	--
iiserm-16	--	1.2 (5.0)	-0.1 (8.8)	--	8.7 (7.0)	-111.5 (80.1)	-59.1 (24.1)
knmi-21	--	--	-4.6 (5.0)	--	2.7 (4.4)	4.9 (60.0)	0.4 (17.6)
knmi-22	-1.5 (4.9)	--	--	-2.5 (4.6)	--	--	--
nust-33	--	6.7 (6.1)	4.3 (9.2)	--	-22.6 (6.8)	48.3 (73.7)	--
latmos-24	--	--	--	--	--	--	--
latmos-25	--	--	--	--	--	--	--
Median from all instruments	**-0.9 (2.8)**	**-0.5 (3.1)**	**-0.4 (5.1)**	**-0.2 (2.4)**	**0.5 (4.3)**	**-12.3 (36.1)**	**-8.7 (12.7)**

Table 6: Mean relative difference from the reference and standard deviation (in percent) for all participating instruments and zenith-sky DOAS data products.

Instrument ID	NO2vis	NO2visSmall	NO2uv	O3vis
bira-4	0.4 (1.0)	0.5 (1.2)	0.9 (2.4)	0.2 (1.0)
iupb-18	0.8 (1.1)	0.8 (1.4)	4.1 (3.0)	0.2 (0.4)
boku-6	2.0 (1.0)	--	--	0.7 (0.7)
cu-boulder-11	3.3 (2.7)	1.3 (2.4)	-3.6 (7.8)	0.5 (1.1)
cu-boulder-12	-0.6 (2.2)	-0.2 (3.1)	-16.5 (21.5)	--
inta-17	1.4 (1.6)	--	--	-0.5 (0.7)
mpic-28	--	0.5 (3.1)	6.3 (6.1)	--
niwa-30	-0.1 (2.8)	--	1.7 (14.4)	--
uto-36	-1.0 (3.4)	-1.6 (2.8)	--	-6.7 (2.4)
auth-3	--	2.1 (3.6)	1.8 (16.5)	--
aiofm-1	--	--	-1.7 (17.5)	--
chiba-9	1.0 (6.0)	5.3 (6.3)	3.2 (16.1)	--
csic-10	--	--	-14.3 (28.1)	--
amoiap-2	0.9 (3.1)	0.0 (3.1)	13.9 (9.3)	--
bsu-5	--	--	1.8 (10.7)	--
iupb-37	4.8 (10.2)	--	--	--
knmi-23	0.3 (1.8)	1.4 (1.7)	2.6 (12.7)	-0.5 (1.4)
luftblick-26	-1.4 (1.5)	-0.2 (1.4)	-0.5 (4.5)	-1.3 (0.7)
luftblick-260	0.5 (1.2)	-0.5 (2.8)	--	-2.6 (5.1)
luftblick-27	-1.7 (1.5)	-1.7 (1.8)	-2.7 (4.7)	-0.4 (0.7)
luftblick-270	-2.5 (1.5)	-1.0 (3.5)	--	-2.5 (5.1)
nasa-31	-1.9 (2.3)	-0.3 (2.3)	6.3 (14.0)	-2.3 (1.3)
nasa-32	-1.1 (1.9)	-0.9 (2.0)	-2.6 (6.0)	-1.3 (0.9)
iuph-19	--	-1.1 (1.7)	-0.2 (4.4)	--
dlrustc-13	-0.8 (2.1)	0.4 (3.0)	-2.2 (5.2)	0.5 (1.7)
dlrustc-14	-2.6 (2.0)	-0.9 (2.1)	-1.6 (4.5)	-5.7 (2.3)
niwa-29	1.3 (6.0)	1.8 (7.9)	-5.2 (8.2)	-0.0 (3.0)
lmumim-35	-3.9 (3.2)	-5.0 (1.9)	-3.8 (4.2)	1.1 (9.7)
cma-7	--	-2.4 (5.1)	1.9 (8.5)	--
cma-8	-2.1 (3.7)	--	--	11.6 (7.4)
iiserm-16	--	4.0 (2.7)	5.6 (13.1)	--
knmi-21	--	--	-19.3 (12.4)	--
knmi-22	1.0 (4.8)	--	--	--
nust-33	--	9.0 (3.7)	22.1 (11.8)	--
latmos-24	-9.2 (6.1)	--	--	3.1 (2.7)
latmos-25	-2.5 (3.7)	--	--	1.0 (1.8)
Median from all instruments	**-0.4 (2.3)**	**-0.1 (2.7)**	**0.3 (8.9)**	**-0.2 (1.5)**

Table 7: Summary of the level of agreement obtained for dSCD measurements during CINDI-2 and typical uncertainties achieved by high quality and standard instruments for the different data products.

Data product	Median agreement level between instruments		Median dSCD fit error (molec/cm^2)	
	Bias (%)	RMS (molec/cm^2)	High quality instruments	Standard instruments
NO2vis	3	$3\ 10^{15}$	$2\ 10^{14}$	$7\ 10^{14}$
NO2visSmall	3	$3.5\ 10^{15}$	$2\ 10^{14}$	$5\ 10^{14}$
NO2uv	3	$4\ 10^{15}$	$6\ 10^{14}$	$1.6\ 10^{15}$
O4vis*	2	$1.5\ 10^{42}$	$1.5\ 10^{41}$	$3\ 10^{41}$
O4uv*	2	$1.5\ 10^{42}$	$3\ 10^{41}$	$8\ 10^{41}$
HCHO	8	$1\ 10^{16}$	$3\ 10^{15}$	$8\ 10^{15}$
O3vis	2	$6\ 10^{17}$	$3\ 10^{17}$	$3\ 10^{17}$
O3uv	4	$1.6\ 10^{17}$	$1.3\ 10^{16}$	$6\ 10^{16}$

* Note: the units for O_4 are molec^2/cm^5

Figure 1: Picture of the CINDI-2 container layout at the main campaign site showing the organisation of the MAX-DOAS instruments on two superposed rows of mobile units (similar to shipping containers)~~containers~~.

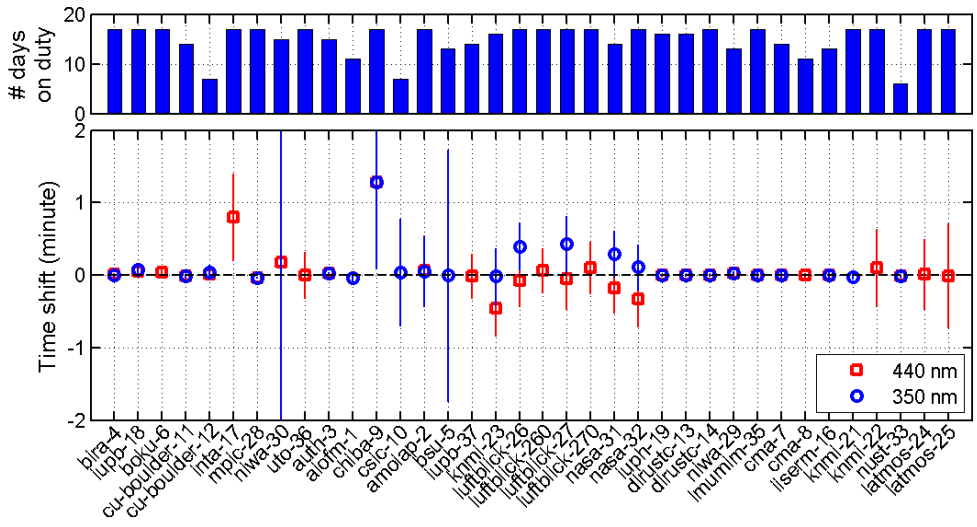

Figure 2: Top panel: The number of days when instruments were on duty during the 17-day intercomparison period. Bottom Panel: The mean and standard deviation of the time deviations (in decimal minutes) observed in the MAX-DOAS measurements as reported by each participating group with respect to the measurement schedule defined for the campaign. Note that the instruments are listed in order of how they are categorised, and this is further explained in Section 4.

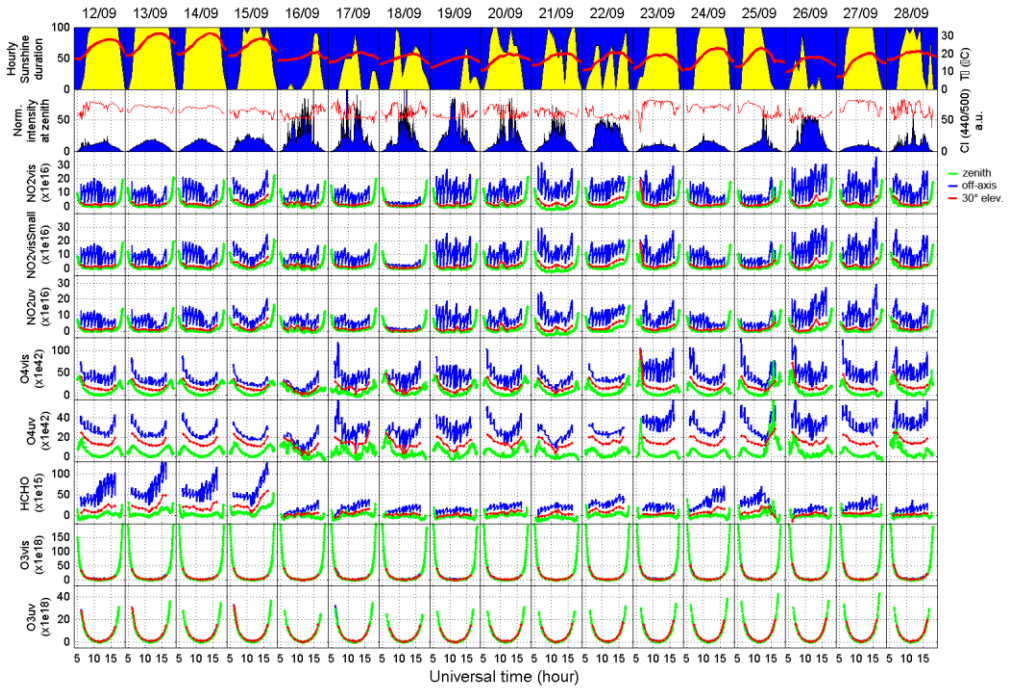

Figure 3: Hourly sunshine duration (yellow area) and temperature at the surface (red line) during the intensive campaign (topmost panel), the intensity measured in the zenith and the colour index (2nd panel from top), and the variability of the various trace gas slant column measurements performed during the semi-blind intercomparison exercise (all other panels). Slant column data measured at the main azimuth viewing direction (287°) with the IUP Bremen instrument (iupb-18) are shown. Green lines and symbols represent zenith-sky measurements, red lines and symbols off-axis data at 30° elevation, and blue lines off-axis measurements up to 15° elevation.

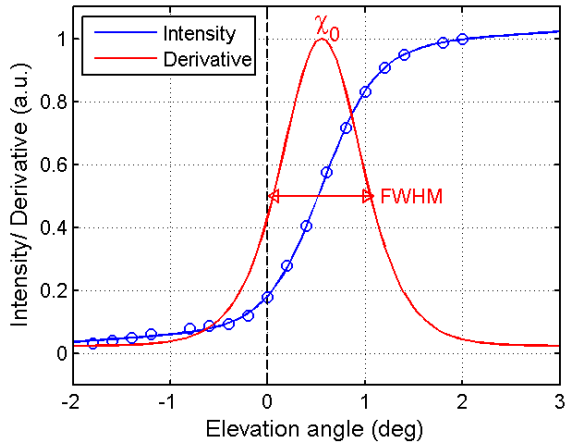

Figure 4: Horizon scans measured by IUP-Bremen on 14 September 2016 in the visible wavelength range. The blue circles display the intensity at 440 nm plotted as a function of the elevation angle reported by the instrument. Measured points are fitted by least-squares minimisation using an error function (blue line) allowing to estimate the horizon elevation (χ_0) and effective field of view (FWHM) (see Section 3.2). The corresponding Gaussian curve (analytical derivative of the fitted blue curve) is represented in red.

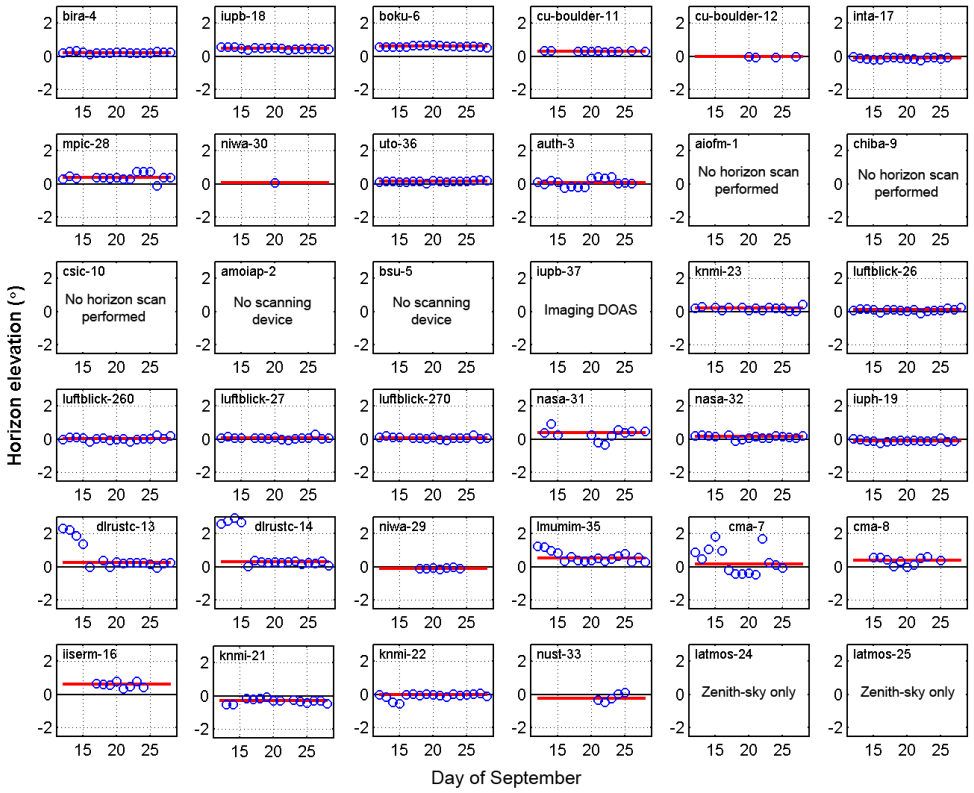

Figure 5: Time series of horizon elevation values (blue circles) derived from daily horizon scans performed with each instrument during the intercomparison period in the visible wavelength range (except for knmi-21). When no data is available for the horizon scan analysis, a short explanation is given. The red lines indicate the median values.

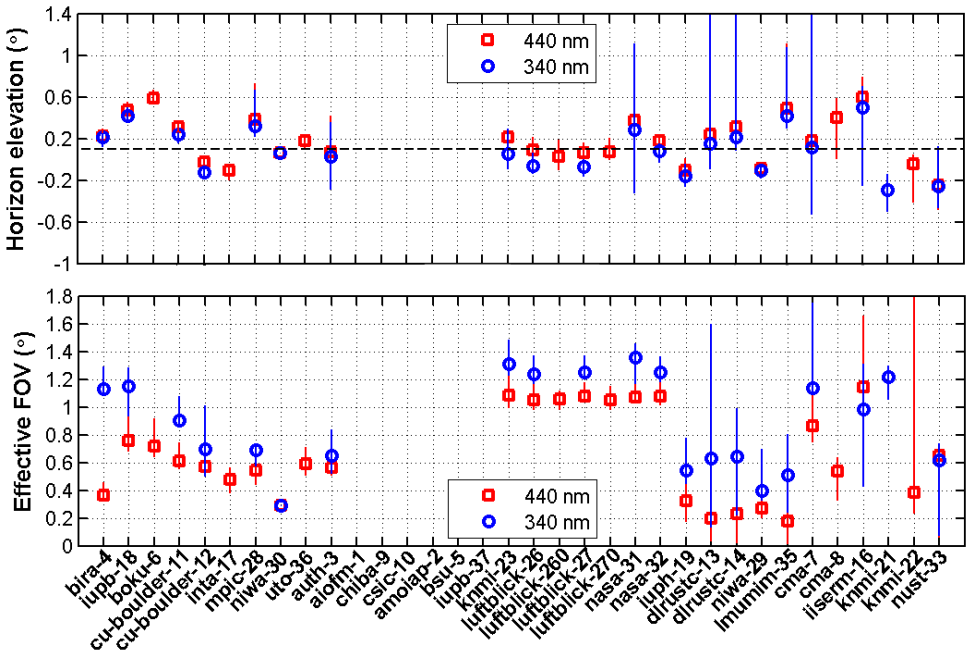

Figure 6: Summary of the average horizon elevation (top panel) and of the field of view (bottom panel), resulting from the horizon scans performed at 340nm and 440nm. Symbols represent median values and the vertical bars 10th and 90th percentiles.

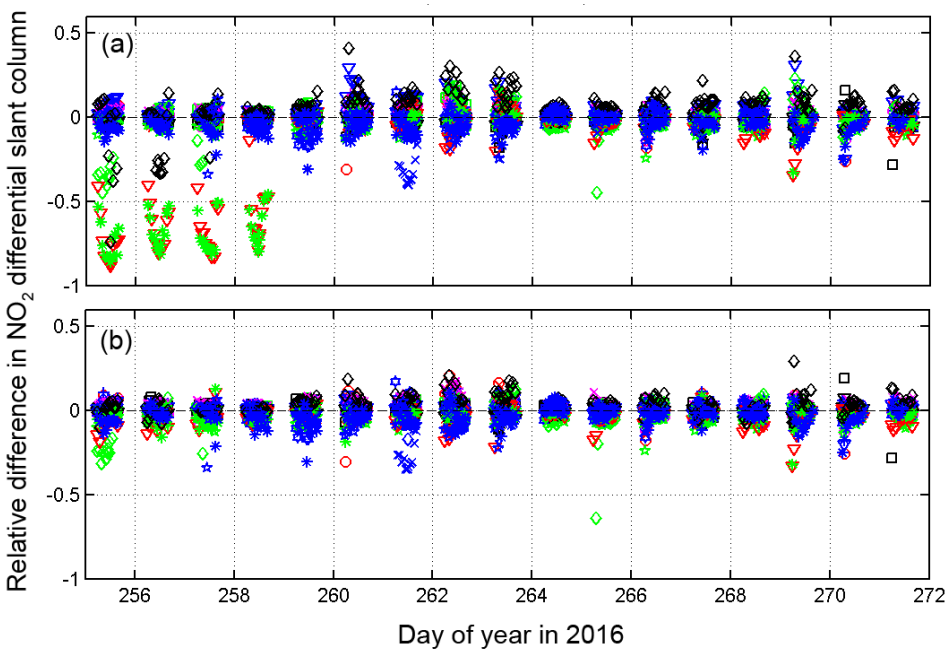
(a)
(b)
0.5
0
-0.5
-1
256
258
260
262
264
266
268
270
272
Relative difference in NO2 differential slant column
Day of year in 2016

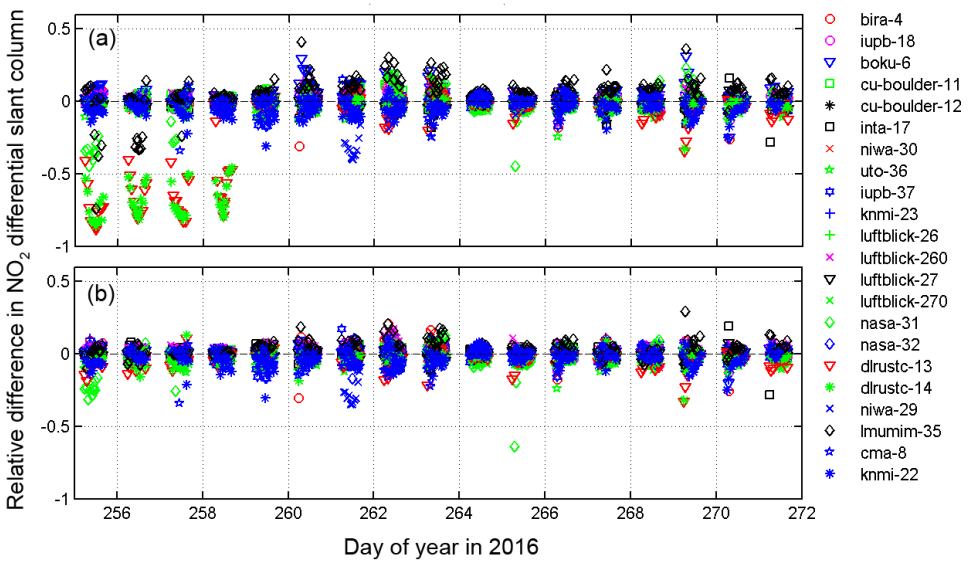
(a)
(b)
0.5
0
-0.5
-1
256
258
260
262
264
266
268
270
272
Relative difference in NO2 differential slant column
Day of year in 2016
bira-4
iupb-18
boku-6
cu-boulder-11
cu-boulder-12
inta-17
niwa-30
uto-36
iupb-37
knmi-23
luftblick-26
luftblick-260
luftblick-27
luftblick-270
nasa-31
nasa-32
dlrustc-13
dlrustc-14
niwa-29
lmumim-35
cma-8
knmi-22

Figure 7: Relative differences of NO_2 dSCDs (in the visible wavelength region) with respect to the median from all instruments measured during the whole semi-blind intercomparison phase for the 287° azimuthal direction and 1° elevation angle. (a) Results before correction for elevation offsets, (b) same results after correction for elevation offsets derived from horizon scans. Colours and symbols represent different instruments.

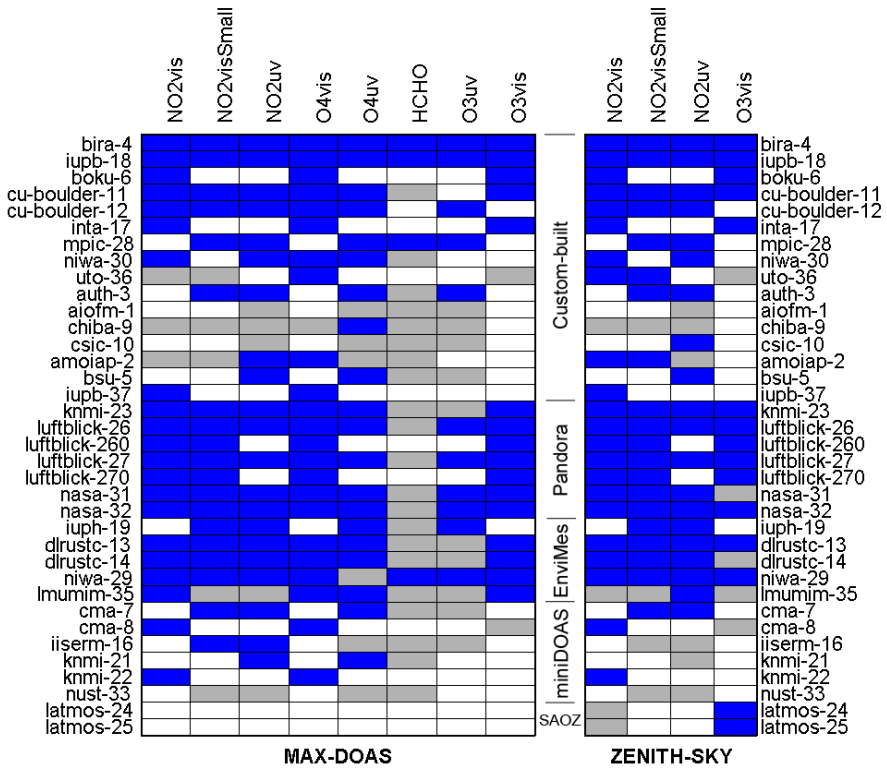

Figure 8: Instrument data sets selected to build the median MAX-DOAS reference (left panel) and zenith-sky (right panel) data sets. Blue marks the data sets included in the median while grey marks the data sets not included and white the ones not available. Note that the instruments are grouped according to their specific design as Custom-built, Pandora, EnviMes, miniDOAS or SAOZ.

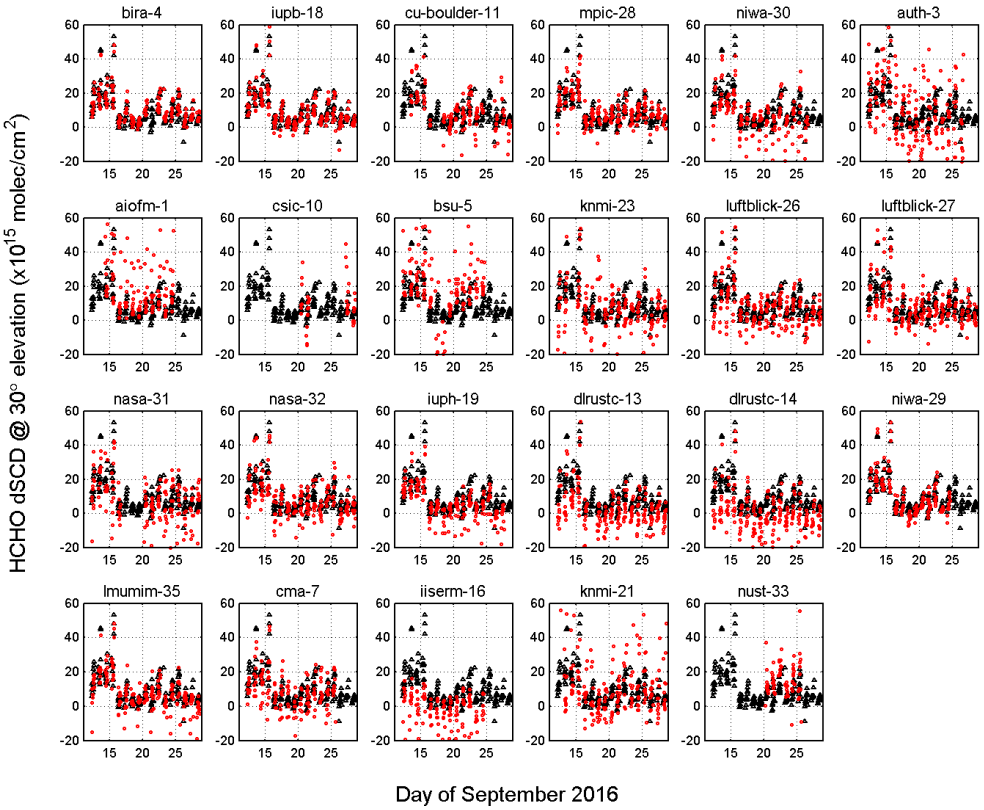

Figure 9: Comparison of HCHO dSCDs retrieved by each group at 30° elevation (red dots), and median values (black triangles). Only the four data sets (bira-4, iupb-18, mpic-28 and niwa-29) showing consistent values and a comparatively low noise level were selected for the calculation of the HCHO median.

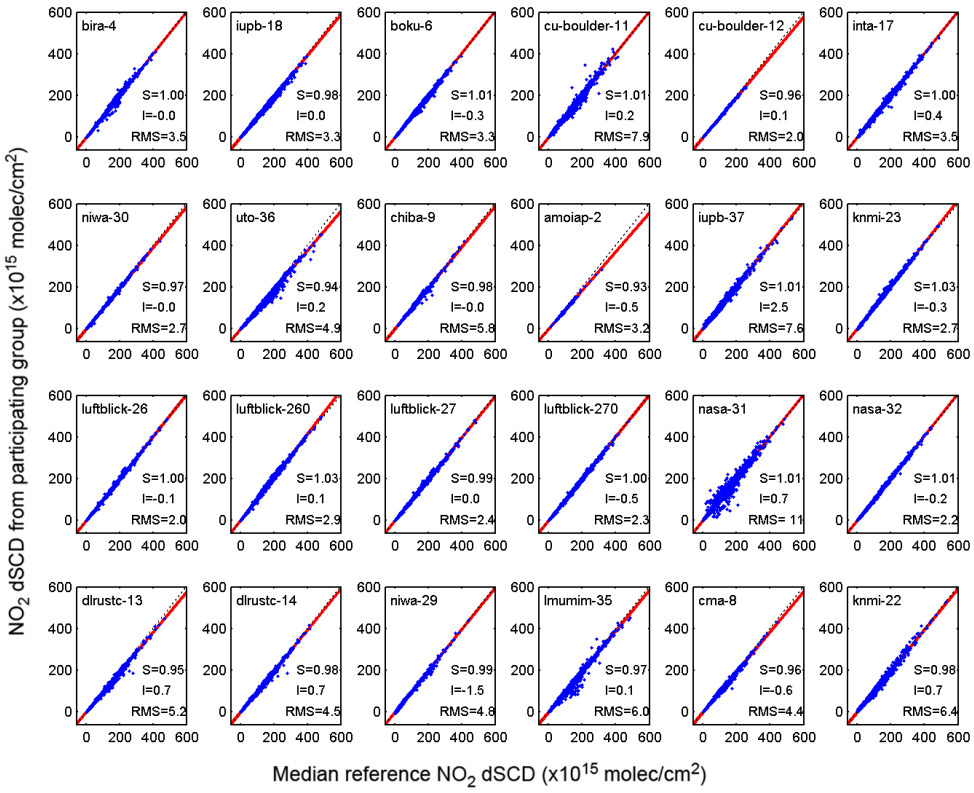

Figure 10: Regression analysis for NO_2 dSCDs (measured in the visible wavelength region) for each instrument which was measuring NO_2 in this wavelength region plotted against median values for the whole semi-blind phase, including all viewing and azimuth angles (blue crosses). The linear regression line is displayed as red line, the 1-to-1 line as a reference as dotted line. Instruments are identified with their affiliation and instrument ID number. S is the slope of the regression, I the intercept and RMS the root-mean-square of the regression residuals.

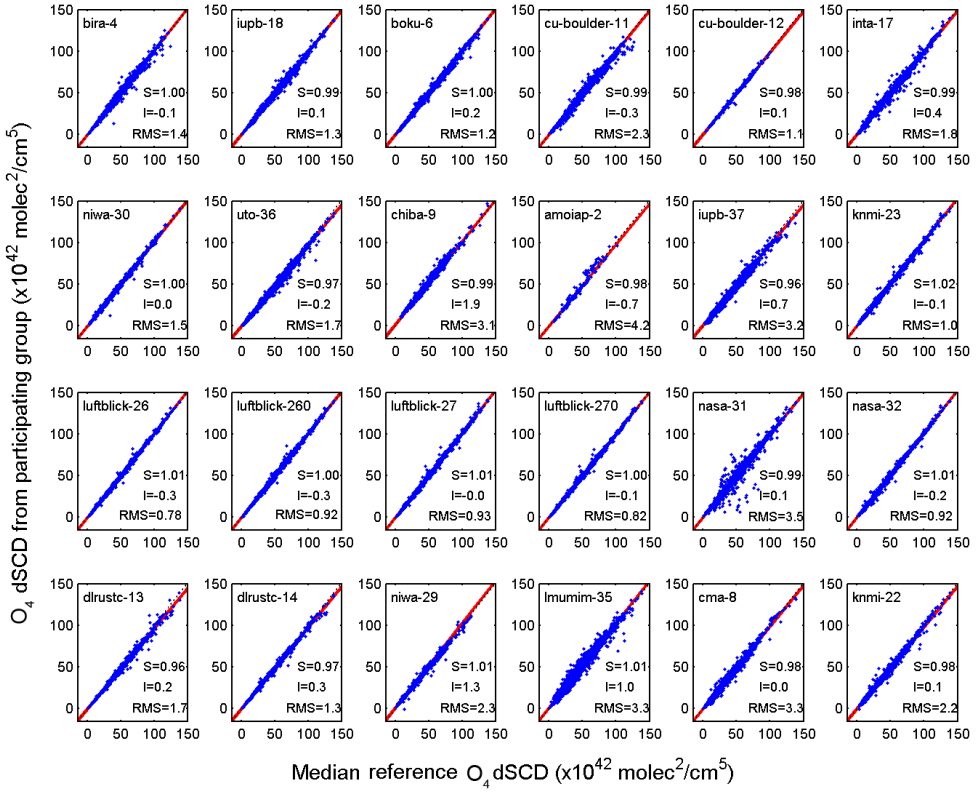

Figure 11: Same as [Figure 10]

~~Figure 10~~ **but for O_4 dSCDs measured in the visible wavelength range.**

Formatted: Font: 9 pt

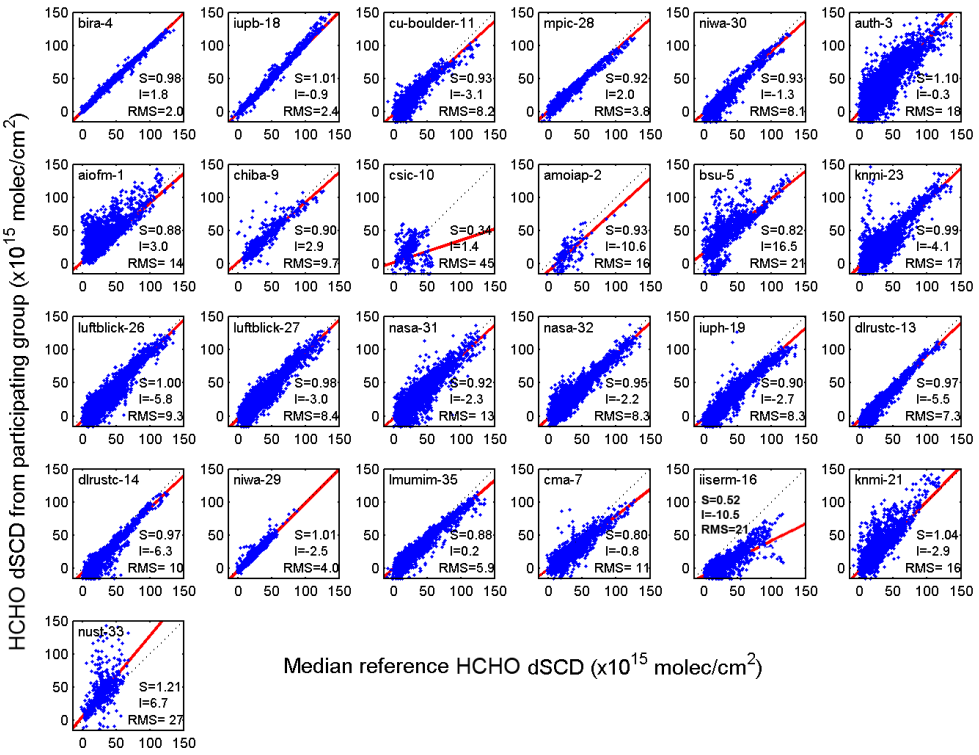

Figure 12: Same as Figure 10~~Figure 10~~ but for HCHO dSCDs.

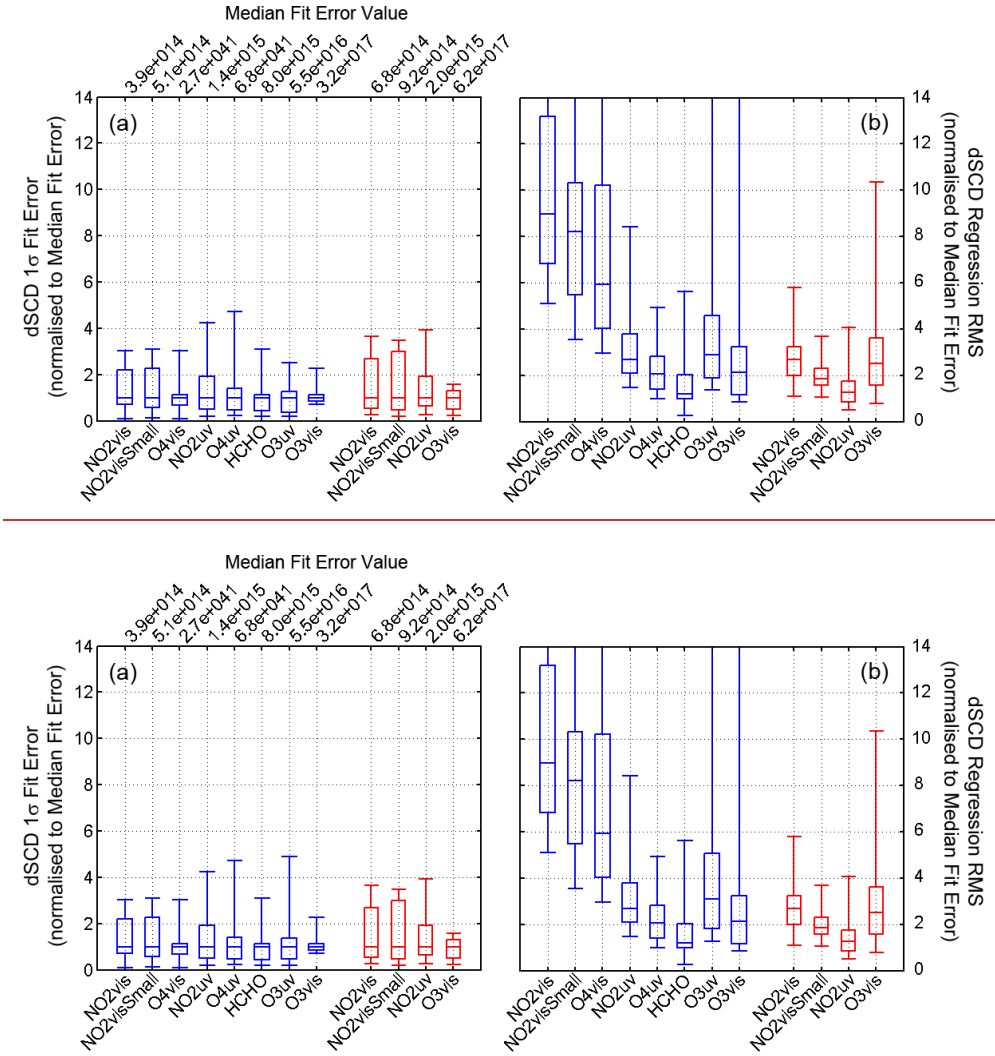

Figure 13: (a) Box-and-whisker plot of the 1 sigma fit error of the dSCDs for the 12 data products, for all instruments and for all elevation angles. MAX-DOAS products are represented in blue and zenith-sky twilight in red. (b) Box-and-whisker plot of the RMS from dSCD regression analyses, again for the 12 data products under investigation.

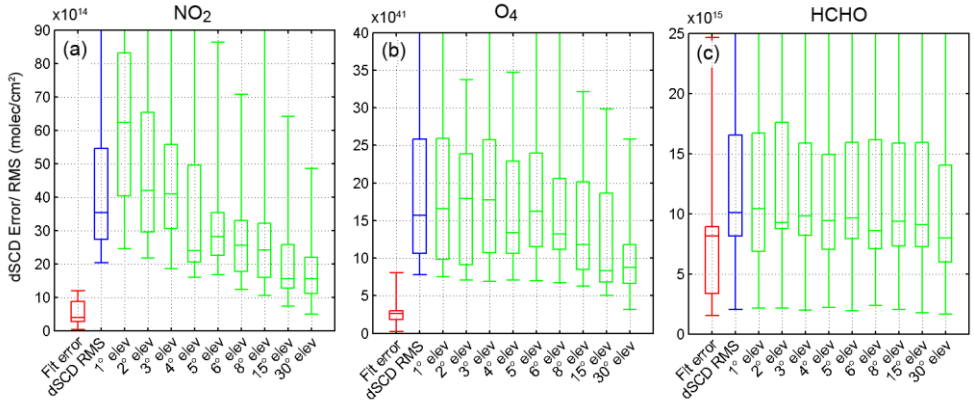

Figure 14: (a) Box-and-whisker plot of the 1 sigma dSCD fit error (red), the regression RMS for all elevation angles (blue) and RMS from dSCD regression analyses sorted as a function of the elevation angle (green) for NO_2 in the visible wavelength range. (b) Same as (a) but for O_4 (visible). (c) Same as (a) but for HCHO.

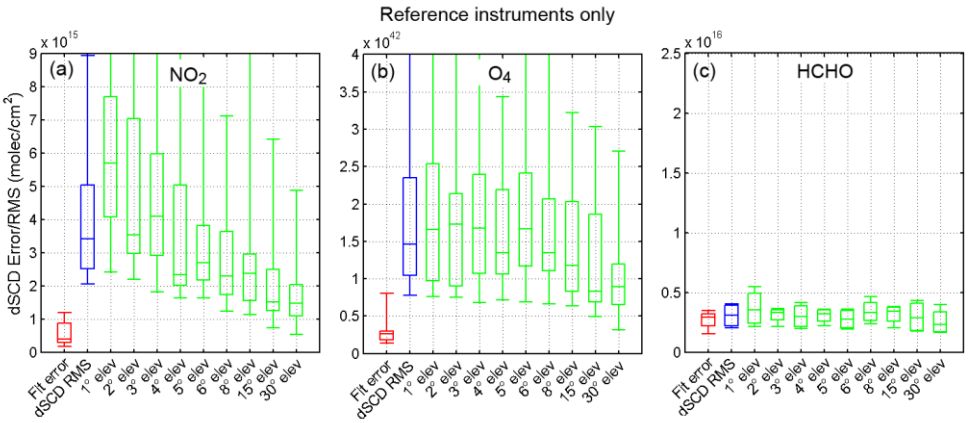

Figure 15: same as Figure 14~~Figure 14~~, but for reference instruments only.

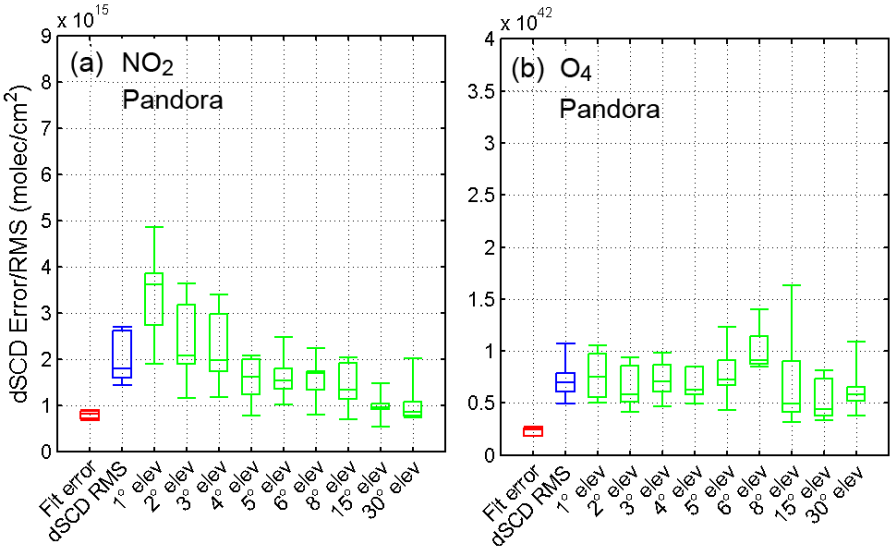

Figure 16: same as Figure 14~~Figure 14~~, but for Pandora instruments only.

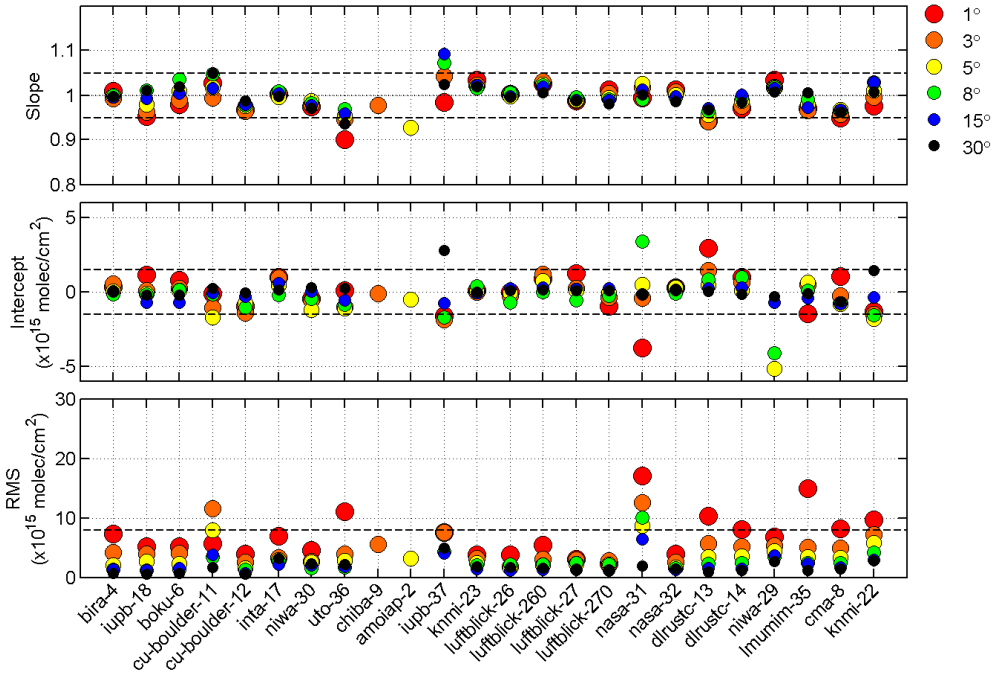

Figure 17: Slope, intercept and RMS of regression plots against the median dSCD reference, for each of the 24 instruments measuring NO_2 in the visible wavelength range (as shown in Figure 10~~Figure 10~~). The values are colour-coded corresponding to the elevation angles (1º to 30º). Apart from a couple of exceptions (chiba-9, amoiap-2), most instruments are measuring the whole range of elevation angles. The dashed lines indicate the limits when comparing the values of the parameters for the different instruments with the aim to identify outliers in a more objective way.~~;~~ Section 4 and Figure 18 explain in more detail how the actual values of the limits were selected ~~are explained in Section 4 and Figure 18~~, and the values are listed in Table 4.

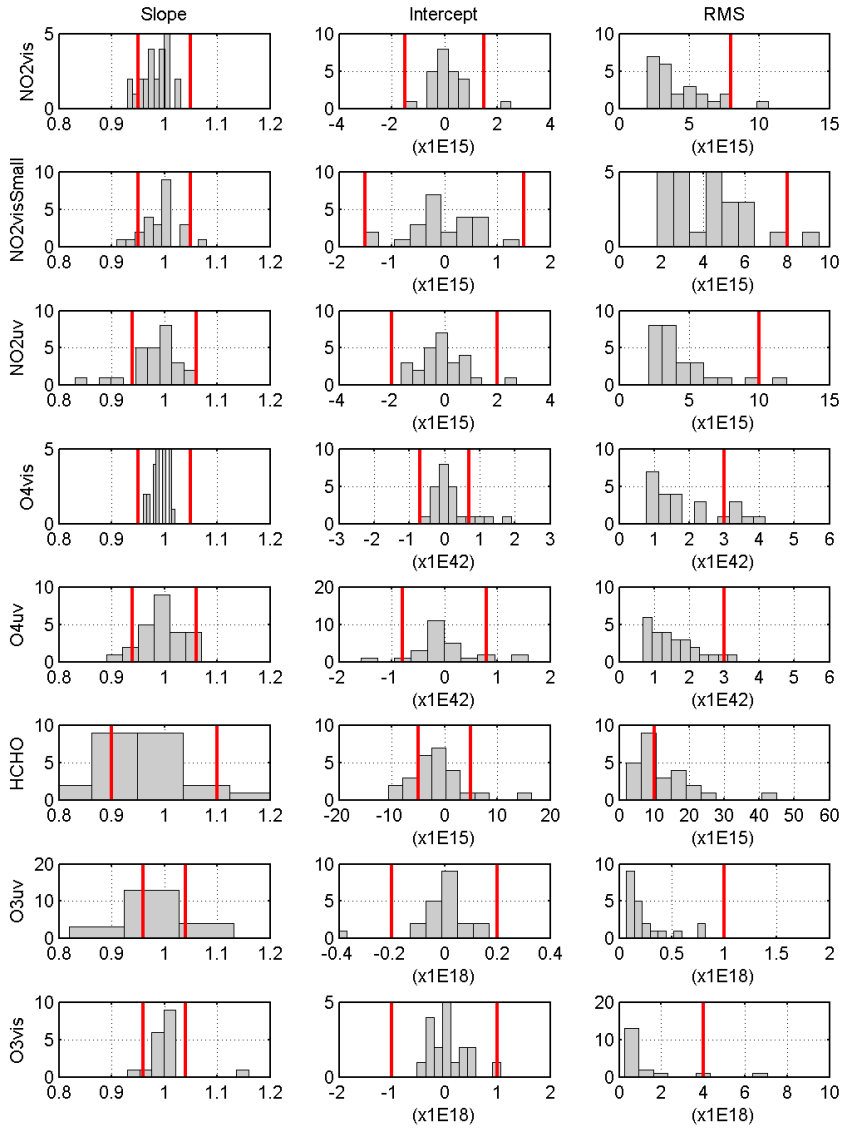
Slope
Intercept
RMS
NO2vis
NO2visSmall
NO2uv
O4vis
O4uv
HCHO
O3uv
O3vis
(x1E15)
(x1E42)
(x1E18)

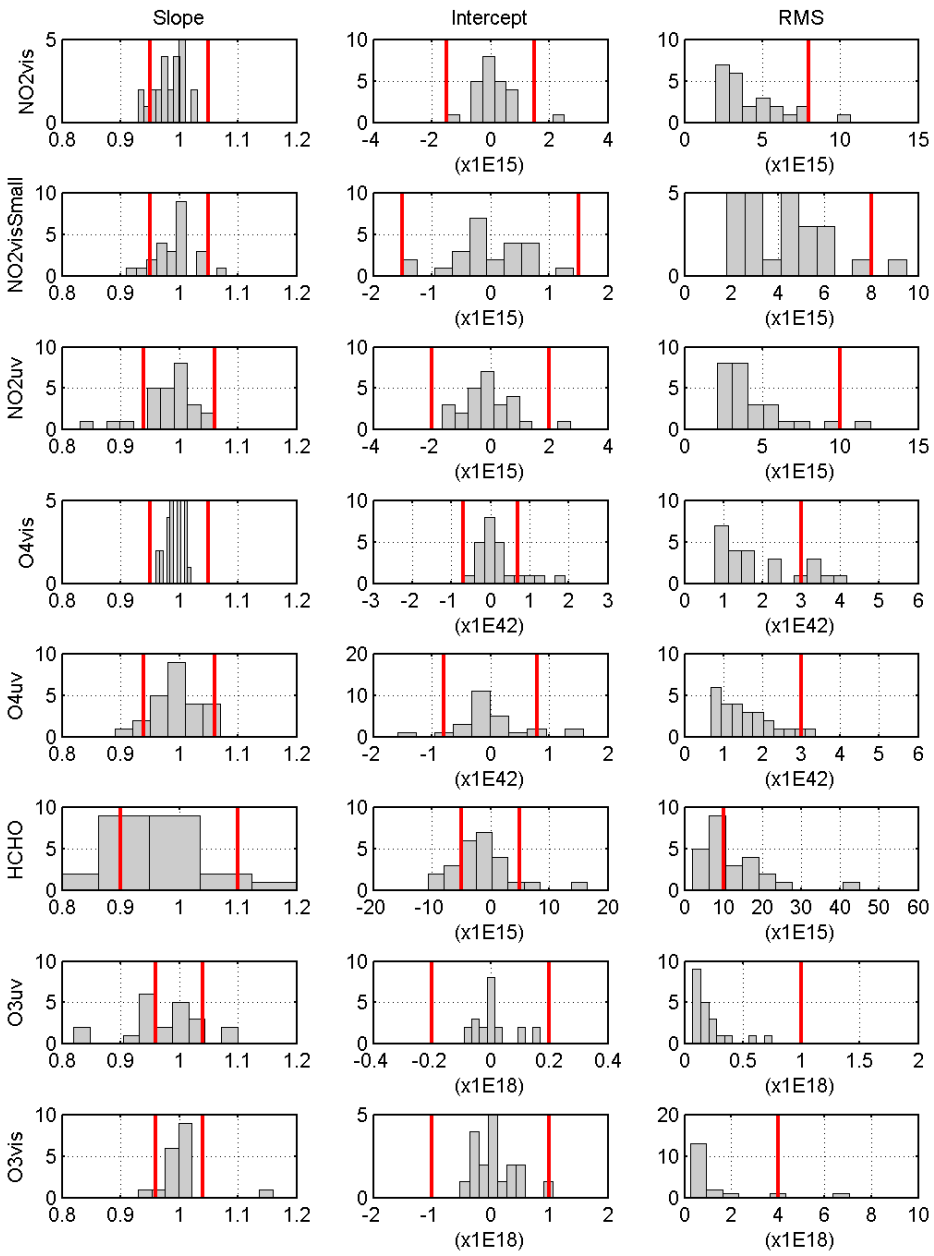
Slope
Intercept
RMS
NO2vis
NO2visSmall
NO2uv
O4vis
O4uv
HCHO
O3uv
O3vis
(x1E15)
(x1E42)
(x1E18)

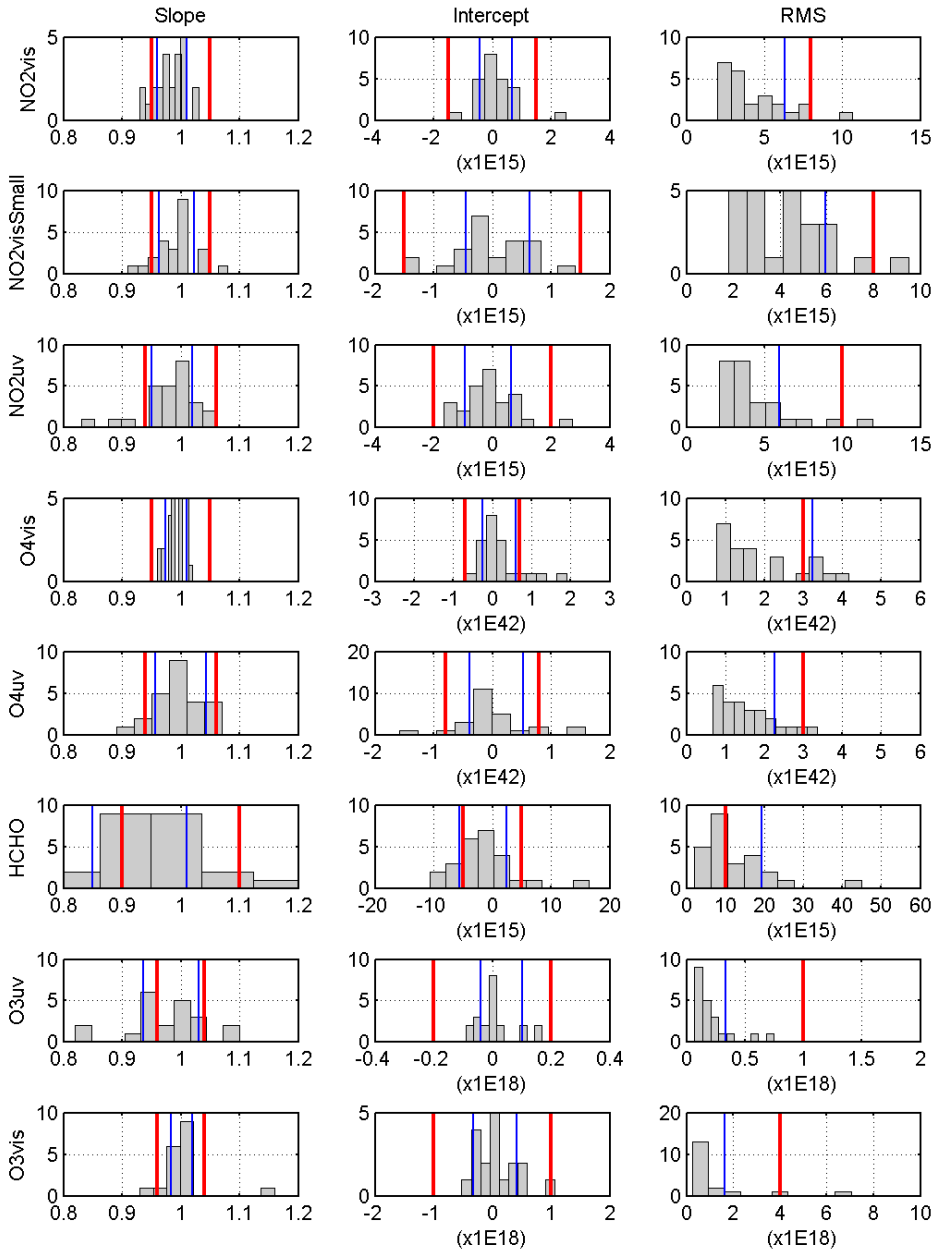

Figure 18: Limits for the assessment criteria for the eight MAX-DOAS data sets shown by red lines. The blue lines represent the percentiles 16 and 84 (84 only for RMS), together with histograms of the slope being displayed in the left column of panels, the intercept in the middle and the RMS in the rightmost panels (see also Table 4).

Formatted: Font: 9 pt

Formatted: Font: 9 pt

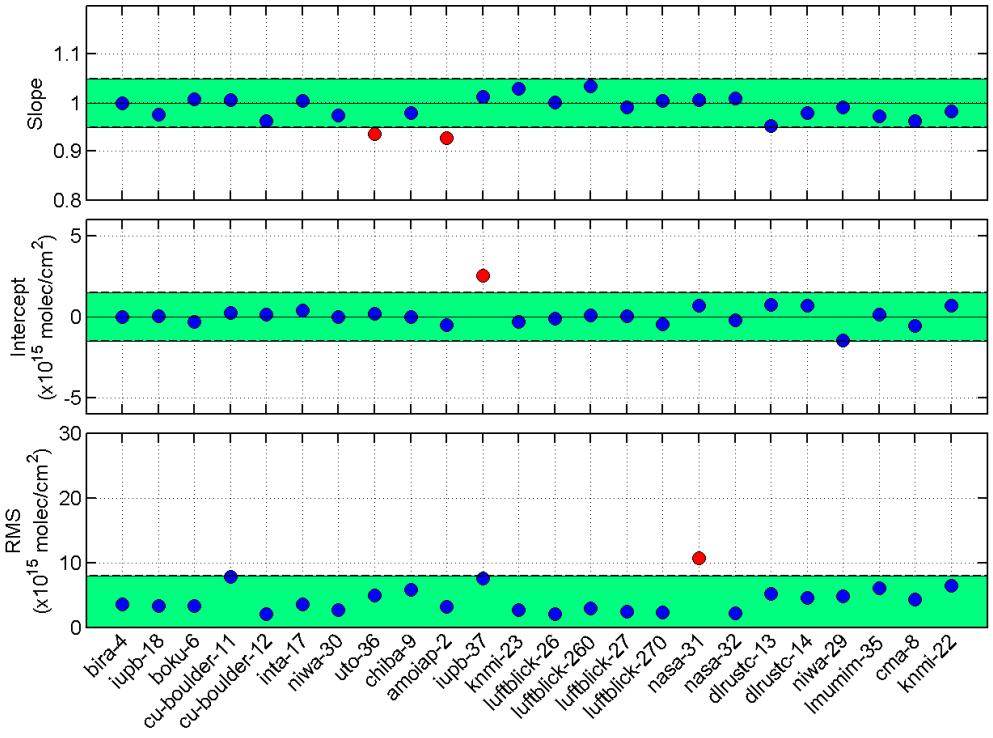

Figure 19: Summary of the NO_2 visible regression statistic shown in Figure 10~~Figure 10~~. The slope, intercept and RMS values are displayed in the top, middle and bottom panel, respectively, for all measurement days, all viewing direction and all elevation angles. The green shading indicates the limits as defined in Table 4 and Figure 18 for NO2vis; the values falling within these limits are plotted in blue, the ones outside the limits in red.

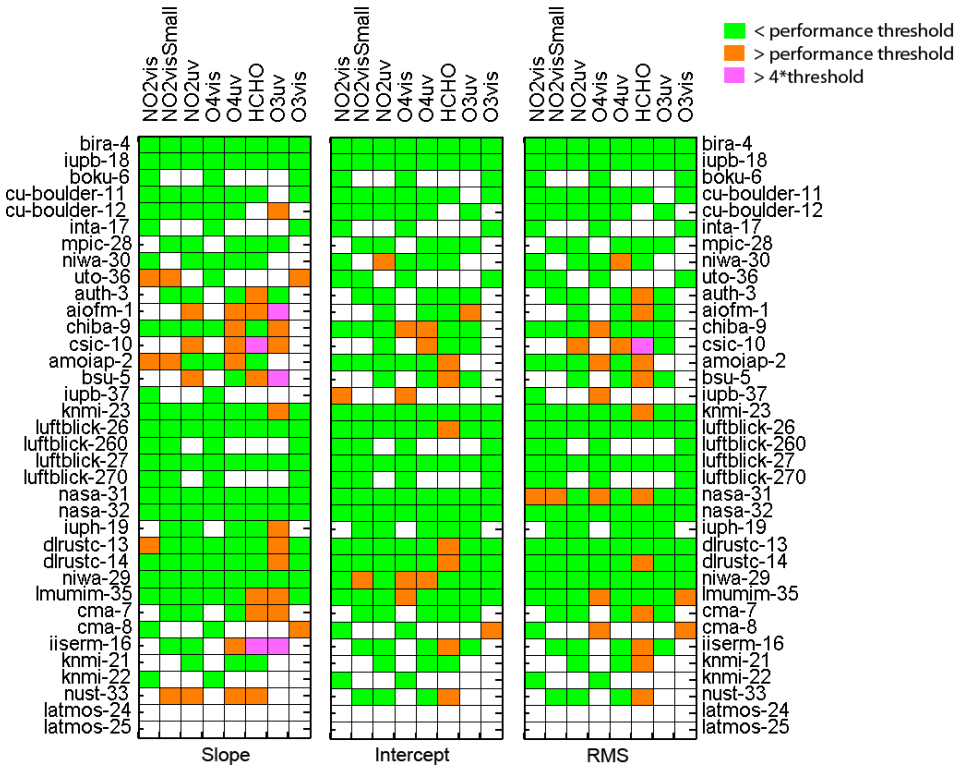
NO2vis
NO2visSmall
NO2uv
O4vis
O4uv
HCHO
O3uv
O3vis
< performance threshold
> performance threshold
> 4*threshold
bira-4
iupb-18
boku-6
cu-boulder-11
cu-boulder-12
inta-17
mpic-28
niwa-30
uto-36
auth-3
aiofm-1
chiba-9
csic-10
amoiap-2
bsu-5
iupb-37
knmi-23
luftblick-26
luftblick-260
luftblick-27
luftblick-270
nasa-31
nasa-32
iuph-19
dlrustc-13
dlrustc-14
niwa-29
lmumim-35
cma-7
cma-8
iiserm-16
knmi-21
knmi-22
nust-33
latmos-24
latmos-25
Slope
Intercept
RMS

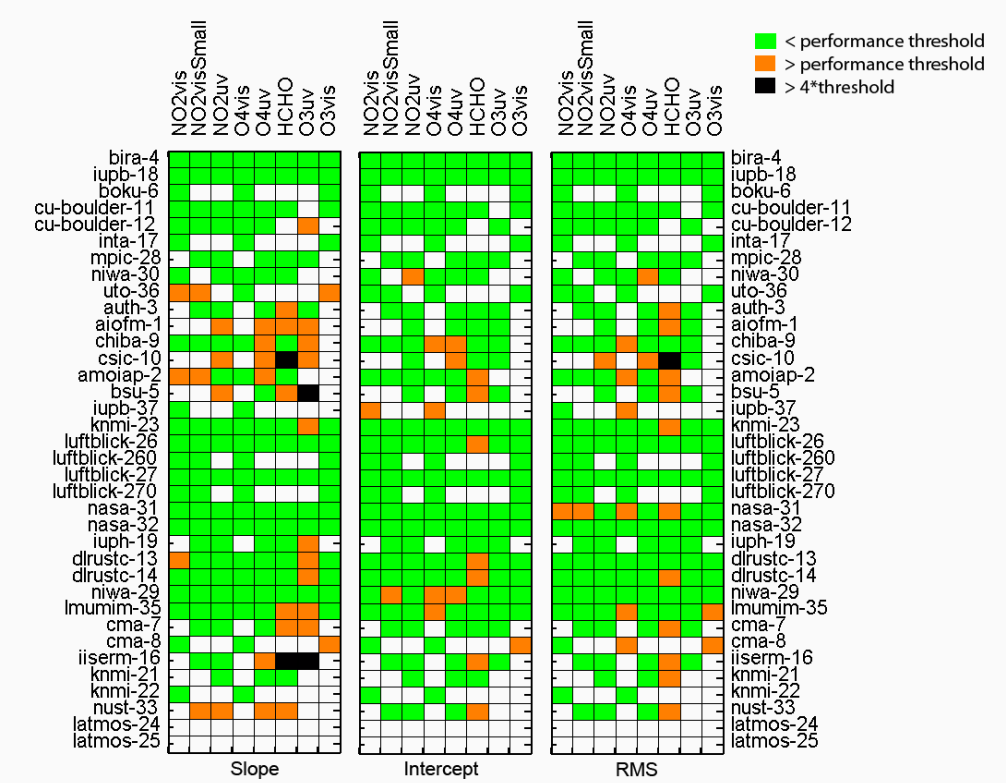

Figure 20: Overview of performance results for the slope, intercept and RMS from the regression analysis displayed for all participating instruments and MAX-DOAS data products. Colour coding denotes if each of the parameters is within the set criteria (green), if the performance threshold is exceeded (orange), or if it is exceeded by more than a factor of 4 (black~~pink~~).

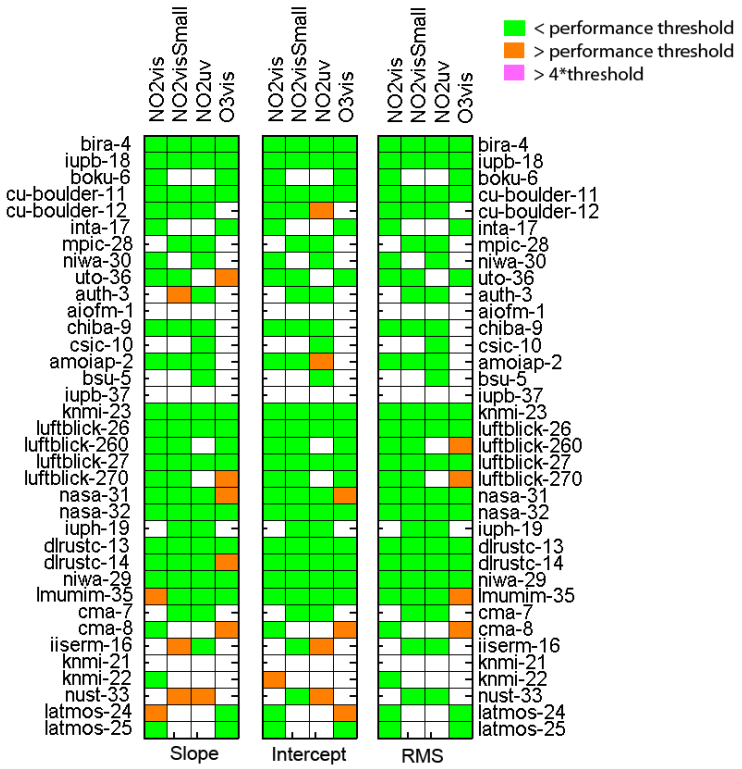
NO2vis
NO2visSmall
NO2uv
O3vis
< performance threshold
> performance threshold
> 4*threshold
bira-4
iupb-18
boku-6
cu-boulder-11
cu-boulder-12
inta-17
mpic-28
niwa-30
uto-36
auth-3
aiofm-1
chiba-9
csic-10
amoiap-2
bsu-5
iupb-37
knmi-23
luftblick-26
luftblick-260
luftblick-27
luftblick-270
nasa-31
nasa-32
iuph-19
dlrustc-13
dlrustc-14
niwa-29
lmumim-35
cma-7
cma-8
iiserm-16
knmi-21
knmi-22
nust-33
latmos-24
latmos-25
Slope
Intercept
RMS

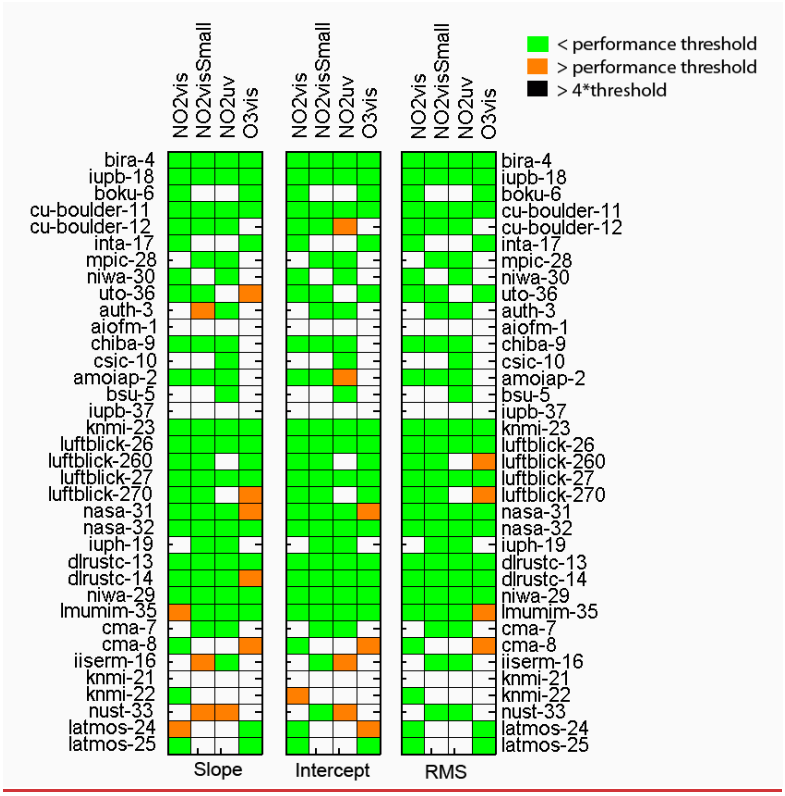
< performance threshold
> performance threshold
> 4*threshold
NO2vis
NO2visSmall
NO2uv
O3vis
bira-4
iupb-18
boku-6
cu-boulder-11
cu-boulder-12
inta-17
mpic-28
niwa-30
uto-36
auth-3
aiofm-1
chiba-9
csic-10
amoiap-2
bsu-5
iupb-37
knmi-23
luftblick-26
luftblick-260
luftblick-27
luftblick-270
nasa-31
nasa-32
iuph-19
dlrustc-13
dlrustc-14
niwa-29
lmumim-35
cma-7
cma-8
iiserm-16
knmi-21
knmi-22
nust-33
latmos-24
latmos-25
Slope
Intercept
RMS

Figure 21: Same as

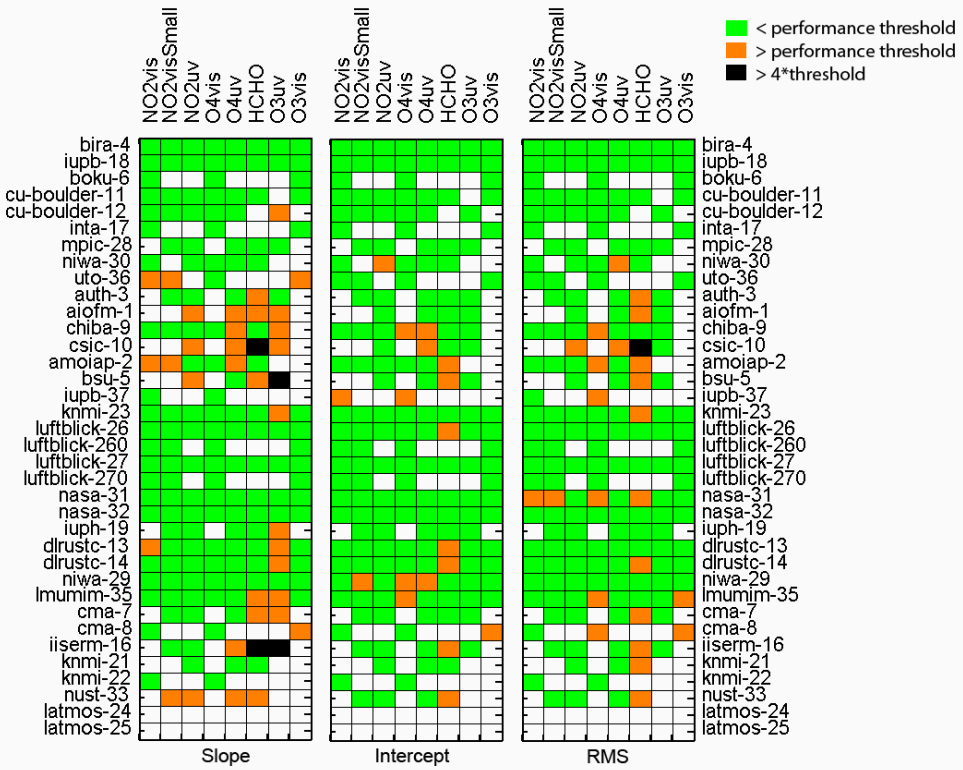

Figure 20~~Figure 20~~ but for the zenith-sky products.

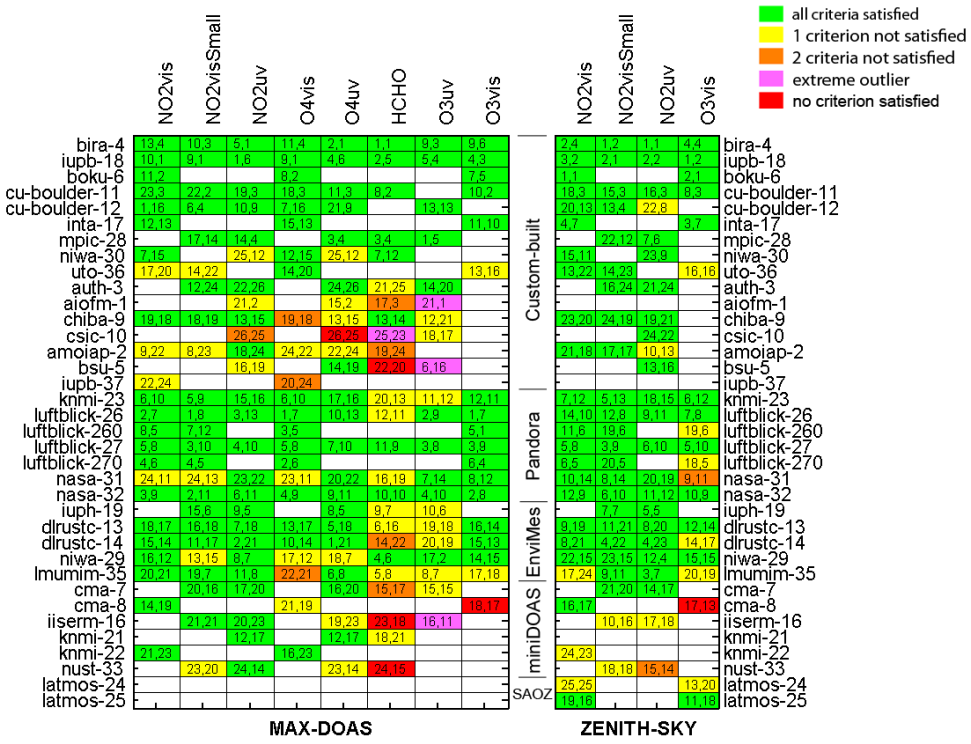
all criteria satisfied
1 criterion not satisfied
2 criteria not satisfied
extreme outlier
no criterion satisfied
NO2vis
NO2visSmall
NO2uv
O4vis
O4uv
HCHO
O3uv
O3vis
Custom-built
Pandora
EnviMes
miniDOAS
SAOZ
MAX-DOAS
ZENITH-SKY

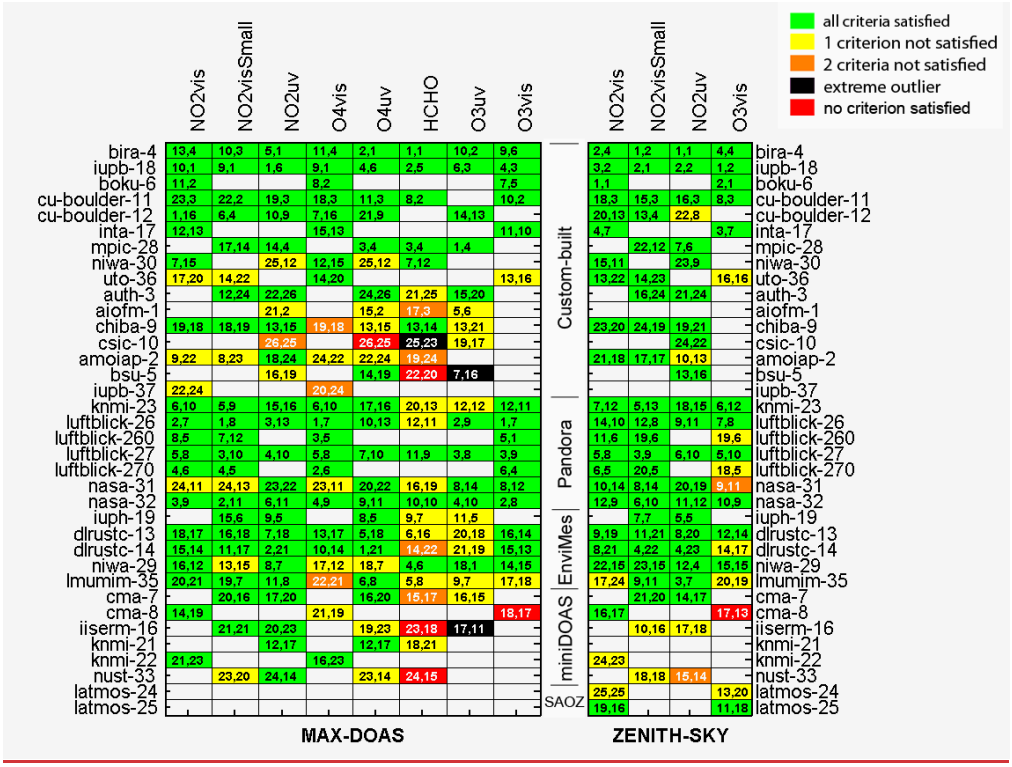

Figure 22: Assessment matrix for all 36 instruments and eight data products for MAX-DOAS, and four data products for zenith-sky mode. Green indicates that all three assessment criteria have been fulfilled, yellow means that one criterion is not satisfied, orange means two are not, red means all three criteria have not been met and blackpink indicates that this data set has at least one extreme outlier. White indicates when data sets were not measured. The two numbers in each box indicate the rating for each product and instrument according to the dSCD regression RMS (first value) and the RMS calculated as part of the data fitting routine (second value). The instruments with the smallest RMS are denoted with the smallest numbers. Note that the instruments are grouped according to their specific design as Custom-built, Pandora, EnviMes, miniDOAS or SAOZ.

Appendix A: DOAS retrieval settings

For each data product, a set of retrieval settings and parameters was prescribed. The use of these settings was mandatory for participation in the semi-blind intercomparison. The tables below summarize the details of the DOAS retrieval configurations used for each data product. The referenced absorption cross-section files are available from the FRM4DOAS web-site (http://frm4doas.aeronomie.be/index.php/documents).

Table A1: DOAS settings for NO_2 and O_4 (VIS range)

Wavelength range	425-490 nm
Fraunhofer reference spectra	Noon zenith spectra averaged between 11:30:00 and 11:40:00 UT
Cross-sections:	
NO_2 (2948 K)	Vandaele et al. (1998) with I_0 correction (SCD of 10^{17} molecules/cm^2) File: no2_2948K_vanDaele.xs
NO_2 (220 K)	Pre-orthogonalized Vandaele et al. (1998) with I_0 correction (SCD of 10^{17} molecules/cm^2) File: no2a_220p2948K_vanDaele_425-490nm.xs
O_3 (223 K)	Serdyuchenko et al. (2014) with I_0 correction (SCD of 10^{20} molecules/cm^2) File: o3_223K_SDY_air.xs
O_4 (293 K)	Thalman and Volkamer (2013) File: o4_thalman_volkamer_293K_inAir.xs
H_2O	HITEMP (Rothman et al., 2010) File: H2O_HITEMP_2010_390-700_296K_1013mbar_air.xs
Ring	RING_QDOAS_SAO2010 File: Ring_QDOAScalc_HighResSAO2010_Norm.xs
Polynomial degree	Order 5 (6 coefficients)
Intensity off-set	Constant

Table A2: DOAS settings for NO_2 and O_4 (alternative VIS range)

Wavelength range	411-445 nm
Fraunhofer reference spectra	Noon zenith spectra averaged between 11:30:00 and 11:40:00 UT
Cross-sections:	
NO_2 (2948 K)	Vandaele et al. (1998) with I_0 correction (SCD of 10^{17} molecules/cm^2) File: no2_2948K_vanDaele.xs
NO_2 (220 K)	Pre-orthogonalized Vandaele et al. (1998) with I_0 correction (SCD of 10^{17} molecules/cm^2) File: no2a_220p2948K_vanDaele_425-490nm
O_3 (223 K)	Serdyuchenko et al. (2014) with I_0 correction (SCD of 10^{20} molecules/cm^2) File: o3_223K_SDY_air.xs
O_4 (293 K)	Thalman and Volkamer (2013)

	File: o4_thalman_volkamer_293K_inAir.xs
H_2O	HITEMP (Rothman et al., 2010) File: H2O_HITEMP_2010_390-700_296K_1013mbar_air.xs
Ring	RING_QDOAS_SAO2010 File: Ring_QDOAScalc_HighResSAO2010_Norm.xs
Polynomial degree	Order 4 (5 coefficients)
Intensity off-set	Constant

Table A3: DOAS settings for NO_2 and O_4 (UV range)

Wavelength range	338-370 nm
Fraunhofer reference spectra	Noon zenith spectra averaged between 11:30:00 and 11:40:00
Cross-sections:	
NO_2 (2948 K)	Vandaele et al. (1998) with I_0 correction (SCD of 10^{17} molecules/cm^2) File: no2_2948K_vanDaele.xs
NO_2 (220 K)	Pre-orthogonalized Vandaele et al. (1998) with I_0 correction (SCD of 10^{17} molecules/cm^2) File: no2a_220p2948K_vanDaele_338-370nm.xs
O_3 (223 K)	Serdyuchenko et al. (2014) with I_0 correction (SCD of 10^{20} molecules/cm^2) File: o3_223K_SDY_air.xs
O_3 (243 K)	Pre-orthogonalized Serdyuchenko et al. (2014) with I_0 correction (SCD of 10^{20} molecules/cm^2) File: o3a_243p223K_SDY_338-370nm.xs
O_4 (293 K)	Thalman and Volkamer (2013) File: o4_thalman_volkamer_293K_inAir.xs
HCHO (297 K)	Meller and Moortgat (2000) File: hcho_297K_Meller.xs
BrO (223 K)	Fleischmann et al. (2004) File: bro_223K_Fleischmann.xs
Ring	RING_QDOAS_SAO2010 File: Ring_QDOAScalc_HighResSAO2010_Norm.xs
Polynomial degree	Order 5 (6 coefficients)
Intensity off-set	Constant

Table A4: DOAS settings for HCHO

Wavelength range	336.5-359 nm
Fraunhofer reference spectra	Noon zenith spectra averaged between 11:30:00 and 11:40:00 UT
Cross-sections:	

HCHO (297 K)	Meller and Moortgat (2000) File: hcho_297K_Meller.xs
NO_2 (2948 K)	Vandaele et al. (1998) with I_0 correction (SCD of 10^{17} molecules/cm^2) File: no2_2948K_vanDaele.xs
O_3 (223 K)	Serdyuchenko et al. (2014) with I_0 correction (SCD of 10^{20} molecules/cm^2) File: o3_223K_SDY_air.xs
O_3 (243 K)	Pre-orthogonalized Serdyuchenko et al. (2014) with I_0 correction (SCD of 10^{20} molecules/cm^2) File: o3a_243p223K_SDY_324-359nm.xs
O_4 (293 K)	Thalman and Volkamer (2013) File: o4_thalman_volkamer_293K_inAir.xs
BrO (223 K)	Fleischmann et al. (2004) File: bro_223K_Fleischmann.xs
Ring	RING_QDOAS_SAO2010 File: Ring_QDOAScalc_HighResSAO2010_Norm.xs
Polynomial degree	Order 5 (6 coefficients)
Intensity off-set	Order 1

Table A5: DOAS settings ozone in the Chappuis band

Wavelength range	450-520 nm
Fraunhofer reference spectra	Noon zenith spectra averaged between 11:30:00 and 11:40:00 UT
Cross-sections:	
O_3 (223 K)	Serdyuchenko et al. (2014) with I_0 correction (SCD of 10^{20} molecules/cm^2) File: o3_223K_SDY_air.xs
O_3 (293 K)	Pre-orthogonalized Serdyuchenko et al. (2014) with I_0 correction (SCD of 10^{20} molecules/cm^2) File: o3a_293p223K_SDY_450-550nm.xs
NO_2 (2948 K)	Vandaele et al. (1998) with I_0 correction (SCD of 10^{17} molecules/cm^2) File: no2_2948K_vanDaele.xs
NO_2 (220 K)	Pre-orthogonalized Vandaele et al. (1998) with I_0 correction (SCD of 10^{17} molecules/cm^2) File: no2a_220p2948K_vanDaele_450-550nm.xs
O_4 (296 K)	Thalman and Volkamer (2013) File: o4_thalman_volkamer_293K_inAir.xs
H_2O	HITEMP (Rothman et al., 2010) File: H2O_HITEMP_2010_390-700_296K_1013mbar_air.xs
Ring	RING_QDOAS_SAO2010 File: Ring_QDOAScalc_HighResSAO2010_Norm.xs
Polynomial degree	Order 5 (6 coefficients)
Intensity off-set	Order 1

Table A6: DOAS settings ozone in the Huggins band

Wavelength range	320-340 nm
Fraunhofer reference spectra	Noon zenith spectra averaged between 11:30:00 and 11:40:00 UT
Cross-sections:	
O_3 (223 K)	Serdyuchenko et al. (2014) with I_0 correction (SCD of 10^{20} molecules/cm^2) File: o3_223K_SDY_air.xs
O_3 (293 K)	Pre-orthogonalized Serdyuchenko et al. (2014) with I_0 correction (SCD of 10^{20} molecules/cm^2) File: o3a_293p223K_SDY_320-340nm.xs
O_3	Non-linear correction terms (Puķīte et al., 2010) Files: o3_SDY_Pukite1_320-340nm.xs and o3_SDY_Pukite2_320-340nm.xs
NO_2 (294 K)	Vandaele et al. (1998) with I_0 correction (SCD of 10^{17} molecules/cm^2) File: no2_294K_vanDaele.xs
HCHO (297 K)	Meller and Moortgat (2000) File: hcho_297K_Meller.xs
Ring	RING_QDOAS_SAO2010 File: Ring_QDOAScalc_HighResSAO2010_Norm.xs
Polynomial degree	Order 3 (4 coefficients)
Intensity off-set	Order 1

Appendix B: History of slant column data set revisions

This appendix provides a history of the slant column data set resubmissions accepted after the formal deadline for participation to the semi-blind intercomparison (18 October 2016). The main motivation for accepting late revisions was to remedy well-identified mistakes. Details of the submitted revisions, including justifications for the changes and corresponding dates, are listed below.

AIOFM (aiofm-1)

Data files resubmitted on 16 October 2017 with two additional corrections applied, which were: (1) A~~a~~ dark current correction and (2) a wavelength shift that needed to be applied with respect to the reference spectrum. The O3uv data set was also resubmitted in September 2019 because an incorrect ozone cross-section was used previously for the data analysis.

AUTH (auth-3)

Data files resubmitted on 17 March 2017. These were corrected for a systematic wavelength shift of the measured spectra.

BIRA-IASB (bira-4)

Revised data submitted on 28 February 2017, with small changes summarized as follows: (1) A correction of an error affecting the dark current subtraction in the UV channel (affecting HCHO, NO2uv, O4uv and O3uv, mostly at large SZA) and (2) an optimisation of the filtering scheme were applied. For the visible products, all measurement points having RMS values exceeding 5 times the daily median RMS calculated in hourly bins were excluded. The same procedure was also applied to the UV products with any data values exceeding 4 times the median being excluded. This approach was found sufficient to exclude outliers due to an electronic instability in the UV channel.

CHIBA (chiba-9)

Data files resubmitted on 11 January 2018, with additional stray-light corrections applied to the measured spectra. This correction was derived as part of the wavelength calibration procedure. Considering the nominal spectral range 310 to 525 nm, 11 discrete wavelength regions (316±5, 336±5, 344±5, 358±5, 374±5, 384±5, 395±5, 410±5, 431±5, 486±10, and 518±5 nm) were selected and analysed. In each spectral window, the spectrum was fitted using an iterative inversion method. The measurement vector consisted of the intensities measured by the MAX-DOAS instrument. The components of the state vector were set to the wavelength shift, the FWHM for the left part of an asymmetric Gaussian instrument line shape (FWHM1), the FWHM for the right part (FWHM2), and the differential slant column (dSCD) of significant absorbers (O_3, NO_2) in the analysed wavelength region. In addition, a scaling polynomial and a constant offset term (or stray-light correction term) were included in the state vector to scale the high-resolution solar spectrum data to the intensities measured by MAX-DOAS.

Formatted: Subscript

Formatted: Subscript

CMA (cam-7, cma-8)

Revised data files were resubmitted on 26 September 2016 for CMA-7 (UV and VisSmall range) and CMA-8 (Vis range). Periods with bad motor connection were filtered out in the resubmitted data. Additionally, fitting of the wavelength shift between measurement spectrum and reference spectrum was added in the revised processing.

CU-Boulder (CU-boulder-11, CU-boulder-12)

Revised data files were submitted for all gases on 4 March 2017. For CU-boulder-11, the resubmitted data were filtered for periods with bad motor connection (when instrument operated in 1D or in zenith geometry), and one corrupt file was corrected. For CU-boulder-12, revised files were only submitted for gases analysed in the UV wavelengths range. Resubmitted data accounted for a

time-dependent etalon identified on the UV spectrometer and fitted as a pseudo absorber with independent shift and stretch. This approach captured the errant signal effectively at longer wavelength but was less effective at shorter wavelengths; no HCHO data were reported. The source of the etalon has since been eliminated.

INTA (inta-17)

Revised data files submitted on 14 February 2017, due to one change in their data analysis routine: The inverse of the actual measurement was used as offset instead of the inverse of the reference spectrum leading to a smaller uncertainty and improved retrievals of the sunrise and sunset slant columns. This change mainly affects twilight data but for consistency the complete data set was reanalysed.

KNMI (knmi-21, knmi-22)

Data files resubmitted on 27 January 2017 with the following corrections: (1) Fitting of the wavelength shift between measurement spectrum and reference spectrum was previously omitted and had to be added. (2) For knmi-22: Due to an instable tripod, the logged angles can only be trusted when the horizon measurements show a consistent horizon from day to day (<0.5° ~~degree~~ difference). The measurements during all other periods have been filtered out.

Formatted: Superscript

LATMOS (latmos-25)

Data files resubmitted data on 4 April 2018, because the data files had to be corrected for detector non-linearity effects that were identified after the campaign. The detector is a Hamamatsu CCD 2048x16 type S11071-1104. The non-linearity of this detector was measured and corrected applying the procedure described in AvaSpec-DLL Manual V9.7.0.0 (p71-73). A stable light source (Xe lamp, VG9 filter and diffuser) was used to measure spectra at different integration times between 50 ms and 1830 ms. The maximum level of the elementary spectrum varies from 400 to 16000 counts. The correlation between the flux (count/s) and the number of counts of an elementary spectrum at several pixels was fitted by a polynomial of degree 7 and this curve was then used to correct raw data as recommended by Avantes.

LMU-MIM (lmumim-35)

Data files resubmitted with two corrections applied on 24 March 2018: (1) The spectra were re-analyzed with a correction for detector non-linearity and the analysis was updated by using offset and dark current spectra. The latter spectra were measured after the CINDI-2 campaign and also corrected for detector non-linearity. (2) The DOAS fit was performed using QDOAS to fit the instrument slit function while for the originally submitted data set a fixed instrument slit function measured with a Hg lamp was used.

LuftBlick/NASA (knmi-23, luftblick-26, 27, 260, 270, nasa-31, 32)

Revised data sets submitted on 4 October 2017. Pandora data during CINDI-2 were processed using BlickP, the native Pandonia Global Network (PGN) software. BlickP allows for fitting of molecular absorption cross-sections of a specific species represented in terms of constant, or linear, or quadratic functions of temperature. Orthogonalization of cross-sections is not allowed. Pandora NO_2 and O_3 slant columns had to be recalculated to "simulate" the case, where cross-sections of the same gas at different temperatures are used in the fitting. In addition, measurements at azimuth angles 95° and 135° at elevation angle of 1° were eliminated due to obstruction. There was also a mistake in the intensity calibration correction in the original submission.

NIWA (niwa-30)

Data files resubmitted for NO_2 in the visible and UV, and for HCHO on 27 March 2017. The data were reprocessed to include a test that detects any bad timing on a spectrum and removes the results for that spectrum. This occasional fault was likely due to last minute logging program changes to enable the one available spectrometer to switch wavelength between the visible and UV regions every quarter hour.

NUST (nust-33)

Data files resubmitted on 10 February 2017, after exploring the relatively larger RMS values. A misalignment of elevation angles was noticed in the analyses due to malfunctioning of the Peltier controller unit and loose gear of the stepper motor. On 15 Sep. 2016, as the instrument was replaced with a new instrument No. 15306 (where a problem with the slit was identified and was adjusted). The new instrument was functioning properly, but there was no lamp experiment to adjust the azimuth direction until 19 Sep 2017. Systematic high RMS values are observed for all elevation angles in the retrieved NO2-visSmall (411- 445 nm) and HCHO DSCDs for the period of 12 – 17 Sep. 2016. Finally, on 19 Sep. 2016, a lamp experiment was performed, and the data showed a relatively large improvement in RMS values from 20 Sep. 2016 onward. After extensive check and quality control, the retrieved slant columns were only submitted for a limited number of days.

1 MAX-DOAS regression results

This section presents detailed results from regression analyses performed for the eight MAX-DOAS data products. In each sub-section below, three plots are provided, showing respectively:

- Scatter plots of the regression between individual data sets and median reference values for all measurement days and all viewing and elevation directions (similar to Figures 10, 11 and 12 of the main manuscript).
- Overview plots of the slope, intercept and RMS from regression analysis for all measurement days and viewing directions, and for several elevation angles (1°, 3°, 5°, 8°, 15°, and 30°) (similar to Figure 15 of the main manuscript).
- Summary overview plots of the slope, intercept and RMS from regression analysis for all measurement days and all viewing and elevation directions. These summarize the details of the performance assessment results, as described in Figure 17 of the main manuscript.

1.1 MAX-DOAS results for NO_2 in the visible range (NO2vis)

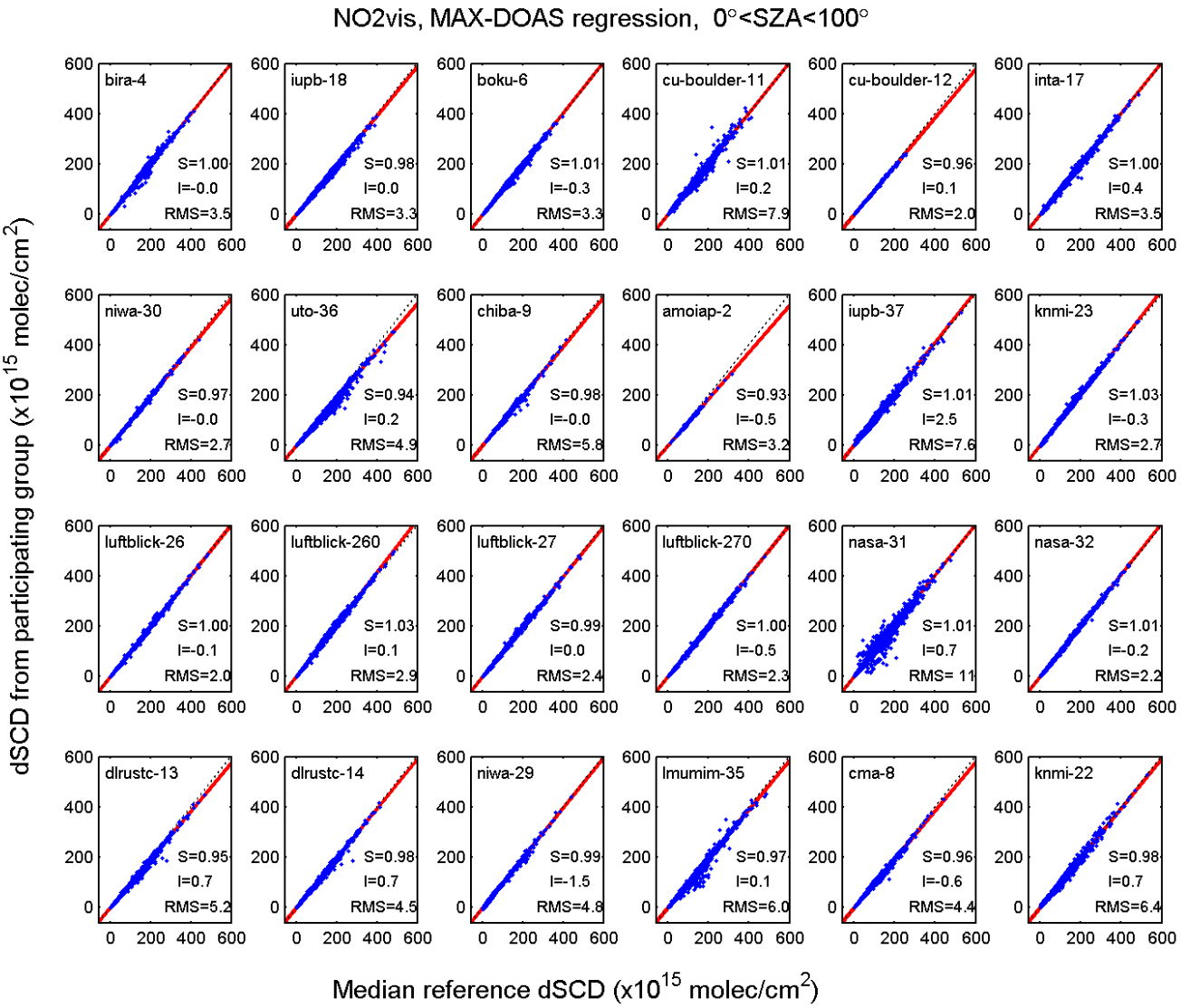

Figure S1: Regression analysis for NO_2 dSCDs (measured in the visible wavelength region), corresponding to Figure 10 in the main manuscript.

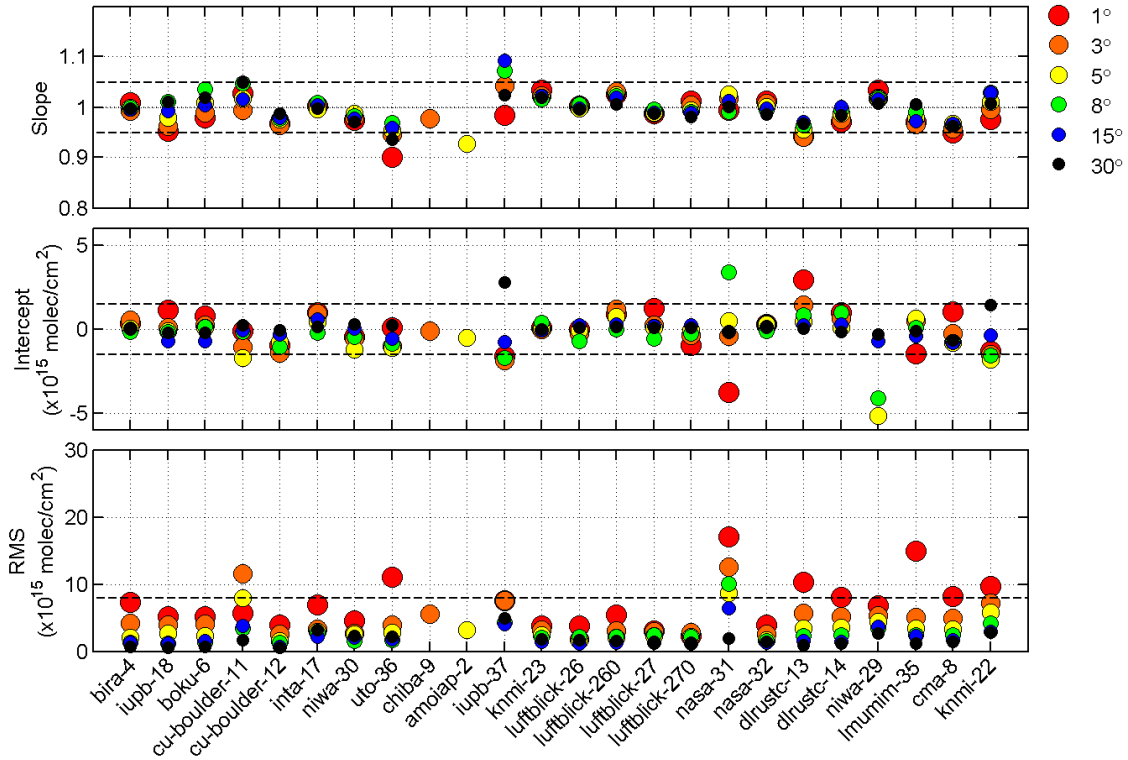

Figure S2: Slope, Intercept and RMS of NO_2 dSCDs against those of the median reference data set, for each instrument measuring NO_2 in the visible range. Colours refer to elevation angles shown top right. This figure is corresponding to Figure 17 in the main manuscript.

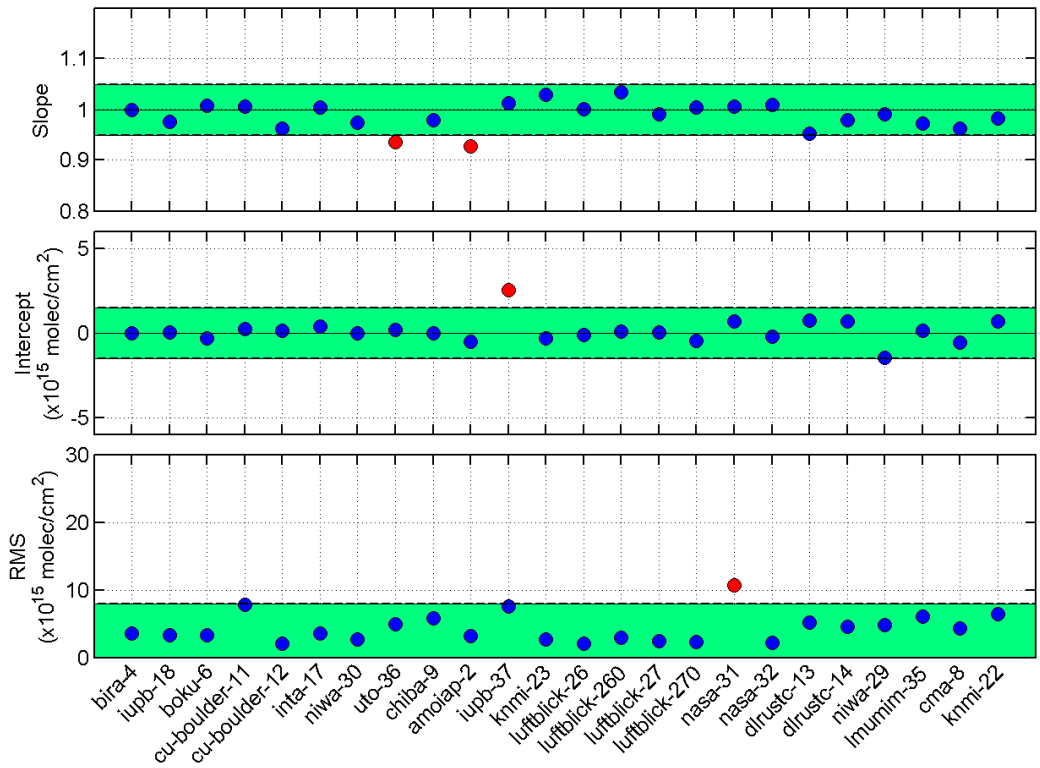

Figure S3: Summary of the regression statistic for NO_2 in the visible range, showing the slope, intercept and RMS values as displayed in Figure S1. The dashed lines show the performance limits as defined in Table 5 of the main manuscript. The values within these limits are plotted in blue, the ones falling outside the limit in red. This figure is corresponding to Figure 17 in the main manuscript.

1.2 MAX-DOAS results for NO_2 in the small visible range (NO2visSmall)

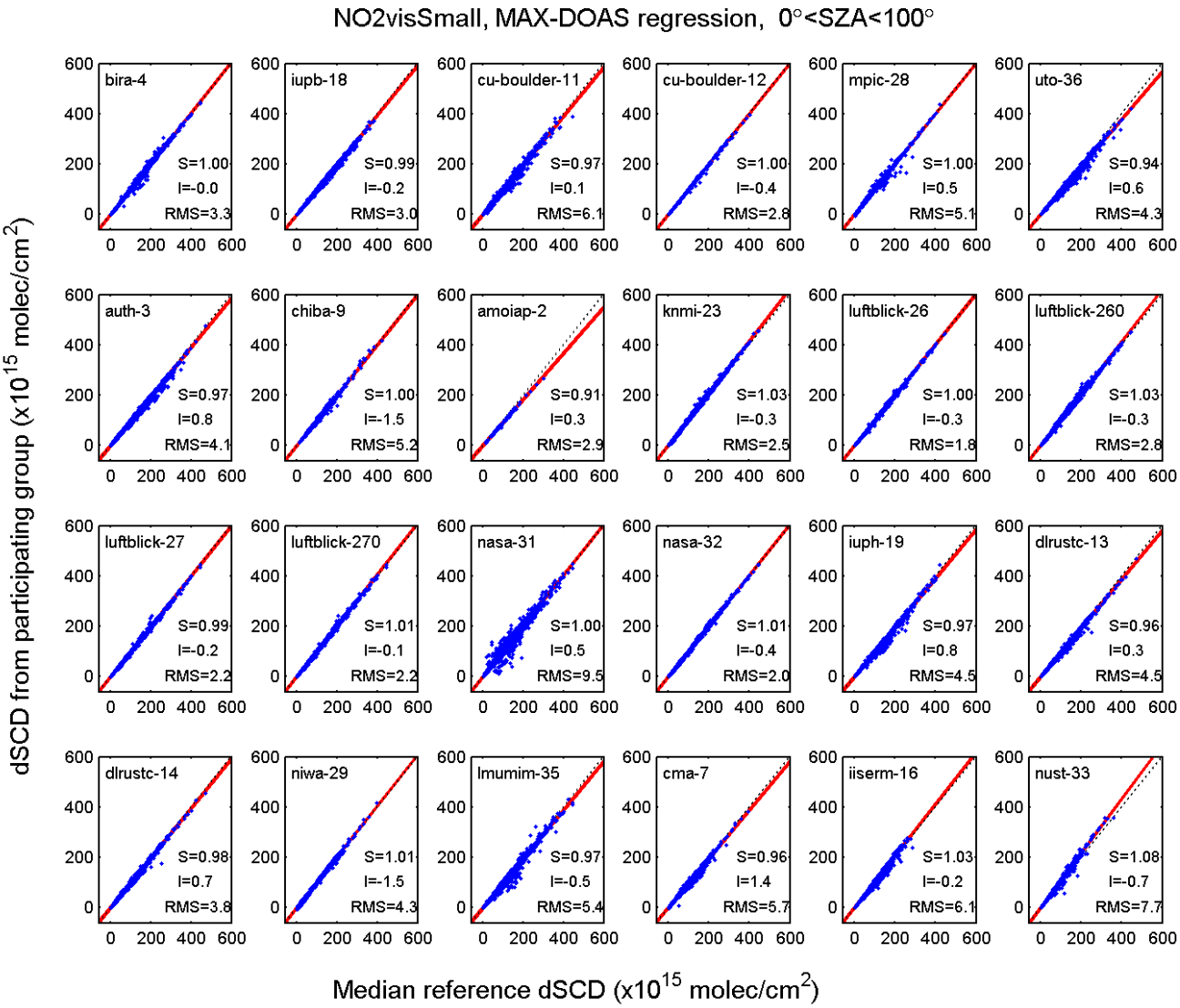

Figure S4: Regression analysis for NO_2 dSCDs (measured in the small visible wavelength region).

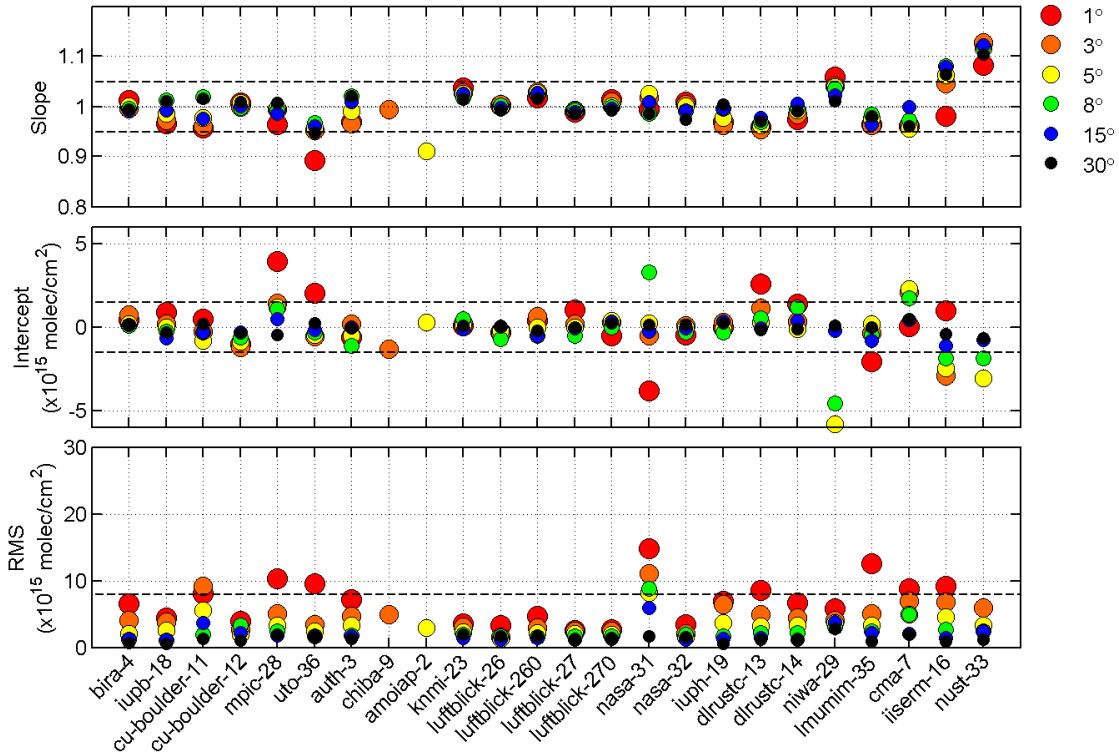

Figure S5: Slope, Intercept and RMS of NO_2 dSCDs against those of the median reference data set, for each instrument measuring NO_2 in the small visible range. Colours refer to elevation angles shown top right.

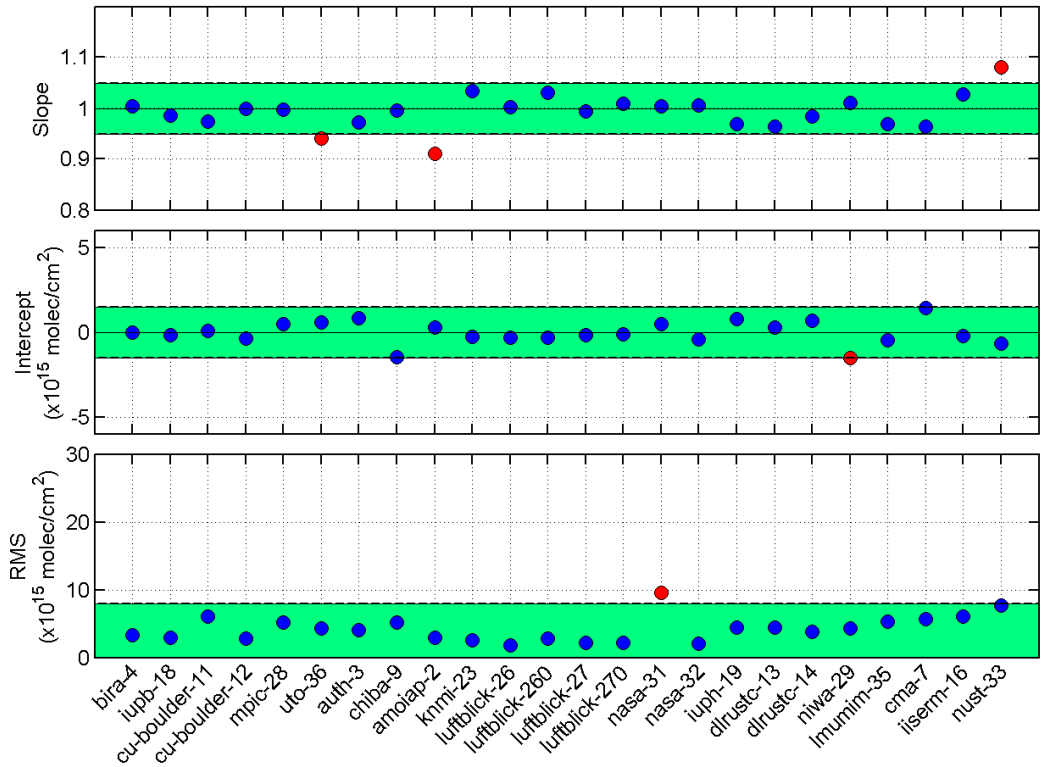

Figure S6: Summary of the regression statistic for NO_2 in the small visible range, showing the slope, intercept and RMS values as displayed in Figure S4. The dashed lines show the performance limits as defined in Table 5 of the main manuscript. The values within these limits are plotted in blue, the ones falling outside the limit in red.

1.3 MAX-DOAS results for NO_2 in the UV range (NO2uv)

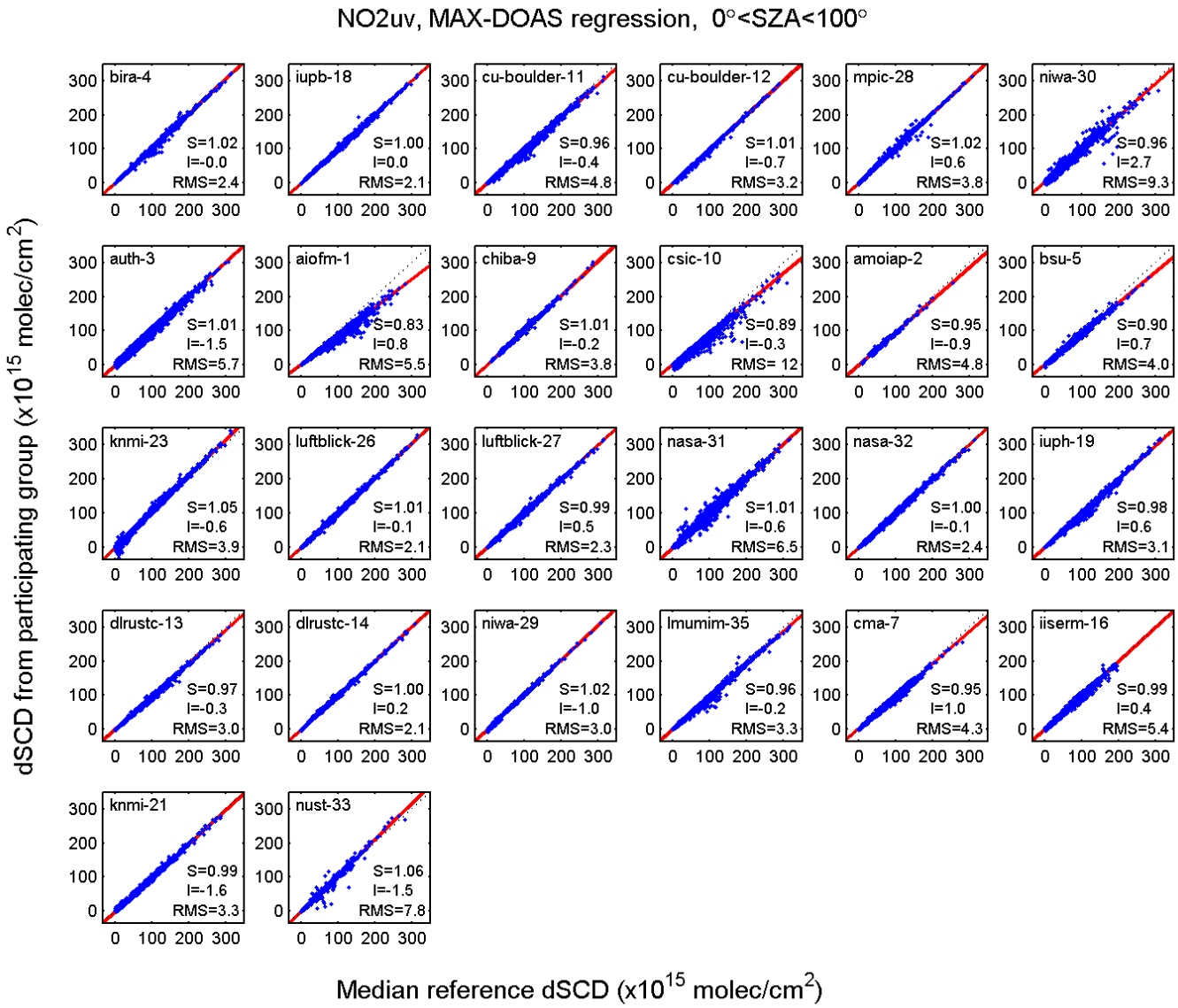

Figure S7: Regression analysis for NO_2 dSCDs (measured in the UV wavelength region).

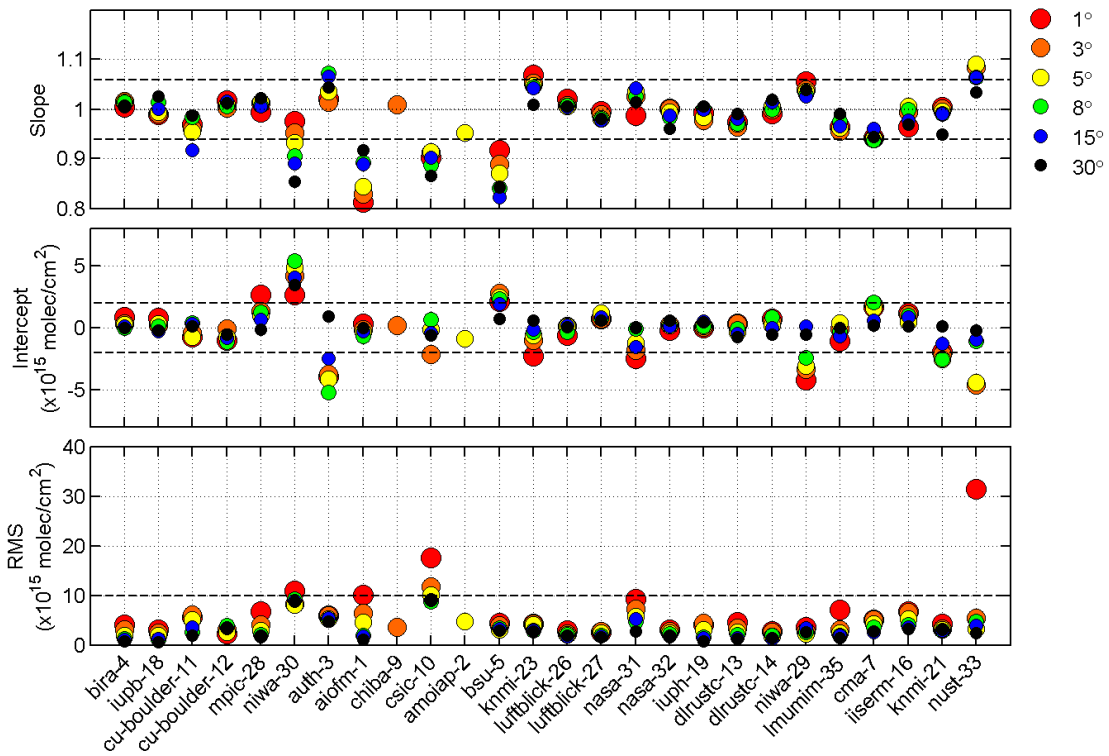

Figure S8: Slope, Intercept and RMS of NO_2 dSCDs against those of the median reference data set, for each instrument measuring NO_2 in the UV range. Colours refer to elevation angles shown top right.

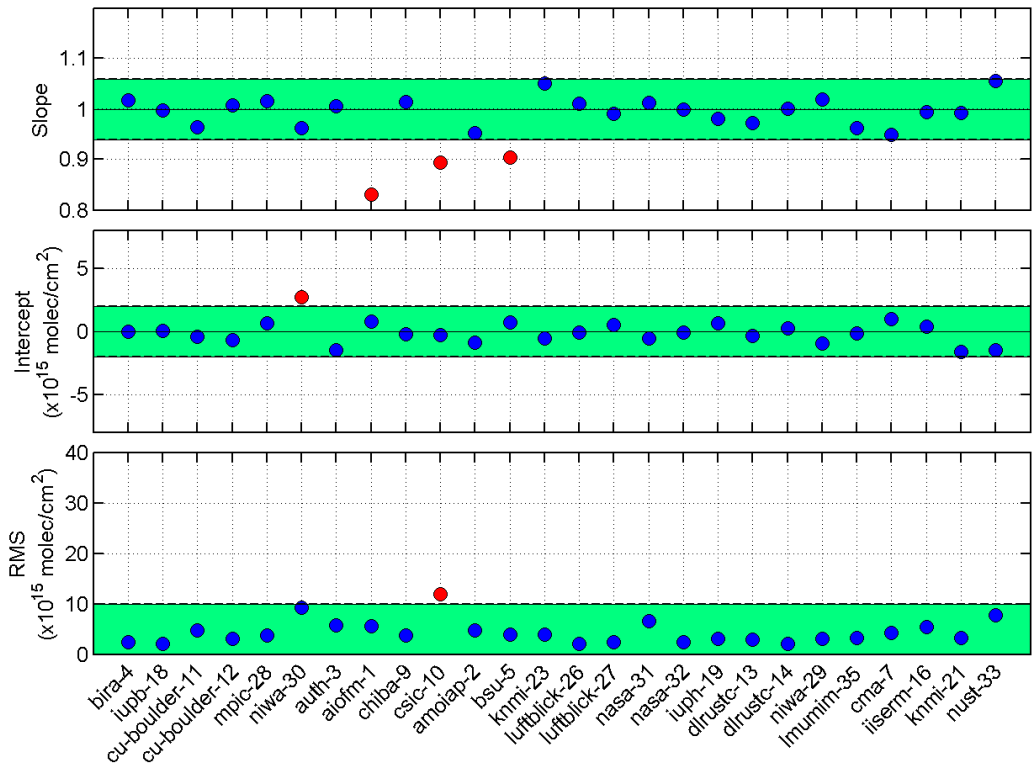

Figure S9: Summary of the regression statistic for NO_2 in the UV range, showing the slope, intercept and RMS values as displayed in Figure S7. The dashed lines show the performance limits as defined in Table 5 of the main manuscript. The values within these limits are plotted in blue, the ones falling outside the limit in red.

1.4 MAX-DOAS results for O_4 in the visible range (O4vis)

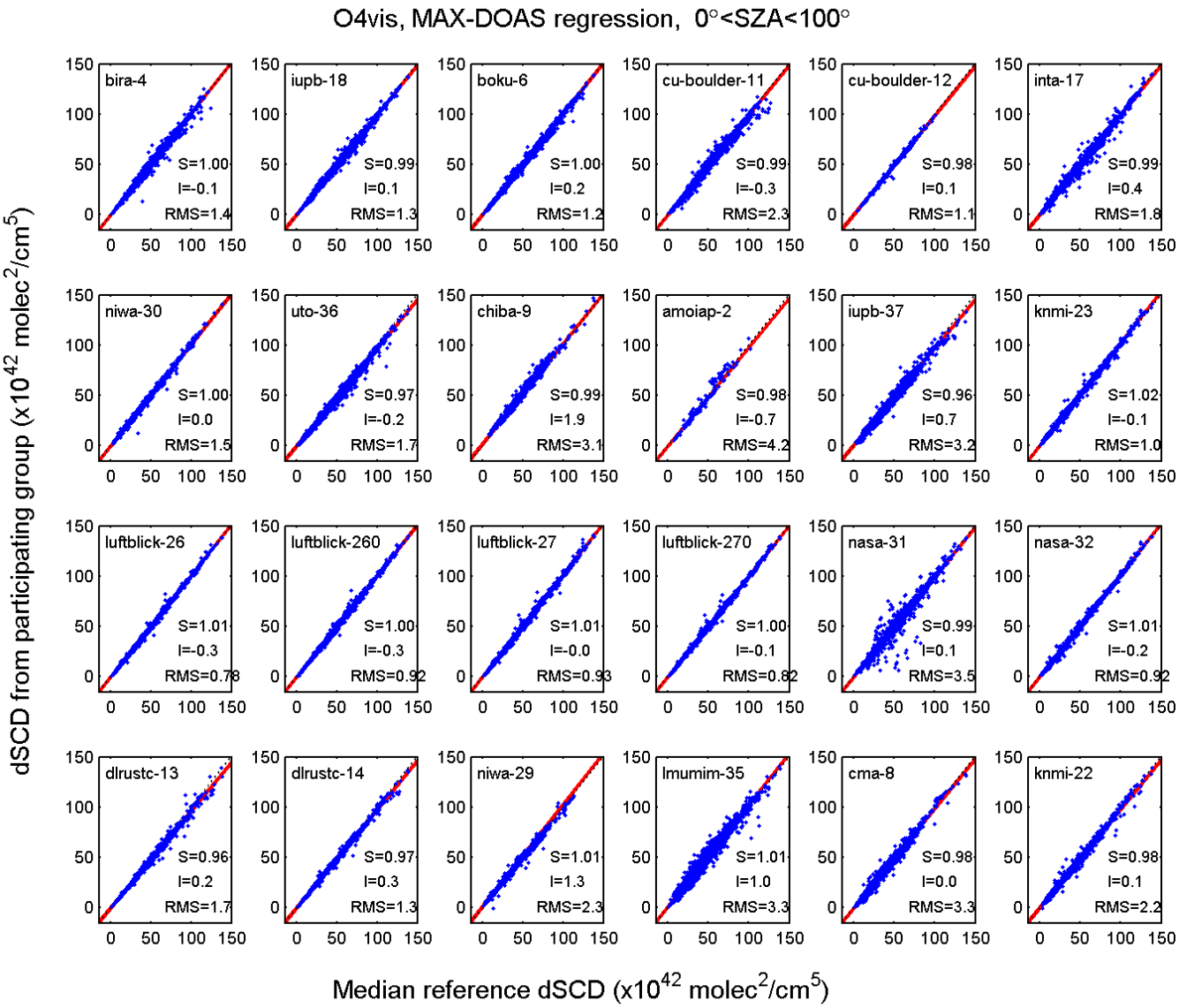

Figure S10: Regression analysis for O_4 dSCDs (measured in the visible wavelength region), corresponding to Figure 11 in the main manuscript.

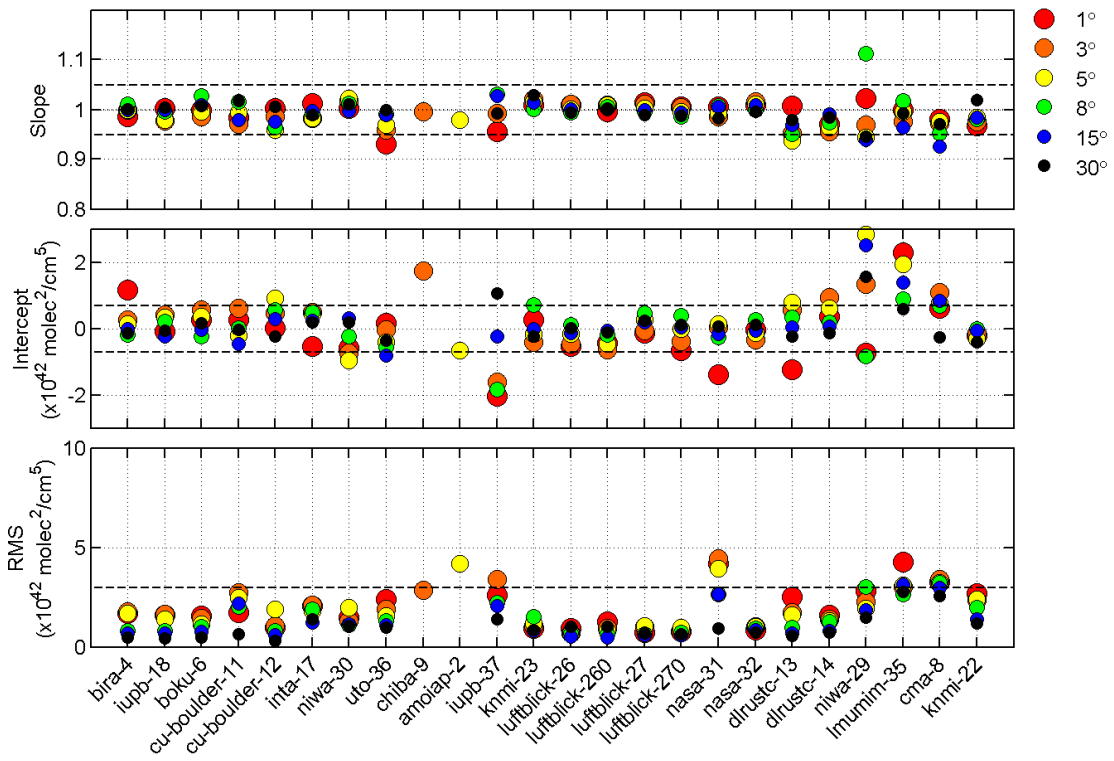

Figure S11: Slope, Intercept and RMS of O_4 dSCDs against those of the median reference data set, for each instrument measuring O_4 in the visible range. Colours refer to elevation angles shown top right.

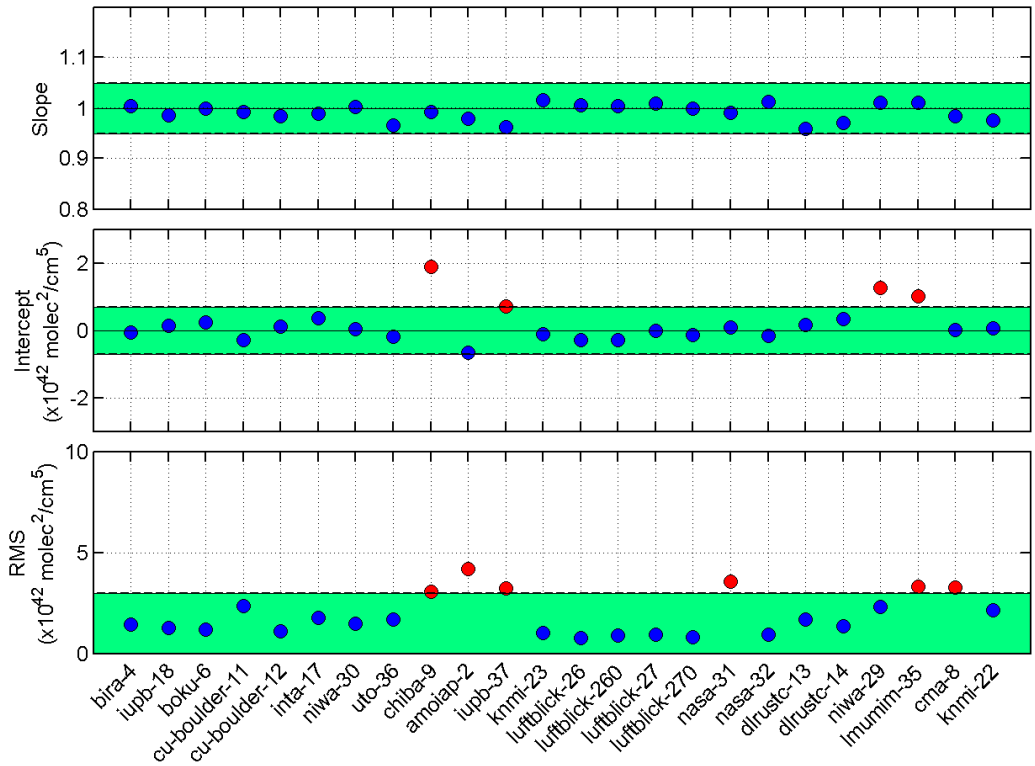

Figure S12: Summary of the regression statistic for O_4 in the visible range, showing the slope, intercept and RMS values as displayed in Figure S10. The dashed lines show the performance limits as defined in Table 5 of the main manuscript. The values within these limits are plotted in blue, the ones falling outside the limit in red.

1.5 MAX-DOAS results for O_4 in the UV range (O4uv)

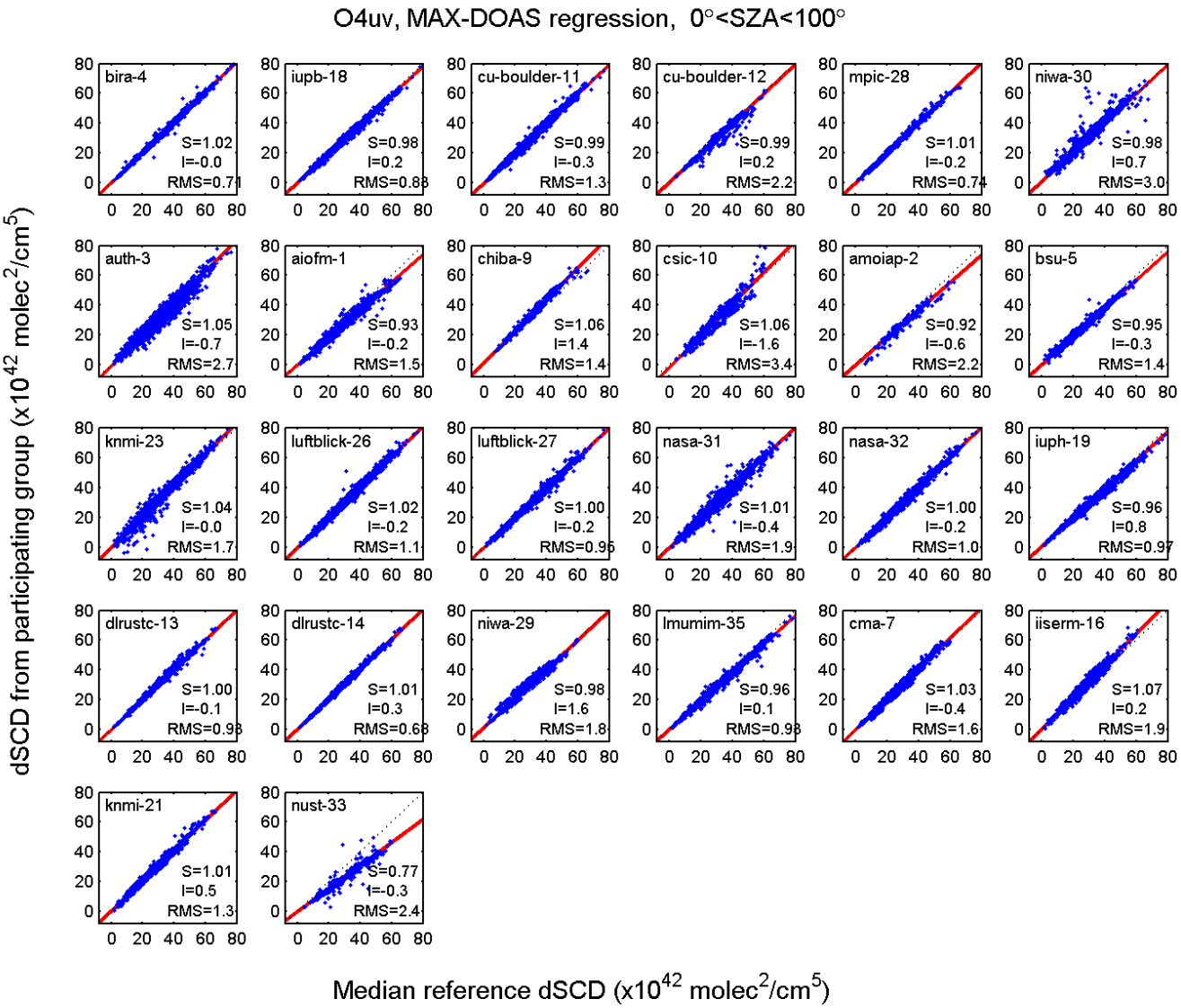

Figure S13: Regression analysis for O_4 dSCDs (measured in the UV wavelength region).

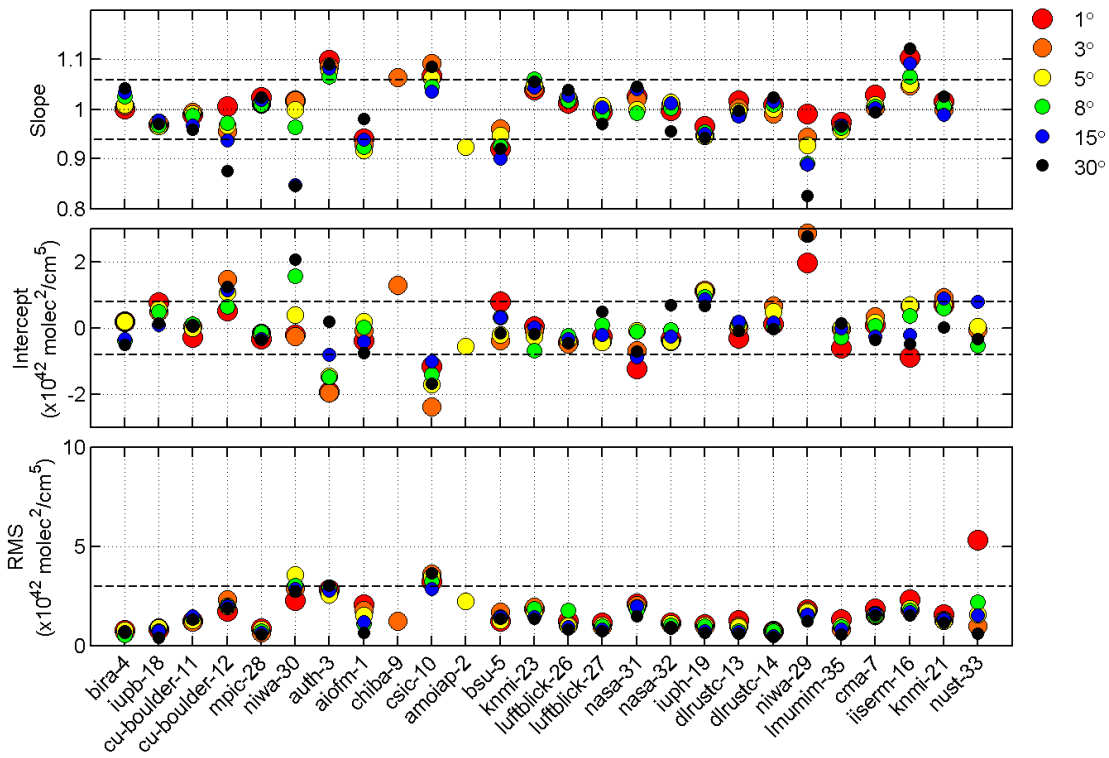

Figure S14: Slope, Intercept and RMS of O_4 dSCDs against those of the median reference data set, for each instrument measuring O_4 in the UV range. Colours refer to elevation angles shown top right.

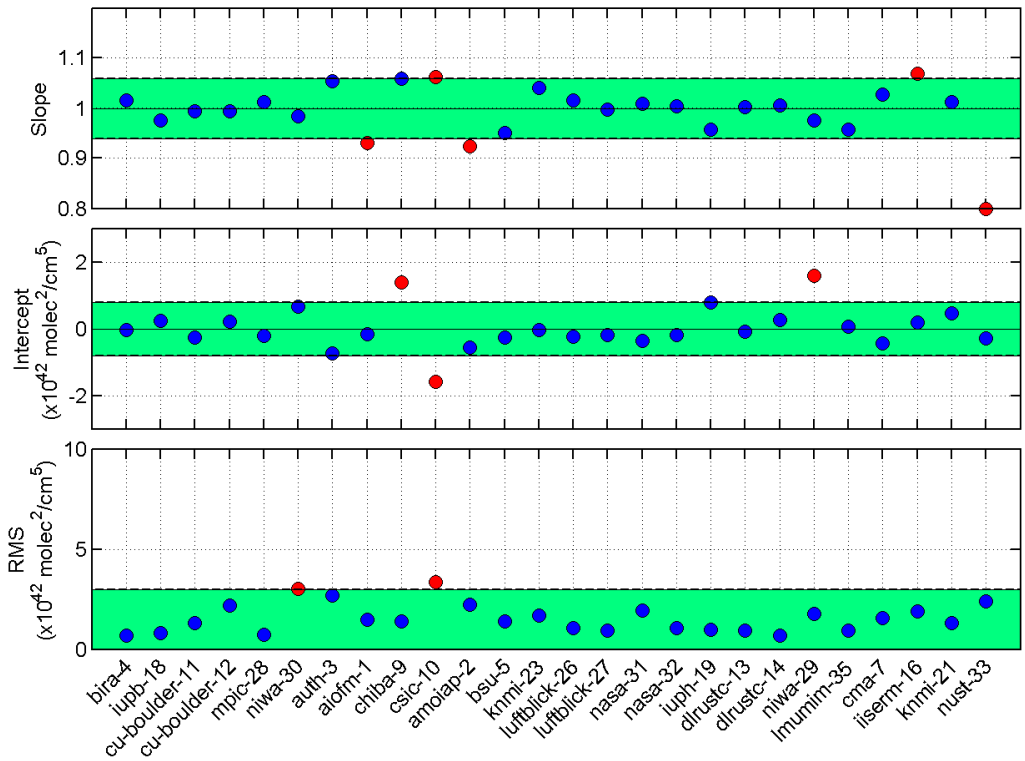

Figure S15: Summary of the regression statistic for O_4 in the UV range, showing the slope, intercept and RMS values as displayed in Figure S13. The dashed lines show the performance limits as defined in Table 5 of the main manuscript. The values within these limits are plotted in blue, the ones falling outside the limit in red.

1.6 MAX-DOAS results for HCHO

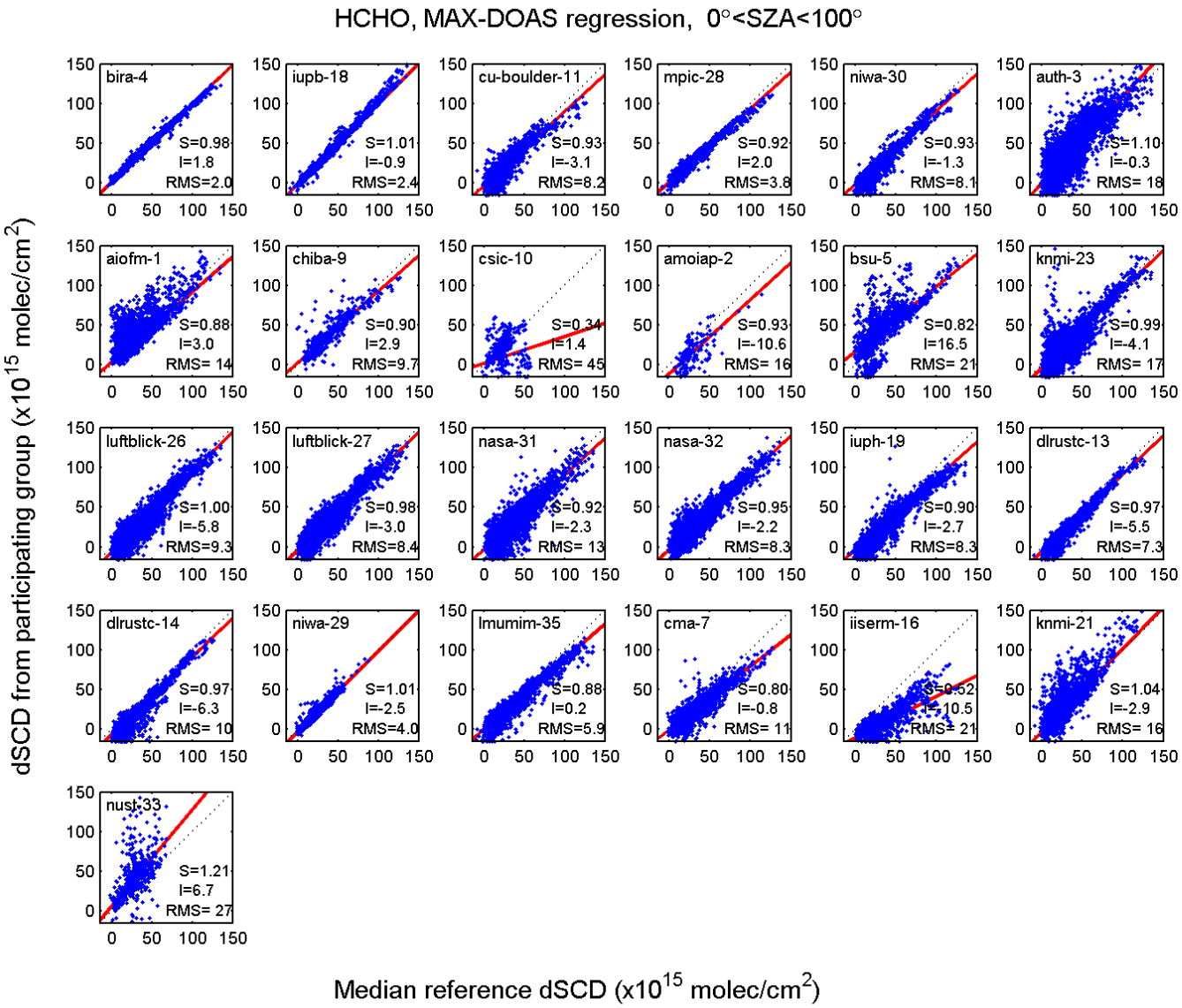

Figure S16: Regression analysis for HCHO dSCDs, corresponding to Figure 12 in the main manuscript.

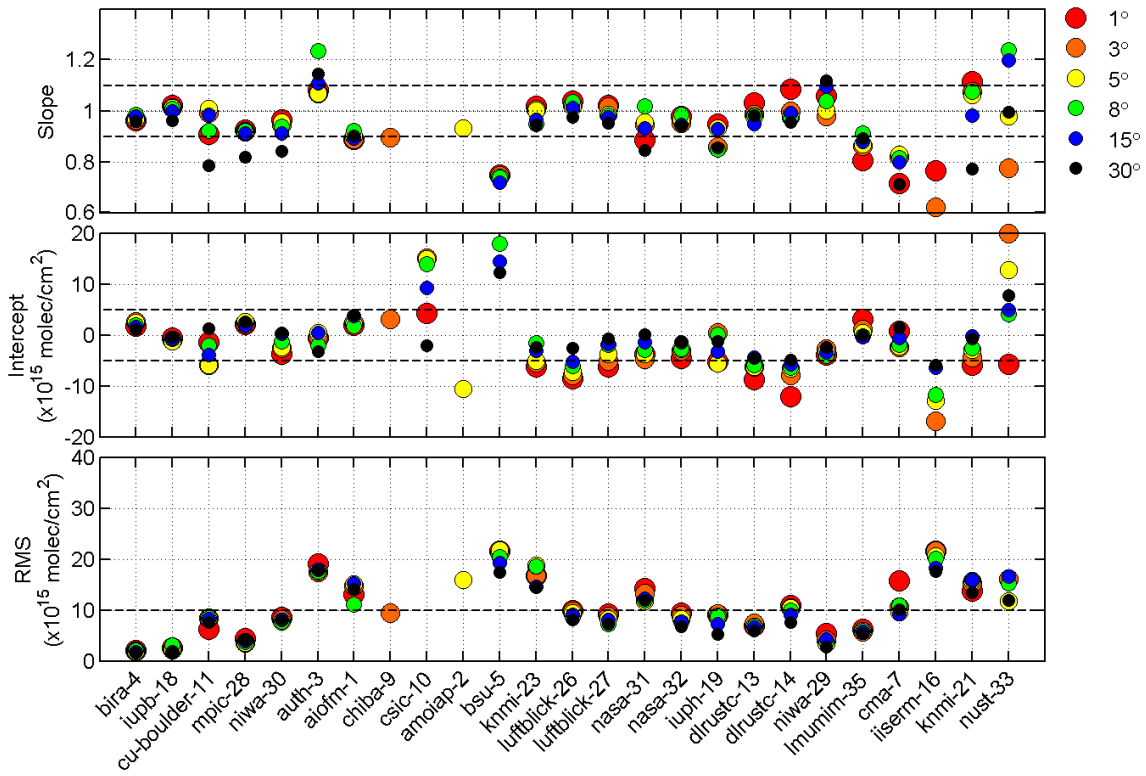

Figure S17: Slope, Intercept and RMS of HCHO dSCDs against those of the median reference data set, for each instrument measuring HCHO. Colours refer to elevation angles shown top right.

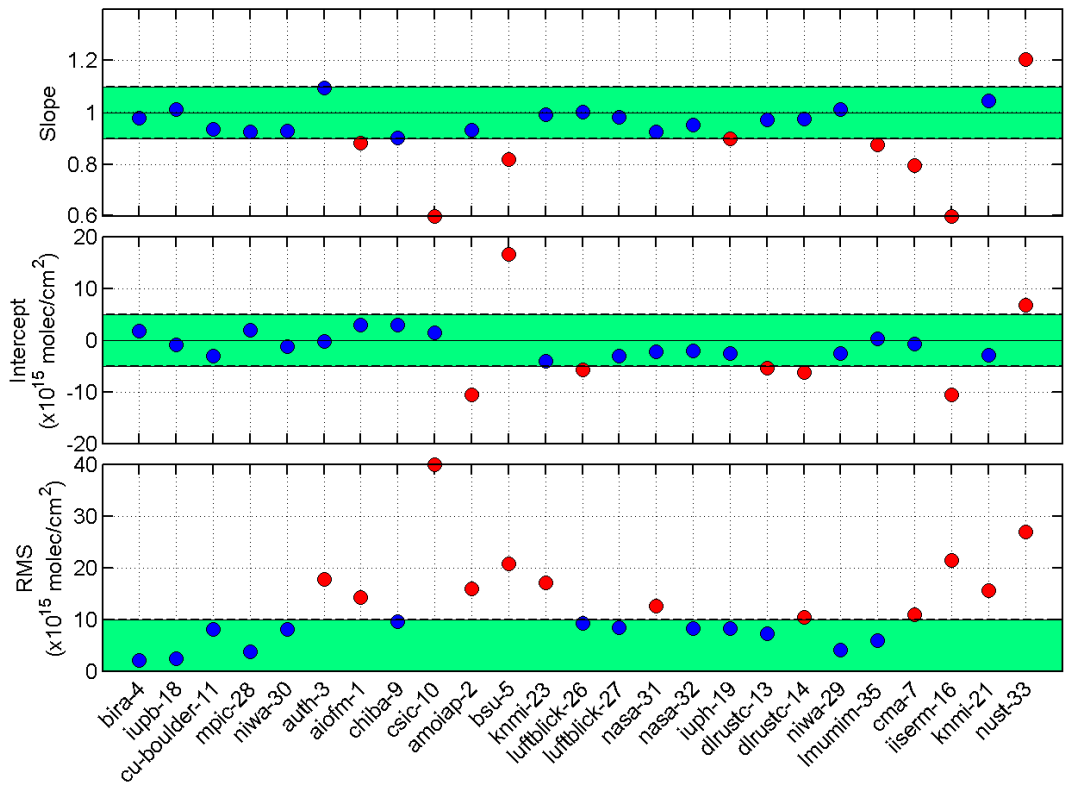

Figure S18: Summary of the regression statistic for HCHO, showing the slope, intercept and RMS values as displayed in Figure S16. The dashed lines show the performance limits as defined in Table 5 of the main manuscript. The values within these limits are plotted in blue, the ones falling outside the limit in red.

1.7 MAX-DOAS results for O_3 in the visible range (O3vis)

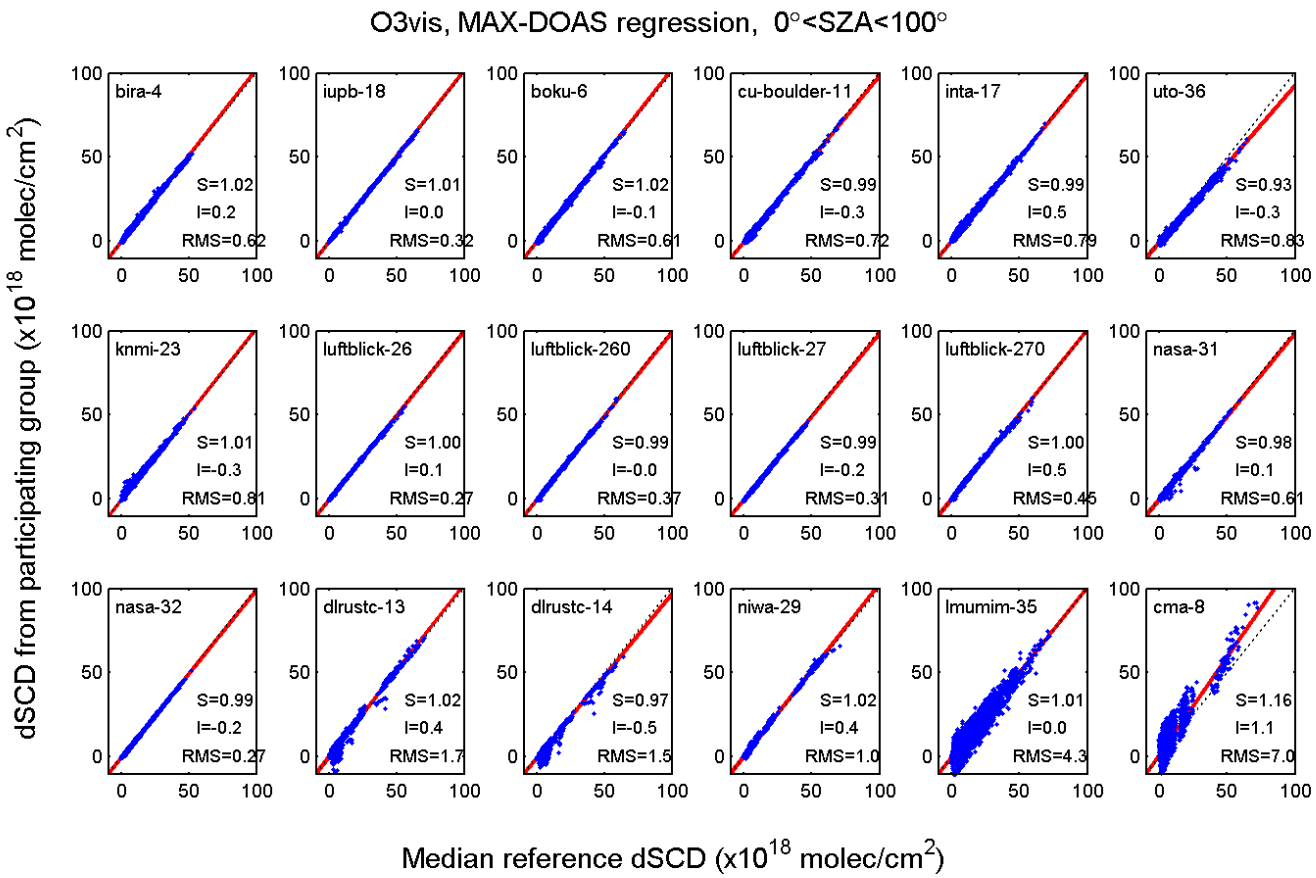

Figure S19: Regression analysis for O_3 dSCDs (measured in the visible wavelength region).

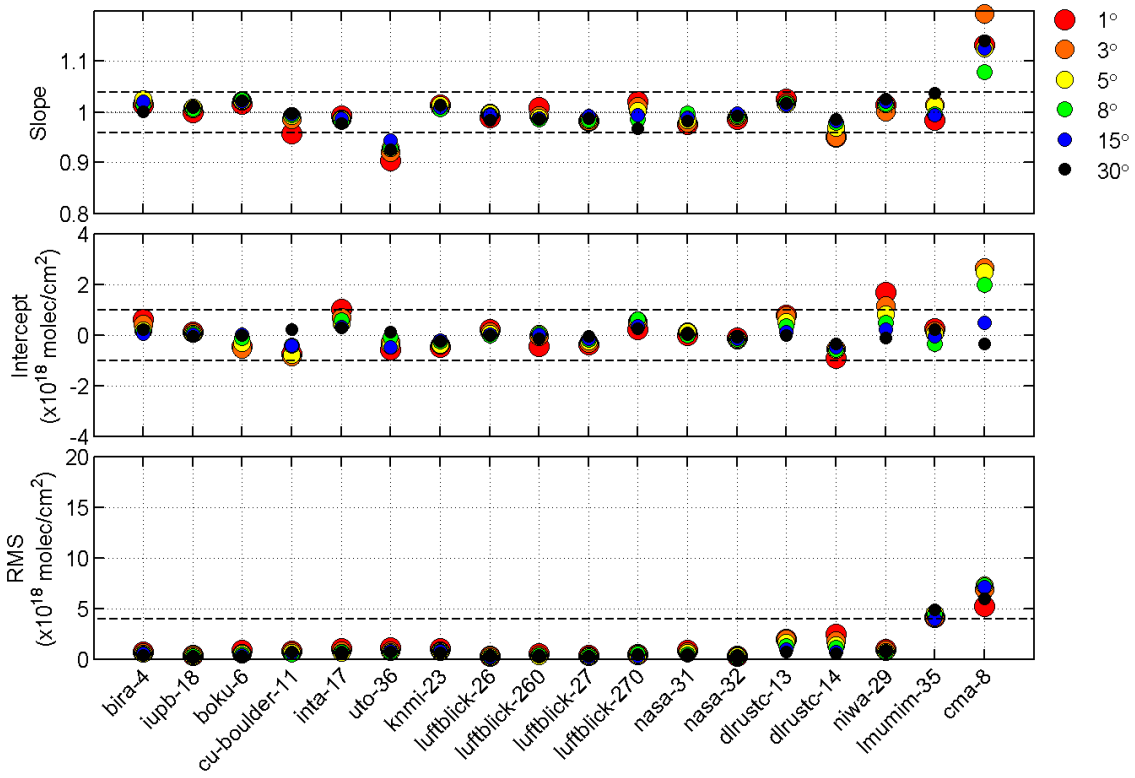

Figure S20: Slope, Intercept and RMS of O_3 dSCDs against those of the median reference data set, for each instrument measuring O_3 in the visible range. Colours refer to elevation angles shown top right.

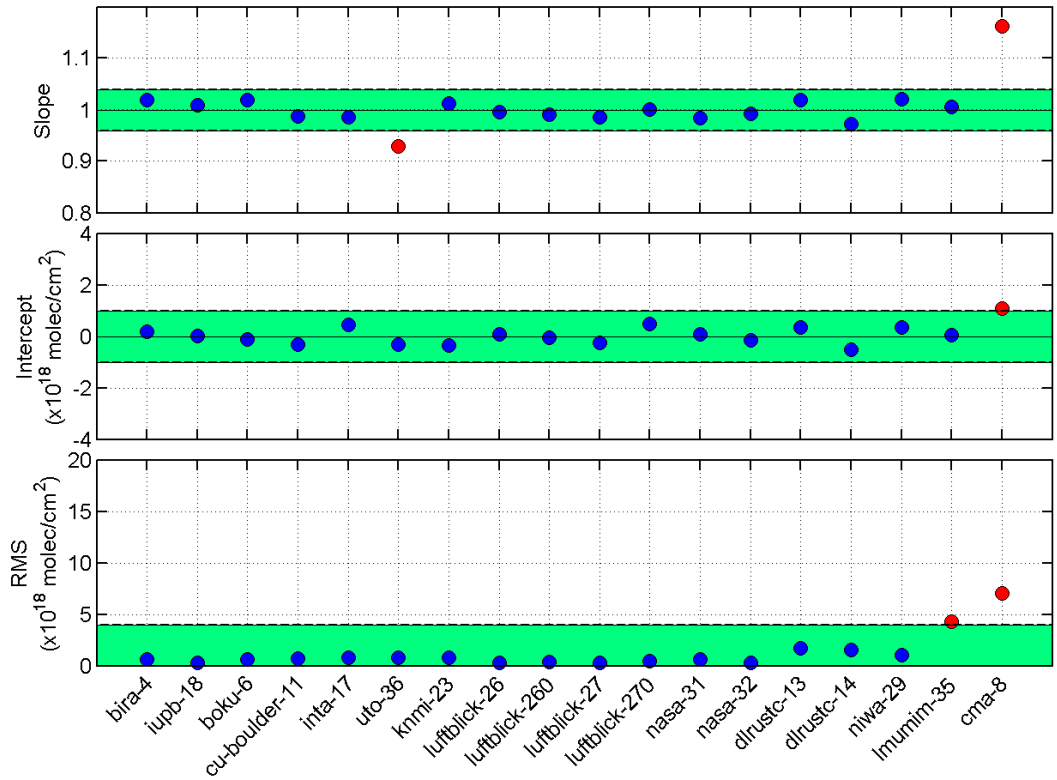

Figure S21: Summary of the regression statistic for O_3 in the visible range, showing the slope, intercept and RMS values as displayed in Figure S19. The dashed lines show the performance limits as defined in Table 5 of the main manuscript. The values within these limits are plotted in blue, the ones falling outside the limit in red.

1.8 MAX-DOAS results for O_3 in the UV range (O3uv)

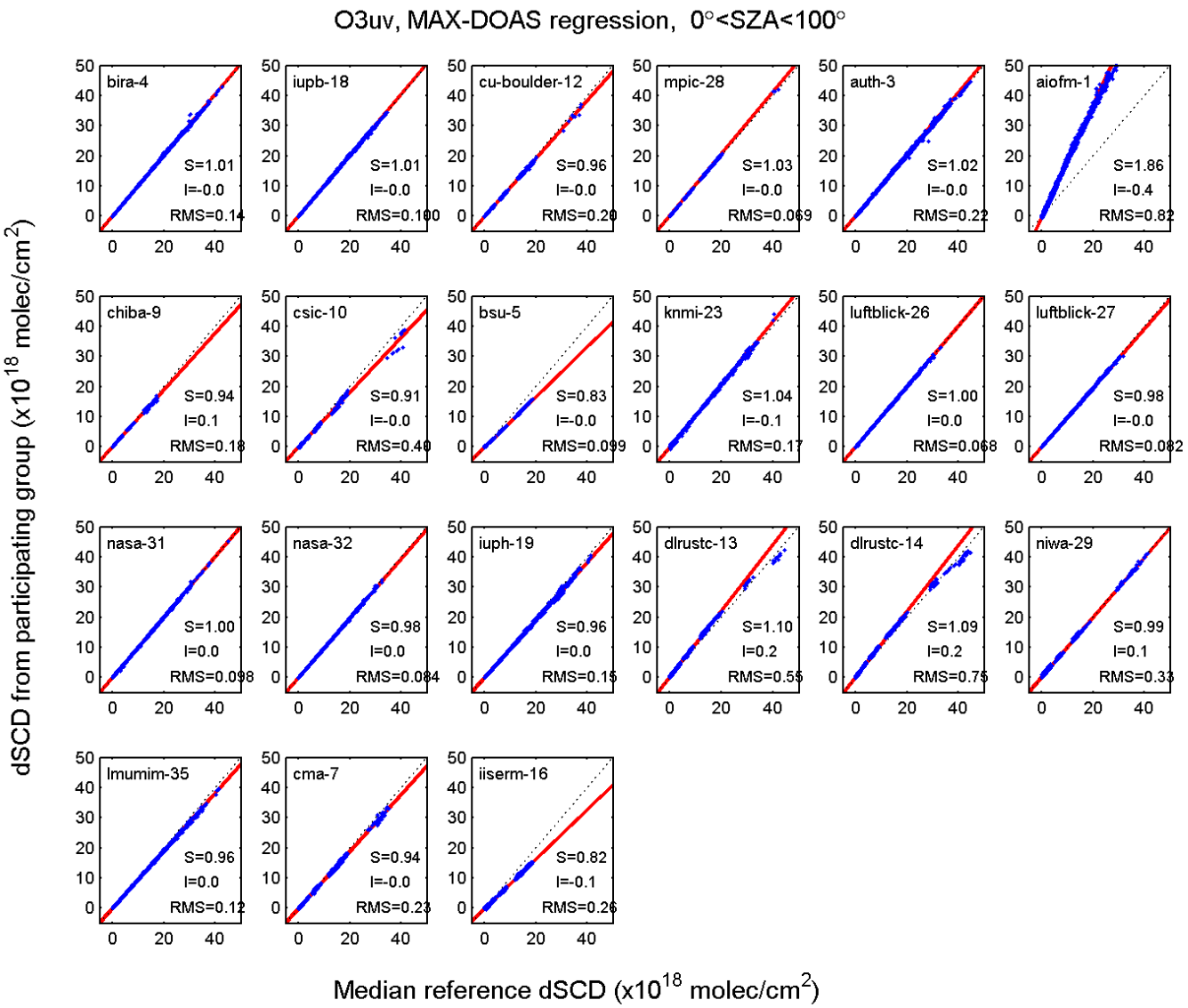
O3uv, MAX-DOAS regression, 0°<SZA<100°
bira-4
S=1.01
I=-0.0
RMS=0.14
iupb-18
S=1.01
I=-0.0
RMS=0.100
cu-boulder-12
S=0.96
I=-0.0
RMS=0.20
mpic-28
S=1.03
I=-0.0
RMS=0.069
auth-3
S=1.02
I=-0.0
RMS=0.22
aiofm-1
S=1.86
I=-0.4
RMS=0.82
chiba-9
S=0.94
I=0.1
RMS=0.18
csic-10
S=0.91
I=-0.0
RMS=0.40
bsu-5
S=0.83
I=-0.0
RMS=0.099
knmi-23
S=1.04
I=-0.1
RMS=0.17
luftblick-26
S=1.00
I=0.0
RMS=0.068
luftblick-27
S=0.98
I=-0.0
RMS=0.082
nasa-31
S=1.00
I=0.0
RMS=0.098
nasa-32
S=0.98
I=0.0
RMS=0.084
iuph-19
S=0.96
I=0.0
RMS=0.15
dlrustc-13
S=1.10
I=0.2
RMS=0.55
dlrustc-14
S=1.09
I=0.2
RMS=0.75
niwa-29
S=0.99
I=0.1
RMS=0.33
lmumim-35
S=0.96
I=0.0
RMS=0.12
cma-7
S=0.94
I=-0.0
RMS=0.23
iiserm-16
S=0.82
I=-0.1
RMS=0.26
dSCD from participating group (x10^18 molec/cm^2)
Median reference dSCD (x10^18 molec/cm^2)

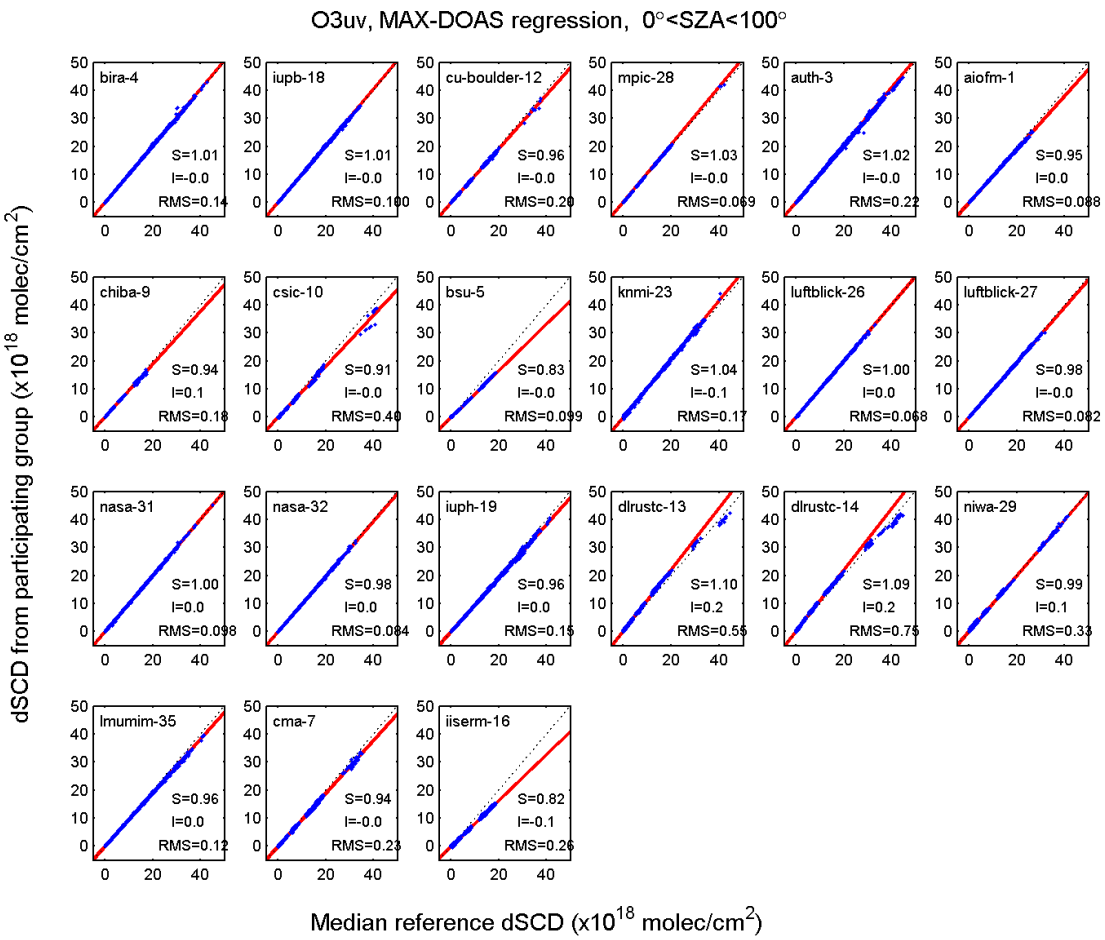

Figure S22: Regression analysis for O_3 dSCDs (measured in the UV wavelength region).

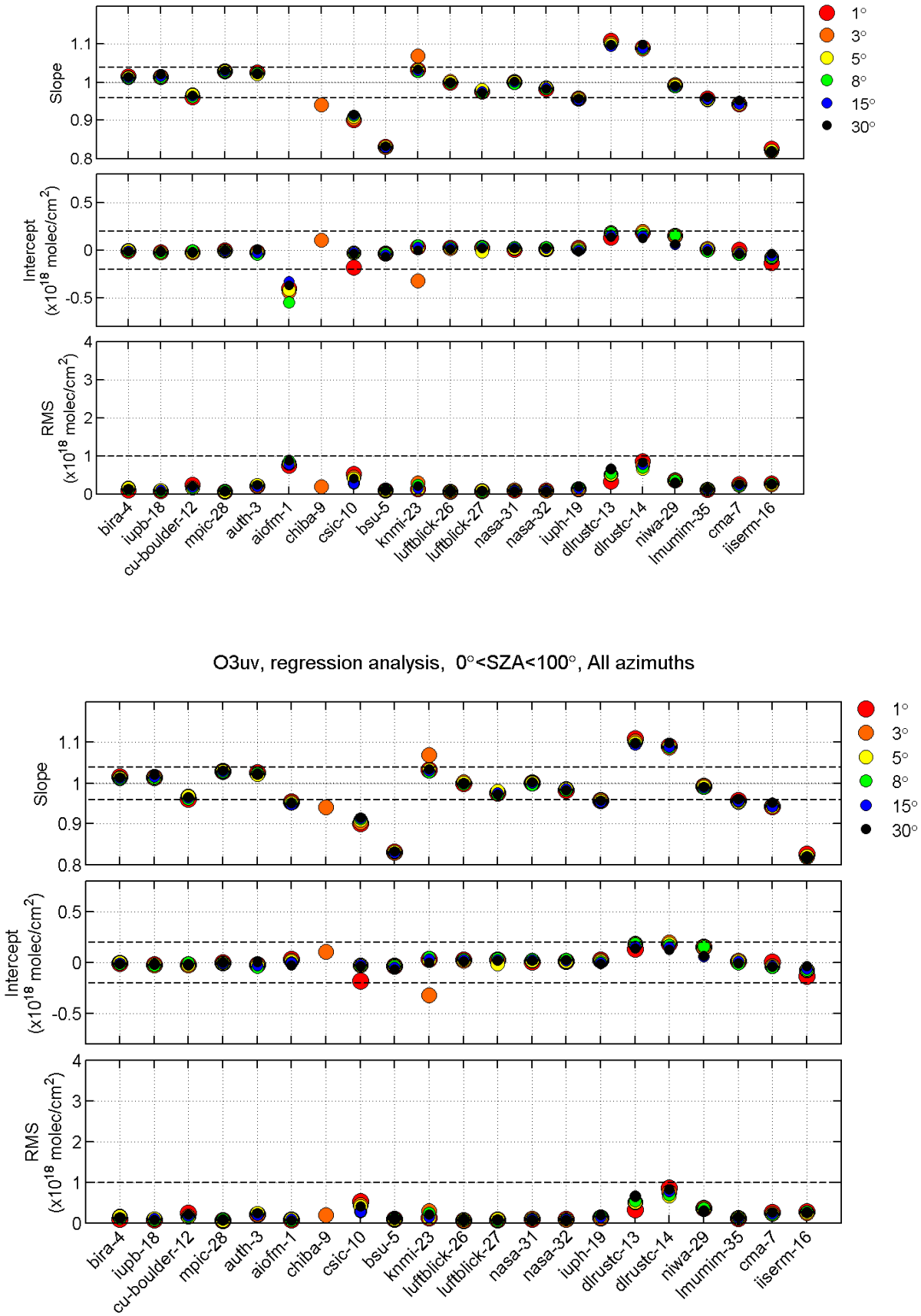

Figure S23: Slope, Intercept and RMS of O_3 dSCDs against those of the median reference data set, for each instrument measuring O_3 in the UV range. Colours refer to elevation angles shown top right.

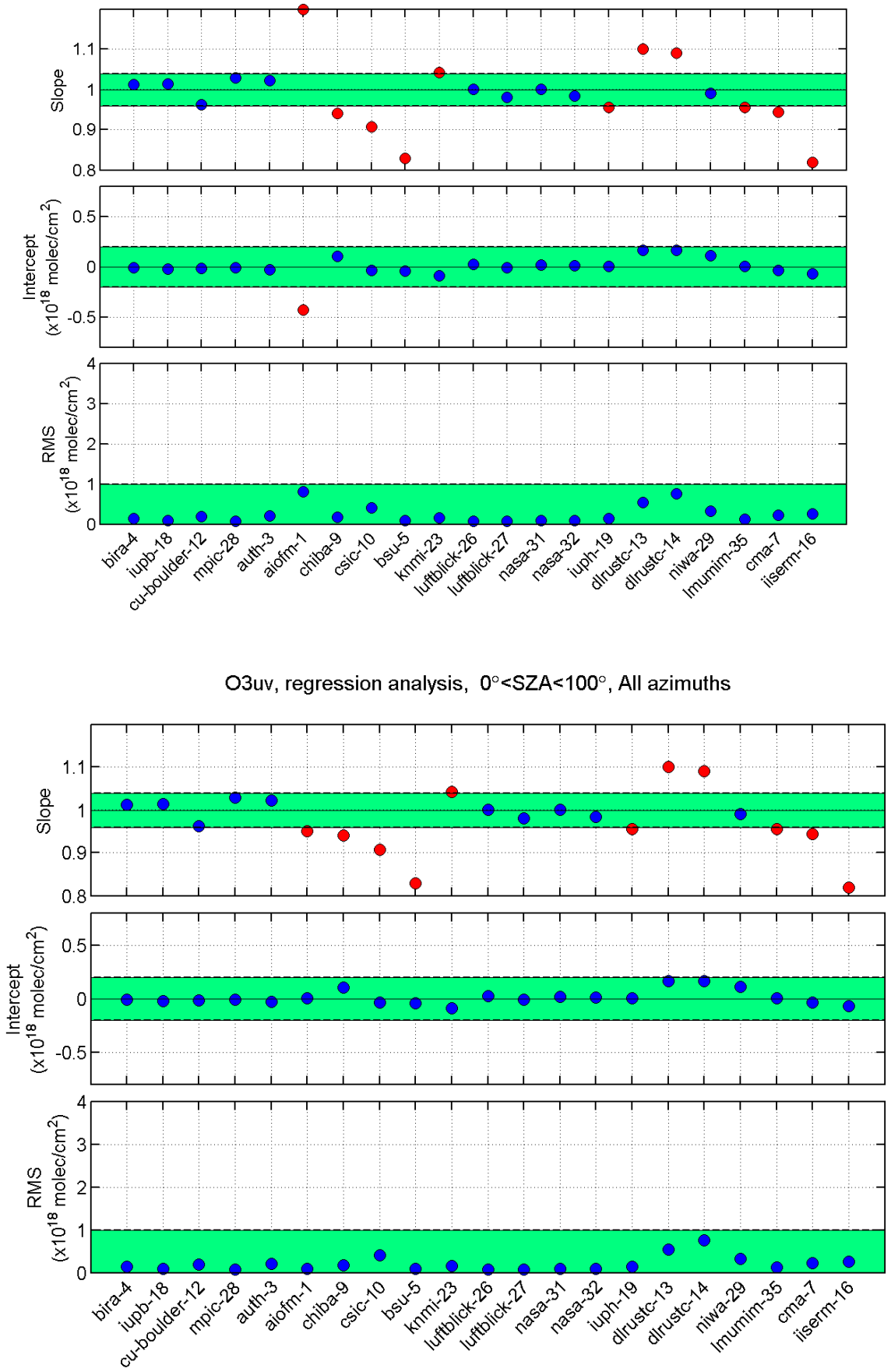

Figure S24: Summary of the regression statistic for O_3 in the UV range, showing the slope, intercept and RMS values as displayed in Figure S22. The dashed lines show the performance limits as defined in Table 5 of the main manuscript. The values within these limits are plotted in blue, the ones falling outside the limit in red.

2 Zenith-sky twilight regression results

This section presents detailed results from regression analyses performed for the four zenith-sky twilight data products. In each sub-section below, two plots are provided, showing respectively:

- scatter plots of the regression between individual data sets and median reference values for all measurement days,
- summary overview plots of the slope, intercept and RMS from regression analysis for all measurement days. These summarize the details of the performance assessment results for zenith-sky twilight measurements as performed within NDACC.

2.1 Zenith-sky results for NO_2 in the visible range (NO2vis)

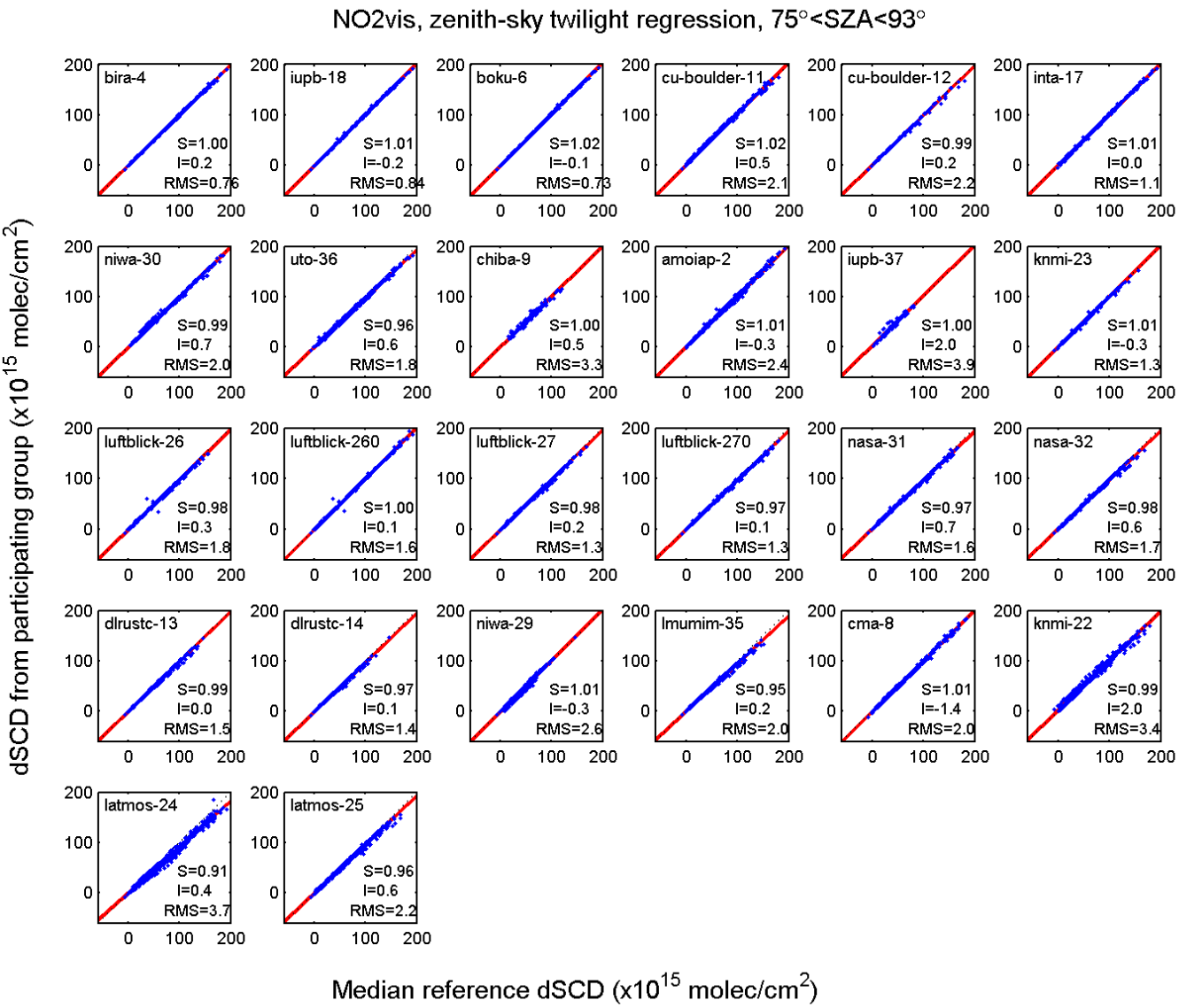

Figure S25: Regression analysis for zenith-sky NO_2 dSCDs (measured in the visible wavelength region).

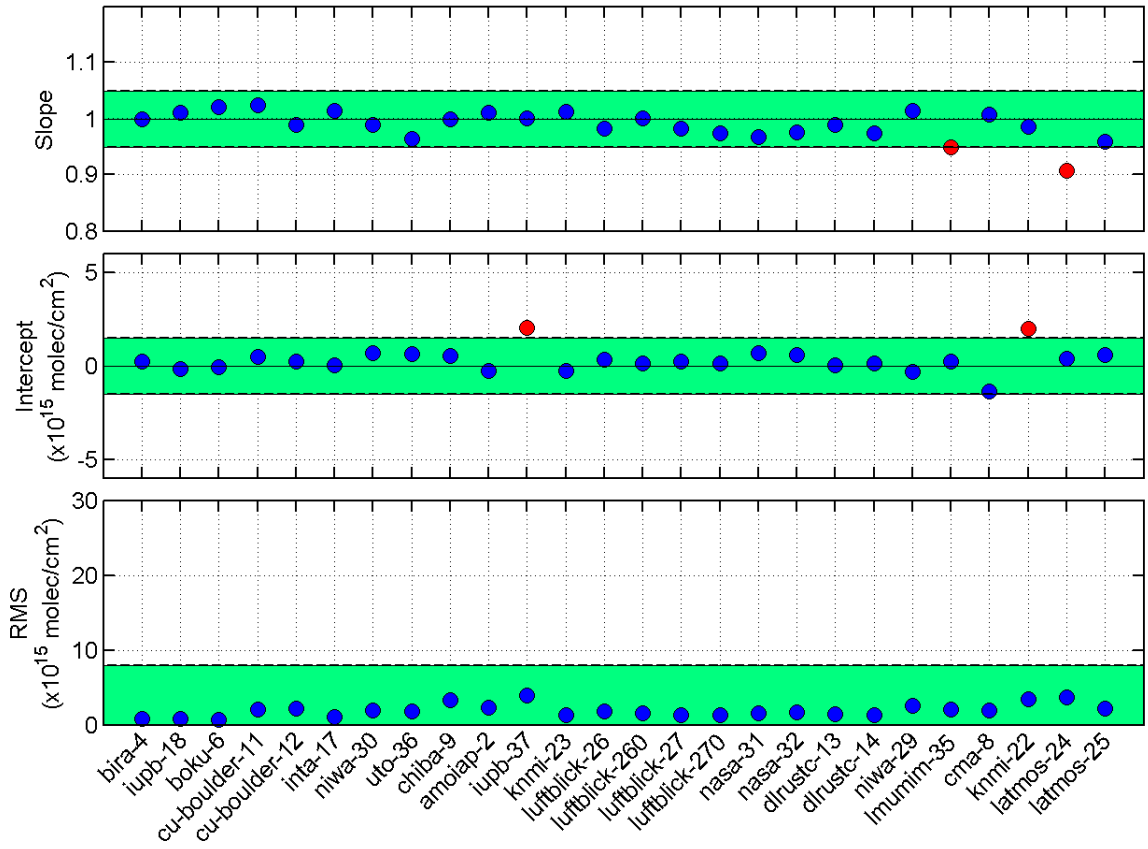

Figure S26: Summary of the regression statistic for zenith-sky NO_2 in the visible range, showing the slope, intercept and RMS values as displayed in Figure S25. The dashed lines show the performance limits as defined in Table 5 of the main manuscript. The values within these limits are plotted in blue, the ones falling outside the limit in red.

2.2 Zenith-sky results for NO_2 in the small visible range (NO2visSmall)

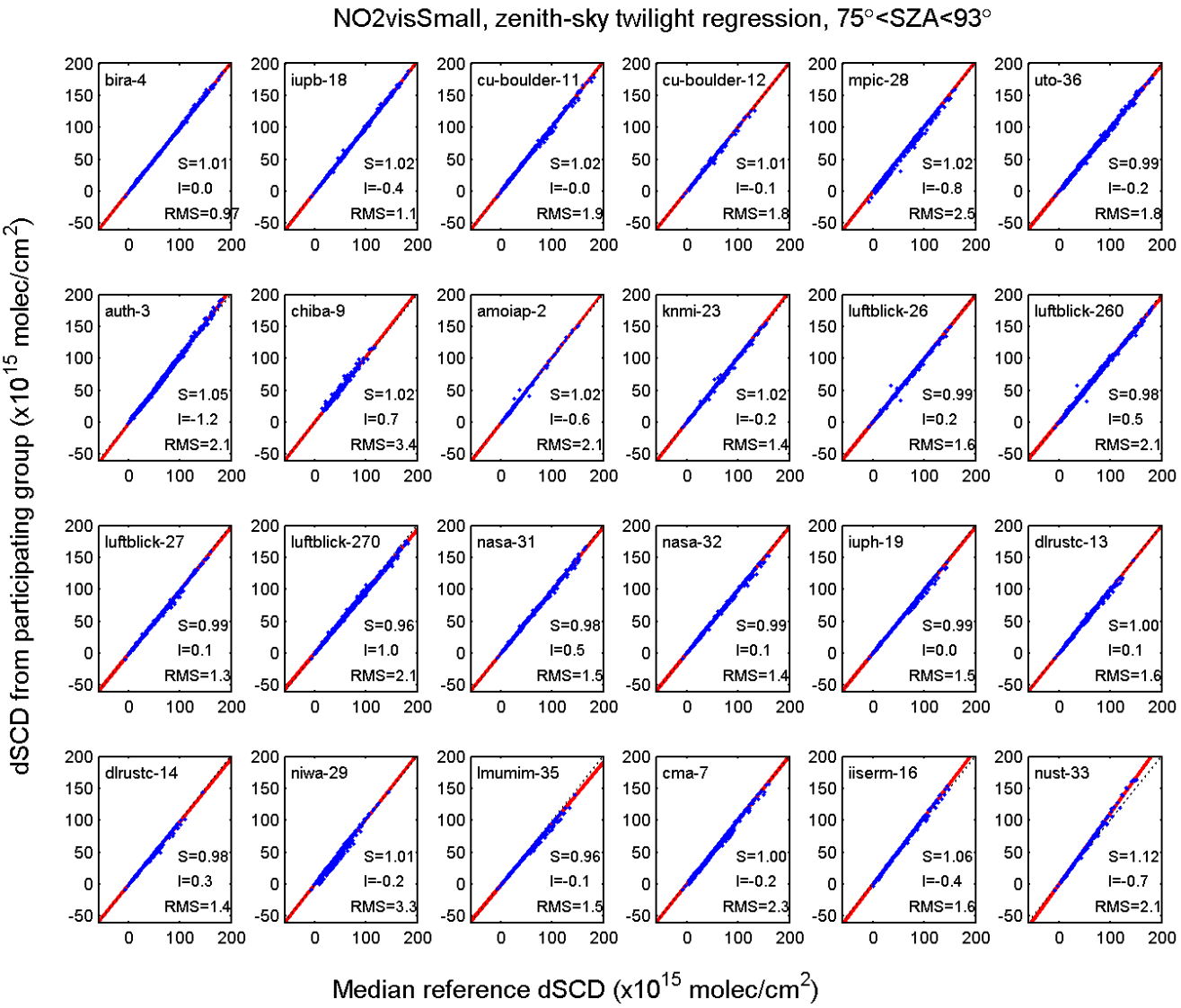

Figure S27: Regression analysis for zenith-sky NO_2 dSCDs (measured in the small visible wavelength region).

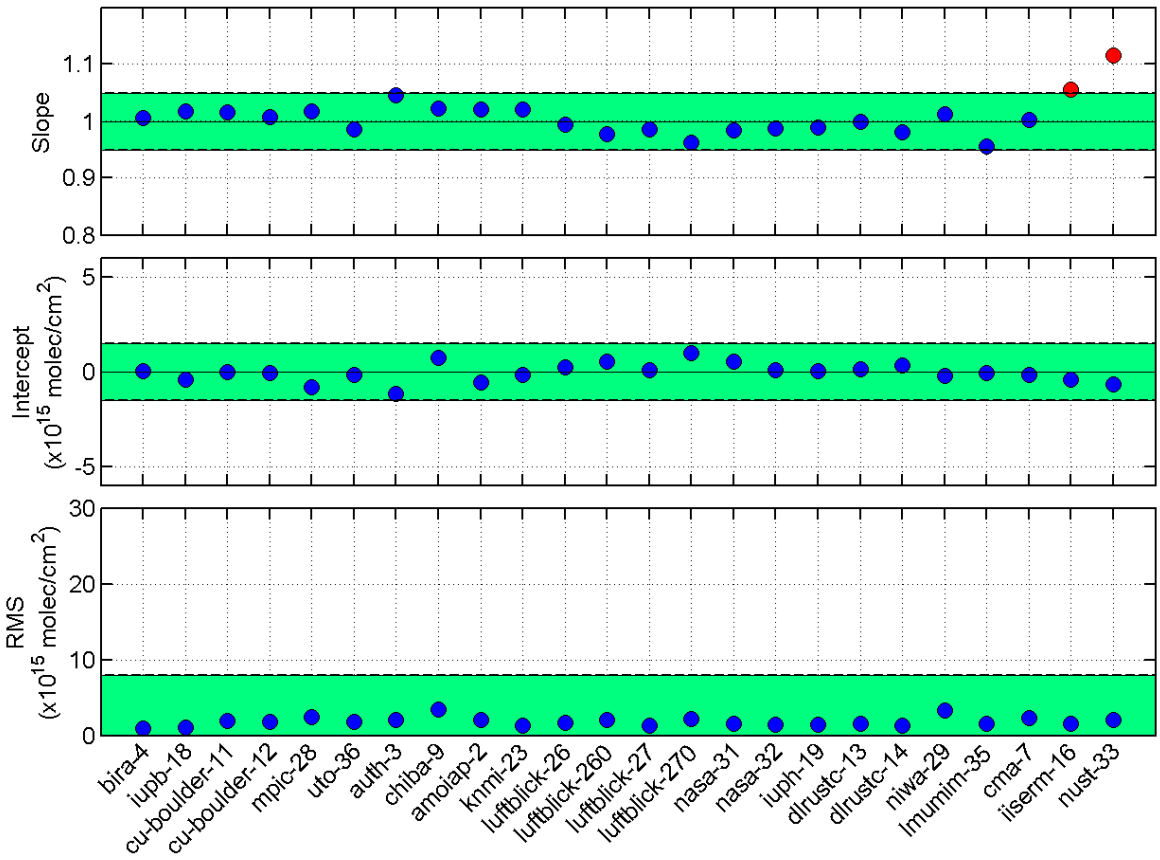

Figure S28: Summary of the regression statistic for zenith-sky NO_2 in the small visible range, showing the slope, intercept and RMS values as displayed in Figure S27. The dashed lines show the performance limits as defined in Table 5 of the main manuscript. The values within these limits are plotted in blue, the ones falling outside the limit in red.

2.3 Zenith-sky results for NO_2 in the UV range (NO2uv)

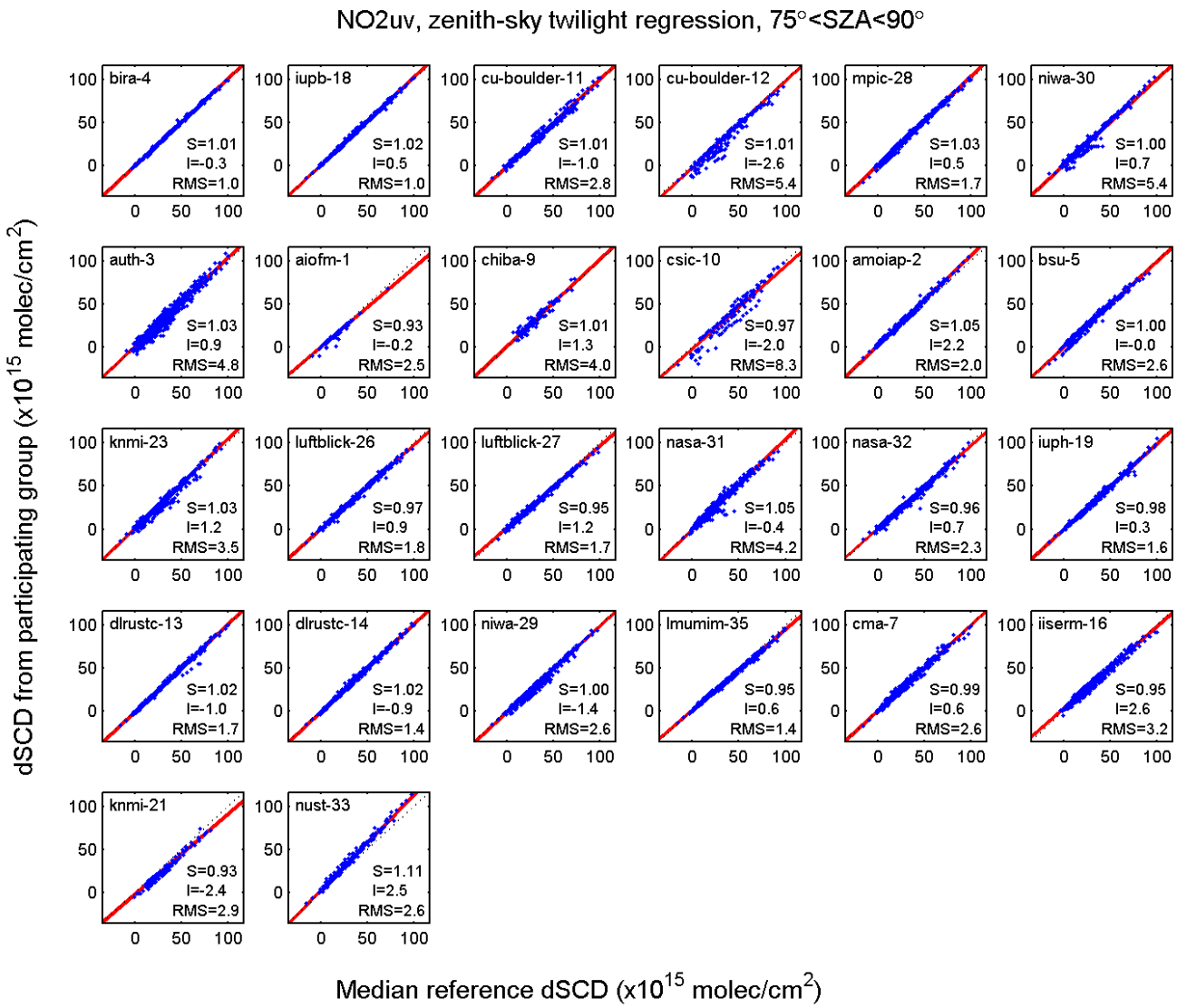

Figure S29: Regression analysis for zenith-sky NO_2 dSCDs (measured in the UV wavelength region).

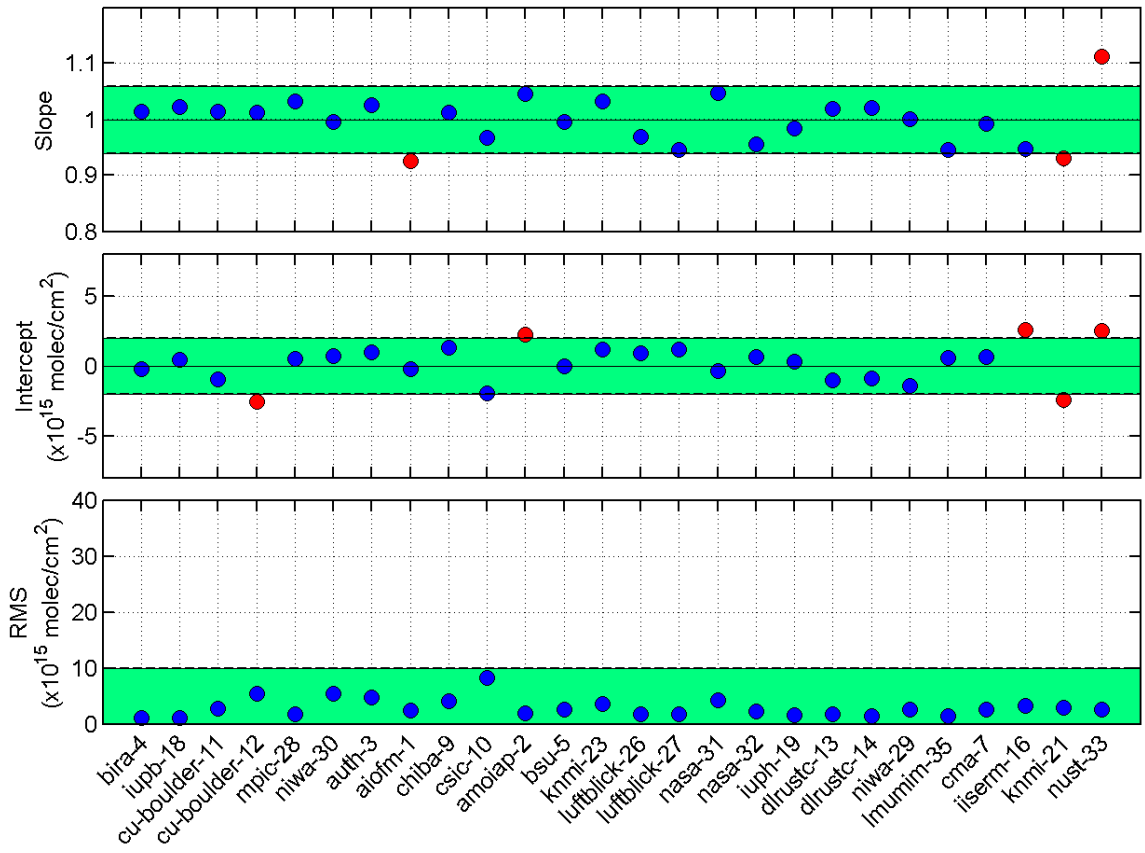

Figure S30: Summary of the regression statistic for zenith-sky NO_2 in the UV range, showing the slope, intercept and RMS values as displayed in Figure S29. The dashed lines show the performance limits as defined in Table 5 of the main manuscript. The values within these limits are plotted in blue, the ones falling outside the limit in red.

2.4 Zenith-sky results for O_3 in the visible range (O3vis)

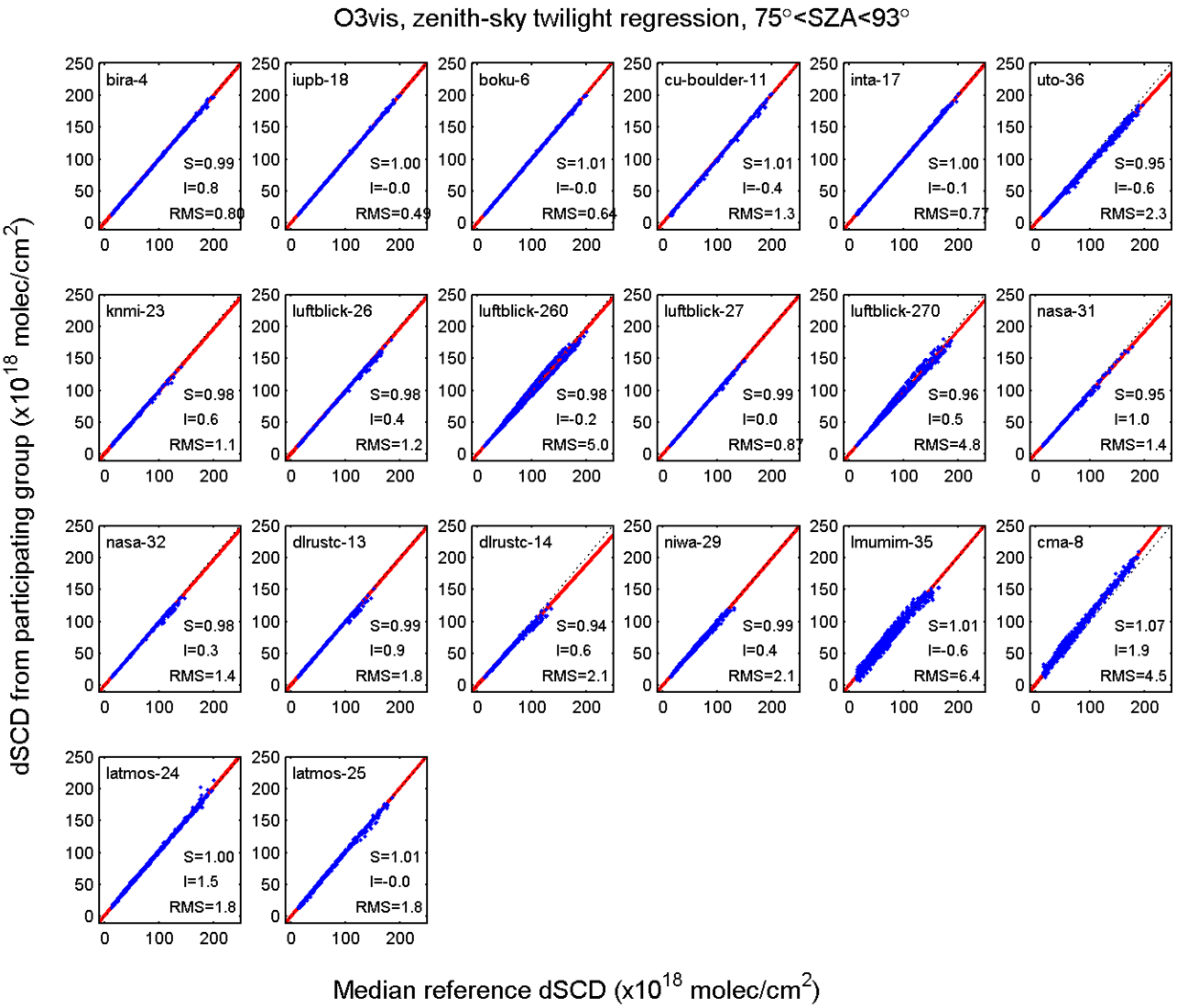

Figure S31: Regression analysis for zenith-sky O_3 dSCDs (measured in the visible wavelength region).

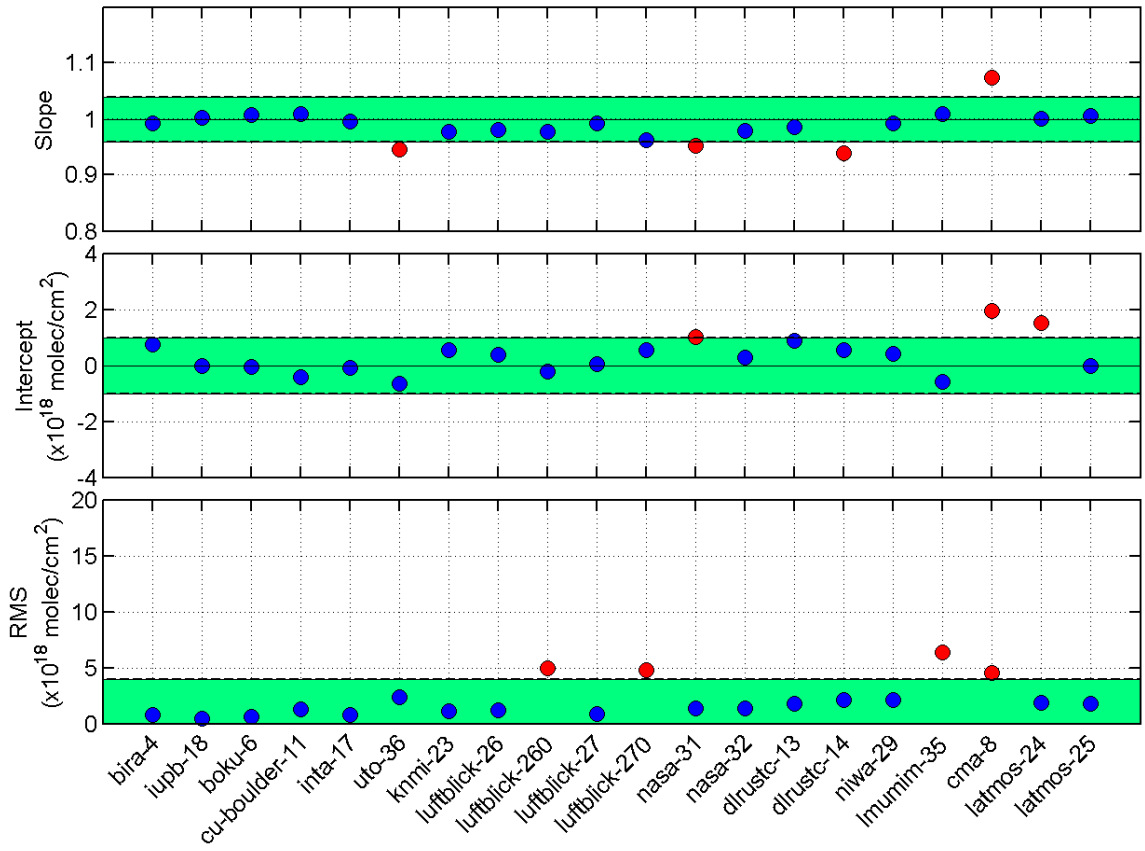

Figure S32: Summary of the regression statistic for zenith-sky O_3 in the visible range, showing the slope, intercept and RMS values as displayed in Figure S31. The dashed lines show the performance limits as defined in Table 5 of the main manuscript. The values within these limits are plotted in blue, the ones falling outside the limit in red.

3 Description and technical characteristics of the CINDI-2 MAX-DOAS and zenith-sky DOAS systems

This section presents the description of all the participating instruments. The following colour coding is used for the different types: yellow for Zenith-sky DOAS, blue for 1D MAX-DOAS and green for 2D MAX-DOAS. The instruments are listed in alphabetical order with respect to their institute acronym which is included in the top of each instrument table as part of the institute name (see also Table 1 in the main manuscript).

Institute: Anhui Institute of Optics and Fine Mechanics, Chinese Academy of Sciences (**AIOFM**), Hefei, China **Responsible person(s):** Ang Li, Pinhua Xie **Contact details:** angli@aiofm.ac.cn, phxie@aiofm.ac.cn	
Instrument type: 2D MAX-DOAS	**Nr:** CINDI-2.01
Overall design of the instrument	**Optical head including telescope:** separated; elevation and azimuth angles fully configurable **Spectrometer type:** Princeton Instrument 150i **Detector type:** Princeton Instrument PIXIS-2K BUV **Optical fibers:** quartz optical fiber, length: 10 m **Filters:** ZWB3(=UG5) **Mirrors: no** **Temperature control of spectrometer/detector:** 35°C /-30°C
Instrument performance	**Spectral range/resolution:** 290-380 (adjustable)/0.35 nm **Azimuthal scan/direct-sun capabilities:** yes/no **Elevation angle capability:** fully configurable **Field of view:** 0.2° **Typical integration time:** 10-60s **Typical scan duration:** 15 minutes
Calibration/characterization procedures	**Elevation angles:** inclinometer **Field of view:** scanning over a light source in the laboratory **Straylight:** **Dark signal:** by using the shutter **Line shape:** Hg lamp in the laboratory **Polarization: -** **Detector nonlinearity:** halogen lamp/dark background **Pixel-to-pixel variability**: halogen lamp/dark background
Spectral analysis software	QDOAS / WinDOAS
Supporting measurements	Video camera, inclinometer, GPS, electronic compass
Reference	Wang Yang, Li Ang, Xie Pin-Hua, Chen Hao, Xu Jin, Wu Feng-Cheng, Liu Jian-Guo, Liu Wen-Qing: Retrieving vertical profile of aerosol extinction by multi-axis differential optical absorption spectroscopy, Acta Phys. Sin., 62(18), 180705, http://dx.doi.org/10.7498/aps.62.180705, 2013.

Institute: A.M.Obukhov Institute of Atmospheric Physics (**AMOIAP**), Russian Academy of Sciences, Moscow, Russia **Responsible person(s):** Alexander Borovski, Oleg V.Postylyakov **Contact details:** alexander.n.borovski@gmail.com oleg.postylyakov@gmail.com		
Instrument type: 2-port DOAS	**Nr:** CINDI-2.02	
Overall design of the instrument	**Optical head including telescope:** separated; 2 telescope units (one for zenith + one for off-axis) **Spectrometer type:** Shamrock303i spectrograph with filter wheel **Detector type:** Newton CCD (DU940N-BU2, 2048×512 pxls) **Optical fibers:** standard fiber cable with two inputs and one output, length: 25 m **Filters:** Andover Corp. filter S86FG11-25 (transmittion from 320 to 700 nm) **Mirrors:** no **Temperature control of spectrometer/detector:** 35°C/-40°C	
Instrument performance	**Spectral range/resolution VIS1:** 420-490 / 0.4 nm **Spectral range/resolution VIS2:** 395-465 / 0.4 nm **Spectral range/resolution VIS3:** 390-530 / 0.9 nm **Spectral range/resolution UV:** 315-385 / 0.4 nm **Azimuthal scan/direct-sun capabilities:** no/no **Elevation angle capability:** two fixed elevation angles (one zenith and one 5°) **Field of view:** 0.3° **Typical integration time:** 1 – 10 s **Typical scan duration:** 30 – 40 s	
Calibration/characterization procedures	**Elevation angles:** adjusted manually using bubble and digital levels **Field of view:** measured in the lab **Straylight:** unknown **Dark signal:** using unilluminated parts of the detector **Line shape:** Hg lamp in the lab, FWHM adjusted during spectra analysis **Polarization:** n/a (use of long depolarizing fiber bundle) **Detector nonlinearity:** unknown **Pixel-to-pixel variability**: unknown	
Spectral analysis software	Andor Solis/own-developed software	
Supporting measurements	n/a	
Reference	I. Bruchkouski, A. Borovski, A. Elokhov, and O. Postylyakov. A layout of two-port DOAS system for investigation of atmospheric trace gases based on laboratory spectrograph, Proc. SPIE, 10035, 100353C, https://doi.org/10.1117/12.2248634, 2016.	

Institute: Physics Department, Section of Applied and Environmental Physics, Laboratory of Atmospheric Physics, Aristotle University of Thessaloniki (**AUTH**), Thessaloniki, Greece **Responsible person(s):** Alkiviadis Bais, Theano Drosoglou **Contact details:** abais@auth.gr, tdroso@auth.gr		
Instrument type: Phaethon mini MAX-DOAS	**Nr:** CINDI-2.03	

Overall design of the instrument	**Optical head including telescope:** separated; elevation and azimuth angles fully configurable **Spectrometer type:** AvaSpec-ULS2048LTEC (Avantes) **Detector type:** SONY2048L (CCD linear array) **Optical fibers:** standard fiber cable with metal silicone jacketing, 800 µm fiber core diameter and overall length of 8 meters **Filters:** filter wheel: neutral density filter + ground quartz diffuser plate for direct-sun, clear aperture for sky-radiance, opaque for dark signal **Mirrors:** no mirrors, plano-convex lens **Temperature control of spectrometer/detector:** 5°C/5°C
Instrument performance	**Spectral range/resolution:** 297-452/0.3-0.4 nm **Azimuthal scan/direct-sun capabilities:** yes/yes **Elevation angle capability:** fully configurable, 0.125° resolution **Field of view:** 1° **Typical integration time:** 200-3000 ms (scattered light) **Typical scan duration:** 10-20 minutes for a sequence of elevation angles
Calibration/characterization procedures	**Elevation angles:** Sighting using the solar disk **Field of view:** white reflecting stripe measurements in laboratory **Straylight:** tunable-laser measurements **Dark signal:** after each scan sequence for all integration times used **Line shape:** laser lines and spectral discharge lamp measurements **Polarization:** zenith radiance measurements at different azimuth angles **Detector nonlinearity:** tunable-laser measurements with varying output **Pixel-to-pixel variability**: tungsten halogen lamp measurements
Spectral analysis software	QDOAS (currently version 2.109.3)
Supporting measurements	None during the campaign
Reference	Drosoglou, T., A. F. Bais, I. Zyrichidou, N. Kouremeti, A. Poupkou, N. Liora, C. Giannaros, M. E. Koukouli, D. Balis, and D. Melas (2017), Comparisons of ground-based tropospheric NO2 MAX-DOAS measurements to satellite observations with the aid of an air quality model over the Thessaloniki area, Greece, Atmos. Chem. Phys., 17(9), 5829-5849; http://dx.doi.org/ 10.5194/acp-17-5829-2017.

Institute: Royal Belgian Institute for space Aeronomy (**BIRA-IASB**), Brussels, Belgium **Responsible person(s):** Christian Hermans and Michel Van Roozendael **Contact details:** christh@aeronomie.be, michelv@oma.be	
Instrument type: 2D MAX-DOAS	**Nr:** CINDI-2.04
Overall design of the instrument	**Optical head including telescope:** separated; elevation and azimuth angles fully configurable; active sun tracking system **Spectrometer type UV:** Newport, model: 74086 **Spectrometer type vis:** Horiba, model: Micro HR **Detector type UV:** CCD Back-illuminated Princeton Instrument Pixis 2K **Detector type vis:** CCD Back-illuminated Princeton Instrument Pixis 100 **Optical fibers:** quartz UV chanel**:** monofiber (l:6m,diam:1000µm)+ bundle(length:2m, 51 fibers 100µm) Vis chanel**:** monofiber (l:6m,diam:800µm)+ bundle(length:2m, 37 fibers 100µm) **Filters:** UV chanel : Filter band U-340 Hoya **Mirrors:** no (for telescope we use lens in quartz) **Temperature control of spectrometer and detector UV:** 30°C/-50°C **Temperature control of spectrometer and detector vis:** 30°C/-50°C
Instrument performance	**Spectral range/resolution UV:** 300–390/0.4 nm **Spectral range/resolution vis:** 405–540/0.7 nm **Azimuthal scan/direct-sun capabilities:** yes/yes **Elevation angle capability:** fully configurable; resolution: <0.1° **Field of view:** <1° **Typical integration time:** total measurement t:60 sec (t min: vis 0.03s, UV 0.1s) **Typical scan duration:** 20 minutes
Calibration/characterization procedures	**Elevation angles:** digital inclinometer in telescope **Field of view:** white light source in lab **Straylight:** double monochromator fed by white light source **Dark signal:** measured as night every day **Line shape:** HgCd lamp in the lab, further adjusted using QDOAS **Polarization:** n/a (use of long depolarising fiber bundle) **Detector nonlinearity:** white light source in the lab **Pixel-to-pixel variability**: white light source in the lab
Spectral analysis software	QDOAS
Supporting measurements	Video camera
Reference	Clémer, K., Van Roozendael, M., Fayt, C., Hendrick, F., Hermans, C., Pinardi, G., Spurr, R., Wang, P., and De Mazière, M.: Multiple wavelength retrieval of tropospheric aerosol optical properties from MAXDOAS measurements in Beijing, Atmos. Meas. Tech., 3, 863-878, https://doi.org/10.5194/amt-3-863-2010, 2010.

Institute: Institute of Meteorology, University of Natural Resources and Life Sciences (**BOKU**), Vienna, Austria **Responsible person(s):** Stefan Schreier **Contact details:** Stefan.Schreier@boku.ac.at		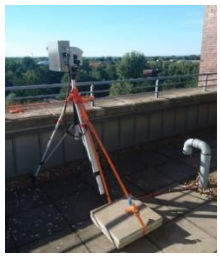
Instrument type: 1 channel scientific grade elevation and azimuth scanning MAX-DOAS	**Nr:** CINDI-2.06	

Overall design of the instrument	**Optical head including telescope:** separated; elevation and azimuth angles fully configurable **Spectrometer type:** Acton Standard Series SP-2356 Imaging Spectrograph **Detector type:** PIX100B-SF-Q-F-A **Optical fibers:** Y-type quartz bundle, diameter: 150µm, length: 25m **Filters:** no **Mirrors:** no **Temperature control of spectrometer and detector:** 35°C/-60°C
Instrument performance	**Spectral range/resolution:** 419–553/0.8 nm **Azimuthal scan/direct-sun capabilities:** yes/no **Elevation angle capability:** fully configurable **Field of view:** 0.8° **Typical integration time:** 30s (off-axis); 60s (zenith) **Typical scan duration:** 10 minutes for 10 elevation angles
Calibration/characterization procedures	**Elevation angles:** geometric alignment of telescope, horizon scan **Field of view:** white light source in lab **Straylight:** not yet characterized **Dark signal:** nightly measurements **Line shape:** HgCd lamp in telescope **Polarization:** - **Detector nonlinearity:** white light source in lab, characterization only **Pixel-to-pixel variability**: white light source in lab, characterization only
Spectral analysis software	NLIN
Supporting measurements	Video camera, HgCd lamp
Reference	Schreier et al., Multiple ground-based MAX-DOAS observations in Vienna, Austria – part 1: Evaluation of horizontal and temporal NO2, HCHO, and CHOCHO distributions and comparison with independent data sets, to be submitted to ACP (2019)

Institute: Belarusian State University (**BSU**), Minsk, Belarus **Responsible person(s):** Ilya Bruchkouski **Contact details:** bruchkovsky2010@yandex.by		
Instrument type: MAX-DOAS one azimuth, catadioptric telescope / MARS-B	**Nr:** CINDI-2.05	

Overall design of the instrument	**Optical head including telescope:** integrated **Spectrometer type:** Oriel MS257 imaging spectrograph (1:4) **Detector type:** Andor DV420-OE 256*1024 pixels CCD **Optical fibers:** n/a **Filters:** red **Mirrors:** yes **Temperature control of detector:** -40°C
Instrument performance	**Spectral range/resolution:** 409-492/0.4 nm + possibly also UV **Azimuthal scan/direct-sun capabilities:** no/no **Elevation angle capability:** fully configurable **Field of view:** 0.2° (azimuth); 1° (elevation) **Typical integration time:** 1-3s **Typical scan duration:** 1.5 minutes (12 elevation angles)
Calibration/characterization procedures	**Elevation angles:** Udo Friess method (laser level, narrow mercury lamp) **Field of view:** measured in the lab **Straylight:** N/A **Dark signal:** 485 ±6 counts **Line shape:** Gaussian **Polarization:** N/A **Detector nonlinearity:** above 25000 counts **Pixel-to-pixel variability**: ±6 counts
Spectral analysis software	Self-made + Windoas
Supporting measurements	Video camera (possibly)
Reference	I. Bruchkouski, V. Dziomin, A. Krasouski. Seasonal variability of the atmospheric trace constituents in Antarctica / I. Bruchkouski [et al.] // Abs. 35-th Canadian Symposium of Remote Sensing (IGARSS-2014), Quèbec, 13-18 July / General Chair Dr. Monique Bernier. – Quebec, 2014. – P. 4098-4100.

Institute: Center for Environmental Remote Sensing (CEReS), Chiba University (**CHIBA**), Chiba, Japan **Responsible person(s):** Hitoshi Irie **Contact details:** hitoshi.irie@chiba-u.jp		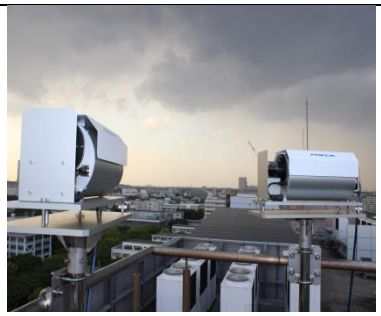
Instrument type: 1 channel scientific grade elevation and azimuth scanning MAX-DOAS	**Nr:** CINDI-2.09	
Overall design of the instrument	**Optical head including telescope:** separated **Spectrometer type:** Ocean Optics Maya2000Pro **Detector type:** Back-thinned, 2D FFT-CCD **Optical fibers:** premium-grade UV/VIS Optical fibre, length - 10 m **Filters:** no **Mirrors:** quartz mirror **Temperature control of spectrometer and detector:** 40°C/40°C	
Instrument performance	**Spectral range/resolution:** 310–515/0.4 nm **Azimuthal scan/direct-sun capabilities:** no/no **Elevation angle capability:** set of 6 elevation angles, values can be adjusted but not the number of angles **Field of view:** <1° **Typical integration time:** 140 seconds **Typical scan duration:** 15 minutes	
Calibration/characterization procedures	**Elevation angles:** Two horizontal levels embedded in the base plate and in a plate holding the reflecting mirror are used to adjust the zero angle of the reflecting mirror. A stepping motor with an angle step of 0.038) is used for controlling the mirror angle. **Field of view:** Characterized by Prede **Stray light:** Subtracted as an offset component in DOAS analysis **Dark signal:** nightly measurements **Line shape:** An asymmetry Gaussian shape is determined during the wavelength calibration. **Polarization:** - **Detector nonlinearity:** characterized by Ocean Optics **Pixel-to-pixel variability**: nightly measurements	
Spectral analysis software	JM2 (Japanese MAX-DOAS profile retrieval algorithm, version 2)	
Supporting measurements	none	
Reference	Irie, H., H. M. S. Hoque, A. Damiani, H. Okamoto, A. M. Fatmi, P. Khatri, T. Takamura, and T. Jarupongsakul, Simultaneous observations by sky radiometer and MAX-DOAS for characterization of biomass burning plumes in central Thailand in January-April 2016, Atmos. Meas. Tech., 12, 599-606, https://doi.org/10.5194/amt-12-599-2019, January 29, 2019.	

Institute: Chinese Academy of Meteorology Science, China Meteorological Administration (**CMA**), Beijing, China **Responsible person(s):** Junli Jin, Jianzhong Ma **Contact details:** jinjunli@camscma.cn		
Instrument type: mini-DOAS Hoffmann UV (#1)	**Nr:** CINDI-2.07	

Overall design of the instrument	**Optical head including telescope:** integrated **Spectrometer type:** Ocean Optics usb 2000 **Detector type:** Sony ILX511 CCD (2048 pixels) **Optical fibers:** n/a **Temperature control of spectrometer/detector:** n/a
Instrument performance	**Spectral range/resolution:** 292-447/0.6-0.8 nm **Azimuthal scan/direct-sun capabilities:** no/no **Elevation angle capability:** fully configurable **Field of view:** 0.8° **Typical integration time:** 1-2 minutes **Typical scan duration:** 15-30 minutes
Calibration/characterization procedures	**Elevation angles:** horizontal scan calibration **Field of view:** not yet characterized **Straylight:** not characterized **Dark signal:** measurement in night or measured with telescope covered, then substracted before spectra analysis **Line shape:** not yet characterized **Polarization:** not yet characterized **Detector nonlinearity:** not yet characterized **Pixel-to-pixel variability**: not yet characterized
Spectral analysis software	WinDOAS
Supporting measurements	none

Institute: Chinese Academy of Meteorology Science, China Meteorological Administration (**CMA**), Beijing, China **Responsible person(s):** Junli Jin, Jianzhong Ma **Contact details:** jinjunli@camscma.cn		
Instrument type: mini-DOAS Hoffmann VIS (#1)	**Nr:** CINDI-2.08	

Overall design of the instrument	**Optical head including telescope:** integrated **Spectrometer type:** Ocean Optics usb 2000 **Detector type:** DET2B-vis (2048 pixels) **Optical fibers:** n/a **Filters:** n/a **Mirrors:** n/a **Temperature control of spectrometer/detector:** n/a
Instrument performance	**Spectral range/resolution:** 399-712/0.6-0.8 nm **Azimuthal scan/direct-sun capabilities:** no/no **Elevation angle capability:** fully configurable **Field of view:** 0.8° **Typical integration time:** 1-2 minutes **Typical scan duration:** 15-30 minutes
Calibration/characterization procedures	**Elevation angles:** horizontal scan calibration **Field of view:** not characterized **Dark signal:** measurement in night or measured with telescope covered, then substracted before spectra analysis **Line shape:** not yet characterized **Polarization:** not yet characterized **Detector nonlinearity:** not yet characterized **Pixel-to-pixel variability**: not yet characterized
Spectral analysis software	WinDOAS
Supporting measurements	none

Institute: Department of Atmospheric Chemistry and Climate (AC2), Spanish National Research Council (**CSIC**), Madrid, Spain **Responsible person(s):** David García, Nuria Benavent, Shanshan Wang **Contact details:** dgarcia@iqfr.csic.es		
Instrument type: MAX-DOAS	**Nr:** CINDI-2.10	

Overall design of the instrument	**Optical head including telescope:** separated; elevation angles fully configurable **Spectrometer type:** Princeton Acton SP2500 **Detector type:** Pixis 2D CCD Camera, 1340x400 pixels **Optical fibers:** Multifiber UV-VIS, 10 m length **Temperature control of spectrometer and detector:** 20-25°C and 70°C
Instrument performance	**Spectral range/resolution:** 300–500/0.5 nm **Azimuthal scan/direct-sun capabilities:** no/no **Elevation angle capability:** fully configurable **Field of view:** approx. 0.7° (estimated using white stripe method) **Typical integration time:** 0.01-1s **Typical scan duration:** 5 minutes
Calibration/characterization procedures	**Elevation angles:** 45 ° **Field of view:** lamp in telescope **Straylight:** - **Dark signal:** by using the shutter **Line shape:** Hg/Ne **Polarization:** - **Detector nonlinearity:** laboratory **Pixel-to-pixel variability**: laboratory
Spectral analysis software	QDOAS
Supporting measurements	Video camera
Reference	Prados-Roman, C., Cuevas, C. A., Hay, T., Fernandez, R. P., Mahajan, A. S., Royer, S.-J., Galí, M., Simó, R., Dachs, J., Großmann, K., Kinnison, D. E., Lamarque, J.-F., and Saiz-Lopez, A.: Iodine oxide in the global marine boundary layer, Atmos. Chem. Phys., 15, 583-593, https://doi.org/10.5194/acp-15-583-2015, 2015.

Institute: University of Colorado (**CU-Boulder**), Boulder, Colorado **Responsible person(s):** Rainer Volkamer, Henning Finkenzeller **Contact details:** Rainer.Volkamer@colorado.edu, Henning.Finkenzeller@colorado.edu	
Instrument type: 3D-MAX-DOAS	**Nr:** CINDI-2.11
Overall design of the instrument	**Optical head including telescope:** separated; elevation and azimuth angles fully configurable; integrating sphere for direct sun measurements **Spectrometer type:** 2 x Acton SP2150 **Detector type:** 2 x PIXIS 400 back-illuminated CCD **Optical fibers:** Monofiber, diameter: 1.25mm, length: 25m connects to Y-type bundle, diameter: 0.145mm, length: 1m **Filters:** BG3/BG38, GG395 **Mirrors:** quartz prisms **Temperature control of spectrometer and detector:** 34°C/-30°C
Instrument performance	**Spectral range/resolution:** 327-470/0.7 & 432–678/1.2 nm **Azimuthal scan/direct-sun capabilities:** yes/yes **Elevation angle capability:** fully configurable **Field of view:** 0.7 degrees (full angle) **Typical integration time:** ~20s **Typical scan duration:** ~8min (12 EA & 12 Az)
Calibration/characterization procedures	**Elevation angles:** geometric alignment, solar aureole/horizon scan **Field of view:** laser pointer backwards **Straylight:** dark areas on CCD **Dark signal:** characterized at night, and by dark areas on CCD **Line shape:** Hg/Kr lamps (external) & QDOAS for wavelength dependency **Polarization:** - **Detector nonlinearity:** Fraunhofer OD at different saturation levels of CCD **Pixel-to-pixel variability**: monitored
Spectral analysis software	QDOAS
Supporting measurements	Webcam, Hg & Kr lamp
Reference	Baidar, S., Oetjen, H., Coburn, S., Dix, B., Ortega, I., Sinreich, R., and Volkamer, R.: The CU Airborne MAX-DOAS instrument: vertical profiling of aerosol extinction and trace gases, Atmos. Meas. Tech., 6, 719-739, https://doi.org/10.5194/amt-6-719-2013 , 2013.

Institute: University of Colorado (**CU-Boulder**), Boulder, Colorado **Responsible person(s):** Rainer Volkamer **Contact details:** Rainer.Volkamer@colorado.edu		
Instrument type: ZS & MAX-DOAS (1D)	**Nr:** CINDI-2.12	

Overall design of the instrument	**Optical head including telescope:** rotating prism, elevation angles fully configurable horizon-to-horizon across zenith **Spectrometer type:** Acton SP2356i & QE65000 **Detector type:** PIXIS 400 back-illuminated CCD & Sony CCD **Optical fibers:** Monofiber, diameter: 1.5mm, length: 10m connects to Y-type bundle, diameter: 0.145mm, length: 1m **Filters:** BG3/BG38 **Mirrors:** quartz prism **Temperature control of spectrometer/detector:** 34°C/-30°C
Instrument performance	**Spectral range/resolution:** 300-466/0.8 & 379–493/0.5 nm **Azimuthal scan/direct-sun capabilities:** no/no **Elevation angle capability:** fully configurable **Field of view:** 0.4 degrees (full angle) **Typical integration time:** ~30s **Typical scan duration:** ~8min
Calibration/characterization procedures	**Elevation angles:** geometric alignment, horizon scan **Field of view:** laser pointer backwards **Straylight:** dark areas on CCD **Dark signal:** characterized at night, and by dark areas on CCD **Line shape:** Hg/Kr lamps (external) & QDOAS for wavelength dependency **Polarization:** - **Detector nonlinearity:** Fraunhofer line distortion at different sat levels **Pixel-to-pixel variability**: monitored
Spectral analysis software	QDOAS
Supporting measurements	Webcam, Hg & Kr lamp
Reference	Coburn, S., Dix, B., Sinreich, R., and Volkamer, R.: The CU ground MAX-DOAS instrument: characterization of RMS noise limitations and first measurements near Pensacola, FL of BrO, IO, and CHOCHO, Atmos. Meas. Tech., 4, 2421-2439, https://doi.org/10.5194/amt-4-2421-2011 , 2011.

Institute 1: Institut fuer Methodik der Fernerkundung (IMF), Deutsches Zentrum fuer Luft- und Raumfahrt e.V. (**DLR**), Wessling, Germany **Institute 2:** School of Earth and Space Sciences, University of Science and Technology of China (**USTC**), Hefei, Anhui, China **Responsible person(s):** Nan Hao (DLR) and Cheng Liu (USTC) **Contact details:** nan.hao@dlr.de, Chliu81@ustc.edu.cn		
Instrument type: 1D MAX-DOAS EnviMeS (#1)	**Nr:** CINDI-2.13 CINDI-2.14	

Overall design of the instrument	**Optical head including telescope:** separated; elevation and azimuth angles fully configurable **Spectrometer type UV and Vis:** Avantes AvaBench-75 **Detector type UV:** Backthinned Hamamatsu CCD (2048 pixel) **Detector type vis:** Backthinned Hamamatsu CCD (2048 pixel) **Optical fibers:** Multifibre (UV), single fibre (VIS), length: 10m **Filters:** UV bandpass filters (BG3) **Mirrors:** none (rotatable prism for elevation angle selection) **Temperature control of spectrometer and detector UV:** 20°C/20°C **Temperature control of spectrometer and detector vis:** 20°C/20°C
Instrument performance	**Spectral range/resolution UV:** 296–460/0.56 nm **Spectral range/resolution vis:** 440–583/0.54 nm **Azimuthal scan/direct-sun capabilities:** yes/no **Elevation angle capability:** fully configurable; step: 0.1° or less **Field of view:** <0.5° **Typical integration time:** 2.5ms -60s **Typical scan duration:** 5 minutes
Calibration/characterization procedures	**Elevation angles:** Point-like light source and laser level **Field of view:** Point-like light source and laser level **Straylight:** Optical filters **Dark signal:** Measurement during the night **Line shape:** Atomic emission lines (Hg/Ne) **Polarization:** n/a (depolarizing fibre) **Detector nonlinearity:** Measurement of artificial light source with varying integration times **Pixel-to-pixel variability**: Halogen lamp
Spectral analysis software	DOASIS
Supporting measurements	Webcam, tilt sensor, GPS

Institute: Indian Institute of Science Education and Research Mohali Department of Earth and Environmental Sciences, Indian Institute of Science Education and Research Mohali (**IISERM**), Punjab, India **Responsible person(s):** Abhishek Kumar Mishra and Vinod Kumar **Contact details:** abhishekkumar.mishra21@gmail.com, vinodkumar@iisermohali.ac.in		
Instrument type: mini-MAX DOAS Hoffmann UV (#2)	**Nr:** CINDI-2.16	

Overall design of the instrument	**Optical head including telescope:** integrated **Spectrometer type UV:** Ocean Optics usb 2000+ **Spectrometer type:** CCD (2048 pixels) **Filters:** no **Mirrors:** - **Temperature control of spectrometer and detector:** Peltier cooler
Instrument performance	**Spectral range/resolution:** 316–466/0.7 nm **Azimuthal scan/direct-sun capabilities:** no/no **Elevation angle capability:** fully configurable; step: 0.1° or less **Field of view:** 0.7° **Typical integration time:** 60ms **Typical scan duration:** ~5 minutes for one full elevation sequence
Calibration/characterization procedures	**Elevation angles:** - Horizon calibration (-3° – 3°) every noon, Distant point source calibration in night **Field of view:** -Point light source **Straylight:** - not characterized **Dark signal:** - Recorded every night **Line shape:** - Gaussian like **Polarization:** - Not characterized **Detector nonlinearity:** - Not characterized **Pixel-to-pixel variability**: - Not characterized
Spectral analysis software	WinDOAS and DOASIS
Supporting measurements	None

Institute: National Institute for Aerospace Technology (**INTA**), Madrid, Spain **Responsible person(s):** Olga Puentedura **Contact details:** puentero@inta.es		
Instrument type: 2D-MAX-DOAS RASAS III	**Nr:** CINDI-2.17	

Overall design of the instrument	**Optical head including telescope:** separated; elevation and azimuth angles fully configurable **Spectrometer type:** Andor Shamrock SR-163i **Detector type:** IDUS Andor BU2 **Optical fibres:** Bundle 100 µm, length: 8 m **Filters:** No **Mirrors:** No **Temperature control of spectrometer/detector:** 17°C/-30ºC
Instrument performance	**Spectral range/resolution:** 420-540/0.55 nm **Azimuthal scan/direct-sun capabilities:** yes/no **Elevation angle capability:** fully configurable **Field of view:** 1° **Typical integration time:** ~1 minute/pointing direction **Typical scan duration:** ~1 minute x number of pointing directions
Calibration/characterization procedures	**Elevation angles:** Inclinometer during operation **Field of view:** Geometrical **Straylight:** HeNe LASER and optical filters **Dark signal:** Measured at constant temperature with different integration times and subtracted during analysis **Line shape:** HgCd lamp **Polarization:** Optical fibre depolarizes the signal **Detector nonlinearity:** Stable source and varying integration times **Pixel-to-pixel variability**: Halogen lamp
Spectral analysis software	LANA software
Supporting measurements	Video camera, inclinometer and GPS
Reference	Puentedura, O., Gil, M., Saiz-Lopez, A., Hay, T., Navarro-Comas, M., Gómez-Pelaez, A., Cuevas, E., Iglesias, J., and Gomez, L.: Iodine monoxide in the north subtropical free troposphere, Atmos. Chem. Phys., 12, 4909-4921, https://doi.org/10.5194/acp-12-4909-2012, 2012.

Institute: Institute of Environmental Physics (**IUP-Bremen**), University of Bremen, Bremen, Germany **Responsible person(s):** Andreas Richter **Contact details:** richter@iup.physik.uni-bremen.de		
Instrument type: 2 channel scientific grade elevation and azimuth scanning MAX-DOAS	**Nr:** CINDI-2.18	
Overall design of the instrument	**Optical head including telescope:** separated; elevation and azimuth angles fully configurable **Spectrometer type UV:** Acton ARC500 **Spectrometer type vis:** Acton ARC500 **Detector type UV:** Princeton NTE/CCD-1340/400-EMB **Detector type vis:** Princeton NTE/CCD-1340/400-EMB **Optical fibers:** Y-type quartz bundle, diameter: 150µm, length: 22m **Filters:** UG5 (UV only) **Mirrors:** no **Temperature control of spectrometer and detector UV:** 35°C/-35°C **Temperature control of spectrometer and detector vis:** 35°C/-30°C	
Instrument performance	**Spectral range/resolution UV:** 305–390/0.5 nm **Spectral range/resolution vis:** 406–579/0.85 nm **Azimuthal scan/direct-sun capabilities:** yes/no **Elevation angle capability:** fully configurable **Field of view:** 1° **Typical integration time:** 60s; 120s for zenith **Typical scan duration:** 15 minutes for 11 elevation angles	
Calibration/characterization procedures	**Elevation angles:** geometric alignment of telescope, horizon scan **Field of view:** white light source in lab **Straylight:** not yet characterized **Dark signal:** nightly measurements **Line shape:** HgCd lamp in telescope **Polarization:** - **Detector nonlinearity:** white light source in lab, characterization only **Pixel-to-pixel variability**: white light source in lab, characterization only	
Spectral analysis software	NLIN	
Supporting measurements	Video camera, HgCd lamp	
Reference	Peters, E., Wittrock, F., Großmann, K., Frieß, U., Richter, A., and Burrows, J. P., Formaldehyde and nitrogen dioxide over the remote western Pacific Ocean: SCIAMACHY and GOME-2 validation using ship-based MAX-DOAS observations, Atmos. Chem. Phys., 12, 11179-11197, doi:10.5194/acp-12-11179-2012, 2012.	

Institute: Institute of Environmental Physics (**IUP-Bremen**), University of Bremen, Bremen, Germany **Responsible person(s):** Enno Peters **Contact details:** Enno.Peters@iup.physik.uni-bremen.de		
Instrument type: single channel scientific grade imaging-DOAS, telescope mounted on pan-tilt-head for azimuthal scans and zenith (reference) pointing, indoor parts equipped in a 19'' rack	**Nr:** CINDI-2.37	

Overall design of the instrument	**Optical head including telescope:** separated; elevation and azimuth angles fully configurable **Spectrometer type:** Andor Shamrock 303i **Detector type:** Andor Newton DU940P-BU, 2048x512 pixel (only inner pixels used for imaging) **Optical fibers:** Fibre bundle with 69 sorted single fibres, diameter: 100µm, length: 15m **Filters:** BG39 **Mirrors:** no **Temperature control of spectrometer and detector:** 35°C/-30°C
Instrument performance	**Spectral range/resolution:** 420 – 500nm/0.8 nm **Azimuthal scan/direct-sun capabilities:** yes/n/a **Elevation angle capability:** fully configurable **Field of view:** vertically approx. 50° total, 1.5° per view, horizontally 1.2° **Typical integration time:** 10s **Typical scan duration:** 10 min for complete horizon scan (10° azimuthal steps 0-360° followed by zenith reference)
Calibration/characterization procedures	**Elevation angles:** between -5 and +30 + regular zenith-sky **Field of view:** white light source in lab **Straylight:** not yet characterized **Dark signal:** manually **Line shape:** HgCd lamp (manually) **Polarization:** - **Detector nonlinearity:** white light source in lab, characterization only **Pixel-to-pixel variability**: white light source in lab, characterization only
Spectral analysis software	NLIN
Supporting measurements	Video camera
Reference	Peters, E., Ostendorf, M.,Bösch, T., Seyler, A., Schönhardt, A., Schreier, S.F., Henzing, J. S., Wittrock, F., Richter, A., Vrekoussis, M., Burrows,J.P., Full-azimuthal imaging-DOAS observations of NO2 and O4 during CINDI-2, submitted to AMT, 2019.

Institute: Institute of Environmental Physics (**IUP-Heidelberg**), University of Heidelberg, Heidelberg, Germany **Responsible person(s):** Udo Friess **Contact details:** udo.friess@iup.uni-heidelberg.de		
Instrument type: 2D MAX-DOAS EnviMeS (#3)	**Nr:** CINDI-2.19	
Overall design of the instrument	**Optical head including telescope:** separated; elevation and azimuth angles fully configurable **Spectrometer type UV and Vis:** Avantes AvaBench-75 **Detector type UV:** Backthinned Hamamatsu CCD (2048 pixel) **Detector type vis:** Backthinned Hamamatsu CCD (2048 pixel) **Optical fibers:** Multifibre (UV), single fibre (VIS), length: 10m **Filters:** UV bandpass filters (BG3) **Mirrors:** none (rotatable prism for elevation angle selection) **Temperature control of spectrometer and detector UV:** 20°C/20°C **Temperature control of spectrometer and detector vis:** 20°C/20°C	
Instrument performance	**Spectral range/resolution UV:** 296–460/0.56 nm **Spectral range/resolution vis:** 440–583/0.54 nm **Azimuthal scan/direct-sun capabilities:** yes/yes **Elevation angle capability:** fully configurable; step: 0.1° or less **Field of view:** <0.5° **Typical integration time:** 2.5ms - 60s **Typical scan duration:** 5 minutes	
Calibration/characterization procedures	**Elevation angles:** Point-like light source and laser level **Field of view:** Point-like light source and laser level **Straylight:** Optical filters **Dark signal:** Measurement during the night **Line shape:** Atomic emission lines (Hg/Ne) **Polarization:** n/a **Detector nonlinearity:** Measurement of artificial light source with varying integration times **Pixel-to-pixel variability**: Halogen lamp	
Spectral analysis software	DOASIS	
Supporting measurements	Webcam, tilt sensor, GPS	
Reference	Lampel, J., Frieß, U., and Platt, U.: The impact of vibrational Raman scattering of air on DOAS measurements of atmospheric trace gases, Atmos. Meas. Tech., 8, 3767-3787, https://doi.org/10.5194/amt-8-3767-2015, 2015.	

Institute: Royal Netherlands Meteorological Institute (**KNMI**), De Bilt, The Netherlands **Responsible person(s):** Ankie Piters **Contact details:** ankie.piters@knmi.nl		
Instrument type: mini-DOAS Hoffmann UV (#3)	**Nr:** CINDI-2.21	

Overall design of the instrument	**Optical head including telescope:** integrated **Spectrometer type:** Ocean Optics usb 2000 **Detector type:** Sony ILX511 CCD (2048 pixels) **Optical fibers:** n/a
Instrument performance	**Spectral range/resolution:** 290-443/0.6 nm **Azimuthal scan/direct-sun capabilities:** no/no **Elevation angle capability:** fully configurable **Field of view:** 0.45° **Typical integration time:** 1-2 minutes **Typical scan duration:** 15-30 minutes
Calibration/characterization procedures	**Elevation angles:** calibration of horizon (+/-0.5 degree) via quick horizon-scan (-3 to +3, very short integration time) **Field of view:** scanning over a light source in the laboratory **Straylight**: not yet characterized **Dark signal:** characterized in the dark room as a function of detector temperature **Line shape:** determined from lamp lines (function of temperature and wavelength) **Polarization:** not yet characterized **Detector nonlinearity:** not yet characterized **Pixel-to-pixel variability**: characterized in the dark room as a function of detector temperature
Spectral analysis software	Own software (Python-based)
Supporting measurements	none
Reference	Vlemmix, T., Piters, A.J.M., Stammes, P., Wang, P., and Levelt, P.F., Retrieval of tropospheric NO2 using the MAX-DOAS method combined with relative intensity measurements for aerosol correction, Atmos. Meas. Tech. 3, 1287-1305, 2010.

Institute: Royal Netherlands Meteorological Institute (**KNMI**), De Bilt, The Netherlands **Responsible person(s):** Ankie Piters **Contact details:** ankie.piters@knmi.nl		
Instrument type: mini-DOAS Hoffmann VIS (#3)	**Nr:** CINDI-2.22	

Overall design of the instrument	**Optical head including telescope:** integrated **Spectrometer type:** Ocean Optics usb 2000+ **Detector type:** Sony ILX511 CCD (2048 pixels)
Instrument performance	**Spectral range/resolution:** 400-600/0.5 nm **Azimuthal scan/direct-sun capabilities:** no/no **Elevation angle capability:** fully configurable **Field of view:** 0.4° **Typical integration time:** 1-2 minutes **Typical scan duration:** 15-30 minutes
Calibration/characterization procedures	**Elevation angles:** calibration of horizon (+/-0.5 degree) via quick horizon-scan (-3 to +3, very short integration time) **Field of view:** scanning over a light source in the laboratory **Straylight**: not yet characterized **Dark signal:** characterized in the dark room as a function of detector temperature **Line shape:** determined from lamp lines (function of temperature and wavelength) **Polarization:** not yet characterized **Detector nonlinearity:** not yet characterized **Pixel-to-pixel variability**: characterized in the dark room as a function of detector temperature
Spectral analysis software	Own software (Python-based)
Supporting measurements	none
Reference	Vlemmix, T, Tropospheric nitrogen dioxide inversions based on spectral measurements of scattered sunlight, PhD Thesis, Technische Universiteit Eindhoven, DOI: 10.6100/IR719874, 2011.

Institute: Royal Netherlands Meteorological Institute (**KNMI**), De Bilt, The Netherlands **Responsible person(s):** Ankie Piters **Contact details:** ankie.piters@knmi.nl		
Instrument type: PANDORA-1S (#1)	**Nr:** CINDI-2.23	
Overall design of the instrument	**Optical head including telescope:** separated; elevation and azimuth angles fully configurable **Spectrometer type:** AvaSpec-ULS2048x64 **Detector type:** 2048 x 64 pixel backthinned non-cooled Hamamatsu CCD **Optical fibers:** single strand 400um core diameter high OH fused silica fiber, 10m long **Filters:** spectral filters (U340 and BP300 to remove visible light), attenuation filters **Mirrors:** no **Temperature control of spectrometer and detector:** 20°C/20°C	
Instrument performance	**Spectral range/resolution UV:** 290-530/0.6 nm **Azimuthal scan/direct-sun capabilities:** yes/yes **Elevation angle capability:** fully configurable **Field of view:** circular, 1.5° (sky mode); 2.5° (sun mode) **Typical integration time:** 2.4ms-300ms (sun), 20ms to 1000ms (sky) **Typical scan duration:** 15-30s per pointing position	
Calibration/characterization procedures	**Elevation angles:** based on astronomical calculations and scanning the solar disc **Field of view:** determined from scanning the solar disc **Stray light:** determined in laboratory from measuring monochromatic input at multiple wavelengths **Dark signal:** determined after each measurement **Line shape:** determined in the laboratory from measurements of several spectral lamps **Polarization:** no residual polarization measured after 10m fiber **Detector nonlinearity:** determined in laboratory from tungsten halogen lamp measurements at different integration times **Pixel-to-pixel variability**: determined in laboratory from tungsten halogen lamp measurement	
Spectral analysis software	Own software (Python-based) and Blick Software Suite (Python-based)	
Supporting measurements	None	
Reference	J. Herman, A. Cede, E. Spinei, G. Mount, M. Tzortziou, and N. Abuhassan, NO2 column amounts from ground-based Pandora and MFDOAS spectrometers using the direct-sun DOAS technique: Intercomparisons and application to OMI validation, J. Geophys. Res., 114, D13307, doi:10.1029/2009JD011848, 2009.	

Institute: Laboratoire Atmosphère, Milieux, Observations Spatiales (**LATMOS**), Guyancourt, France **Responsible person(s):** Andrea Pazmino **Contact details:** andrea.pazmino@latmos.ipsl.fr, Manuel.pinharanda@latmos.ipsl.fr	
Instrument type: Système d'Analyse par Observation Zénithale (SAOZ) **Nr:** CINDI-2.24	
Overall design of the instrument	**Optical head including telescope:** n/a **Spectrometer type:** Jobin-Yvon CP200 flat field **Detector type:** 1024 NMOS diode array from Hamamatsu **Optical fibers:** n/a **Filters:** no **Mirrors:** Yes **Temperature control of spectrometer and detector:** no
Instrument performance	**Spectral range/resolution:** 270–640/1.3 nm **Azimuthal scan/direct-sun capabilities:** n/a **Elevation angle capability:** n/a **Field of view:** 20^{o} **Exposure time:** 0.19 s - 5 x measurement cycle (adjusted automatically) **Measurement cycle:** 60 s (programmable)
Calibration/characterization procedures	**Elevation angles:** n/a **Field of view:** n/a **Straylight:** n/a **Dark signal:** shutter **Line shape:** wavelength calibration based on reference spectrum **Polarization:** Est-West fixed direction of the entrance slit **Detector nonlinearity:** exposure time calibrated to 12000 counts in elementary spectrum **Pixel-to-pixel variability**: dark background
Spectral analysis software	SAM version 5.9
Supporting measurements	GPS
Reference	Pazmiño A., O3 and NO2 vertical columns using SAOZ UV-Visible spectrometer, EPJ Web of Conferences, Vol 9: ERCA 9 – From the Global Mercury Cycle to the Discoveries of Kuiper Belt Objects, p. 201-214, doi:10.1051/epjconf/201009016, 2010.

Institute: Laboratoire Atmosphère, Milieux, Observations Spatiales (**LATMOS**), Guyancourt, France **Responsible person(s):** Andrea Pazmino **Contact details:** andrea.pazmino@latmos.ipsl.fr, Manuel.pinharanda@latmos.ipsl.fr	
Instrument type: Mini Système d'Analyse par Observation Zénithale (mini-SAOZ)	**Nr:** CINDI-2.25

Overall design of the instrument	**Optical head:** separated **Spectrometer type:** Cerny-Turner, grating 600 grooves/mm **Detector type:** 2048x16 CCD back-thinned from Hamamatsu **Optical fibers:** HGC950; diameter: 950 µm; length:10 m **Filters:** OSC-UB **Temperature control of spectrometer and detector:** n/a
Instrument performance	**Spectral range/resolution:** 270–820/0.7 nm **Azimuthal scan/direct-sun capabilities:** n/a **Elevation angle capability:** n/a **Field of view:** 8° **Exposure time:** 0.037 s - 5 x measurement cycle (adjusted automatically) **Measurement cycle:** 60 s (programmable)
Calibration/characterization procedures	**Elevation angles:** n/a **Field of view:** n/a **Straylight:** n/a **Dark signal:** shutter **Line shape:** wavelength calibration based on reference spectrum **Polarization:** n/a **Detector nonlinearity:** exposure time calibrated to 12000 counts in elementary spectrum spectrum (semi-blind campaign) Characterisation using stable light source at different integration time (after campaign) **Pixel-to-pixel variability**: dark background
Spectral analysis software	SAOZ.gui Version 1.25-50f870
Supporting measurements	GPS
Reference	Piters, A. J. M. et al.: The Cabauw Intercomparison campaign for Nitrogen Dioxide measuring Instruments (CINDI): design, execution, and early results, Atmos. Meas. Tech., 5(2), 457-485, 2012, doi:10.5194/amt-5-457-2012, 2012.

Institute: Meteorologisches Institut, Ludwig-Maximilians-Universität München (**LMU-MIM**), Munich, Germany **Responsible person(s):** Mark Wenig **Contact details:** mark.wenig@physik.uni-muenchen.de, lok.chan@ physik.uni-muenchen.de		
Instrument type: 2D MAX-DOAS EnviMeS (#4)	**Nr:** CINDI-2.35	

Overall design of the instrument	**Optical head including telescope:** separated; elevation and azimuth angles fully configurable **Spectrometer type UV:** Avantes AvaBench-75 **Spectrometer type vis:** Avantes AvaBench-75 **Detector type UV:** Backthinned Hamamatsu CCD (2048 pixel) **Detector type vis:** Backthinned Hamamatsu CCD (2048 pixel) **Optical fibers:** Multifibre (UV), single fibre (VIS), length: 10m **Filters:** UV bandpass filters (BG3) **Mirrors:** N/A **Temperature control of spectrometer and detector UV:** 20°C/20°C **Temperature control of spectrometer and detector vis:** 20°C/20°C
Instrument performance	**Spectral range/resolution UV:** 305–460/0.56 nm **Spectral range/resolution vis:** 430–650/0.54 nm **Azimuthal scan/direct-sun capabilities:** yes/yes **Elevation angle capability:** fully configurable **Field of view:** <0.5° **Typical integration time:** 2.5ms -60s **Typical scan duration:** 15 min
Calibration/characterization procedures	**Elevation angles:** tilt sensor **Field of view:** not yet characterized **Straylight:** not yet characterized **Dark signal:** not yet characterized **Line shape:** not yet characterized **Polarization:** not yet characterized **Detector nonlinearity:** not yet characterized **Pixel-to-pixel variability**: not yet characterized
Spectral analysis software	DOASIS
Supporting measurements	Two video cameras, inclinometer
Reference	Lampel, J., Frieß, U., and Platt, U.: The impact of vibrational Raman scattering of air on DOAS measurements of atmospheric trace gases, Atmos. Meas. Tech., 8, 3767-3787, https://doi.org/10.5194/amt-8-3767-2015, 2015.

Institute: **LuftBlick**, Mutters, Austria **Responsible person(s):** Alexander Cede **Contact details:** alexander.cede@luftblick.at		
Instrument type: PANDORA-2S (#2 & #3)	**Nr:** CINDI-2.26 CINDI-2.27	

Overall design of the instrument	**Optical head including telescope:** separated; elevation and azimuth angles fully configurable **Spectrometer type:** AvaSpec-ULS2048x64 (one for UV and one for vis) **Detector type:** 2048 x 64 pixel backthinned non-cooled Hamamatsu CCD (one for UV and one for vis) **Optical fibers:** single strand 400um core diameter high OH fused silica fiber, 10m long **Filters:** spectral filters (U340 and BP300 to remove visible light), attenuation filters **Mirrors:** no **Temperature control of spectrometer and detector UV:** 20°C/20°C **Temperature control of spectrometer and detector VIS:** 20°C/20°C
Instrument performance	**Spectral range/resolution UV:** 280 - 540/0.6 nm **Spectral range/resolution vis:** 380 - 900/1.1 nm **Azimuthal scan/direct-sun capabilities:** yes/yes **Elevation angle capability:** fully configurable **Field of view:** circular, 1.5° (sky mode); 2.8° (sun mode) **Typical integration time:** 2.4ms-300ms (sun), 20ms to 1000ms (sky) **Typical scan duration:** 15-30s per pointing position
Calibration/characterization procedures	**Elevation angles:** based on astronomical calculations and scanning the solar disc **Field of view:** determined from scanning the solar disc **Stray light:** determined in the laboratory from measuring monochromatic input at different wavelengths **Dark signal:** determined after each measurement **Line shape:** determined in the laboratory from measurements of several spectral lamps **Polarization:** no residual polarization measured after 10m fiber **Detector nonlinearity:** determined in laboratory from tungsten halogen lamp measurements at different integration times **Pixel-to-pixel variability**: determined in laboratory from tungsten halogen lamp measurements
Spectral analysis software	Blick Software Suite (Python-based)
Supporting measurements	None
Reference	J. Herman, A. Cede, E. Spinei, G. Mount, M. Tzortziou, and N. Abuhassan, NO2 column amounts from ground-based Pandora and MFDOAS spectrometers using the direct-sun DOAS technique: Intercomparisons and application to OMI validation, J. Geophys. Res., 114, D13307, doi:10.1029/2009JD011848, 2009.

Institute: Max-Planck Institute for Chemistry (**MPIC**), Mainz, Germany **Responsible person(s):** Thomas Wagner **Contact details:** thomas.wagner@mpic.de		
Instrument type: TubeMAX-DOAS	**Nr:** CINDI-2.28	
Overall design of the instrument	**Optical head including telescope:** separated; elevation angles fully configurable **Spectrometer type:** Avantes **Detector type:** CCD **Optical fibers:** quartz fibre bundle, length: 5 m **Filters:** BG3 (UV) **Mirrors:** no **Temperature control of spectrometer and detector:** 20°C/20°C	
Instrument performance	**Spectral range/resolution:** 305–464/0.6 nm **Azimuthal scan/direct-sun capabilities:** no/no **Elevation angle capability:** fully configurable **Field of view:** 0.7^{o} **Typical integration time:** 60s **Typical scan duration:** 15 minutes (depends on sequence)	
Calibration/characterization procedures	**Elevation angles:** performed at the campaign using laser device or water level **Field of view:** performed at the campaign using laser device or water level **Straylight:** has to be quantified **Dark signal:** measured on site and corrected **Line shape:** almost symmetric Gaussian-like, almost not dependent on wavelength **Polarization:** - **Detector nonlinearity:** characterised in the laboratory **Pixel-to-pixel variability**: -	
Spectral analysis software	Windoas and QDOAS	
Supporting measurements	Video camera	
Reference	Donner, S., Mobile MAX-DOAS measurements of the tropospheric formaldehyde column in the Rhein-Main region. Master Thesis, Universität, Mainz,http://hdl.handle.net/11858/00-001M-0000-002C-EB17-2, 2016.	

Institute: **NASA**-Goddard (Greenbelt, Maryland) **Responsible person(s):** Jay Herman **Contact details:** jay.r.herman@nasa.gov, Elena Spinei (elena.spinei@nasa.gov)		
Instrument type: PANDORA-1S (#4 & #5)	**Nr:** CINDI-2.31 CINDI-2.32	

Overall design of the instrument	**Optical head including telescope:** separated; elevation and azimuth angles fully configurable **Spectrometer type:** AvaSpec-ULS2048x64 (one for 285 – 530 nm) **Detector type:** 2048 x 64 pixel backthinned non-cooled Hamamatsu CCD **Optical fibers:** single strand 400um core diameter high OH fused silica fiber, 10m long **Filters:** spectral filters (U340 and BP300 to remove visible light), attenuation filters **Mirrors:** no **Temperature control of spectrometer and detector UV:** 20°C/20°C **Temperature control of spectrometer and detector VIS:** 20°C/20°C
Instrument performance	**Spectral range/resolution UV:** 280-540/0.6 nm **Azimuthal scan/direct-sun capabilities:** yes/yes **Elevation angle capability:** fully configurable **Field of view:** circular, 1.6° (sky mode); 2.8° (sun mode) **Typical integration time:** 2.4ms-300ms (sun), 20ms to 1000ms (sky) **Typical scan duration:** 15-30s per pointing position
Calibration/characterization procedures	**Elevation angles:** based on astronomical calculations and scanning the solar disc **Field of view:** determined from scanning the solar disc **Stray light:** determined in laboratory from measuring monochromatic input at multiple wavelengths **Dark signal:** determined after each measurement **Line shape:** determined in the laboratory from measurements of several spectral lamps **Polarization:** no residual polarization measured after 10m fiber **Detector nonlinearity:** determined in laboratory from tungsten halogen lamp measurements at different integration times **Pixel-to-pixel variability**: determined in laboratory from tungsten halogen lamp measurement
Spectral analysis software	Blick Software Suite (Python-based)
Supporting measurements	None
Reference	J. Herman, A. Cede, E. Spinei, G. Mount, M. Tzortziou, and N. Abuhassan, NO2 column amounts from ground-based Pandora and MFDOAS spectrometers using the direct-sun DOAS technique: Intercomparisons and application to OMI validation, J. Geophys. Res., 114, D13307, doi:10.1029/2009JD011848, 2009.

Institute: National Institute of Water and Atmospheric Research (**NIWA**), Lauder, New Zealand **Responsible person(s):** Richard Querel, Paul Johnston **Contact details:** richard.querel@niwa.co.nz		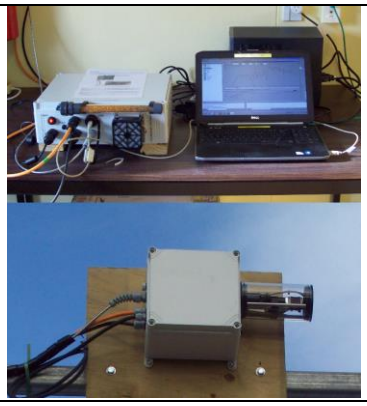
Instrument type: EnviMeS 1D MAX-DOAS (#3)	**Nr:** CINDI-2.29	

Overall design of the instrument	**Optical head including telescope:** elevation angle configurable **Spectrometer type UV:** Avantes AvaBench-75 **Spectrometer type vis:** Avantes AvaBench-75 **Detector type UV:** Backthinned Hamamatsu CCD (2048 x 64 pixels) **Detector type vis:** Backthinned Hamamatsu CCD (2048 x 64 pixels) **Optical fibers:** Multifibre (6 x UV), single fibre (1 x VIS), length: 10m **Filters:** UV bandpass filter (BG3), VIS bandpass filter (BG40) **Mirrors:** Rotating glass quartz prism as entrance optic **Temperature control of spectrometer and detector UV:** 20 °C / 20 °C **Temperature control of spectrometer and detector vis:** 20 °C / 20 °C
Instrument performance	**Spectral range/resolution UV:** 305–457 nm / 0.7 nm **Spectral range/resolution vis:** 410–550 nm / 0.7 nm **Azimuthal scan/direct-sun capabilities:** no **Elevation angle capability:** fully configurable; step: 0.1° or less **Field of view:** <0.5° **Typical integration time:** 2.5ms -60s **Typical scan duration:** 60 s
Calibration/characterization procedures	**Elevation angles:** Calibrated tilt meter and level **Field of view:** not measured **Straylight:** not measured **Dark signal:** shutter blocks light path in scanning head **Line shape:** taken from Hg lamp spectra **Polarization:** 10 m fibre effectively depolarizes incoming light **Detector nonlinearity:** observations of a temperature stabilized LED with several different exposure times, assuming LED to be constant intensity. **Pixel-to-pixel variability**: Not tested
Spectral analysis software	DOASIS, STRATO
Supporting measurements	Tilt sensor (for elevation angle), PTU
Reference	Lampel, J., Frieß, U., and Platt, U.: The impact of vibrational Raman scattering of air on DOAS measurements of atmospheric trace gases, Atmos. Meas. Tech., 8, 3767-3787, https://doi.org/10.5194/amt-8-3767-2015, 2015.

Institute: National Institute of Water and Atmospheric Research (**NIWA**), Lauder, New Zealand **Responsible person(s):** Richard Querel, Paul Johnston **Contact details:** richard.querel@niwa.co.nz		 
Instrument type: Lauder Acton275 MAX-DOAS	**Nr:** CINDI-2.30	
Overall design of the instrument	**Optical head including telescope:** elevation angle configurable **Spectrometer type UV/Vis:** Acton 275 with grating control **Detector type UV/Vis:** Backthinned Hamamatsu CCD (1044 x 128pixels x 24um) **Optical fibers:** Multifibre with 100um fibres, input end circular 1mm diam, length: 12m **Filters:** **Mirrors:** Front silvered rotating mirror and quartz lens optic. **Temperature control of detector:** -20 °C	
Instrument performance	**Spectral range/resolution: multi band configurable; typical two bands are: alternating** 290–363 nm and 400-460; 0.6 nm **Azimuthal scan/direct-sun capabilities:** no **Elevation angle capability:** fully configurable; step: < 0.1° **Field of view:** about 0.5° **Typical integration time:** 16ms -20s **Typical scan duration:** 60 s (but flexible)	
Calibration/characterization procedures	**Elevation angles:** Bubble level on mirror and external laser level **Field of view: m**easured using laser level **Straylight:** estimated using Schott filters to cut light at shorter wavelengths.<1e-2 ? **Dark signal:** night spectra or manual scan **Line shape:** taken from Hg and other line lamp spectra **Polarization:** 12 m fibre effectively depolarizes incoming light **Detector nonlinearity:** quantified by comparing observations of a clear sky with and without neutral density filter. **Pixel-to-pixel variability**: measured with white lamp.	
Spectral analysis software	STRATO (Lauder, NIWA)	
Supporting measurements	GPS time, Camera possible.	

Institute: National University of Sciences and Technology (**NUST**), Islamabad, Pakistan **Responsible person(s):** Muhammad Fahim Khokhar and Junaid Khayyam Butt **Contact details:** fahim.khokhar@iese.nust.edu.pk, jkb2ravian@gmail.com		
Instrument type: Mini MAX-DOAS	**Nr:** CINDI-2.33	
Overall design of the instrument	**Optical head including telescope:** integrated **Spectrometer type:** Czerny-Turner spectrometer **Detector type:** 1 dimensional CCD (Sony ILX511, 2048 individual pixels) **Optical fibers:** n/a **Filters:** n/a **Mirrors:** n/a **Temperature control of spectrometer and detector:** n/a	
Instrument performance	**Spectral range/resolution:** 320–465/0.7 nm **Azimuthal scan/direct-sun capabilities:** no/no **Elevation angle capability:** fully configurable; 1 degree resolution **Field of view:** ~1.2^{o} **Typical integration time:** 10-60s **Typical scan duration:** 20 minutes	
Calibration/characterization procedures	**Elevation angles:** water/sprit level **Field of view:** n/a **Straylight:** n/a **Dark signal:** manual procedure **Line shape:** n/a **Polarization:** n/a **Detector nonlinearity:** n/a **Pixel-to-pixel variability**: n/a	
Spectral analysis software	QDOAS (version:2.111) / WinDOAS	
Supporting measurements	GPS but not integrated	

Institute: Department of Physics, University of Toronto (**UTO**), Toronto, Canada **Responsible person(s):** Kristof Bognar, Xiaoyi Zhao, Kimberly Strong **Contact details:** kbognar@physics.utoronto.ca, xizhao@atmosp.physics.utoronto.ca, strong@atmosp.physics.utoronto.ca		 
Instrument type: PEARL-GBS instrument (MAX-DOAS, ZSL-DOAS, and DS)	**Nr:** CINDI-2.36	
Overall design of the instrument	**Optical head including telescope:** separated; elevation and azimuth angles fully configurable **Spectrometer type:** Jobin Yvon Triax-180 triple-grating spectrometer **Detector type:** back-illuminated cooled CCD with 2048 x 512 pixels **Optical fibers:** fiber bundle (37 HOH mapped fibres, spot-to-slit), spot end diameter: ~0.8 mm, length: 6 m **Filters:** Filter wheel containing one empty slot, four metallic neutral density filters (31.6%, 1%, 0.1%, 0.01% transmittance) and a UV diffuser **Mirrors:** UV-enhanced aluminum (suntracker) **Temperature control of spectrometer and detector:** 25°C/-70°C	
Instrument performance	**Spectral range/resolution:** 340–560/0.75 nm **Azimuthal scan/direct-sun capabilities:** yes/yes **Elevation angle capability:** fully configurable **Field of view:** 0.6° **Typical integration time:** 50-140 s **Typical scan duration:** 12-23 minutes for 9 elevation angles	
Calibration/characterization procedures	**Elevation angles:** calibrated by levelling the suntracker **Field of view:** calculated analytically **Straylight:** determined using a red filter and a halogen lamp **Dark signal:** determined from a series of closed shutter measurements **Line shape:** assumed to be Gaussian **Polarization:** determined using a polarizer and a halogen lamp; fiber bundle mostly depolarizes incoming light **Detector nonlinearity:** <0.4% as given by the CCD manufacturer **Pixel-to-pixel variability**: not characterized	
Spectral analysis software	Raw data is processed using in-house MATLAB code and analysis is performed using the QDOAS software	
Supporting measurements	Webcam	
Reference	A. Fraser, C. Adams, J.R. Drummond, F. Goutail, G. Manney, and K. Strong. The Polar Environment Atmospheric Research Laboratory UV-Visible Ground-Based Spectrometer: First Measurements of O_3, NO_2, BrO, and OClO Columns. *J. Quant. Spectrosc. Radiat. Transfer*, **110 (12)**, 986-1004, 2009.	